



# Geologic Field-Trip Guide of Volcaniclastic Sediments from Snow- and Ice-Capped Volcanoes—Mount St. Helens, Washington, and Mount Hood, Oregon



Scientific Investigations Report 2017–5022–F

**Cover:** *Top.* Photograph of open breach of the Mount St. Helens crater taken from the Pumice Plain looking south-southeast. Eroded deposits in foreground are 1980 pyroclastic density current deposits. The smooth ramp leading up to crater floor is the sliding surface of the 1980 debris avalanche. The composite lava dome (1980–1986 and 2004–2008) is partly visible (largely in shadow) at back of crater. USGS photograph by T. Pierson, 2012. *Bottom.* Photograph of Mount Hood summit looking northeast from Zigzag Canyon, which has incised the debris fan on the southwest flank of the volcano. Stratified late Pleistocene and Holocene volcanoclastic sediments, emplaced by block-and-ash flows and lahars, are visible in the canyon walls overlying a lava flow near the bottom of the canyon. USGS photograph by T. Pierson, 2003.

# **Geologic Field-Trip Guide of Volcaniclastic Sediments from Snow- and Ice-Capped Volcanoes—Mount St. Helens, Washington, and Mount Hood, Oregon**

By Thomas C. Pierson, Lee Siebert, Christopher J. Harpel, and Kevin M. Scott

Scientific Investigations Report 2017–5022–F

**U.S. Department of the Interior  
U.S. Geological Survey**

**U.S. Department of the Interior**  
RYAN K. ZINKE, Secretary

**U.S. Geological Survey**  
James F. Reilly II, Director

U.S. Geological Survey, Reston, Virginia: 2018

For more information on the USGS—the Federal source for science about the Earth, its natural and living resources, natural hazards, and the environment—visit <https://www.usgs.gov> or call 1–888–ASK–USGS.

For an overview of USGS information products, including maps, imagery, and publications, visit <https://store.usgs.gov>.

Any use of trade, firm, or product names is for descriptive purposes only and does not imply endorsement by the U.S. Government.

Although this information product largely is in the public domain, it may also contain copyrighted materials as noted in the text. Permission to reproduce copyrighted items must be secured from the copyright owner.

Suggested citation:

Pierson, T.C., Siebert, L., Harpel, C.J., and Scott, K.M., 2018, Geologic field-trip guide of volcanoclastic sediments from snow- and ice-capped volcanoes—Mount St. Helens, Washington, and Mount Hood, Oregon: U.S. Geological Survey Scientific Investigations Report 2017–5022–F, 97 p., <https://doi.org/10.3133/sir20175022F>.

ISSN 2328-0328 (online)

## Preface

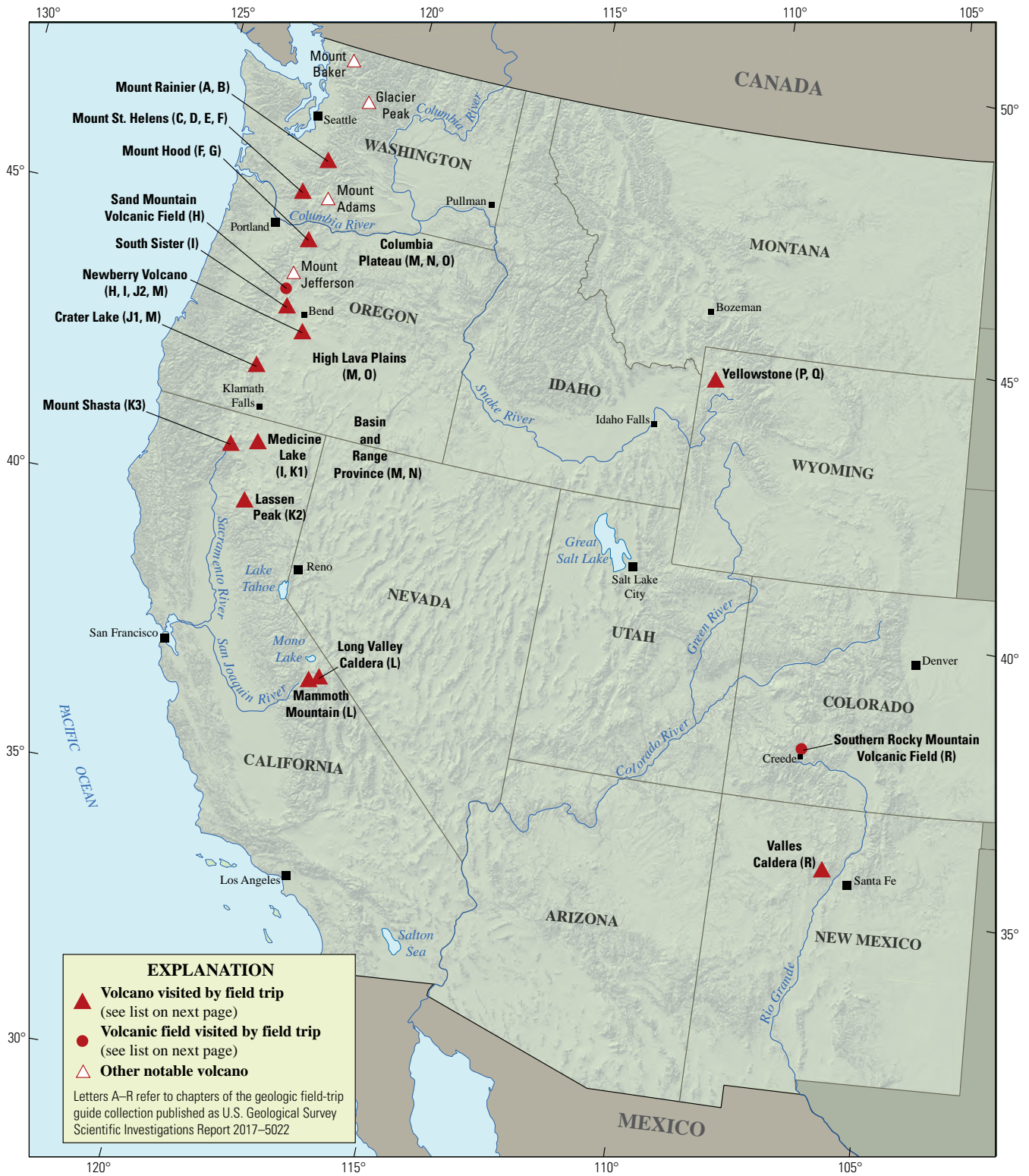
The North American Cordillera is home to a greater diversity of volcanic provinces than any comparably sized region in the world. The interplay between changing plate-margin interactions, tectonic complexity, intra-crustal magma differentiation, and mantle melting have resulted in a wealth of volcanic landscapes. Field trips in this series visit many of these landscapes, including (1) active subduction-related arc volcanoes in the Cascade Range; (2) flood basalts of the Columbia Plateau; (3) bimodal volcanism of the Snake River Plain-Yellowstone volcanic system; (4) some of the world's largest known ignimbrites from southern Utah, central Colorado, and northern Nevada; (5) extension-related volcanism in the Rio Grande Rift and Basin and Range Province; and (6) the spectacular eastern Sierra Nevada featuring Long Valley Caldera and the iconic Bishop Tuff. Some of the field trips focus on volcanic eruptive and emplacement processes, calling attention to the fact that the western United States provides opportunities to examine a wide range of volcanological phenomena at many scales.

The 2017 Scientific Assembly of the International Association of Volcanology and Chemistry of the Earth's Interior (IAVCEI) in Portland, Oregon, marks the first time that the U.S. volcanological community has hosted this quadrennial meeting since 1989, when it was held in Santa Fe, New Mexico. The 1989 field-trip guides are still widely used by students and professionals alike. This new set of field guides is similarly a legacy collection that summarizes decades of advances in our understanding of magmatic and tectonic processes of volcanic western North America.

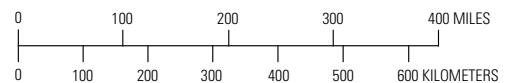
The field of volcanology has flourished since the 1989 IAVCEI meeting, and it has profited from detailed field investigations coupled with emerging new analytical methods. Mapping has been enhanced by plentiful major- and trace-element whole-rock and mineral data, technical advances in radiometric dating and collection of isotopic data, GPS (Global Positioning System) advances, and the availability of lidar (light detection and ranging) imagery. Spectacularly effective microbeam instruments, geodetic and geophysical data collection and processing, paleomagnetic determinations, and modeling capabilities have combined with mapping to provide new information and insights over the past 30 years. The collective works of the international community have made it possible to prepare wholly new guides to areas across the western United States. These comprehensive field guides are available, in large part, because of enormous contributions from many experienced geologists who have devoted entire careers to their field areas. Early career scientists are carrying forward and refining their foundational work with impressive results.

Our hope is that future generations of scientists as well as the general public will use these field guides as introductions to these fascinating areas and will be enticed toward further exploration and field-based research.

Michael Dungan, University of Oregon  
Judy Fierstein, U.S. Geological Survey  
Cynthia Gardner, U.S. Geological Survey  
Dennis Geist, National Science Foundation  
Anita Grunder, Oregon State University  
John Wolff, Washington State University  
Field-trip committee, IAVCEI 2017



Map of the western United States showing volcanoes and volcanic fields visited by geologic field trips scheduled in conjunction with the 2017 meeting of the International Association of Volcanology and Chemistry of the Earth's Interior (IAVCEI) in Portland, Oregon, and available as chapters in U.S. Geological Survey Scientific Investigations Report 2017–5022. Shaded-relief base from U.S. Geological Survey National Elevation Dataset 30-meter digital elevation model data.



<b>Chapter letter</b>	<b>Title</b>
A	Field-Trip Guide to Volcanism and Its Interaction with Snow and Ice at Mount Rainier, Washington
B	Field-Trip Guide to Subaqueous Volcaniclastic Facies in the Ancestral Cascades Arc in Southern Washington State—The Ohanapecosh Formation and Wildcat Creek Beds
C	Field-Trip Guide for Exploring Pyroclastic Density Current Deposits from the May 18, 1980, Eruption of Mount St. Helens, Washington
D	Field-Trip Guide to Mount St. Helens, Washington—An overview of the Eruptive History and Petrology, Tephra Deposits, 1980 Pyroclastic Density Current Deposits, and the Crater
E	Field-Trip Guide to Mount St. Helens, Washington—Recent and Ancient Volcaniclastic Processes and Deposits
F	Geologic Field-Trip Guide of Volcaniclastic Sediments from Snow- and Ice-Capped Volcanoes—Mount St. Helens, Washington, and Mount Hood, Oregon
G	Field-Trip Guide to Mount Hood, Oregon, Highlighting Eruptive History and Hazards
H	Field-Trip Guide to Mafic Volcanism of the Cascade Range in Central Oregon—A Volcanic, Tectonic, Hydrologic, and Geomorphic Journey
I	Field-Trip Guide to Holocene Silicic Lava Flows and Domes at Newberry Volcano, Oregon, South Sister Volcano, Oregon, and Medicine Lake Volcano, California
J	Overview for Geologic Field-Trip Guides to Mount Mazama, Crater Lake Caldera, and Newberry Volcano, Oregon
J1	Geologic Field-Trip Guide to Mount Mazama and Crater Lake Caldera, Oregon
J2	Field-Trip Guide to the Geologic Highlights of Newberry Volcano, Oregon
K	Overview for Geologic Field-Trip Guides to Volcanoes of the Cascades Arc in Northern California
K1	Geologic Field-Trip Guide to Medicine Lake Volcano, Northern California, Including Lava Beds National Monument
K2	Geologic Field-Trip Guide to the Lassen Segment of the Cascades Arc, Northern California
K3	Geologic Field-Trip Guide to Mount Shasta Volcano, Northern California
L	Geologic Field-Trip Guide to Long Valley Caldera, California
M	Field-Trip Guide to a Volcanic Transect of the Pacific Northwest
N	Field-Trip Guide to the Vents, Dikes, Stratigraphy, and Structure of the Columbia River Basalt Group, Eastern Oregon and Southeastern Washington
O	Field-Trip Guide to Flood Basalts, Associated Rhyolites, and Diverse Post-Plume Volcanism in Eastern Oregon
P	Geologic Field-Trip Guide to the Volcanic and Hydrothermal Landscape of Yellowstone Plateau, Montana and Wyoming
Q	Field-Trip Guide to the Petrology of Quaternary Volcanism on the Yellowstone Plateau, Idaho and Wyoming
R	Field-Trip Guide to Continental Arc to Rift Volcanism of the Southern Rocky Mountains—Southern Rocky Mountain, Taos Plateau, and Jemez Volcanic Fields of Southern Colorado and Northern New Mexico

## Contributing Authors

### **Boise State University**

Brittany D. Brand  
Nicholas Pollock

### **Colgate University**

Karen Harpp  
Alison Koleszar

### **Durham University**

Richard J. Brown

### **Eastern Oregon University**

Mark L. Ferns

### **ETH Zurich**

Olivier Bachmann

### **Georgia Institute of Technology**

Josef Dufek

### **GNS Science, New Zealand**

Natalia I. Deligne

### **Hamilton College**

Richard M. Conrey

### **Massachusetts Institute of Technology**

Timothy Grove

### **National Science Foundation**

Dennis Geist (also with  
Colgate University and  
University of Idaho)

### **New Mexico Bureau of Geology and Mineral Resources**

Paul W. Bauer  
William C. McIntosh  
Matthew J. Zimmerer

### **New Mexico State University**

Emily R. Johnson

### **Northeastern University**

Martin E. Ross

### **Oregon Department of Geology and Mineral Industries**

William J. Burns  
Lina Ma  
Ian P. Madin  
Jason D. McClaughry

### **Oregon State University**

Adam J.R. Kent

### **Portland State University**

Jonathan H. Fink (also with  
University of British Columbia)  
Martin J. Streck  
Ashley R. Streig

### **San Diego State University**

Victor E. Camp

### **Smithsonian Institution**

Lee Siebert

### **Universidad Nacional Autónoma de San Luis Potosí**

Damiano Sarocchi

### **University of California, Davis**

Kari M. Cooper

### **University of Liverpool**

Peter B. Kokelaar

### **University of Northern Colorado**

Steven W. Anderson

### **University of Oregon**

Ilya N. Binderman  
Michael A. Dungan  
Daniele McKay (also with  
Oregon State University and  
Oregon State University,  
Cascades)

### **University of Portland**

Kristin Sweeney

### **University of Tasmania**

Martin Jutzeler  
Jocelyn McPhie

### **University of Utah**

Jamie Farrell

### **U.S. Army Corps of Engineers**

Keith I. Kelson

### **U.S. Forest Service**

Gordon E. Grant (also with  
Oregon State University)

### **U.S. Geological Survey**

Charles R. Bacon  
Andrew T. Calvert  
Christine F. Chan  
Robert L. Christiansen  
Michael A. Clyne  
Michael A. Cosca  
Julie M. Donnelly-Nolan

Benjamin J. Drenth

William C. Evans

Judy Fierstein

Cynthia A. Gardner

V.J.S. Grauch

Christopher J. Harpel

Wes Hildreth

Richard P. Hoblitt

Peter W. Lipman

Jacob B. Lowenstern

Jon J. Major

Seth C. Moran

Lisa A. Morgan

Leah E. Morgan

L.J. Patrick Muffler

Jim O'Connor

John S. Pallister

Thomas C. Pierson

Joel E. Robinson

Juliet Ryan-Davis

Kevin M. Scott

William E. Scott

Wayne (Pat) Shanks

David R. Sherrod

Thomas W. Sisson

Mark Evan Stelten

Weston Thelen

Ren A. Thompson

Kenzie J. Turner

James W. Vallance

Alexa R. Van Eaton

Jorge A. Vazquez

Richard B. Waitt

Heather M. Wright

### **U.S. Nuclear Regulatory Commission**

Stephen Self (also with University of  
California, Berkeley)

### **Washington State University**

Joseph R. Boro

Owen K. Neill

Stephen P. Reidel

John A. Wolff

### **Acknowledgments**

Juliet Ryan-Davis and Kate Sullivan created the overview map, and Vivian Nguyen created the cover design for this collection of field-trip guide books. The field trip committee is grateful for their contributions.



## Contents

Introduction.....	1
Context and Terminology .....	1
Defining Flow Types at Volcanoes .....	2
Sediment-Gas Flows .....	2
Sediment-Water Flows .....	2
Criteria for Differentiating Volcaniclastic Deposits .....	4
Pyroclastic Density Current Deposits .....	4
Pyroclastic-Fall Deposits.....	5
Volcanic Debris-Avalanche Deposits.....	5
Lahar Deposits.....	6
Volcano-Fluvial Deposits .....	7
Glacial Deposits Composed of Volcaniclastic Particles .....	8
Volcaniclastic Deposits of Mount St. Helens.....	9
Holocene Eruptive Activity.....	9
Deposits in the Toutle River Drainage Basin.....	11
Flow Processes in 1980 and Associated Deposits.....	11
March 1982 Lahar and Associated Deposits .....	15
Post-1980 Sediment Redistribution.....	15
Toutle River Lahars from Older Eruptive Periods.....	18
Deposits in the Lewis River Drainage Basin .....	18
Volcaniclastic Deposits of Mount Hood.....	19
Holocene Eruptive Activity.....	21
Timberline Eruptive Period .....	21
Old Maid Eruptive Period.....	23
Deposits in the Sandy River Drainage Basin .....	23
Deposits in the White River Drainage Basin .....	26
Polallie-age Flow Deposits.....	26
Old Maid-age Flow Deposits.....	26
Road Log and Description of Field Trip Stops .....	27
Day 1: Debris-Avalanche and Lahar Deposits in the Toutle River Valley, Mount St. Helens..	27
Day 2: Pyroclastic density current, pyroclastic-fall, lahar, and volcano-fluvial deposits in Lewis River drainage, Mount St. Helens .....	49
Day 2: Alternative Route 1 .....	61
Day 2: Alternative Route 2 .....	63
Day 3: Hyaloclastites, glacial tills, and other diamicts in the Hood River and Sandy River basins, Mount Hood.....	67
Day 4: Distal lahar and volcano-fluvial deposits downstream of Mount Hood .....	79
Stratigraphy of Timberline-age Section.....	89
Historical accounts of the Sandy River delta during and following the Old Maid eruptive period.....	89
Acknowledgments.....	89
References Cited.....	91

## Figures

1. Quaternary chronologic and morphologic history of Mount St. Helens .....	10
2. Map showing full extent of volcanoclastic sediment deposition by the May 18, 1980, and later 1980 eruptions of Mount St. Helens .....	12
3. Aerial photograph of Mount St. Helens taken from the International Space Station in 2009.....	13
4. Shaded-relief map showing the impacts of various volcanic and volcanoclastic processes to the Mount St. Helens area in 1980 .....	14
5. Composite lithostratigraphic sections of the May 18, 1980, lateral blast pyroclastic surge deposit.....	15
6. Plot of suspended sediment yields in surrounding rivers since the May 1980 Mount St. Helens eruption .....	16
7. Shaded-relief maps showing topographic changes in the North Fork Toutle River valley after the May 1980 Mount St. Helens eruption.....	17
8. Photograph of an outcrop of pre-1980 volcanoclastic deposits along the Swift Creek riverbank.....	18
9. Two photographic views of Mount Hood .....	19
10. Map showing Mount Hood and the three main river systems that drain the volcano.....	20
11. Simplified surficial geologic map of the Mount Hood debris fan showing recognized deposits of Old Maid and Timberline age.....	22
12. Photographic examples of secondary lahar deposits originating as remobilized dome-collapse pyroclastic density current deposits in the upper Sandy River canyon.....	22
13. Longitudinal profile of the Sandy River channel, starting at Crater Rock—the source volcanic vent—and continuing downstream to the confluence with the Columbia River .....	23
14. Old Maid Flat, the main sediment source of the Sandy River .....	24
15. Schematic stratigraphic relations between Timberline- and Old Maid-age deposits along the Sandy River at Oxbow Regional Park.....	25
16. Photograph of sediment fill in the lower Sandy River valley at Oxbow Regional Park.....	26
17. Photograph of thick, incised sediment fill composed of pyroclastic density current and lahar deposits in the head of White River canyon .....	26
18. Map of locations of planned stops and optional stops for the Mount St. Helens area on Days 1 and 2 of the field trip .....	27
19. Shaded-relief map of proximal volcanoclastic deposits at Mount St. Helens.....	28
20. Historical photographic view of Silver Lake with the snow-capped pre-1980 cone of Mount St. Helens in the distance.....	29
21. Reconstructed lahar-flow cross sections at peak discharge (assuming synchronicity with peak stage) of lahars PC1 and PC3 in the North Fork Toutle River valley at Kid Valley .....	30
22. Pine Creek eruptive period stratigraphy based on 1980–83 exposures in the North Fork Toutle River valley .....	30
23. Photographs of Pine Creek-age deposits.....	31
24. Photograph of vertical tree mold encased by flood plain facies of PC1 and PC3 lahar deposits.....	32
25. Conceptual diagram of origin and transformation of the South Fork Toutle River lahar .....	33
26. Photographs of lahar deposits at Harry Gardner Park.....	33
27. Aerial photographic view of the North Fork Toutle River lahar on the afternoon of May 18, 1980.....	34
28. Stage hydrograph at USGS gaging station 14243000, Cowlitz River at Castle Rock, for May 18–19, 1980.....	34

29. Photographs of North Fork Toutle River lahar deposits.....	35
30. Photograph of the 575-meter-wide sediment retention structure on the North Fork Toutle River .....	36
31. Sketch of features visible from Castle Lake viewpoint.....	36
32. Line drawings and photographs depicting 1980 debris-avalanche kinematics .....	39
33. Summary of 1980 debris avalanche components before and after edifice collapse .....	40
34. Photographs of barren Mount St. Helens 1980 debris-avalanche deposit shortly after emplacement .....	41
35. Sketch of the view towards Mount St. Helens from the Science and Learning Center at Coldwater.....	41
36. Photograph of rusted logging equipment damaged and partly buried by the lateral blast.....	42
37. Photograph of logs of trees blown down by 1980 lateral blast.....	42
38. Views of the 1980 eruption impacts from Johnston Ridge Observatory .....	43
39. Photograph of Spirit Lake looking east from Harry's Ridge .....	44
40. Map of the Coldwater Lake area.....	45
41. Photographs of the 1980 debris-avalanche deposit near Coldwater Lake.....	46
42. Schematic longitudinal cross section through the middle part of the debris-avalanche deposit located within the North Fork Toutle River valley .....	47
43. Cross-sectional profiles of the North Fork Toutle River.....	48
44. Photograph of a low terrace in the North Fork Toutle River valley .....	48
45. Locations of Day 2 planned stops and optional stops on the south and southeast sides of Mount St. Helens.....	49
46. Schematic cross section of Lewis River valley.....	50
47. Failure of the Swift Reservoir power canal dam.....	51
48. Cross-sectional view of deposits of the Swift Creek eruptive stage exposed in the Lewis River valley near the mouth of Swift Creek.....	52
49. Topographic map of the southeast quadrant of Mount St. Helens showing Day 2 stops .....	53
50. Photographic view of the south flank of Mount St. Helens between 8:33 and 8:34 a.m. on May 18, 1980.....	54
51. Map of volcanic slopes and river channels on west, south, and east flanks of Mount St. Helens that were impacted by May 18, 1980, lahars.....	55
52. Pyroclastic-fall, pyroclastic density current, and lahar deposits at Stratigraphy Viewpoint along the Pine Creek-Muddy River debris fan margin .....	56
53. Close-up photographs of two volcanoclastic units at Stratigraphy Viewpoint .....	58
54. Signs of passage left by 1980 lahars other than major deposits .....	59
55. Cross-sectional photographic view of Pine Creek-age lahar deposits and volcano-fluvial layers in quarry at Stop 8.....	59
56. Photograph of a Cougar-age debris-avalanche deposit at Cedar Flats.....	60
57. Lake-level record for Swift Reservoir on May 18, 1980, and reconstructed hydrographs for the Pine Creek and Muddy River lahars as they entered Swift Reservoir .....	61
58. Evidence of lahars in the lower Muddy River.....	62
59. Colorized digital elevation model of the Portland area.....	64
60. Large landslides in Columbia Gorge.....	65
61. Photograph of headscarps of the Bonneville landslide and Red Bluffs landslide in the background, with the truncated toe of the Bonneville landslide deposit in the left foreground.....	67
62. Locations of planned stops and optional stops for field trip Days 3 and 4 at Mount Hood.....	68

63.	Deposits of a late Pliocene basaltic hyaloclastite delta, located along Interstate 84, just west of Hood River, Oregon.....	69
64.	Photographs of edifice-collapse deposits from the Hood River lahar at Mount Hood.....	70
65.	Location of planned stops and optional stops on Days 3 and 4 that are proximal to Mount Hood.....	71
66.	Photographs of the Eliot Branch lahar source and deposit.....	72
67.	Eliot Branch channel before and after deposition of the Eliot Branch debris flow, with the Parkdale lava flow largely blocking the channel.....	73
68.	Impacts of Polallie Creek debris flow on December 25, 1980, on the east side of Mount Hood.....	74
69.	Photograph of small glaciers remaining on Mount Hood.....	75
70.	Photographs of glacial till deposits at Bennett Pass.....	75
71.	Photographs of lithic pyroclastic density current and secondary lahar deposits in the upper White River valley.....	77
72.	History of debris-flow damage to the Oregon Route 35 bridge crossing the White River.....	78
73.	Photograph of the Timberline Lodge on the southwest flank of Mount Hood in winter.....	79
74.	Photographs of volcanoclastic deposits of mainly Old Maid age exposed at Old Maid Flat, about 15 kilometers downstream of Mount Hood.....	81
75.	Photographic view of Sandy River from Jonsrud viewpoint outside of Sandy, Oregon.....	82
76.	Shaded-relief map of the lower Sandy River with geology of the Sandy River delta shown.....	83
77.	Simplified cross sections along the low-gradient depositional reach of the Sandy River in Oxbow Regional Park.....	84
78.	Digital elevation model with 2-meter resolution of the Sandy River at Oxbow Regional Park.....	85
79.	Photographs of sediments emplaced during the Old Maid eruptive period at Oxbow Regional Park.....	87
80.	Holocene stratigraphy and chronology at Stop 9, as exposed in a riverbank outcrop along the west bank of the Sandy River delta.....	88
81.	Photographs of lithofacies within the uppermost Timberline-age lahar deposit exposed at the mouth of the Sandy River.....	90

## Tables

1.	Categories of rock fragments comprising volcanic sediments, based on fragment origin.....	3
2.	Time-discrete flow events and mechanical flow types involving two-phase flows of solid and fluid mixtures at volcanoes.....	3
3.	Major eruptive, noneruptive geomorphic, and glacial events recorded at Mount Hood during the past 100,000 years.....	21

## Conversion Factors

[International System of Units to U.S. customary units]

<b>Multiply</b>	<b>By</b>	<b>To obtain</b>
<b>Length</b>		
centimeter (cm)	0.3937	inch (in.)
millimeter (mm)	0.03937	inch (in.)
meter (m)	3.281	foot (ft)
meter (m)	1.094	yard (yd)
kilometer (km)	0.6214	mile (mi)
inch (in.)	2.54	centimeter (cm)
inch (in.)	25.4	millimeter (mm)
foot (ft)	0.3048	meter (m)
mile (mi)	1.609	kilometer (km)
<b>Area</b>		
square kilometer (km <sup>2</sup> )	0.3861	square mile (mi <sup>2</sup> )
<b>Volume</b>		
cubic meter (m <sup>3</sup> )	264.2	gallon (gal)
cubic meter (m <sup>3</sup> )	35.31	cubic foot (ft <sup>3</sup> )
cubic meter (m <sup>3</sup> )	1.308	cubic yard (yd <sup>3</sup> )
cubic kilometer (km <sup>3</sup> )	0.2399	cubic mile (mi <sup>3</sup> )
<b>Flow rate</b>		
meter per second (m/s)	3.281	foot per second (ft/s)
meter per second (m/s)	2.237	miles per hour (mi/h)
meter per year (m/yr)	3.281	foot per year ft/yr)
centimeter per year (cm/yr)	0.3937	inch per year (in/yr)
cubic meter per second (m <sup>3</sup> /s)	35.31	cubic foot per second (ft <sup>3</sup> /s)
<b>Mass</b>		
metric ton (t)	1.102	ton, short [2,000 lb]
metric ton (t)	0.9842	ton, long [2,240 lb]
ton, short [2,000 lb]	0.9072	metric ton (t)

Temperature in degrees Celsius (°C) may be converted to degrees Fahrenheit (°F) as  $^{\circ}\text{F} = (1.8 \times ^{\circ}\text{C}) + 32$ .

Temperature in degrees Fahrenheit (°F) may be converted to degrees Celsius (°C) as  $^{\circ}\text{C} = (^{\circ}\text{F} - 32) / 1.8$ .



# Geologic Field-Trip Guide of Volcaniclastic Sediments from Snow- and Ice-Capped Volcanoes—Mount St. Helens, Washington, and Mount Hood, Oregon

By Thomas C. Pierson<sup>1</sup>, Lee Siebert<sup>2</sup>, Christopher J. Harpel<sup>1</sup>, and Kevin M. Scott<sup>1</sup>

## Introduction

This field guide for the International Association of Volcanology and Chemistry of the Earth's Interior (IAVCEI) Scientific Assembly 2017 focuses on volcaniclastic sediments from Mount St. Helens in Washington and Mount Hood in Oregon. The trip spends four days in the field and includes nine stops at each volcano. For completeness, this guidebook also includes sixteen optional stops in the Mount St. Helens area and three in the Mount Hood area. These two volcanoes provide excellent depositional records of the broad spectrum of volcanic hazards that involve the flow or fall of volcaniclastic particles. At the field-trip stops we will contrast and compare the different types of deposits—sediments that can be frustratingly difficult to distinguish from one another. Correct identification of deposit origin leads to a better understanding of hazards that can impact vulnerable communities at particular volcanoes.

During this four-day field trip, we will spend two days in the Mount St. Helens area and two days near Mount Hood. On the first day, we will visit debris-avalanche and lahar deposits in the Toutle River valley in Washington. The second day will focus on pyroclastic density current, pyroclastic-fall, lahar, and volcano-fluvial deposits in the Lewis River drainage system near Mount St. Helens. On the third day, we will visit hyaloclastites, glacial tills, and other diamicts in the Hood River and Sandy River basins near Mount Hood. The fourth and final day will focus on distal lahar and volcano-fluvial deposits downstream of Mount Hood.

What follows is an in-depth introduction to the deposits studied on this field trip. We provide criteria that are observable in the field to aid in differentiating between pyroclastic density current, pyroclastic-fall, debris-avalanche, lahar, water-flood, and glacial deposits. We also introduce the Holocene eruptive histories of Mount St. Helens and Mount Hood and discuss the processes responsible for deposit emplacement. Field-trip stops

and features of interest along the route are described in detail in a road log that provides daily cumulative mileage.

## Context and Terminology

Volcaniclastic sediments<sup>3</sup> encompass fragmental geologic deposits composed of volcanic rock particles transported and deposited by pyroclastic processes, geomorphic processes, or a combination of the two. Thus, they record the history of both pyroclastic processes that are typically hot and dry and volcano-hydrologic processes that are typically cool and involve mixtures of fragmental rock debris and water. The bulk of volcaniclastic sediments are produced by explosive eruptions that generate large volumes of tephra and other fragmental rock debris. Explosive eruptions are most common at volcanoes of intermediate and silicic composition in volcanic arcs. All processes emplacing volcaniclastic sediments can be hazardous, but some can be more hazardous than others.

Terminology for volcaniclastic particles and deposits is not entirely consistent. Here, we adhere to the definitions used by White and Houghton (2006). Primary volcaniclastic particles and deposits are those emplaced by or during the eruption of rock that is fragmented during the eruption process itself or during gravitational collapse of still-hot lava domes or flows. Specific depositional processes include pyroclastic density currents (PDCs)—including block-and-ash flows—tephra fall, and primary lahars. Secondary volcaniclastic particles and deposits result from the remobilization and redeposition of primary deposits by gravity-driven mass flows or through mobilization and transport by flowing water, ice, or air. Major depositional processes in this case include debris avalanches, lahars, water floods, and glaciers.

The geologic, sedimentologic, and stratigraphic characteristics of primary volcaniclastic deposits have been classified and well documented over the years, but the characteristics of secondary volcaniclastic deposits have received much less attention (for example, Fisher, 1961, 1966; Walker, 1971; Wright and others, 1980, 1981; Fisher and Schmincke, 1984; Cas and Wright, 1987; McPhie and others, 1993; Branney and Kokelaar, 2002; White and Houghton, 2006). Most of this attention came after a string of late 20th century eruptions demonstrated the danger and long reach of processes emplacing these sediments (Manville and others, 2009):

<sup>1</sup>U.S. Geological Survey.

<sup>2</sup>Smithsonian Institution.

<sup>3</sup>The term sediment, in the singular, is usually applied to particulate material held in suspension in water or deposited from suspension. The term in the plural is generally applied to all types of fragmental deposits, not just those carried by a flowing fluid (Neuendorf and others, 2005).

## 2 Geologic Field-Trip Guide of Volcaniclastic Sediments from Snow- and Ice-Capped Volcanoes

the May 18, 1980, eruption of Mount St. Helens (United States), the November 13, 1985, eruption of Nevado del Ruiz (Colombia), and the June 15, 1991, eruption of Mount Pinatubo (Philippines). Most detailed descriptions of secondary volcaniclastic deposits are process-specific or location-specific. Reviews and overviews that have generalized the characteristics of secondary volcaniclastic deposits more broadly have been limited in scope and detail, and they do not make direct detailed comparisons with primary volcaniclastics (for example, Smith, 1986; Cas and Wright, 1987; McPhie and others, 1993; Manville and others, 2009).

Fragmental volcanic deposits are notoriously difficult to identify and interpret in the field for a variety of reasons (Orton, 1996):

- A wide variety of both eruptive and noneruptive depositional processes can produce fragmental deposits with similar characteristics.
- Depositional processes commonly evolve over short periods and distances, causing deposits with different characteristics to overlap spatially and grade into each other.
- Textural and compositional variations can have multiple causes.
- Mineral grains and glass fragments are susceptible to chemical alteration in harsh volcanic environments, which can change deposit appearance.
- Localized flow paths and variations in sediment supply and transport can result in spatially irregular deposits.
- Deposits are highly erodible and can have ephemeral residence times in the geologic record.
- Deposits are vulnerable to disruption and burial by subsequent volcanic or volcano-tectonic activities and processes.

As most field volcanologists already recognize, fragmental deposits emplaced subaerially by primary volcanic processes (PDCs and tephra fall), those emplaced by secondary volcano-hydrologic processes (debris avalanches, lahars, and muddy floods), and even those emplaced by alpine glaciers on the flanks of volcanoes, can all look similar in outcrop. This field trip is organized to provide opportunities to visit a wide range of deposit types, so that the critical and often subtle physical differences among these deposits can be examined and discussed. Except for the hyaloclastites to be seen on Day 3, the sediments visited during this field trip were deposited in subaerial settings. Deposition in marine or lacustrine environments is complicated by size- and density-controlled settling behavior of particles through a water column, which affects grain-size distributions and stratification differently than on land.

Classification of deposits composed of volcanic rock fragments has been based on clast-forming processes (Fisher, 1961, 1966; Fisher and Schmincke, 1984), on transport and depositional processes (Cas and Wright, 1987), and on a combination of both (McPhie and others, 1993; White and Houghton, 2006) (table 1). Regardless of the classification scheme, volcanologists agree that rock fragments that originate at volcanoes as solidified particles of erupting lava and then move to their place of deposition by nonvolcanic geomorphic processes constitute a separate and important category of volcanic deposits—termed secondary volcaniclastic deposits (Orton, 1996; Manville and others, 2009).

### Defining Flow Types at Volcanoes

Primary and secondary volcaniclastic deposits are commonly emplaced by flow processes involving a solid phase (volcaniclastic particles) and a fluid phase (water or gas). The spectrum of two-phase gravity flows occurring subaerially at volcanoes are generally grouped into four basic categories of time-discrete flow events—pyroclastic density currents, debris avalanches, lahars, and floods. In terms of flow mechanics, we can describe four basic flow types, but flow types do not always have a one-to-one correlation with flow events (table 2). These flow types comprise two varieties of sediment-gas flow and two varieties of sediment-water flow:

#### Sediment-Gas Flows

- Dry to damp granular flow. The dominant fluid phase is gas; particle-particle interactions primarily control flow behavior.
- Dry to damp fluid flow. The dominant fluid phase is gas; fluid properties primarily control flow behavior.

#### Sediment-Water Flows

- Water-saturated granular flow. The dominant fluid phase is water; particle-particle interactions primarily control flow behavior.
- Water-saturated fluid flow. The dominant fluid phase is water; fluid properties primarily control flow behavior. Dilute lahars (hyperconcentrated flows) behave as non-Newtonian fluids, but water floods behave as Newtonian fluids.

Boundaries between flow types are not sharp, either in terms of flow behavior or the characteristics of the deposits they emplace. Each flow type has the potential of transforming from one to another as the proportions of fluids to solids or



**Table 1.** Categories of rock fragments comprising volcanic sediments, based on fragment origin. The two basic types of volcanic sediments—sediments composed of particles of volcanic rock—are volcanoclastic and epiclastic sediments. Blank spaces indicate origins that were not addressed by the referenced authors.

Origin of volcanic rock fragments	White and Houghton (2006)	McPhie and others (1993)	Cas and Wright (1987)	Fisher and Schmincke (1984)
Fragments of volcanic rock formed and dispersed by any process	Volcanic	Volcanoclastic	Volcanoclastic	Volcanoclastic
Rock fragments ejected from a volcanic vent, regardless of eruption cause, fragment origin, or fragment composition	Primary volcanoclastic	Pyroclastic	Pyroclastic	Pyroclastic
Particles formed by fragmentation and ejection of magma in an eruption		Pyroclastic (juvenile)		Pyroclastic
Particles formed by steam-driven explosion		Pyroclastic		Hydroclastic
Particles formed by quench-shattering of lava in contact with water, water-saturated sediment, or ice		Autoclastic (hyaloclastic)	Autoclastic	Hydroclastic
Fragments of lava formed by mechanical fragmentation of flowing (and solidifying) lava flows or domes		Pyroclastic (autoclastic)	Pyroclastic	Autoclastic
Fragments of previously formed rock (volcanic or nonvolcanic) incorporated into a pyroclastic deposit	Lithic	Lithic	Lithic	Lithic
Lithic fragments of nonvolcanic rock or volcanic rock not related to the erupting volcano	Accidental lithic	Accidental lithic	Accidental lithic	Accidental lithic
Lithic fragments of volcanic rock originating not from the erupting volcano but from a previous eruption	Accessory lithic	Accessory lithic	Accessory lithic	Accessory lithic
Lithic fragments of nonvesiculated juvenile magma in contrast to pumice from the same eruption	Cognate lithic	Cognate lithic	Cognate lithic	Cognate lithic
Primary volcanoclastic rock fragments remobilized from an unconsolidated deposit at its initial site of deposition and transported to another site (one or more times) by nonvolcanic geomorphic processes	Secondary volcanoclastic	Resedimented volcanoclastic	Epiclastic	Secondary pyroclastic (reworked pyroclastic)
Particles formed by physical breakdown of lithified volcanic or nonvolcanic rock, whether fresh or weathered	Epiclastic	Volcanogenic sedimentary (epiclastic)	Epiclastic	Epiclastic

**Table 2.** Time-discrete flow events and mechanical flow types involving two-phase flows of solid and fluid mixtures at volcanoes.

Flow event	Flow type <sup>1</sup>	Dominant fluid phase	Factors that determine flow behavior <sup>2</sup>
Debris avalanche	Dry to damp granular flow	Gas	Particle interactions >> fluid properties
Concentrated pyroclastic density current (pyroclastic flow)	Dry to damp granular flow	Gas	Particle interactions > fluid properties
Dilute pyroclastic density current (pyroclastic surge)	Dry to damp fluid flow	Gas	Fluid properties > particle interactions
Concentrated lahar (debris flow)	Water-saturated granular flow	Water	Particle interactions ≈ fluid properties
Dilute lahar (hyperconcentrated flow)	Water-saturated fluid flow	Water	Fluid properties > particle interactions
Water flood	Water-saturated fluid flow	Water	Fluid properties >> particle interactions

<sup>1</sup>Small amounts of gas (typically air) are commonly found in water-saturated sediment mixtures (as much as ~5 percent by volume) and similarly small amounts of liquid water may be found in dry flows.

<sup>2</sup>Relative importance indicated by mathematical symbols: >>, much greater than; >, greater than; ≈, approximately equal.

particle-size distributions change (through sediment entrainment or selective deposition) and as flow kinetic energy (manifest as granular temperature or turbulence) increases or decreases (Iverson and Vallance, 2001; Iverson, 2005; Pierson, 2005). Different flow types emplace subtly different sedimentary deposits that, in most cases, have characteristically identifiable sedimentologic, stratigraphic, and morphologic properties. Flows having sediment concentrations near the transformation boundaries between flow types, however, emplace deposits that can be particularly hard to identify.

Flow events involving two-phase flow in volcanic settings typically do not travel their entire flow paths as a single flow type; instead they commonly transform from one flow type to another (Scott, 1988a; Smith and Lowe, 1991; Vallance and Scott, 1997). For example, a crater-lake outburst flood can begin as a water flood, entrain sediment and transform over a short distance to become a debris-flow lahar, then transition more gradually to a hyperconcentrated-flow lahar through selective deposition of coarse sediment and dilution by water input from tributary streams, and finally change back to a water flood through continued dilution (Waitt and others, 1983; Pierson and Scott, 1985; Pierson, 1999). As in this example, flow transformations can go in either direction, with the flow mixture becoming more concentrated or more dilute with time and distance traveled. Despite alternative definitions of the term flow transformation (for example, Fisher, 1983), transformations involving change from one flow type to another are not necessarily related to changes in hydraulic flow states or regimes, such as laminar/turbulent, subcritical/supercritical, steady/unsteady, or uniform/nonuniform flow transitions, but hydraulic changes may accompany changes in flow type nevertheless. Flow transformations have been observed or inferred in all types of volcanic granular and fluid flows.

## Criteria for Differentiating Volcaniclastic Deposits

### Pyroclastic Density Current Deposits

Pyroclastic density currents (PDCs) are density-stratified flows containing variably dispersed mixtures of juvenile rock fragments (usually hot) of varying particle size and density, plus some fraction of entrained accidental particles, magmatic gases, and entrained air (Fisher and Schmincke, 1984; Cas and Wright, 1987; Carey, 1991; Freundt and others, 2000; Valentine and Fisher, 2000; Wilson and Houghton, 2000; Branney and Kokelaar, 2002; Sarocchi and others, 2011; Sulpizio and others, 2014; Dufek and others, 2015). Most commonly driven by gravity, PDCs can also be driven by impulsive forces from phreatic or magmatic explosions (for example, base surges or directed blasts). Flow is typically highly turbulent when particle-gas mixtures are dilute and more laminar when highly concentrated. Such flows vary both temporally and spatially in bulk density, composition, temperature, transport mechanics, and velocity as they move. Emplacement

temperatures for relatively small, dry PDCs have been measured as high as about 850 °C, but temperatures can reach 1,000 °C for large silicic ignimbrites (Hoblitt and Kellogg, 1979; Banks and Hoblitt, 1981; Voight and Davis, 2000; Charbonnier and Gertisser, 2008; Bryan and others, 2010; Brown and Andrews, 2015). On the other hand, emplacement temperatures can be less than 100 °C for wet PDCs triggered by phreatic eruptions, phreatomagmatic eruptions, or eruptions through water bodies (Moore, 1967; Fisher and Waters, 1970; Lorenz, 1974).

PDC deposits exhibit a wide range of lithofacies that include poorly sorted diamicts, as well as stratified and unstratified gravels, gravelly sands, sandy gravels, and sands. This variability reflects the variety of eruption styles, rates, components, and depositional conditions that produce them (Sparks and others, 1973; Lorenz, 1974; Wilson and Walker, 1982; Fisher and Schmincke, 1984; Cas and Wright, 1987; Branney and Kokelaar, 2002). PDC deposits can closely resemble lahar deposits in outcrop. Characteristic features to aid in the identification of relatively fresh (unaltered) PDC deposits include:

- Sediment mixture compositions wholly or mostly monomictic (composed of particles of a single rock species—that is, from a single magma batch).
- Lithofacies of concentrated PDCs typically massive, commonly coarse grained, and commonly graded (inverse, normal, or both).
- Lithofacies of dilute PDCs commonly stratified, with either sharp or diffuse bedding contacts, but can be massive; crosscutting contacts common within depositional units.
- Low-angle crossbedding common in finer grained deposits.
- Moderate to very poor sorting (We report sorting values ( $\sigma$ ) as the Inclusive Graphic Standard Deviation of the particle size ( $\phi$ ), as defined by Folk, 1974).
- Consistency generally friable (dry)/soft (moist) owing to paucity of fine particles, unless cemented by vapor-phase alteration or welding.
- Evidence of high emplacement temperature common (but not required), including fragments of charred vegetation, bread-crusted or prismatically jointed clasts, pinkish deposit surface coloration, welded zones, and uniform thermoremanent magnetic orientation of clasts.
- Bubble vesicles typically absent, except in deposits from phreatic or phreatomagmatic eruptions, due to elutriation of fines; however, matrix may contain small voids between particles (a miniature open-work structure).
- Sub-2-millimeter (mm) size fraction (ash) dominated by crystals in concentrated PDC deposits and by vitric shards in dilute PDC deposits.

- Subvertical gas-escape pipes common (elutriated conduits, often with surrounding cylindrical zones hardened by vapor-phase mineral sublimation and oxidation).

## Pyroclastic-Fall Deposits

Subaerial pyroclastic-fall deposits are emplaced by the lofting of volcanic rock particles into the air by eruptive processes and their subsequent gravity-driven fallout through the air back to earth. Lofting is accomplished by (1) explosive ballistic ejection or pressurized jetting of solid rock fragments or molten lava spatter from volcanic vents and (2) suspension of relatively fine-grained particles in turbulent air currents by heat-driven convection and wind, either directly from source vents or from elutriation of ash from PDCs that are undergoing clast fragmentation during downslope movement (Walker, 1981; Fisher and Schmincke, 1984; Cas and Wright, 1987; Wilson and Houghton, 2000; Houghton and others, 2000; Branney and Kokelaar, 2002).

Pyroclastic-fall deposits are typically better sorted than most volcaniclastic sediments and bedded lithofacies may superficially resemble volcano-fluvial deposits—the main difference being that the latter are found only as horizontal fills in channels and on valley floors, whereas air-fall tephra mantle the entire landscape with slope-parallel deposits. Sedimentologic variations reflect differences in eruption magnitudes, styles, rates, and components, as well as distance from the source vent, wind velocities, and wind directions (Walker, 1981; Fisher and Schmincke, 1984; Cas and Wright, 1987; Wilson and Houghton, 2000; Houghton and others, 2000; Houghton and Carey, 2015). Characteristic features of fresh pyroclastic-fall deposits include:

- In time-equivalent stratigraphic units, particle mixtures usually are wholly or mostly monomictic (for example, an aphyric rhyolite pumice with 75 weight percent  $\text{SiO}_2$ , or a hornblende- and plagioclase-phyric low-silica dacite).
- In tephra sequences from prolonged eruptions or eruptions involving magma mixing, composition may be oligomictic (composed of a single rock type; for example, a rhyolite with compositional variation) or polymictic (composed of different rock types; for example, rhyolite and basalt).
- Depositional units can be stratified or massive, but stratification is common.
- Both lithic and juvenile particles are typically angular.
- Commonly moderately to well sorted.
- Bedding is plane-parallel with beds and laminae reflecting orientation of underlying topography; little to no deposition on slopes steeper than angle of repose unless wet (cohesive) or anchored by vegetation.
- Beds laterally continuous over long distances with relatively uniform thickness.
- Beds commonly graded (normal or inverse).
- Bedding contacts may be sharp but are commonly diffuse.
- Deposits well sorted with respect to aerodynamic size equivalence of particles (for example, fine dense ash particles may fall together with scoriaceous lapilli).
- Accretionary lapilli, cored lapilli, or ash pellets common, but not always well preserved.
- Intergranular voids common (size in proportion to particle size).
- Bubble vesicles commonly found only in fine ash from phreatic or phreatomagmatic eruptions; rarely found in ash layers subjected to heavy rainfall.
- Friable (dry)/soft (moist) consistency; loose packing.
- Leaves and fine twigs distributed throughout accumulations of coarse tephra in forested terrain (not in discrete layers); commonly such vegetal debris is progressively stripped from overhanging trees by abrasion from tephra fall.

## Volcanic Debris-Avalanche Deposits

Volcanic debris avalanches are rapid, unsaturated, gravitational flows of non-coherent, unsorted granular mixtures of rock fragments (parts of failed edifice with or without juvenile lava) and ice, soil, wood fragments, and other debris entrained during transport, with varying amounts of air, volcanic gases, or liquid water in the dilated interstices between particles (Ui, 1983, 1989; Voight and others, 1983; Schuster and Crandell, 1984; Siebert, 1984, 1996; Ui and others, 2000; van Wyk de Vries and Davies, 2015). Volumetric water contents in these flows may vary from 0 to about 30 percent. Flow mechanics are principally controlled by inertial and frictional forces between moving particles and between the particles and the bed (Savage, 1984; Iverson and Vallance, 2001), but movement also involves rigid-body frictional sliding at the outset before disaggregation and deformation of the failed mass occurs.

Major lithofacies of volcanic debris-avalanche deposits include (1) mixed facies—disaggregated and well-mixed solid rock fragments ranging from clay-size grains to blocks larger than 10 meters (m) (that is, a mixture of clasts and matrix, where matrix is defined as particles less than 2 mm in diameter) and (2) block facies—deposits dominated by very large, highly fractured, unconsolidated to semi-consolidated pieces of the failed edifice that have been transported mostly intact to their point of deposition (Glicken, 1996). Characteristic identifying features include:

- Hummocky surface topography composed of irregularly shaped and distributed hills (hummocks) that are commonly tens to hundreds of meters in diameter and that have intervening closed depressions.

## 6 Geologic Field-Trip Guide of Volcaniclastic Sediments from Snow- and Ice-Capped Volcanoes

- Polymictic sediment composition (that is, composed of particles of multiple types of volcanic rock with or without accidental nonvolcanic rock fragments).
- Abundant large debris blocks composed of pervasively fractured, unconsolidated to semi-consolidated segments of the failed source volcanic edifice that commonly retain their original primary stratification.
- Unusually thick depositional units (commonly greater than 100 m) that are devoid of primary stratification.
- Steep, sharply defined lateral and frontal margins.
- Abrupt color changes from the uniform neutral grays and browns of the mixed-material facies to more intense colors (typically black, white, tan, red, orange, or yellow) of relatively fresh or hydrothermally altered, intact rock units from the failed edifice.
- Jigsaw fracturing of blocks, even down to the size of sand grains.
- Angular shape of clasts and particles smaller than 2 mm in matrix; clasts commonly fractured extensively.
- Clastic dikes relatively common, with irregular margins and variable orientation.
- Plastic deformation of small blocks common—including elongation, folding, smearing, and contorting.
- Absence of true stratification, although intra-deposit shearing can produce subhorizontal shear zones that resemble bedding.
- Large clasts/blocks commonly clustered within outcrops (that is, large particles tend not to be randomly or uniformly distributed in outcrops).
- Mixed facies (small clasts and matrix) very or extremely poorly sorted.
- Absence of bubble vesicles and grading.
- Absence of strongly developed fabrics.
- Absence of fluid-escape structures (in most cases).

### Lahar Deposits

Lahars are discrete, rapid, gravity-driven flows involving fully saturated, high-concentration mixtures of water and solid particles (fragments of rock, ice, wood, and other debris) originating from volcanoes (Smith and Fritz, 1989; Smith and Lowe, 1991; Vallance, 2000; Vallance and Iverson, 2015). Lahar flow types include both debris flow and hyperconcentrated flow—two distinct flow types that commonly occur within a single lahar and both of which behave as non-Newtonian fluids (Crandell, 1971; Smith and Lowe, 1991; Pierson, 2005). Thus, a lahar is not

a flow type but rather a high-discharge flow event that commonly includes both debris flow and hyperconcentrated flow. When lahars occur in channels occupied by streams, their faster high-concentration flow fronts commonly push stream water ahead and mix with it. This creates wedges of muddy water, similar to bow waves, that become part of the lahars but precede the high-concentration parts. In some cases, these dilute “bow waves” produce the highest stages and peak discharges of lahars (Pierson and Scott, 1985; Cronin and others, 1999; Dinehart, 1999).

Deposits emplaced by the debris-flow phases of lahars are massive (unstratified) diamicts that can commonly be described as very/extremely poorly sorted muddy sandy gravels or muddy gravelly sands. In terrains affected by recent eruptions, fine-particle (silt and clay) content is commonly less than 10 weight percent, but the proportion can be as high as 25 weight percent if lahars originate from edifice failures (for example, Vallance and Scott, 1997). In levees or deposit margins where clasts are concentrated and matrix material has been partly or entirely removed, deposits typically have an openwork structure with virtually no fines or even sand. Single debris-flow depositional units are commonly graded but never stratified—this is a key distinguishing characteristic. Single flow units are seldom thicker than 1–2 m, unless ponded behind barriers or flow constrictions. However, sequences of multiple flow units can be many meters thick. If flow units are deposited in quick succession, such as by successive flow surges during a single lahar, sharp contacts may not form between flow units (Major, 1997). Characteristic identifying features of deposits emplaced by debris flows include:

- Massive internal structure; no stratification (bedding).
- Very poor to extremely poor sorting (generally greater than  $2.0\phi$ ).
- Both clast-supported and matrix-supported structures possible.
- Polymictic sediment compositions in most cases, although lahars can start as monomictic mixtures (for example, particles from a dome collapse) and become progressively oligomictic or polymictic with distance traveled as bed material from stream valleys is entrained.
- Matrix (particles less than 2 mm) and clasts packed tightly together in deposit interiors—no openwork structure except in flow levees and deposit margins, where fluid matrix has flowed or been washed away.
- Bubble vesicles (~1 mm) common throughout deposits.
- Debris-flow deposit outcrops relatively uniform and homogeneous in appearance; no abrupt changes in color, texture, or spatial distribution of clasts and matrix within single flow units.
- Both inverse and normal grading common, sometimes both in a single flow unit with inverse grading at base and normal grading at top; some deposits ungraded.

- Clast fabric commonly weak, although strong fabric may be observed with elongate woody debris on deposit surfaces. Imbrication can develop in boulder bed forms.
  - Clasts generally not fractured.
  - Uncharred wood fragments common (if trees encountered along flow path).
  - No evidence of high heat (in most cases). Hot lahars are less than 100 °C, but remobilization of PDC deposits or sediments containing charcoal from wildfires may entrain charcoal fragments in lahar deposits.
  - Relatively fine-grained basal layers (also called sole layers) and post-depositional dewatering cap layers may be present.
  - Water-escape structures (subvertical elutriated pipes) may be present in deposits of relatively dilute noncohesive flows, but these are uncommon.
  - Cobbles and boulders commonly show gross rounding, although surfaces not smoothed; pebbles typically are angular unless the lahar entrained stream gravel.
  - Flat to slightly convex deposit surfaces, commonly studded randomly with boulders protruding above the surface of deposits.
  - Extensive damage to trees growing near the main axis of flow, but relatively minor damage along flow margins; tree trunks typically coated in a thin layer of sandy mud.
  - Lateral flow levees constructed of undifferentiated debris mixtures, concentrations of boulders (commonly with openwork structure), or battered logs.
  - Hard (dry)/firm (moist) consistency—high degree of consolidation, particularly in cohesive debris-flow lahar deposits; deposits break off in chunks rather than individual particles when dug or struck with tools.
- 2.0 $\phi$ ; most deposits range between 1.1 and 1.6 $\phi$  (Scott, 1988a; Cronin and others, 2000).
- Deposits typically stratified, although channel facies deposits can be massive.
  - Bedding is characteristically horizontal and plane parallel; contacts between beds are typically faint or diffuse.
  - Low-angle crossbedding from migrating upper regime bed forms may be observed. High-angle (ripple- and dune-type) cross-stratification (that is, bedding angles steeper than about 15° from plane of channel bed) has never been reported.
  - Isolated outsized clasts (cobbles and in some cases boulders) in outcrops of otherwise sandy beds are common; outsized clasts also common on surfaces of fresh deposits.
  - Thin, bedding-parallel laminations of clayey silt to silty fine sand (cap layers) commonly mark contacts between depositional units. Flow pulses within a single lahar may emplace separate flow units with cap layers.
  - Cap layers commonly deformed into dish structures—water escape structures, formed by upward migration of pore fluid during deposit consolidation.
  - Layers of bubble vesicles may be concentrated beneath silty cap layers (concentrated during upward migration of pore water).
  - Soft-sediment deformation common (caused by undrained loading).
  - Consistency slightly hard (dry)/slightly firm (moist). Massive deposits not as firm or hard as debris-flow lahar deposits. When dry outcrops are kicked or struck, deposits typically break off to produce some fragile chunks and some raveling of individual grains.

Deposits emplaced by the hyperconcentrated-flow phases of lahars may exhibit lithofacies that can range from (1) massive, relatively fine-grained, clast-supported gravelly sand diamicts to (2) faintly or diffusely horizontally bedded gravelly sands (with bedding commonly interrupted by isolated gravel lenses and outsized clasts) to (3) distinctly bedded alternating layers of sand and fine gravel. The coarser, more massive lithofacies generally occur along channel axes (channel facies) and are distinguished from sandier, more distinctly bedded lithofacies (lateral or overbank facies) along channel margins (Pierson and Scott, 1985; Scott, 1988a; Cronin and others, 2000). Hyperconcentrated-flow deposits tend to become progressively finer grained and more distinctly bedded with distance from source. Characteristic sedimentologic features of hyperconcentrated-flow deposits include:

- Sorting values between those of debris-flow and water-flood deposits, namely in the range of about 0.9 to

## Volcano-Fluvial Deposits

Volcano-fluvial deposits are mainly emplaced by volcanic water floods—turbulent, high-discharge floods of muddy water transporting very high sediment loads from relatively small drainage basins in volcanically disturbed landscapes. However, volcano-fluvial deposits also include sediments emplaced by smaller discharge and much lower concentration streamflows, which commonly rework and change the character of muddy flood deposits. Volcanic water-flood deposits generally have more in common with flash floods in arid terrains than with meteorologic floods in large, well-vegetated drainage basins. Commonly triggered by heavy rainfall, they can also be generated by lake outbreaks and glacier outbursts. Like lahars, volcanic water floods are discreet flow events, but by definition

these flows have sediment concentrations below the threshold of hyperconcentrated flow and behave as Newtonian fluids. Though generally not as destructive as lahars at equivalent discharges, volcanic water floods nevertheless typically transport enormous quantities of sediment and have significant geomorphic impacts on river channels.

Volcanic water-flood deposits are typically stratified and can range from bouldery conglomerates to finely laminated fine sands and silts, depending on channel slope, proximity to sediment sources, and discharges of the floods that emplaced them. Characteristic deposit features include:

- Most deposits well stratified—water-flow deposits nearly everywhere show distinct bedding with sharp boundaries between beds or laminae owing to abrupt changes in grain size during deposition. However, in deposits without much variation in grain size, bedding may be faint or appear massive. Strata commonly millimeters to centimeters in thickness. Bioturbation may obscure original bedding.
- Stratified deposits moderately to moderately well sorted—generally from 0.5 to 0.9 $\phi$  for sandy deposits (Scott, 1988a; Letsinger, 1994). Deposits containing gravel can be more poorly sorted.
- Consistency very friable or loose (dry)/soft to very soft (moist). Sediment grains in dry outcrops ravel easily when disturbed.
- High-angle (greater than 15°) dune or ripple crossbedding common.
- Absence of bubble vesicles.
- Openwork structure common in gravelly facies.
- Imbrication of non-equant clasts common, with the flattest surface dipping upstream.
- Ungraded in most cases (upward fining may be observed locally).
- Polymictic sediment compositions; reworked epiclastic particles commonly mixed with fresh volcaniclastic particles.

Volcanic water-flood deposits are typically aggradational, rather than erosional, because the amount of sediment supplied to a river far exceeds its transport capacity. Fluvial reworking of such flood deposits can be surmised from localized disconformities, formed where reincision of the aggradational channel fill by post-flood lower discharge flow (either the tail of the flood itself or later flows) cuts across flood-deposit strata and redeposits beds that are commonly finer grained and more finely bedded.

## Glacial Deposits Composed of Volcaniclastic Particles

Deposits emplaced by flowing glacial ice are termed tills and include two basic types: lodgment till and ablation till (Neuendorf and others, 2005). Lodgment tills are mixtures of fragmental rock debris that are overridden, deformed, and highly compacted by glaciers. Ablation tills consist of (1) supraglacial rock debris initially emplaced on glacier surfaces by nonglacial processes (mass movement or fluvial transport) and (2) englacial rock debris entrained within glacier ice, both of which are later lowered to the ground surface (without significant compaction) by ice stagnation and melting. These two types of tills can have very different sediment properties and deposit morphology. Alpine glacier deposits and landforms are the types most often encountered on the flanks of volcanoes having sufficiently high altitude or latitude.

Volcaniclastic deposits transported and redeposited by glacial ice typically have only a few differences distinguishing them from other volcaniclastic sediments. Both lodgment tills and ablation tills can closely resemble deposits of debris-flow lahars and debris avalanches. If only sediment textures in outcrop are examined, it may difficult to say whether a diamict has been emplaced by glacial ice; recognition of glacial landforms is also important. Characteristic features of alpine glacial tills include:

- Aggradational landforms, including thin irregular till sheets emplaced on ridges as well as in valleys, lateral and end moraines (may be found in valleys beyond base of volcanic edifice), and kettle holes (or ponds).
- Erosional features, including faceted, striated, bullet-shaped clasts found within the deposit, as well as glacial striations, crescentic chatter marks, and polishing on surfaces of lava flows.
- Extreme compaction possible (but not required); compacted deposits may display fissility (flaky, subhorizontal foliation).
- Generally polymictic sediment mixture compositions (possibly monomictic or oligomictic near source).
- Lack of grading.
- Well-developed fabric in lodgment till; weak or no fabric in ablation till.
- Unusually high clay contents in matrix of tills from large glaciers.
- Crushed, flattened logs and vegetation found only beneath the diamict (not mixed in).
- Very thin deposits relative to areal coverage; deposits may be discontinuous.

## Volcaniclastic Deposits of Mount St. Helens

Mount St. Helens is one of the youngest and most active volcanoes in the Cascades volcanic arc, as well as one of the most explosive (Mullineaux, 1996; Crandall, 1987; Clynne and others, 2005; Clynne and others, 2008) (fig. 1). Over its history it has produced a wide variety and large volume of volcaniclastic sediments. This mountain, known as Loowit by some native peoples, is an intermediate-composition stratovolcano, much of it built within the last 2,500 years (fig. 1B). The modern cone has been largely constructed of (1) a dacitic dome complex as its foundation; (2) andesitic to basaltic lava flows, scoriaceous pyroclastic units, and a few small dacitic lava domes forming its outer flanks; and (3) prior to the 1980 eruption, a central core composed of a large dacitic lava dome that was removed by the 1980 debris avalanche. Today the edifice hosts a 2-kilometer (km)-wide and 600-m-deep, horseshoe-shaped crater (crater rim maximum elevation 2,550 m (8,363 feet, ft) above sea level. The crater is open to the north and partly filled by both a composite dacitic lava dome (extruded 1980–1986 and 2004–2008) and by an advancing glacier—arguably the newest glacier in the world (formed since 1986) and one of the few that is growing.

### Holocene Eruptive Activity

Eruptive activity at Mount St. Helens includes four major eruptive stages dating back to about 300,000 years ago. Details of the eruptive activity and products are summarized below from Mullineaux (1996), Crandell (1987), Clynne and others (2005, 2008), and Michael Clynne (written commun., 2012) (fig. 1A). Three Pleistocene eruptive stages were followed in the Holocene by the Spirit Lake stage, which is subdivided into seven eruptive periods, including the modern period that began in 1980. Ages are reported in calendar years (C.E.) or in thousands of years before present (ka). Refer to figure 1A for alphabetic names of tephra layers and sets.

1. **Ape Canyon stage** volcanism included explosive eruptions and lava dome emplacement west of the current edifice during two distinct periods, about 300–250 ka and 160–35 ka. The explosive eruptions producing diagnostic biotite-bearing tephra set C around 40 ka are among the largest eruptions at Mount St. Helens (Mullineaux, 1996). Extensive aggradational fill deposits containing Ape Canyon stage rocks are preserved in terraces in the lower Lewis River valley.
2. **Cougar stage** (28–18 ka) was probably the most active stage prior to the modern Spirit Lake stage. Activity included construction of dacite domes, large PDCs, tephra emissions, and a very large debris avalanche on the south flank of the volcano, followed by a large explosive eruption that culminated in the largest lava flow (andesite) at Mount St. Helens. Lahar and volcanic fluvial deposits caused aggradation in the middle and lower reaches of the Lewis River.
3. **Swift Creek stage** (16–12.8 ka) eruptive activity involved the growth of unstable lava domes and explosive eruptions producing two major ash layers and numerous PDCs and lahars. During this time, three extensive fans of pyroclastic debris were emplaced on the volcano's flanks. This stage was followed by about 9,000 years of dormancy.
4. **Spirit Lake stage** (3.9 ka to present) has seven named eruptive periods separated by dormant intervals of decades to centuries.
  - A. **Smith Creek eruptive period** (3.9–3.3 ka) had major explosive eruptions that produced the voluminous set-Y tephra (Mullineaux, 1986, 1996). The Yn tephra layer (3.5 ka) was emplaced by the largest known explosive eruption of Mount St. Helens (approximately 10 times larger than the May 18, 1980, eruption), with a dense-rock equivalent volume of 4 cubic kilometers (km<sup>3</sup>) that extends about 900 km north-northeast into Canada (Carey and others, 1995). At least four other Y tephra were erupted during this period.
  - B. The **Pine Creek eruptive period**, from about 3.0–2.5 ka, was a period of major dome building, including the light-colored dacitic lava domes prominent in the current crater walls of Mount St. Helens. Tephra set P eruptions during the Pine Creek period were relatively modest in size. This period also included emplacement of two large debris avalanches in the north (Hausback and Swanson, 1990; Hausback, 2000). Associated lahars in the North Fork Toutle River, formed by breakout(s) of the ancestral debris avalanche-dammed Spirit Lake, were the largest Holocene volcaniclastic flows at Mount St. Helens (Scott, 1988b).
  - C. The **Castle Creek eruptive period**, from about 2.2–1.9 ka, marked a change to variable composition eruptions that, in addition to dacitic lava domes, produced both explosive eruptions and lava flows of basaltic to dacitic composition, with associated lahars and PDCs. By the end of the Castle Creek period, the volcano had been transformed from a cluster of lava domes to a composite volcano with an elevation of about 2,450 m (fig. 1B).
  - D. The ensuing short-lived **Sugar Bowl eruptive period**, from 850–900 C.E., included eruption of the

10 Geologic Field-Trip Guide of Volcaniclastic Sediments from Snow- and Ice-Capped Volcanoes

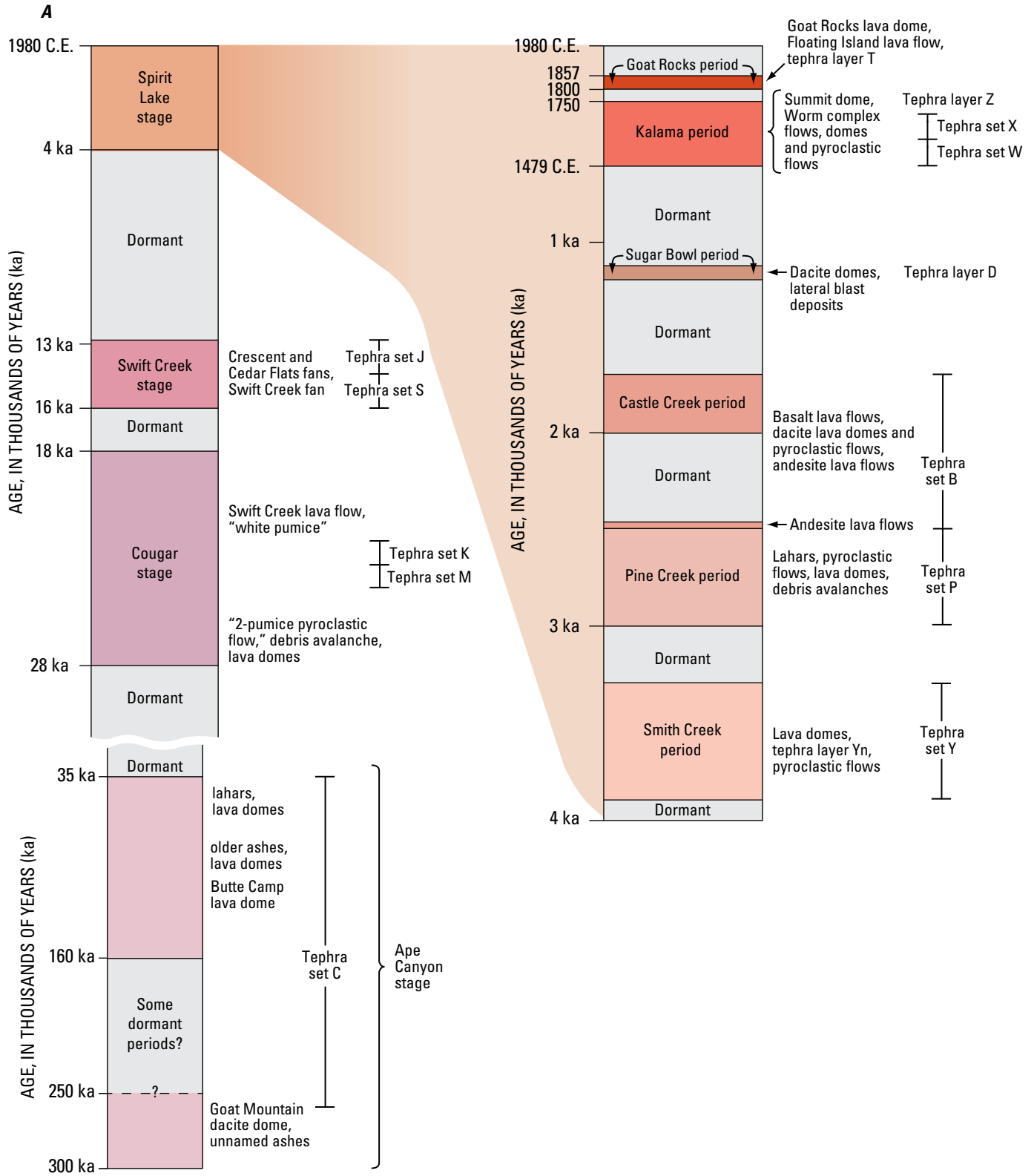


**Figure 1.** Quaternary chronologic and morphologic history of Mount St. Helens. *A.* Eruptive history of Mount St. Helens with Holocene Spirit Lake eruptive stage subdivided into eruptive periods at the right. Ages are given in calendar years (C.E.) or in thousands of years ago (ka). Note that time scales are not linear. *B.* Inferred morphologic evolution of Mount St. Helens edifice. Edifice-collapse events interrupted growth during the Cougar stage, the Pine Creek eruptive period, and the modern eruptive period. Both diagrams modified from Clyne and others (2005).



B

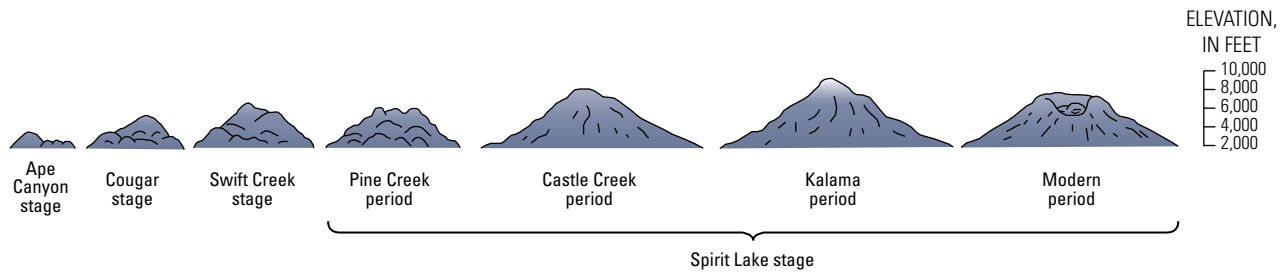


Figure 1.—Continued

Sugar Bowl dome and other flank lava domes and a small north-northeast directed lateral explosion.

- E. The **Kalama eruptive period**, from 1470–1720 C.E., began with two closely spaced, large-volume eruptions (producing the Wn and We tephra) dendrochronologically dated at 1479 and 1482 C.E. (Yamaguchi and Hoblitt, 1995). These explosive eruptions were followed by PDC emplacement and the eruption of tephra layer X around 1500 C.E. Andesitic PDCs accompanied extrusion of the sinuous Worm Flows lava complex on the south and southeast flanks ending around 1570 C.E. Thereafter, a large summit lava dome grew to completely fill the crater between about 1620 and 1720 C.E.; summit dome growth was accompanied by lithic PDCs and lahars on all sides of the volcano. This sequence of activity brought Mount St. Helens to its pre-1980 configuration and maximum elevation of 2,950 m.
- F. The **Goat Rocks eruptive period**, from 1800–1857 C.E., began with eruption of the T tephra in 1800 C.E. Extrusion of the Goat Rocks lava dome on the north flank took place between 1831 and 1857 and was accompanied by minor explosive eruptions, which were witnessed by early explorers, settlers, and Native Americans (Mullineaux and Crandell, 1981). Minor phreatic explosions also were reported in 1898, 1903, and 1921, after the Goat Rocks eruptive period ended (Majors, 1980), and were likely related to the Goat Rocks hydrothermal system.
- G. The **modern eruptive period** commenced in March 1980 with intrusion of a cryptodome into the upper volcanic edifice, phreatic eruptions, and marked edifice deformation and culminated in the Volcanic Explosivity Index 5 Plinian eruption of May 18, 1980 (Lipman and Mullineaux, 1981). This eruption was triggered by a sector collapse of the north side of the volcanic edifice. The May 18 eruption was followed by five smaller explosive eruptions during the summer and fall of 1980. From October 1980 to October 1986, lava extrusion of highly viscous dacite built a 305-m-high (1,000-ft)

lava dome in 17 eruptive episodes. Lava extrusion recommenced in October 2004 with the more or less continuous extrusion of semi-solid dacitic lava, which produced numerous lava spines and a new 455-m-high (1,500-ft) lava dome over the next 3+ years (until early 2008). The closely monitored eruptions of this period have led to major new understandings of eruptive and volcaniclastic processes in volcanic arcs and have sparked the development of new monitoring techniques (Sherrod and others, 2008). A recent compilation of eyewitness accounts describes the impact of the May 18, 1980, eruption on residents, visitors, first responders, public officials, and scientists (Waitt, 2015).

Physical impacts and deposits from the 1980 eruptions at Mount St. Helens, particularly the May 18 eruption, significantly changed the landscape surrounding the volcano and severely altered river channels draining the volcano (Lombard and others, 1981; Major and others, 2000, 2009) (figs. 2, 3). Today, many of those features and deposits are being modified, eroded, or buried by ongoing surficial processes and recolonization by forest vegetation.

## Deposits in the Toutle River Drainage Basin

The Toutle River and its tributaries drain the north and northwest flanks of the volcano and have accumulated volcaniclastic sediments from Mount St. Helens over multiple eruptive periods (figs. 2–4). Most of the volcaniclastic deposits from the 1980 eruptions of Mount St. Helens are found in this drainage basin. Volcaniclastic deposits in the upstream half of the North Fork Toutle River basin are dominated by debris-avalanche and PDC deposits, but also contain pyroclastic-fall and lahar deposits. The southern fork and main stem of the Toutle River are dominated by lahar deposits.

## Flow Processes in 1980 and Associated Deposits

The May 18, 1980, eruption began with a catastrophic rockslide and debris avalanche that was one of the largest globally in history, filling 60 square kilometers (km<sup>2</sup>) of the North Fork Toutle valley with 2.8 km<sup>3</sup> of debris and reaching as far as 28 km

## 12 Geologic Field-Trip Guide of Volcaniclastic Sediments from Snow- and Ice-Capped Volcanoes

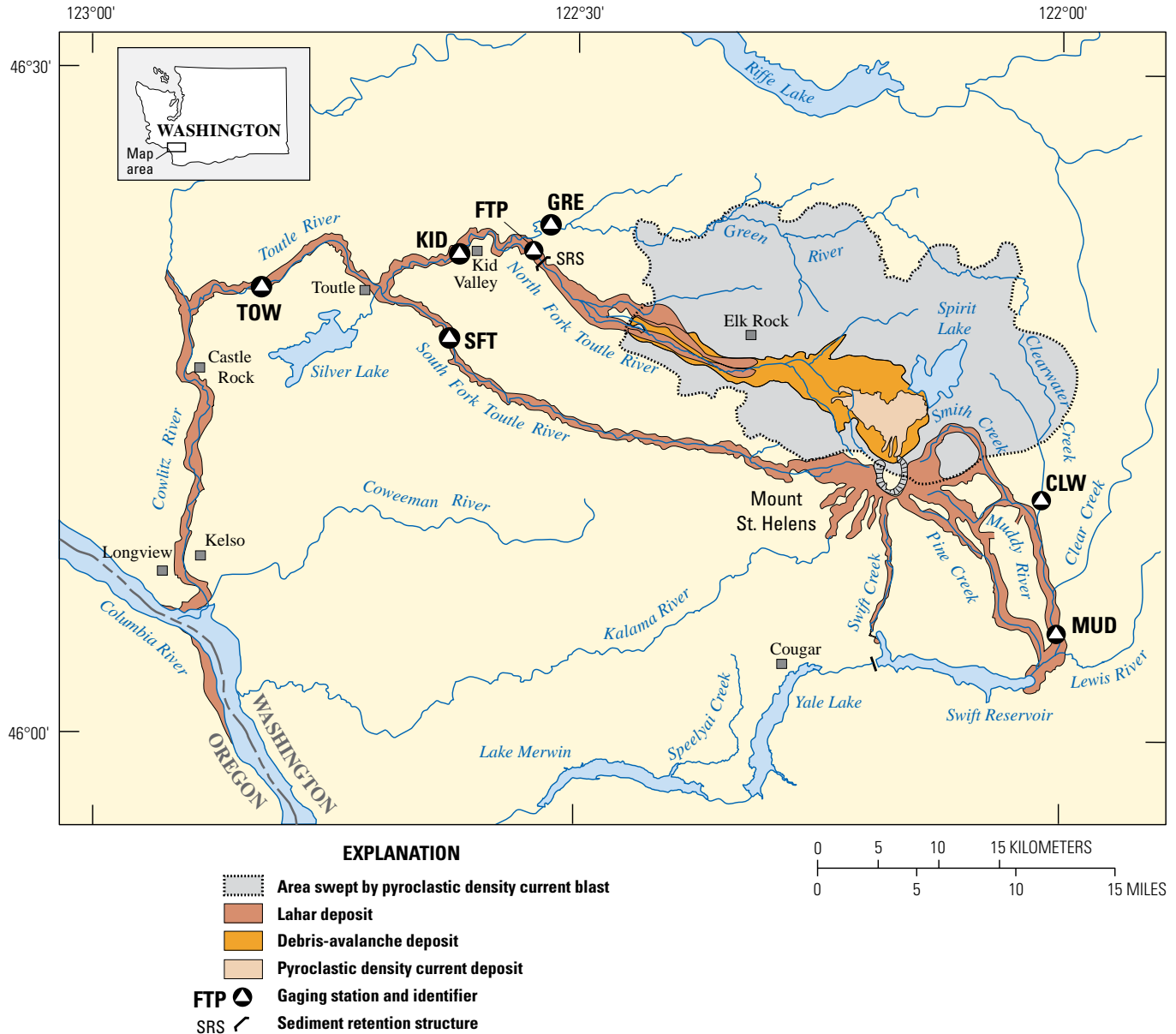


**Figure 2.** Map showing full extent of volcaniclastic sediment deposition by the May 18, 1980, and later 1980 eruptions of Mount St. Helens (J.J. Major, written commun., 2016). Labeled triangle symbols are locations of stream gages used in monitoring sediment yield: Tower Road (TOW), Kid Valley (KID), South Fork Toutle (SFT), fish trap (FTP), Green River (GRE), Clearwater Creek (CLW), and Muddy River (MUD).

downstream in 10–12 minutes (Voight and others, 1981, 1983; Glicken, 1996). Peak velocity at the base of the volcano was about 70 meters per second (m/s); the average velocity was 35 m/s. High-velocity debris entering Spirit Lake pushed a water wave up-valley to an elevation 260 m above lake level. Its deposit redammed the lake outlet, raised the surface elevation of the new Spirit Lake about 60 m, and filled the upper North Fork Toutle River valley with hummocky, poorly sorted debris to a maximum depth of 180 m (average depth 45 m)—only a fraction of which has been eroded since. Although elevated pore pressures and seismically induced deformation may have contributed to the failure, modeling by Reid and others (2010) shows that progressive shear strength reduction due to cryptodome intrusion

and gravitational loading could have provoked edifice collapse, even in the absence of transiently elevated pore-fluid pressures or seismic disturbance.

Rapid unloading of the hydrothermal-magmatic system in the upper edifice by retrogressive edifice collapse triggered a catastrophic directed volcanic explosion. A wide variety of terms has been applied to this relatively dilute PDC, but we follow others in using the term “lateral blast” to acknowledge the directed component and initial explosive thrust of the density current (Hoblitt and others, 1981). The lateral blast devastated an area of 600 km<sup>2</sup> over a broad arc west-northwest to east-northeast of the volcano, removing trees proximally, causing extensive radial and flow-parallel tree blowdown, and leaving singed standing trees at



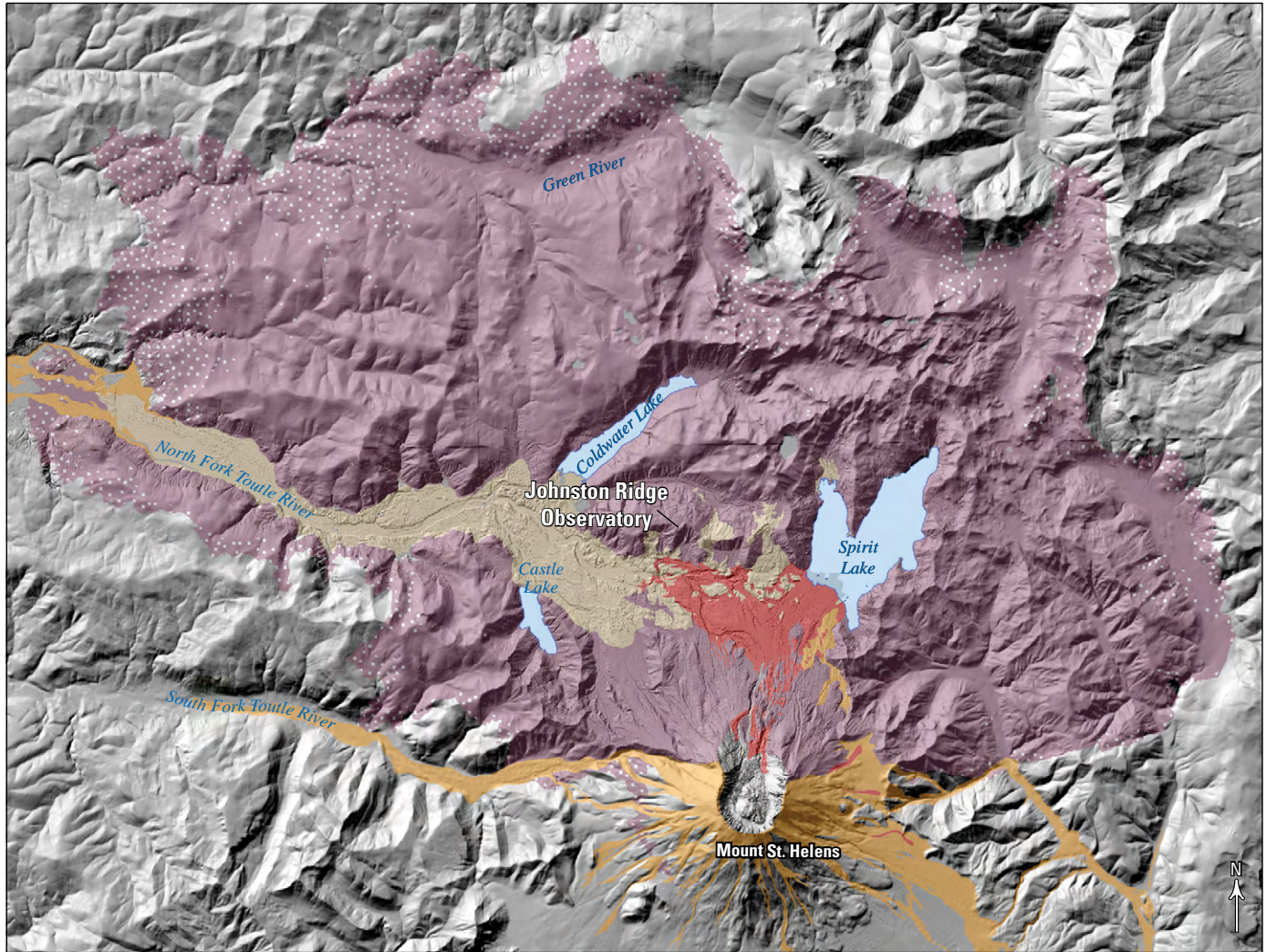
**Figure 3.** Aerial photograph of Mount St. Helens taken from the International Space Station in 2009. View is to the west. Crater breach opens to the north and adjacent lava domes from 2004–2008 (left) and 1980–1986 (right) are visible inside the crater. The 1980 debris-avalanche deposit is the thick valley-fill sediment extending westward within the North Fork Toutle River valley (toward top of photograph). The largely still unvegetated “blast zone” extends across most of the right half of the photograph. NASA astronaut photograph ISS018-E-5643, acquired October 28, 2008, available at <http://earthobservatory.nasa.gov/>.

the distal margins (Hoblitt and others, 1981; Moore and Sisson, 1981; Waitt, 1981).

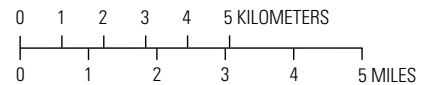
Lateral-blast deposits vary across the upper North Fork Toutle River basin. Their grayish color and lithic-rich composition contrast with the whitish pumiceous deposits emplaced later by May 18 PDCs and open-vent tephra fall. Typical sections include a basal fines-poor A1 layer that can include organic material with pebble-size cryptodome dacitic fragments, a friable A2 layer, portions of which display bedded surge layers, and a thin overlying A3 air-fall layer that may contain accretionary lapilli (Waitt, 1981) (fig. 5). Hoblitt (2000) noted evidence for a second blast explosion that may have been phreatomagmatic because of lower proportions of juvenile clasts.

Following emplacement of the debris avalanche and the lateral blast, a vertical open-vent phase of the May 18 eruption produced a Plinian eruption column and dacitic pyroclastic-fall deposits—including pumice lapilli in proximal areas and ash in distal areas downwind to the east (Sarna-Wojcicki and others, 1981). Secondary PDCs derived from remobilization






of lateral-blast deposits on steep valley walls ponded in South Coldwater Creek valley, covering much of the debris-avalanche deposit that overtopped Johnston Ridge (Hoblitt and others, 1981; Fisher and others, 1987; Fisher, 1990). Collapse of the eruption column produced pumiceous PDCs that descended the north flank of Mount St. Helens, traveling 7–8 km from the vent and formed a pyroclastic debris apron south of Johnston Ridge, locally known as Pumice Plain (Rowley and others, 1981; Criswell, 1987). Secondary small-scale phreatic eruptions originating from water-ice interaction with still-hot pumice deposits produced explosion pits rimmed by bedded pyroclastic surge layers. Smaller pumiceous PDCs formed during subsequent explosive eruptions between May 25 and October 16, 1980 (Christiansen and Peterson, 1981). Two types of lahars occurred in the Toutle River drainage basin on May 18: (1) a granular, fines-poor lahar, triggered almost instantly by rapid snowmelt produced by PDCs scouring snow and ice and (2) a muddy, slightly more fines-rich lahar (3–5 weight percent silt and clay), triggered by liquefaction of the debris-avalanche deposit over



Shaded relief from 2009 U.S. Army Corps of Engineers 1-meter light detection and ranging (lidar) data



**EXPLANATION**

-  Area affected by lateral blast with variable deposition
-  Zone of standing dead (singed) trees
-  Debris-avalanche deposit
-  May 18 and later pumiceous pyroclastic density current deposit
-  May 18 lahar deposit—Overlies parts of the debris-avalanche deposit

**Figure 4.** Shaded-relief map showing the impacts of various volcanic and volcanoclastic processes to the Mount St. Helens area in 1980 (Lipman and Mullineaux, 1981). Shaded relief from 2009 U.S. Army Corps of Engineers 1-meter light detection and ranging (lidar) data.

a period of hours. The granular lahar coursed down the South Fork Toutle River within minutes of the 8:32 a.m. onset of the May 18 eruption, starting as a debris flow and becoming progressively more dilute as it coursed downstream (Cummins, 1981; Janda and others, 1981). It transformed fully to hyperconcentrated flow after mixing with North Fork Toutle River water at the confluence of the two forks. The larger fines-rich North Fork Toutle River lahar initiated from “mud springs” coalescing

over several hours on the debris-avalanche deposit in the early afternoon of May 18. The mud springs were generated by seismically induced liquefaction of the fresh debris-avalanche deposit in the upper North Fork Toutle River valley (Fairchild, 1985). The South Fork Toutle River lahar flowed about 43 km as a debris flow before transforming to hyperconcentrated flow. The North Fork Toutle River lahar, by contrast, traveled 93 km to the Columbia River entirely as a debris flow.

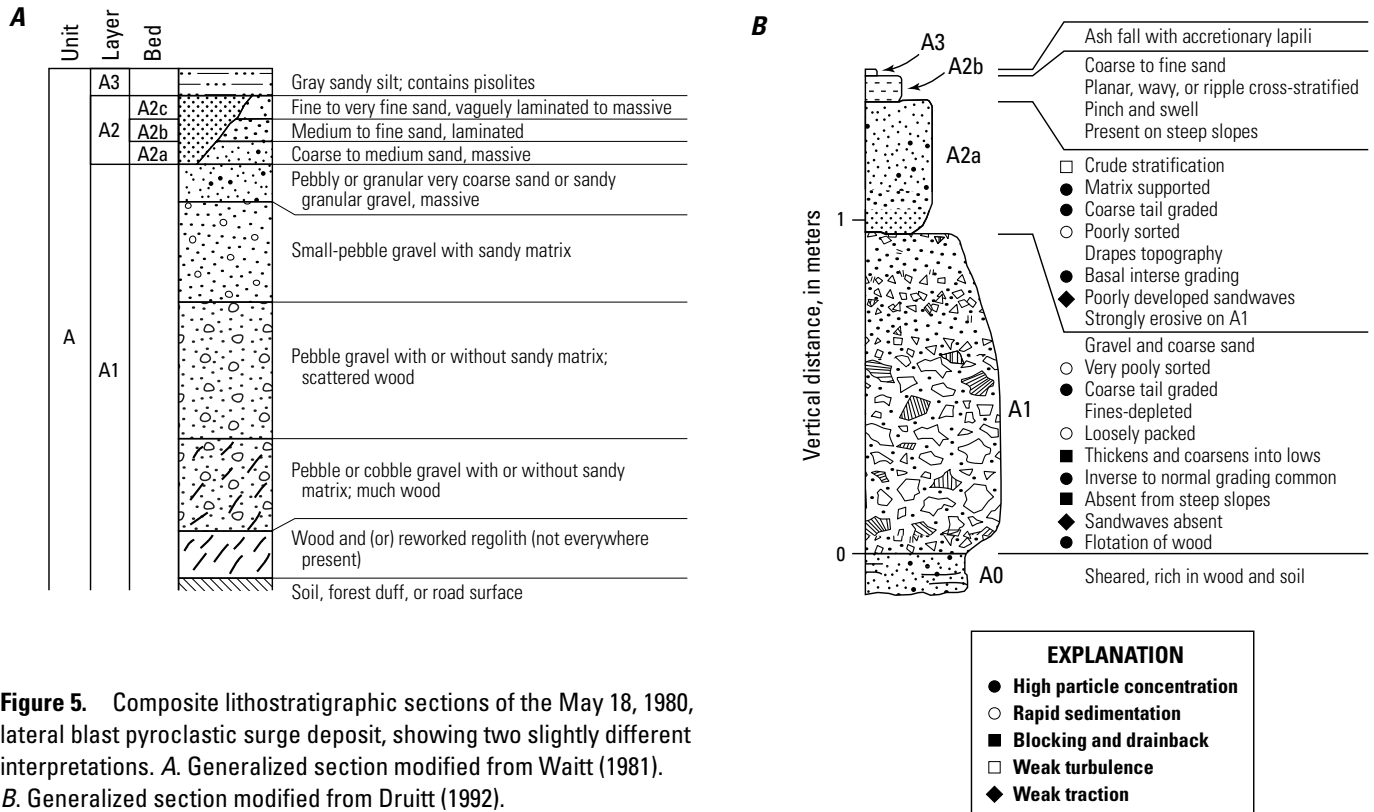


**Figure 5.** Composite lithostratigraphic sections of the May 18, 1980, lateral blast pyroclastic surge deposit, showing two slightly different interpretations. *A.* Generalized section modified from Waitt (1981). *B.* Generalized section modified from Druitt (1992).

### March 1982 Lahar and Associated Deposits

The largest post-1980 lahar at Mount St. Helens took place in 1982. On March 19, nearly instantaneous melting of snow and ice by a large explosion during lava dome extrusion sprayed snow-covered crater walls with incandescent rock debris, triggered avalanches of rapidly melting snow, and released 4 million cubic meters (m<sup>3</sup>) of water and hot rock debris from the crater. The flowing mixture transformed to a debris flow through erosion and incorporation of sediment by the time it reached the base of the volcano (Waitt and others, 1983; Pierson and Scott, 1985; Pierson, 1999). Over the next 81 km that it traveled down the Toutle River, the lahar became progressively dilute as water from the overtaken river was ingested and coarse sediment was deposited (Pierson and Scott, 1985). The debris flow transformed to hyperconcentrated flow starting about 27 km downstream of the crater. At 43 km from the crater, the lahar had completely transformed to hyperconcentrated flow (Dinehart, 1999). The lahar reached the Cowlitz River confluence, 83 km downstream from the crater, in approximately 5 hours. Flow-front velocity averaged 4.6 m/s.

The hyperconcentrated phase of the 1982 lahar deposited an unusual, faintly stratified, coarse sand with isolated outsized clasts and gravel lenses—the first systematically described deposits emplaced by hyperconcentrated flow (Pierson and Scott, 1985). Unfortunately, almost all of these deposits have been eroded away. Similar deposits have since

been described in lahar channels and in the geologic record at a number of other volcanoes worldwide, indicating that lahars are more common than had been recognized prior to 1985.

### Post-1980 Sediment Redistribution

Large-scale erosion and mobilization of May 18 volcaniclastic deposits (primary and secondary) flushed a huge volume of sediment down the Toutle River, requiring extensive and prolonged engineering intervention by the U.S. Army Corps of Engineers in order to prevent catastrophic inundation and flooding of downstream communities (Willingham, 2005). Without intervention, the lower Toutle and Cowlitz Rivers would have experienced significant channel aggradation.

Long-term monitoring of stream erosion and sediment transport since 1980 has revealed that initial sediment yields following the 1980 eruption were several hundred times above background and that the magnitude of yields depended on the type and degree of disturbance to subcatchments (Major and others, 2000). Levels of suspended sediment were highest and lasted longest in the upper North Fork Toutle River drainage, which was impacted by the 1980 debris avalanche (fig. 6). In contrast, lower sediment yields of shorter duration occurred in the Green River catchment, which was deforested and covered only with thin lateral-blast (pyroclastic-surge) and pyroclastic-fall deposits. The sediment yields recorded immediately after the eruption declined sharply over the next five years, but have remained well above background levels until the present.

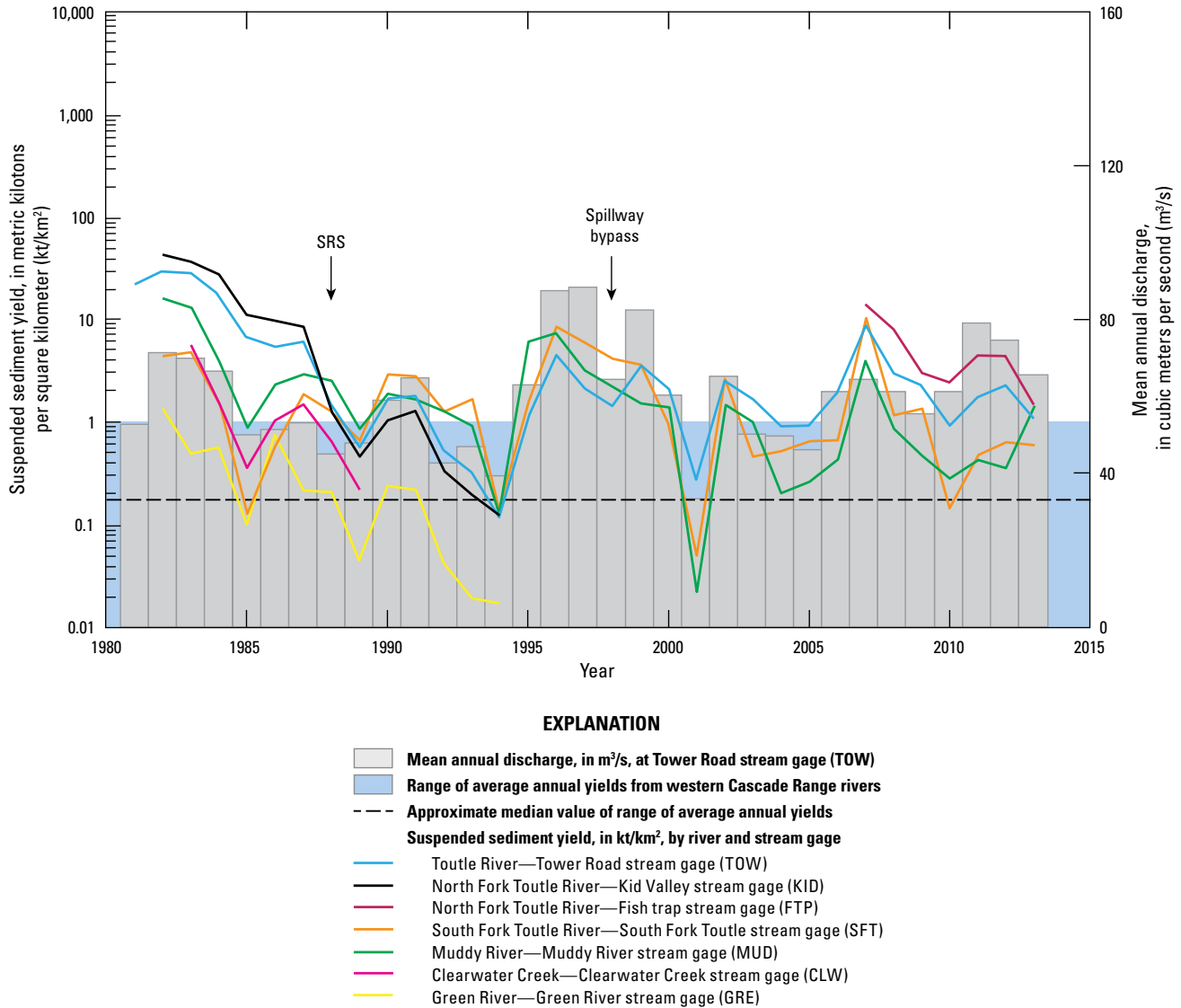


**Figure 6.** Plot of suspended sediment yields (in metric kilotons per square kilometer, kt/km<sup>2</sup>) in surrounding rivers since the May 1980 Mount St. Helens eruption (J.J. Major, written commun., 2016). Stream gage locations are marked in figure 2. Gray-shaded bar graph depicts mean annual discharge (in cubic meters per second, m<sup>3</sup>/s) at Tower Road station (TOW) on the Toutle River near its confluence with the Cowlitz River (blue line). Background blue shading shows the range of average annual yields from western Cascade Range rivers. The dashed horizontal line is the approximate median value of the range of average annual yields. SRS marks the completion date of the sediment retention structure; “spillway bypass” indicates when water and sediment began passing over the SRS spillway in 1998.

The initial rapid decline in sediment yield in the Toutle River basin was due to stabilization of tephra deposits remaining on hill slopes, as demonstrated by annual yields from the Green River basin (affected only by tephra deposition) returning to pre-eruption levels within five years (Collins and Dunne, 1986; Major and others, 2000). In other Toutle River subbasins, continuing high sediment yields were caused primarily by channel erosion of debris-avalanche and lahar deposits rather than hillside erosion. Such channel erosion has continued to produce sediment yields about 10–50 times

greater than probable pre-eruption levels for more than three decades.

In the North Fork Toutle River valley, channel erosion during the second decade after the eruption (1987–1999) was concentrated along a 6-km-long area at and upstream of a valley constriction near Elk Rock in the middle of the debris-avalanche deposit (fig. 7). During the following decade (1999–2009), erosion was more evenly distributed along the channel, incising into the middle and upper parts of the avalanche deposit with increasing lateral erosion of tall stream banks. In 1987–1989, construction

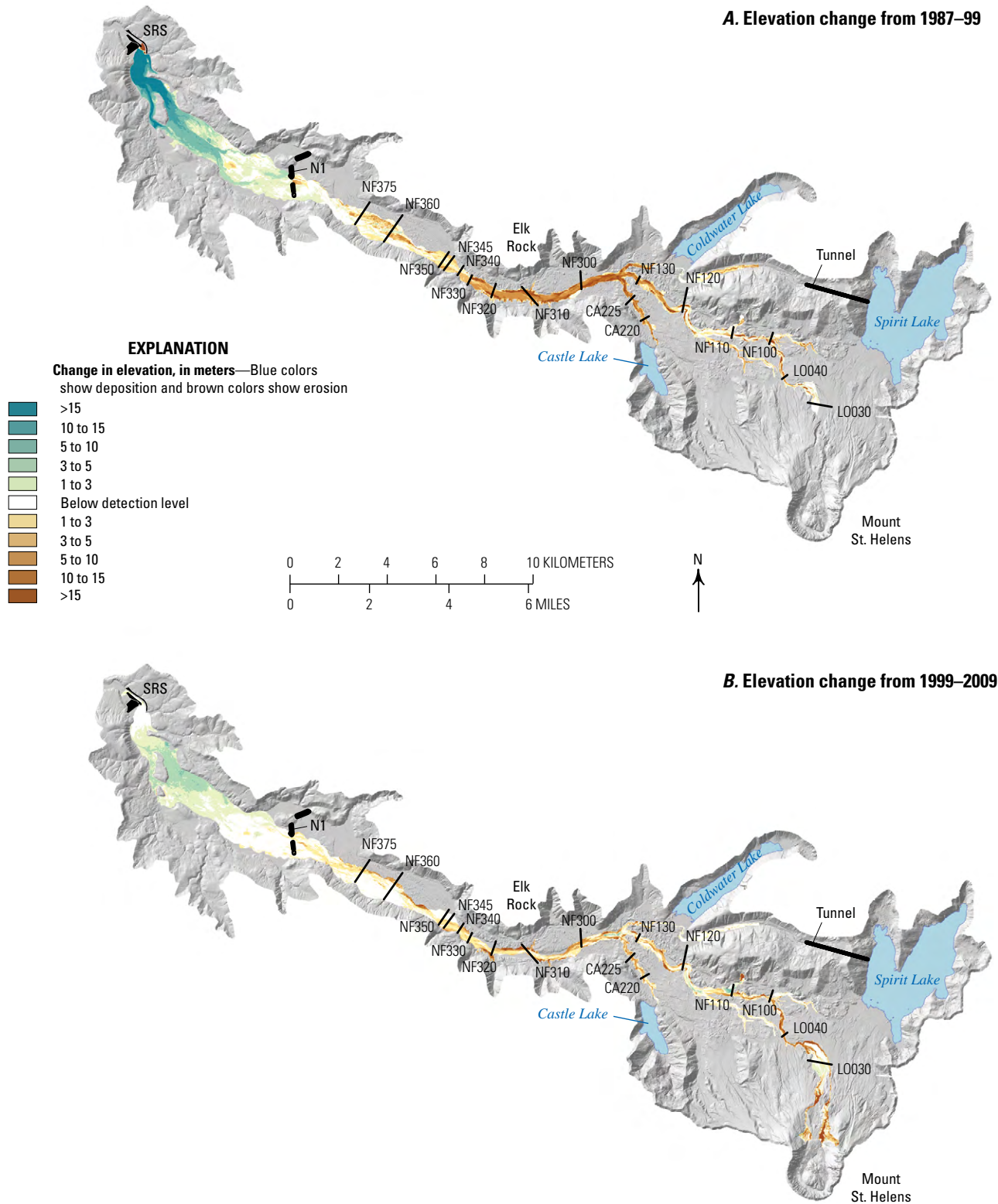


**Figure 7.** Shaded-relief maps showing topographic changes in the North Fork Toutle River valley after the May 1980 Mount St. Helens eruption (Mosbrucker, 2014). *A.* Digital elevation models of topographic difference derived from comparison of aerial photographs taken in 1987 and 1999. *B.* Digital elevation models of topographic difference derived from comparison of 1999 aerial photographs with 2009 U.S. Army Corps of Engineers light detection and ranging (lidar) data. SRS, sediment retention structure, completed in 1989; N1, former small retention structure constructed in early 1980s. Selected long-term monitoring cross section sites, used for data verification, are labeled.

of a sediment dam—the sediment retention structure—forced sediment deposition within the valley downstream of these erosion-prone areas, burying the toe of the debris-avalanche deposit.

Despite the focused erosion of the debris-avalanche deposit, the bulk of this massive sediment reservoir is still in place. As of 2010, stream erosion or local mass-failure processes have modified only about 20 percent of the debris-avalanche deposit planimetric area and only about 13 percent of the deposit volume has been eroded (J.J. Major, written commun., 2016).

## Toutle River Lahars from Older Eruptive Periods

The distal North Fork Toutle River valley downstream of the North and South Fork Toutle River confluence exposes lahar deposits spanning much of the history of Mount St. Helens (Scott, 1988a). Terraces near the confluence preserve a sequence of lahar deposits dating back to late Pleistocene time: (1) a lahar deposit of Swift Creek age (16–12.8 ka), (2) lahar deposits of Smith Creek age (3.9–3.3 ka), and (3) lahar deposits of Pine Creek age (3.0–2.5 ka). The four Pine Creek-age lahar deposits are interpreted to have been generated by outbreak floods released from the ancestral Spirit Lake, a lake repeatedly formed by damming caused by debris-avalanche deposits (Scott, 1988a). The lahars contain clasts composed almost entirely of well-rounded river gravel, suggesting that they could only have been deposited by large floods entraining sediment from the Toutle River bed.

The recurrence interval of Toutle River lahars is one lahar every few centuries over the past 4,000 years, determined for lahars of sufficient volume to reach 50 km downstream. However, lahar occurrence is not randomly distributed, but concentrated in eruptive periods. The average recurrence interval of large lahars during the last 4,000 years, if only eruptive periods are considered, is 130 years (at least 15 lahars during the 1,930 years within eruptive periods) (Scott, 1989).

## Deposits in the Lewis River Drainage Basin

A variety of Mount St. Helens volcaniclastic sediments can be found in the Lewis River basin, the system that drains the south and east flanks of Mount St. Helens (Crandell and Mullineaux, 1973; Major and Scott, 1988; Clynne and others, 2008) (figs. 2, 8). Key tributaries affected by eruptions at Mount St. Helens include Smith Creek, Clearwater Creek, Muddy River, Pine Creek, and Swift Creek. In addition, three major hydropower reservoirs (Swift Reservoir, Yale Lake, and Lake Merwin) are found along the main stem of the Lewis River, which extends from the volcanic edifice to the Columbia River confluence, about 90 km downstream. All of the Pleistocene eruptive stages of Mount St. Helens and several eruptive periods of the Holocene Spirit Lake eruptive stage (fig. 1) are named for features and deposits in the Lewis River drainage.

A huge volume of volcaniclastic material was produced during the Cougar eruptive stage (28–18 ka). A very large Cougar-age debris avalanche originated from near the location of the present-day edifice (Mullineaux and Crandell, 1981; Clynne and others, 2008). The avalanche traveled about 17 km, filled the valley with a deposit 200–300 m thick and 1–2 km<sup>3</sup> in volume, and dammed the Lewis River at the present-day site of the Swift Creek confluence (Clynne and others, 2008). Subsequent overtopping of the blockage and lake drainage caused flooding downstream to the Columbia River and contributed to aggradation of at least 75 m in the lower Lewis River valley. This flooding is analogous to what occurred in the North Fork Toutle River during the Pine Creek eruptive period. Avalanche occurrence was immediately followed by the explosive eruptions that produced the dacitic “two-pumice” PDC (24.4 ka) (Clynne and others, 2008). The PDC deposit buries the debris-avalanche deposit to depths of 100–200 m without evidence for intervening erosion or soil formation. After a hiatus of several thousand years, deposits from the Swift Creek eruptive stage (16–12.8 ka) buried Cougar stage deposits in the Lewis River drainage and produced the Cedar Flats debris fan southeast of the volcano. This feature is dominated by an assemblage of deposits, including lahars and dome-collapse PDC deposits, about 100 m thick. Following another dormant period, abundant lahar, PDC, and volcano-fluvial deposits of the Smith Creek (3.9–3.3 ka), Pine Creek (3.0–2.5 ka), and modern (1980 to present) eruptive periods were emplaced within in the Swift Creek, Pine Creek, and Muddy River drainages.

On the morning of May 18, 1980, after the start of the Mount St. Helens eruption, major snowmelt-generated lahars flowed down Pine Creek and Muddy River, depositing about  $1.4 \times 10^7$  m<sup>3</sup> of lithic debris in Swift Reservoir in less than an hour (Pierson, 1985). A smaller similar lahar descended Swift Creek



**Figure 8.** Photograph of an outcrop of pre-1980 volcaniclastic deposits along the Swift Creek riverbank. The thick lowest unit was emplaced by the “two-pumice” pyroclastic density current that was erupted during the Cougar stage. The largest blocks visible are about 2 meters in diameter. The soil developed on this deposit (dark band) is overlain by a whitish lahar deposit of Swift Creek age. Smithsonian Institution photograph by L. Siebert, 2016.



at the same time and, during the afternoon, a pumiceous lahar was generated by snowmelt from column-collapse PDCs. On the northeast flank of the volcano, a complex assemblage of deposits from the lateral blast and resultant snowmelt lahars was emplaced in Smith Creek (Brantley and Waitt, 1988). As in the case of the lahars in Pine Creek and Muddy River, initial lahar flow velocities in the upper Smith Creek tributaries were high (greater than 30 m/s). Deposits emplaced in Smith Creek include ponded lateral-blast (PDC) deposits and secondary PDC deposits derived from valley sides and lahars that are capped by a tephra-fall unit containing accretionary lapilli (lateral blast unit A3) (fig. 5). This stratigraphy indicates emplacement of the entire Smith Creek sequence in less than 30 minutes (Brantley and Waitt, 1988).

## Volcaniclastic Deposits of Mount Hood

Mount Hood is an intermediate composition stratovolcano, composed largely of andesite and some low-silica dacite (58.0–64.5 weight percent SiO<sub>2</sub>), and is capped by perennial snow and glacial ice. It is located along the crest of the Cascade Range about 120 km east of Portland, Oregon, and 56 km south of the Columbia River (Wise, 1969; Scott, Gardner, and others, 1997; Scott, Pierson, and others, 1997; Scott and Gardner, 2017) (figs. 9, 10). The present volcanic edifice—composed of lava domes, lava flows, and interbedded volcaniclastic deposits—is approximately 50 km<sup>3</sup> in volume (Sherrod and Scott, 1995). Its summit stands 3,427 m (11,241 ft) above sea level. Mount

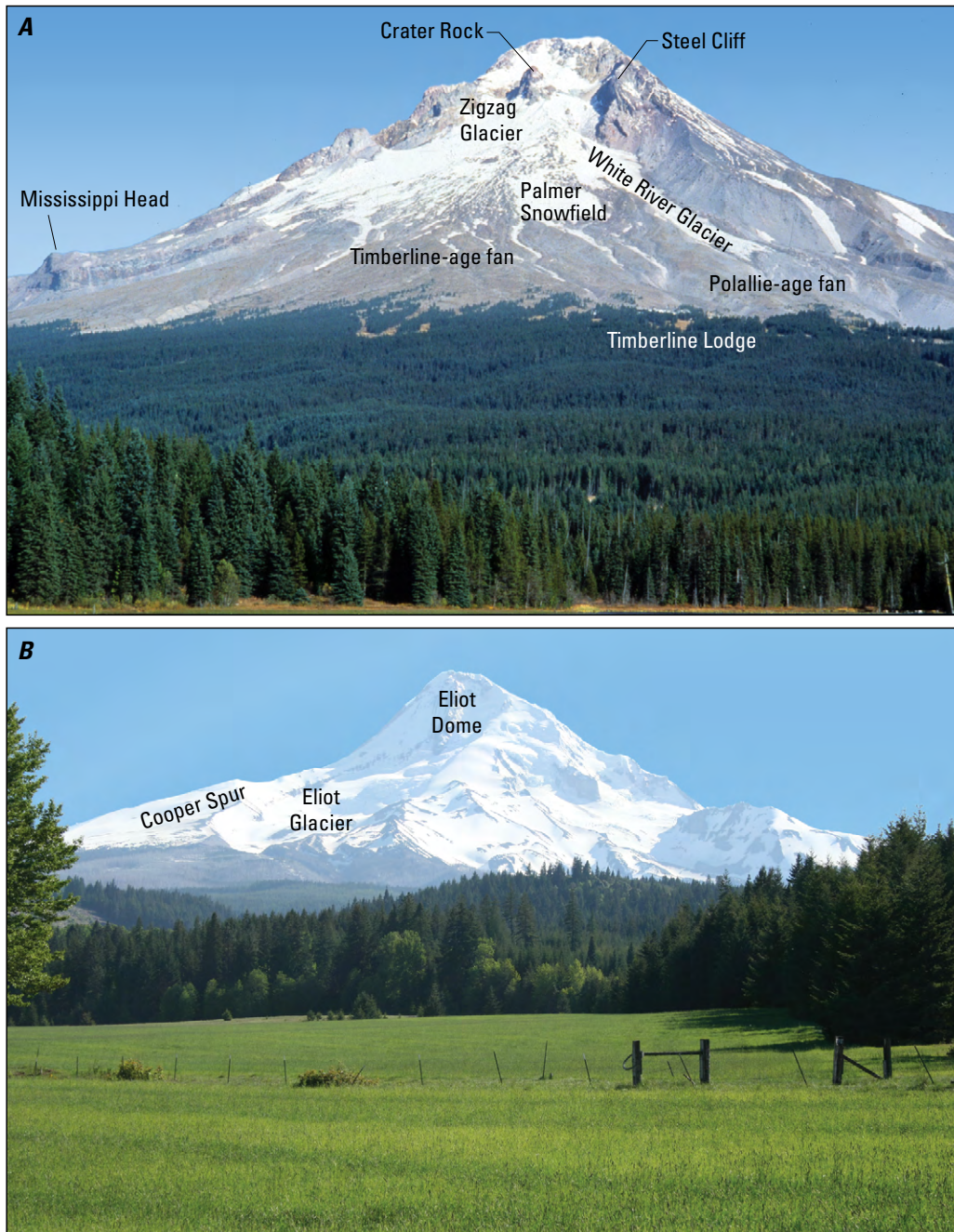


**Figure 9.** Two photographic views of Mount Hood. *A.* Southwest flank of Mount Hood with key features labeled. Collapsing lava domes located at the site of present-day Crater Rock (dome remnant) produced the pyroclastic debris fan extending downhill during the Timberline (~450 C.E.) and Old Maid (1781–1793 C.E.) eruptive periods. Activity during the Polallie eruptive period (30,000–15,000 calendar years ago) sent flows down the White River. Modified from Pierson and others (2009). *B.* North flank of Mount Hood viewed from the Hood River valley looking south. Cooper Spur is thought to be part of the collapse scarp of the late Pleistocene Hood River debris avalanche and lahar. Smithsonian Institution photograph by L. Siebert, 2013.

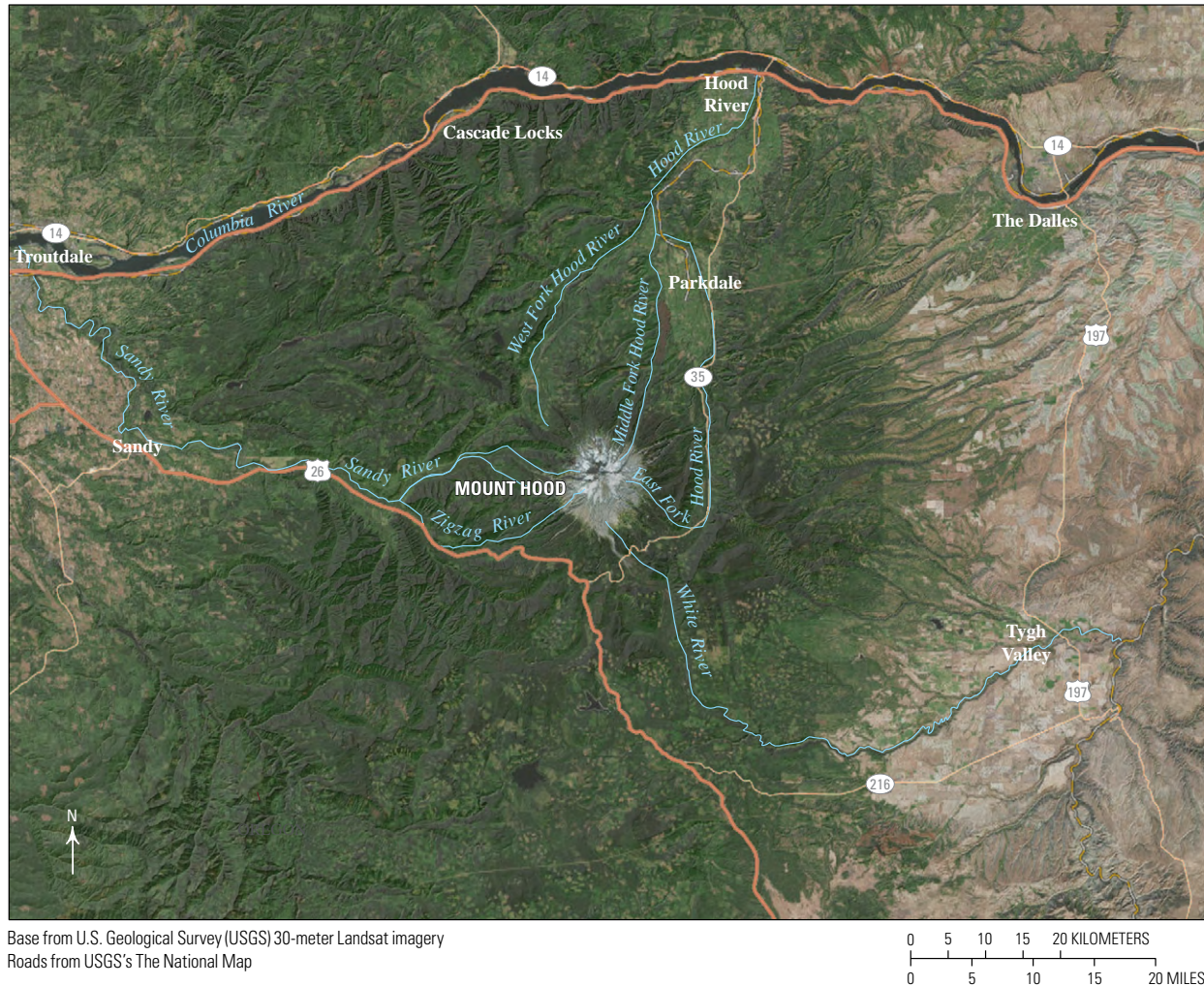


**Figure 10.** Map showing Mount Hood and the three main river systems that drain the volcano.

Hood differs from Mount St. Helens and other Cascade Range volcanoes in the relatively uniform chemistry of its eruptive products over its 500,000 year history and in its lack of highly explosive eruptions. Effusive eruptions and lava dome growth dominate its recent activity, along with associated lithic PDCs and lahars.

Construction of the Mount Hood edifice began about 1.5 million years ago (Ma) with eruptions from vents within several kilometers of the current vent. By about 500 thousand years ago (ka), lavas were added from other vents closer to the present summit (Sherrod and Scott, 1995; Scott, Gardner, and others, 1997; Scott and Gardner, 2017). The reversely magnetized 1.2 Ma basaltic to andesitic Sandy Glacier volcano underlies the west flank of Mount Hood (Wise, 1969). Lava flows dominate, but the upper part of Sandy Glacier volcano is composed of a thick sequence of diamicts that were probably deposited chiefly by block-and-ash flows and lahars. Prior to 300 ka, several Pleistocene-age basaltic-andesite volcanoes grew on what is now the north flank of Mount Hood. Most

of the present Mount Hood edifice is composed of lava flows of Pleistocene age and most of the upper cone is formed of flows younger than about 150 ka (Scott, Gardner, and others, 1997; Scott and Gardner, 2017). Pleistocene lava flows were overridden by glaciers during the Last Glacial Maximum (about 20 to 33 ka), and many remain partly buried by moraines.

Mount Hood has produced both effusive and moderately explosive eruptions during the past 100,000 years, including dormant periods of variable length (table 3) (Scott and Gardner, 2017). Most volcanic activity since about 30 ka has consisted of lava-dome growth and collapse, which fed numerous PDCs, and the eruption of stubby lava flows on the summit and upper flanks. The last of the Pleistocene eruptive activity produced lava domes, PDCs, lahars, and tephra over the period from about 30 to 15 ka—an interval of multiple poorly dated eruptive episodes broadly defined as the Polallie eruptive period, which coincides with maximum glacial ice cover on the volcano. Eruptive products during this interval impacted valleys surrounding the volcano.

**Table 3.** Major eruptive (orange-yellow), noneruptive geomorphic (beige), and glacial (blue) events recorded at Mount Hood during the past 100,000 years. Modified from Scott, Gardner, and others (1997).

[ka, thousand years ago; cm, centimeters]

Date or age	Event	Deposits
20th and 21st centuries	Debris flows in Sandy, White, and Hood Rivers	Debris-flow deposits
1859, 1865 C.E.	Minor explosive eruptions	Scattered pumice
Late 19th century	Late neoglacial advance	Prominent, sharp-crested moraines
1781–1793 C.E.	Dome-building eruption of Old Maid eruptive period	Silica-rich andesite lava dome (Crater Rock); dome-collapse pyroclastic density current and lahar deposits; minor tephra
~500 years ago	Debris flows in Zigzag River	Debris-flow deposits
~1 ka	Debris flows in upper Sandy River (not syneruptive)	Debris-flow deposits
~1.5 ka	Dome-building eruption(s) of Timberline eruptive period	Silica-rich andesite lava dome; dome-collapse pyroclastic density current and lahar deposits; minor tephra
~7.7 ka	Mafic eruption from satellite vent north of Mount Hood (near Parkdale)	Basaltic andesite lava flow
~20–11 ka	Waning phases of Evans Creek glaciation	Moraines
~20–13 ka	Dome-building eruptions of Polallie eruptive period	Silica-rich andesite lava dome; dome-collapse pyroclastic density current and lahar deposits; minor tephra
~25–20 ka	Maximum extent of Evans Creek glaciation	Belts of moraines in most valleys
~30–20 ka	Dome-building eruptions	Silica-rich andesite lava dome; dome-collapse pyroclastic density current and lahar deposits
~50–30 ka	Lava-flow eruptions from central vent	Andesite lava flows of Cathedral Ridge and Tamanawas Falls
~100–60 ka	Sector-collapse debris avalanche from north flank of Mount Hood	Avalanche transformed to Hood River lahar and flowed to the Columbia River

## Holocene Eruptive Activity

Dome-building eruptions occurred at Mount Hood during its two most recent eruptive periods: (1) the Timberline eruptive period about 1.5 ka, and (2) the Old Maid eruptive period that occurred slightly more than 200 years ago, with historically documented explosions (phreatic?) occurring throughout the mid-19th century (Crandell, 1980; Cameron and Pringle, 1986, 1987; Scott, Gardner, and others, 1997; Pierson and others, 2011; Scott and Gardner, 2017). Eruptions during both Holocene eruptive periods produced multiple dome-collapse lithic PDCs and lahars but very little air-fall tephra. The Timberline eruptive period began with a flank collapse that sent a large lahar down the Sandy River and left the active vent surrounded by a scarp-bounded, horseshoe-shaped failure scar open to the southwest. Flows of primary and secondary volcanoclastic fragments during both eruptive periods were therefore directed southwest and emplaced on a steep pyroclastic debris fan on the southwest flank of the volcano (fig. 9A, 11). The Holocene debris fan extends 6–10 km downslope of the Holocene eruptive vent on the south flank of the volcano and sheds sediment into two of the

three river systems draining Mount Hood—the Sandy and White Rivers (fig. 10, 11). In addition to sediment storage of primary PDC and lahar deposits on the debris fan itself, substantial volumes of these sediments were remobilized by lahars and floods during and following volcanic activity, and moved into the heads of confined canyons beyond the toe of the fan in both the upper Sandy and White River drainages (fig. 12). This combined fan and valley-head stockpile of stored sediment became the sediment source for decades-long periods of post-eruption sediment remobilization. The third major drainage basin on Mount Hood, the northward-flowing Hood River, does not receive sediment from Holocene eruptions. The Holocene vent location is marked today by a remnant of the most recent lava dome, named Crater Rock.

## Timberline Eruptive Period

Holocene eruptive activity at Mount Hood began about 1,500 years ago and follows nearly 10,000 years of quiescence. Timberline-age eruptive products are dominated by the deposits of lithic PDCs and accompanying ash clouds and extend at least 12 km from the vent (Scott, Gardner, and others, 1997). They

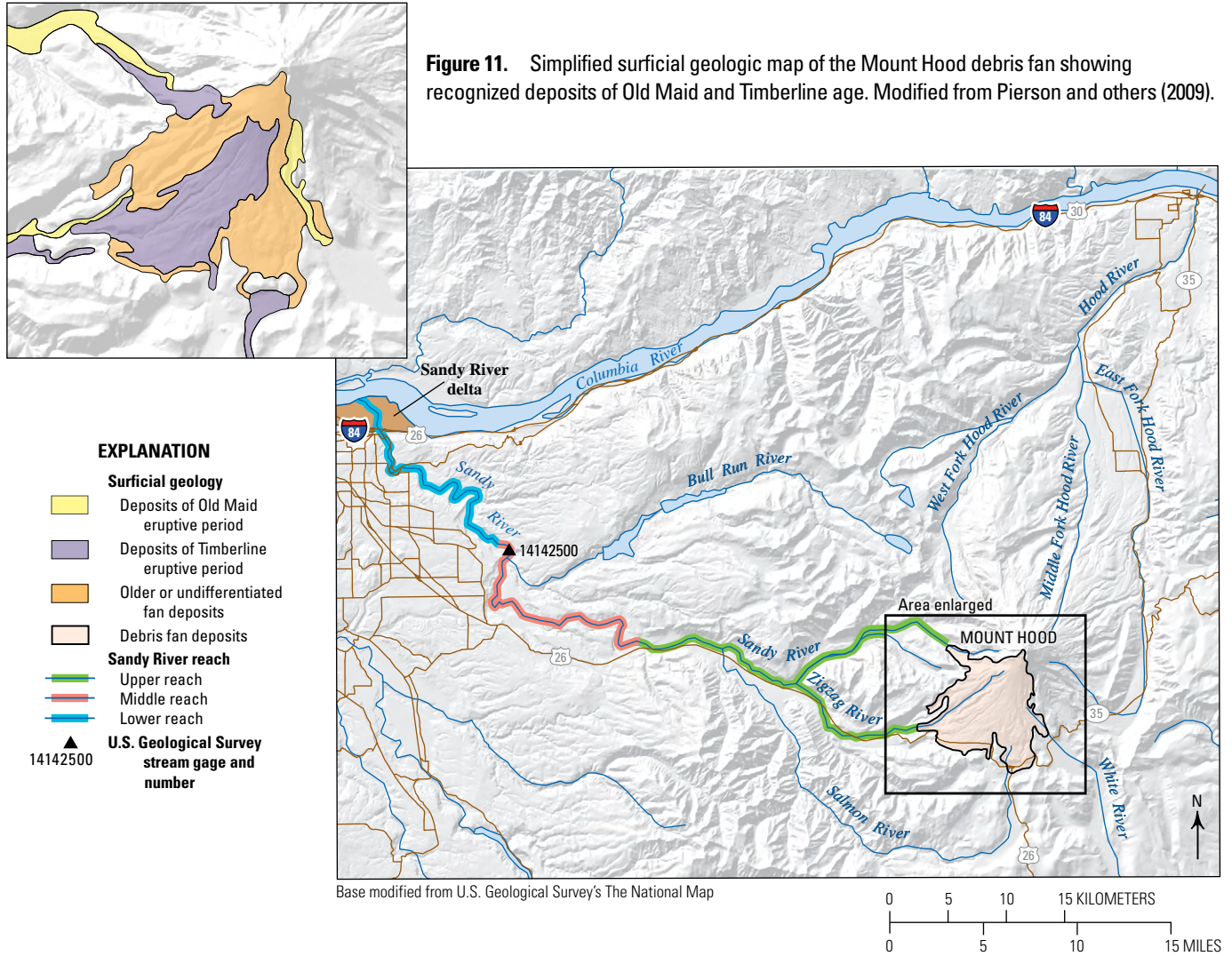


**Figure 11.** Simplified surficial geologic map of the Mount Hood debris fan showing recognized deposits of Old Maid and Timberline age. Modified from Pierson and others (2009).



**Figure 12.** Photographic examples of secondary lahar deposits originating as remobilized dome-collapse pyroclastic density current deposits in the upper Sandy River canyon. *A.* Timberline-age lahar deposit containing a large, prismatic block, indicating a dome-collapse origin for the block. Trenching tool shovel handle is 55 centimeters long. *B.* A thick pink-colored lahar deposit of Timberline age, overlain by a ~50-centimeter-thick gray lahar deposit of Old Maid age. USGS photographs by T.C. Pierson, 2005.

were generated by multiple gravitational collapses of a growing lava dome, as inferred from radial fracturing and microvesicular texture observed within many clasts in these deposits. Lahars were mobilized by water from rapid snowmelt mixing with the PDCs and probably also by heavy rain (Crandell, 1980; Cameron and Pringle, 1986; Scott, Gardner, and others, 1997; Pierson and others, 2011). Deposits of Timberline age are found in all of the rivers that drain the debris fan but are sparse in the White River drainage, suggesting that a topographic barrier blocked the head of the White River during this period (Scott, Gardner, and others, 1997). Timberline deposits within the fan itself are locally as thick as 100 m (Cameron and Pringle, 1986). The surficial distribution of Timberline deposits in the fan suggests that the source lava dome must have been at or very near the present site of Crater Rock on the upper southwest flank of the volcano.

The age of the Timberline eruptive period was originally defined from about 300 to 600 C.E., on the basis of four dated samples (Crandell, 1980). More recent unpublished dates have narrowed this range to a decades-long interval centered at about 450 C.E. (Scott and Gardner, 2017; W.E. Scott, written commun., 2016). Paleomagnetic data from the Mount Hood edifice, supported by stratigraphic and weathering evidence, suggest that Timberline eruptive activity was divided into two episodes separated by at least several decades (Scott, Pierson, and others, 1997; Scott and Gardner, 2017).

### Old Maid Eruptive Period

Another dome-building eruption occurred during the late 18th century Old Maid eruptive period, when about  $2 \times 10^8 \text{ m}^3$  dense-rock equivalent of hypersthene-hornblende dacite was extruded (Crandell, 1980). More than 90 percent of the extruded

magma was converted to fragmental debris and deposited on the flanks of the volcano by multiple phreatic explosions and dome-collapse lithic PDCs. About half of that debris was delivered to two headwater tributaries of the Sandy River.

Recent tree-ring dating, augmented by correlation of geochemical signatures from individual annual rings of trees affected by PDC ash clouds, indicates that Old Maid dome-building began in 1781 C.E. and lasted until 1793 C.E. (Sheppard and others, 2010; Pierson and others, 2011). Other tree-ring evidence suggests that a PDC occurred between 1795 and 1805 in the White River valley (Lawrence, 1948; Cameron and Pringle, 1987). Eyewitness accounts of minor explosions (possibly phreatic) were reported in 1859 and 1865 by early settlers (Scott, Gardner, and others, 1997), but a precise end to the Old Maid eruptive period has not been defined.

### Deposits in the Sandy River Drainage Basin

A variety of volcaniclastic sediments from Mount Hood are found in sequences of eroded fill terraces along the Sandy River. This river and its major sediment-transporting tributary, the Zigzag River, drain the northwestern part of the debris fan and the west flank of Mount Hood (fig. 12). The river is incised 100–500 m into late Tertiary bedrock and early to middle Quaternary volcanic sediments that were shed westward from the Cascades crest, forming the western piedmont of the Cascades at this latitude (Trimble, 1963; Sherrod and Scott, 1995). The river valley remains narrowly confined and relatively steep until just before it reaches its confluence with the Columbia River, about 87 km downstream (fig. 13). Here the Sandy River has built a 10 km<sup>2</sup> delta extending about 3 km into the Columbia River valley. Drainage area of the

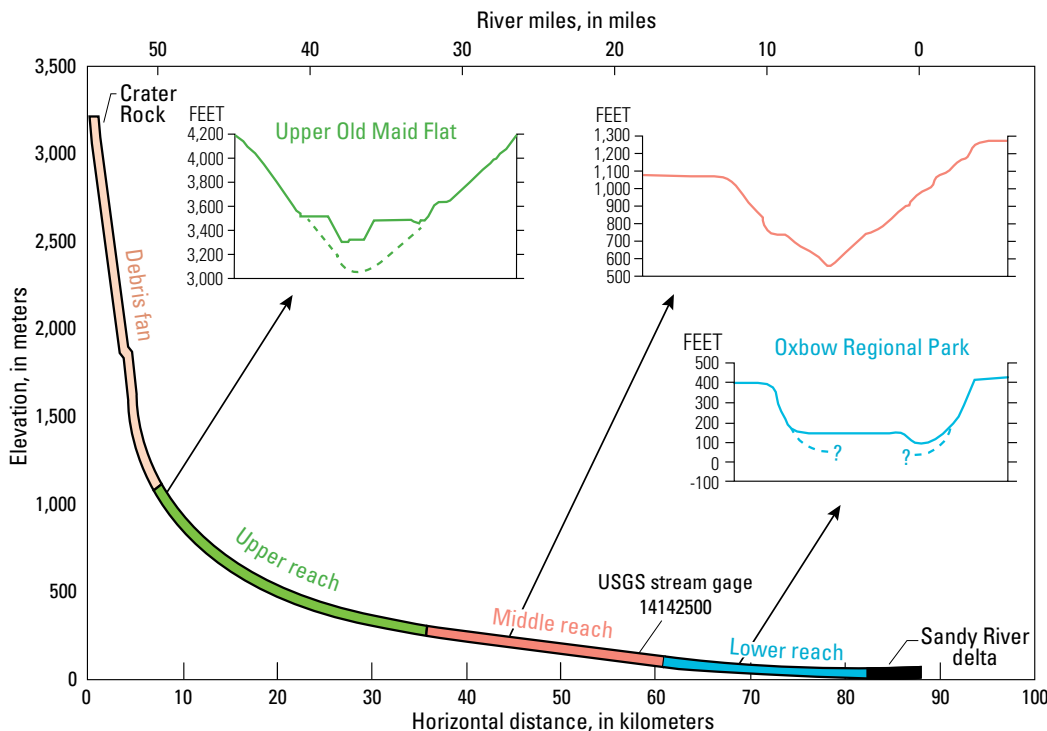
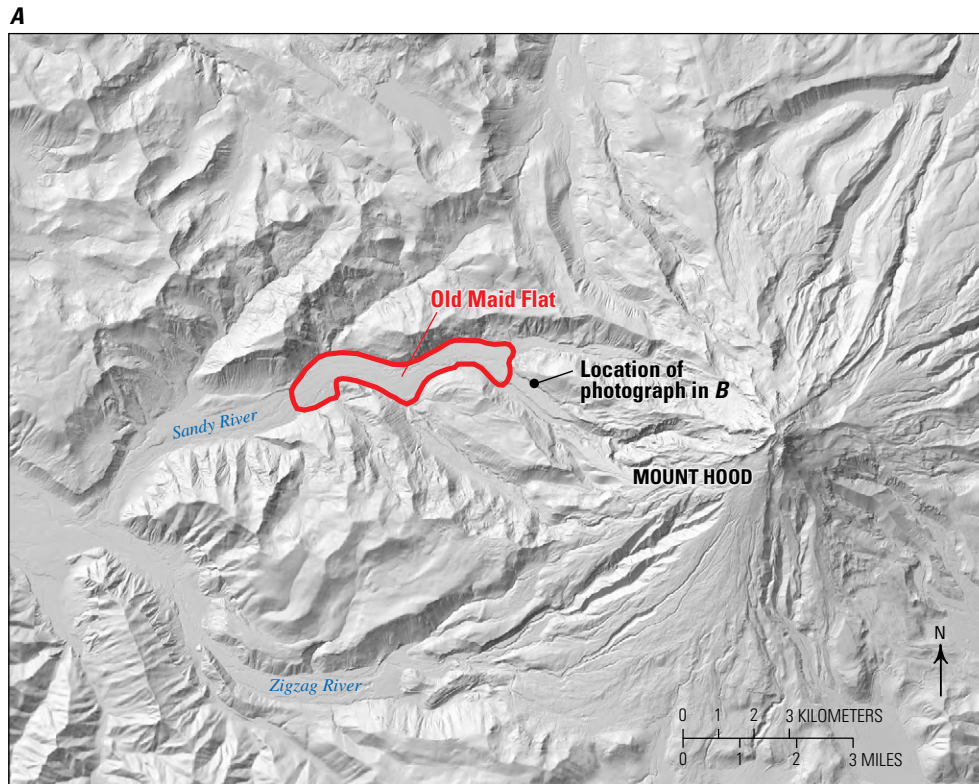


**Figure 13.** Longitudinal profile of the Sandy River channel, starting at Crater Rock—the source volcanic vent—and continuing downstream to the confluence with the Columbia River. The upper, middle, and lower reaches of the river (shown in fig. 11) are indicated and selected cross sections of the valley within each reach are shown. Profile derived from USGS 30-meter digital National Elevation Dataset and USGS 1:24,000 digital line graph. Vertical exaggeration is 9.3x. Modified from Pierson and others (2011).



Shaded relief from U.S. Geological Survey 3-meter light detection and ranging (lidar) data



**Figure 14.** Old Maid Flat, the main sediment source of the Sandy River. *A.* Shaded-relief map of the west flank of Mount Hood, with the wide, flat-floored valley known as Old Maid Flat outlined. Shaded relief from USGS 3-meter light detection and ranging (lidar) data. *B.* Photograph of a thick (40–60 meters) sediment-fill terrace in the upper part of Old Maid Flat, taken approximately from the location marked in *A.* View looks to the southeast. USGS photograph by T. Pierson, 2005.

Sandy River is about 1,130 km<sup>2</sup> upstream of a stream gage (USGS 14142500) located 58 km downstream from Crater Rock (fig. 13). Peak discharge of record at this gage (in 1964) is 2,390 cubic meters per second (m<sup>3</sup>/s). Mean annual flow was 66 m<sup>3</sup>/s prior to flow regulation in 1915.

Wedges of volcaniclastic sediment that thin downstream have accumulated in the heads of the Sandy and Zigzag Rivers since the late Pleistocene to a combined thickness of as much as 200 m (fig. 13), including some Polallie-age sediments that are mostly buried. Remnants of these valley fills have remained active sediment sources to the present time. They continue to provide above-normal sediment volumes to the Sandy River during winter storms, affecting bank stability and flood hazards along the river. The upper Sandy River sediment wedge is 16 km long; its slightly incised top surface forms a broad valley floor known locally as Old Maid Flat (figs. 13, 14). Sediments exposed in riverbanks at Old Maid Flat are dominated by lahar deposits and poorly sorted water-flood deposits of Old Maid age. Rapid deposition of these sediments engulfed standing forest trees, the evidence for which are numerous vertical shafts (tree wells) on Old Maid Flat that remain today after the wood rotted away. Most of the lahars recorded by deposits in Old Maid Flat did not travel much

farther than 20–30 km downstream. Only four Holocene lahars are presumed to have traveled the full 87 km from the vent to the Columbia River: three Timberline lahars documented on the delta (Rapp, 2005) and one Old Maid lahar that was at least 3 m deep a few kilometers upstream of the river mouth and recorded by a thin paleoterrace deposit (Pierson and others, 2011).

Volcaniclastic deposits downstream of Old Maid Flat in the Sandy River valley are dominated by lahar and volcano-fluvial deposits of Timberline age. The estimated bulk volume of fragmental material produced during this eruptive period is 1.0–2.0 km<sup>3</sup> (Scott and Gardner, 2017). Timberline lahar deposits (with a veneer of Old Maid-age deposits) now fill the entire Sandy River valley floor in the area from Wildwood to Welches (fig. 10). Large lahar-transported boulders still dot the flat valley floor in this zone.

Deposits in the lower Sandy River valley (60–84 km downstream) and in the Sandy River delta are composed mainly of volcano-fluvial sediments. At Oxbow Regional Park (~68 km downstream), an aggradational valley-fill sequence of Timberline age is as much as 30 m thick (fig. 15), whereas a similar sequence emplaced during the Old Maid eruptive period is at most 23 m thick (figs. 15, 16) (Pierson and others, 2009). Aggradation at this

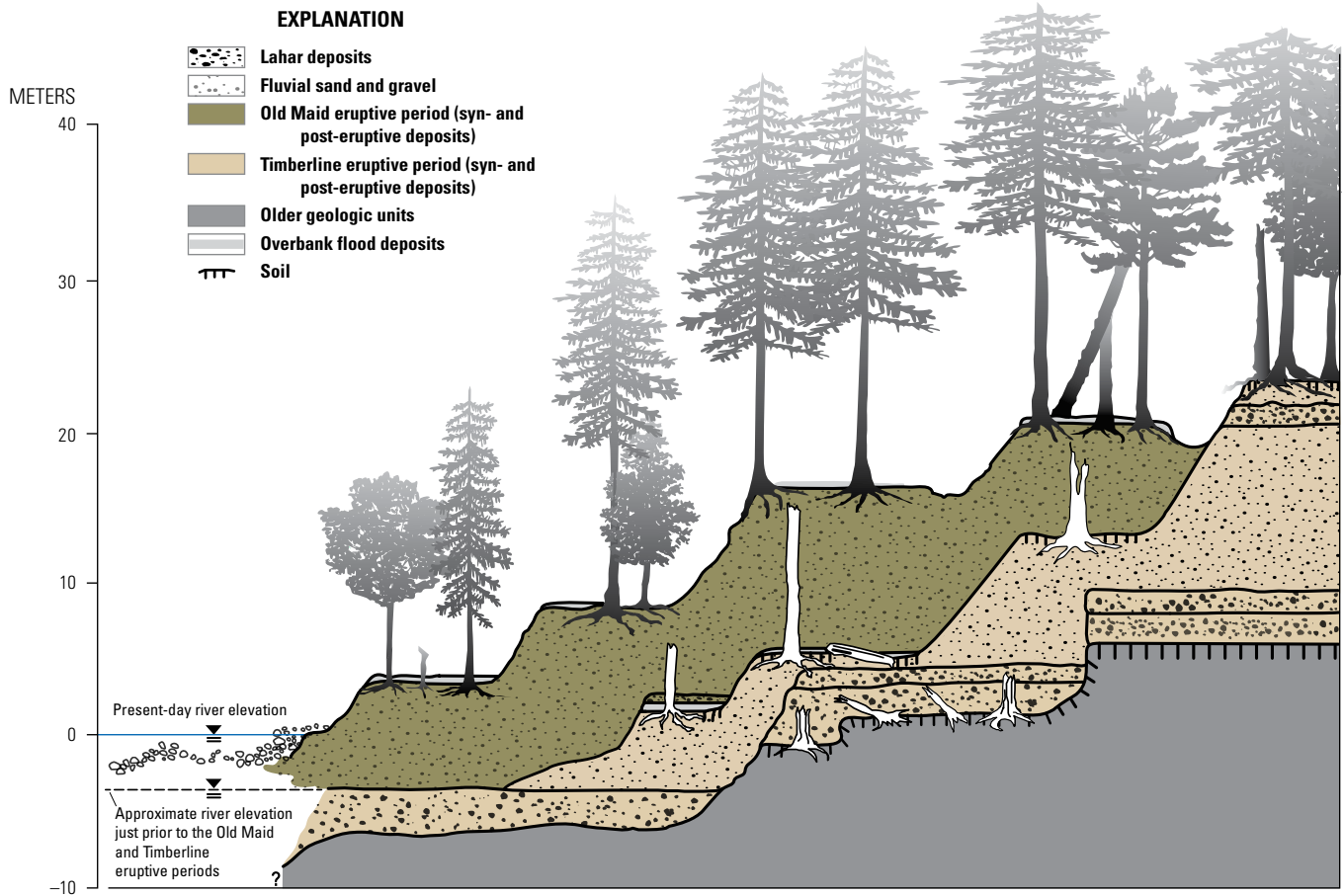


**Figure 15.** Schematic stratigraphic relations between Timberline- and Old Maid-age deposits along the Sandy River at Oxbow Regional Park. The figure depicts present and former channel levels, exposed terrace surfaces, buried paleoterraces, and buried forests 68–70 kilometers downstream of Mount Hood. Modified from Pierson and others (2009).



**Figure 16.** Photograph of sediment fill in the lower Sandy River valley at Oxbow Regional Park (67 kilometers downstream of Mount Hood), where an Old Maid-age aggradational sequence of volcaniclastic lahar and volcano-fluvial deposits can be seen on the riverbank. These deposits buried a forest that was growing on Timberline-age river terraces. The remains of trees killed in 1781 C.E. are still standing, recently exhumed by bank erosion. USGS photograph by T.C. Pierson, 2009.

site during both the Timberline and Old Maid eruptive periods was rapid enough to bury entire old growth forests before the wood in the trees could rot. During the Old Maid eruptive period when data on timing are available, aggradation during the 12-year period of dome growth averaged about 2 meters per year but was likely episodic and faster for short periods of time, presumably in response to major winter storms. On the delta, older aggradational volcano-fluvial units dating to about 5.0 ka have been found in drill cores (Rapp, 2005), but no volcanic activity of that age has been documented. Some high terraces in the lower Sandy River valley are formed of Polallie-age (late Pleistocene) volcaniclastic deposits (Everts and others, 2013).

## Deposits in the White River Drainage Basin

Significant volumes of volcaniclastic deposits of Polallie and Old Maid age are preserved on the steep upper flank of Mount Hood within the White River drainage. Lahar deposits of Old Maid age are also found in a low-gradient reach 65–70 km downstream of the vent (Tygh Valley). Only the steep upper reach of the river and the lower reach spanning from Tygh Valley to the Deschutes River confluence are easily accessible by foot because the river flows for much of its length through a remote and deeply incised canyon in which sediment transport dominates over deposition.

Debris flows and hyperconcentrated flows still regularly occur in the upper White River valley, mobilized during rainstorms by bank erosion and slope failures of the abundant loose volcaniclastic debris in headwater V-notch canyons (fig. 17). Multi-day, high-intensity storms generated by “atmospheric



**Figure 17.** Photograph of thick, incised sediment fill composed of pyroclastic density current and lahar deposits in the head of White River canyon. View is to the north from the Timberline Trail, a few miles east of Timberline Lodge. Canyon walls are composed mainly of Polallie-age deposits, locally capped by Timberline-age deposits. The lower level inset terrace, with its eroded surface sloping eastward, is composed of deposits emplaced during the Old Maid eruptive period. USGS photograph by T.C. Pierson, 2007.

“rivers”, such as occurred in February 1996 and November 2006, are particularly effective in generating high-concentration flows. In recent years, such events have caused channel aggradation that has episodically buried the Oregon Route 35 bridge in bouldery debris. These episodes have been costly for the Oregon State Department of Transportation in their efforts to maintain the bridge crossing. However, a few years ago the bridge was raised and extended laterally to facilitate debris passage and prevent blockage.

## Polallie-age Flow Deposits

Lahar and PDC deposits of Polallie age in the upper White River are remnants of a broad and discontinuous apron of late Pleistocene volcaniclastic debris. The current White River canyon cuts into this apron. Polallie-age deposition, synchronous with the Last Glacial Maximum at Mount Hood, did not emplace deposits on high-elevation valley floors, owing to occupation of the valleys by glacier ice that shielded their floors from direct deposition (Crandell, 1980). Some units of late Polallie age locally formed kame terraces at lower elevations as the glaciers shrank in size.

## Old Maid-age Flow Deposits

Inset within upper White River canyon walls (composed of Polallie-age deposits) are two sequences of volcaniclastic deposits comprising a set of Old Maid-age syneruptive lithic PDC deposits and lahars and a slightly younger set of Old Maid depositional units comprising only lahar deposits (Crandell, 1980) (fig. 17). Both sequences were formed by deposition from dome-collapse PDCs, snowmelt lahars, and subsequent rain-triggered lahars.



## Road Log and Description of Field-Trip Stops

This road log gives mileage and GPS coordinates for regular and optional stops associated with this field trip. Cumulative mileage is calculated for each day from the starting point given (number at left in log). Some of the optional stops require travel along spur roads off of the main trip route. The distances traveled for these spur routes are not included in the cumulative trip mileage.

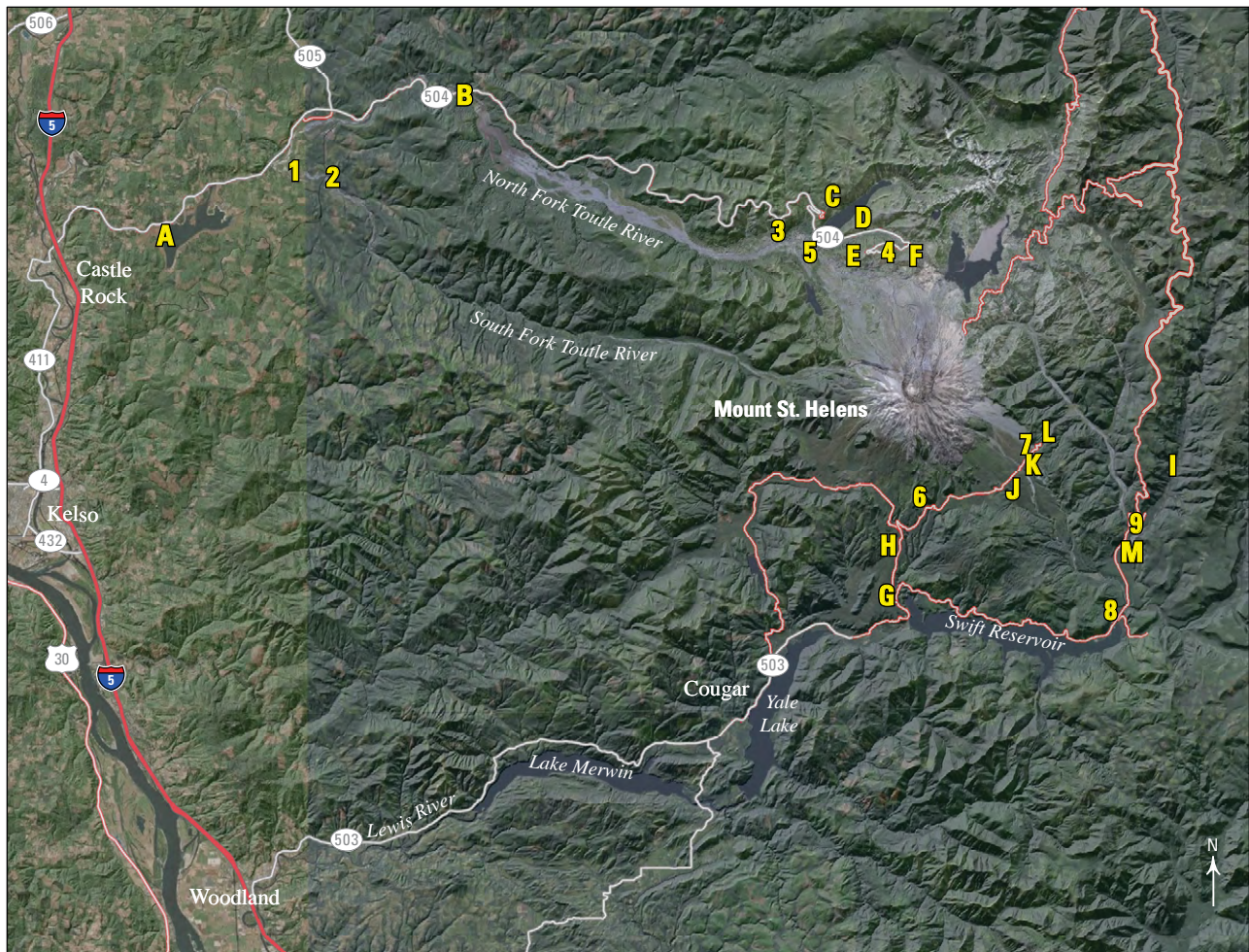
Some of the stops in this guidebook are on public land and require permits, such as a Northwest Forest Pass or seasonal Sno-Park Permit. Stops on private land may require permission for access. Such stops are noted in the log.

Snowfall in the Cascades arrives early and stays late. Owing to snow cover, many of the stops in this guidebook generally will not be accessible by vehicle from October to June, and it is advisable to check the current conditions prior to any trip during the spring or fall.

## Day 1: Debris-Avalanche and Lahar Deposits in the Toutle River Valley, Mount St. Helens

This field trip log begins in Castle Rock, Washington, although the 2017 IAVCEI field trip begins and ends in Portland, Oregon. From Portland, drive 1.75 hours north on Interstate 5. Take Exit 49 for Castle Rock off I-5 and turn right (to head east) at the traffic light at the end of the exit ramp. Continue east to the next traffic light. You are now at the intersection of Mount St. Helens Way NE, Dougherty Drive NE, and Old Pacific Highway North. Start your odometer here and begin traveling east on Mount St. Helens Way NE, which becomes State Route 504 (S.R. 504). Watch for a sign advising that the Mount St. Helens Visitor Center at Silver Lake and Seaquest State Park are ahead.

Day 1 field trip stops emphasize deposits of the 1980 eruption in the North Fork Toutle River (fig. 18). A more detailed map of stops proximal to the edifice shows the exposed 1980 debris-avalanche and pumiceous PDC deposits (fig. 19).

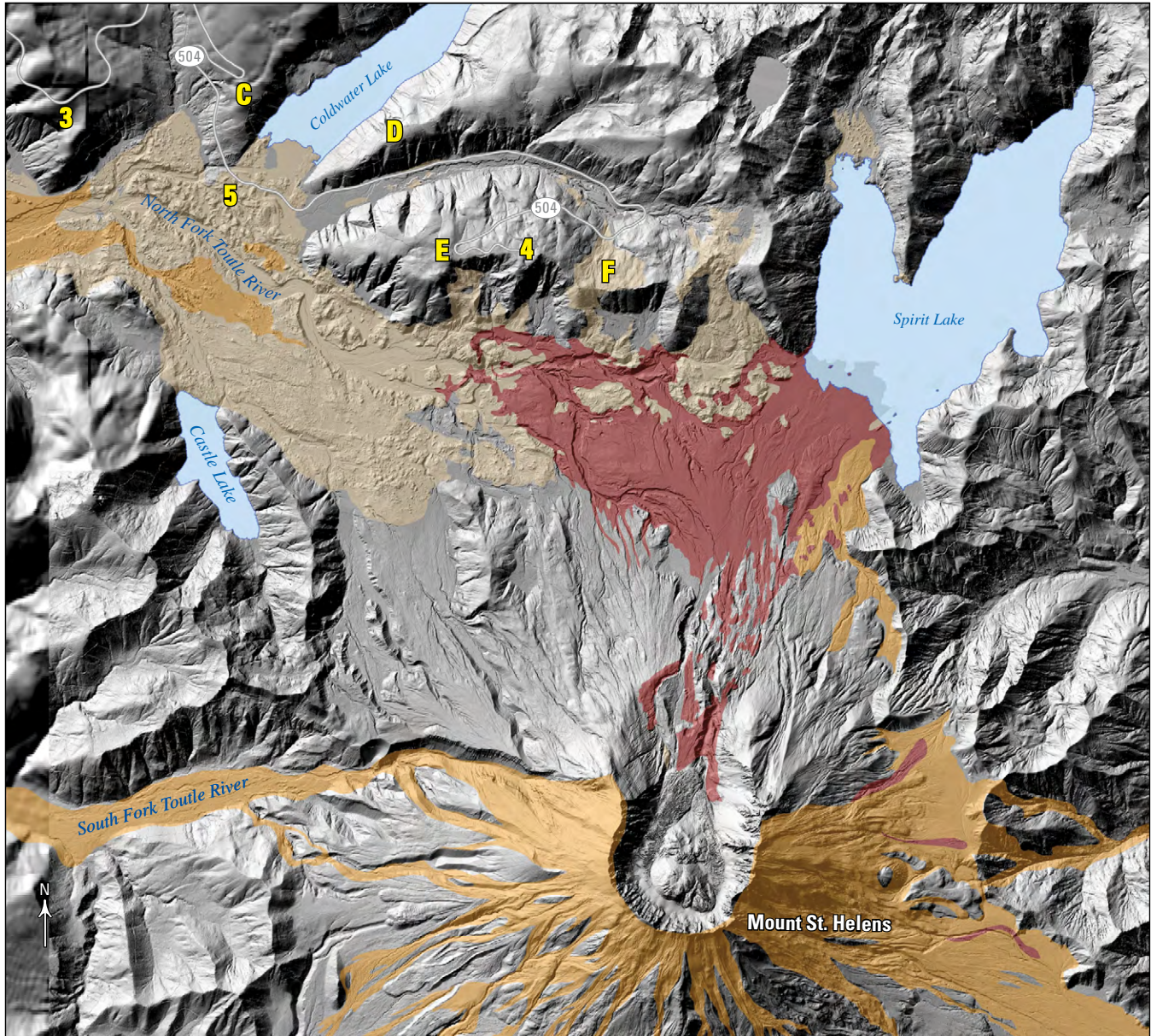


Base from U.S. Geological Survey (USGS) 30-meter Landsat imagery  
Shaded relief and roads from USGS's The National Map

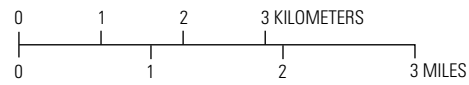
**EXPLANATION**  
**5** Field-trip stop—Number is planned stop; letter is optional stop

0 5 10 15 KILOMETERS  
 0 5 10 15 MILES

**Figure 18.** Map of locations of planned stops (numbers) and optional stops (letters) for the Mount St. Helens area on Days 1 and 2 of the field trip.



Shaded relief from 2009 U.S. Army Corps of Engineers  
light detection and ranging (lidar) data  
Roads from the U.S. Geological Survey's The National Map



**EXPLANATION**

- Debris-avalanche deposit
- May 18 and later pumiceous pyroclastic density current deposit
- May 18 lahar deposit—Overlies parts of the debris-avalanche deposit
- 5** Field-trip stop—Number is planned stop; letter is optional stop

**Figure 19.** Shaded-relief map of proximal volcaniclastic deposits at Mount St. Helens. Visible in the crater is the composite lava dome, extruded in 1980–1986 (northern third of dome) and again in 2004–2008 (southern two thirds of dome). Yellow numbers mark planned field trip stops and letters mark optional stops (as in fig. 18). Shaded relief from 2009 U.S. Army Corps of Engineers light detection and ranging (lidar) data; roads from the USGS National Map.

0.0 Head east on Mount St. Helens Way NE from the intersection with Dougherty Drive NE and Old Pacific Highway North.

**5.1 Optional Stop A—Mount St. Helens Visitor Center at Silver Lake (lat 46.2952° N, long 122.8228° W)**  
Pull off at the Mount St. Helens Visitor Center at Silver Lake on the right side of the road. This was the original Mount St. Helens visitor center before others were constructed closer to the volcano. It is now part of a Washington State park and contains exhibits focusing on the 1980 eruption. A boardwalk trail provides access to Silver Lake, with views of Mount St. Helens in the distance (fig. 20). This lake, 12 km<sup>2</sup> in area but only 1–3 m deep, was formed when deposits from two huge Toutle River lahars blocked a broad tributary valley about 2.6 ka during the Pine Creek eruptive period. The lake is drained by Outlet Creek, and lake level is controlled for the convenience of the large number of homes along the lakeshore. From the north shore of the lake the field trip route continues for about 15 miles (mi; 24 km) on the surface of this extensive lahar deposit.

When you are finished at this stop, turn right out of the parking lot onto S.R. 504 and continue traveling east. When you enter the town of Toutle, watch for your next turn, which will be shortly after passing the school on the north side of the road.

10.4 Turn right onto South Toutle Road. Your next turn is just on the left.

**10.5 Stop 1—Pine Creek-age lahars at Outlet Creek (lat 46.3238° N, long 122.7299° W)** Turn left into the recycling center and follow the access road until it begins to loop around to the east. Park your car at the end of the access road. Walk about 200 ft east through the forest to the edge of Outlet Creek to view exposures of Pine Creek-age lahars. The outcrop is located at lat 46.3241° N, long 122.7280° W.

Outcrops on the north side of Outlet Creek expose three Pine Creek-age lahar deposits PC1, PC2, and PC3. Based on estimated peak flows, PC1 and PC3 were the largest and second largest Holocene lahars from Mount St. Helens, respectively (Scott, 1988a, 1988b, 1989). The PC1 lahar had a peak discharge of 200,000–300,000 m<sup>3</sup>/s (approximate average discharge of the Amazon River) and was about 30 m deep at distances of 30–50 km from the volcano (fig. 21) (Scott, 1988b, 1989). Such a flow rate places it among the world's largest floods (O'Connor and Costa, 2005). The only water source large enough to produce such large lahars would have been outbreak floods from precursors to Spirit Lake—the lake repeatedly formed



**Figure 20.** Historical photographic view of Silver Lake with the snow-capped pre-1980 cone of Mount St. Helens in the distance, 50 kilometers to the east-southeast. Photograph by J. Boyd Ellis.

by debris-avalanche dams blocking off a small basin on the north side of Mount St. Helens (Hausback and Swanson, 1990; Hausback, 2000). A debris-dammed ancestral Spirit Lake as the source for the Pine Creek-age lahars is also inferred from (1) abundant well-rounded river cobbles and pebbles that show large-scale entrainment of sediment from the Toutle River bed (such sediment entrainment is common in massive turbulent water floods), and (2) megaclasts of hydrothermally altered dacite in the lahar deposits (indicating erosion of a debris-avalanche deposit). Thus, the Pine Creek-age deposits (figs. 22, 23) show what might have happened if the current Spirit Lake, dammed in 1980, had not been engineered to prevent overtopping of the 1980 blockage.

Deposits from the PC1 and PC3 lahars at Stop 1 (and nearby) show that the lake-outbreak floods entrained sufficient sediment to form debris flows. PC1 deposits in this area are as much as 6–8 m thick and locally contain large fragile clasts of the unconsolidated debris-avalanche deposit that formed the lake blockage. Farther downstream, the flows transformed to hyperconcentrated lahars. Throughout this area “tree wells” (fig. 24) can be found marking where trees on terraces were encased by lahar deposits but remained upright. Subsequent decay of the wood left vertical shafts that provided preferred pathways for tree roots.

When you are finished at the site, return to the car and depart the recycling center parking lot. Turn left onto South Toutle Road. When you cross the bridge over the South Fork Toutle River, you are close to your next turn (5 minute drive).

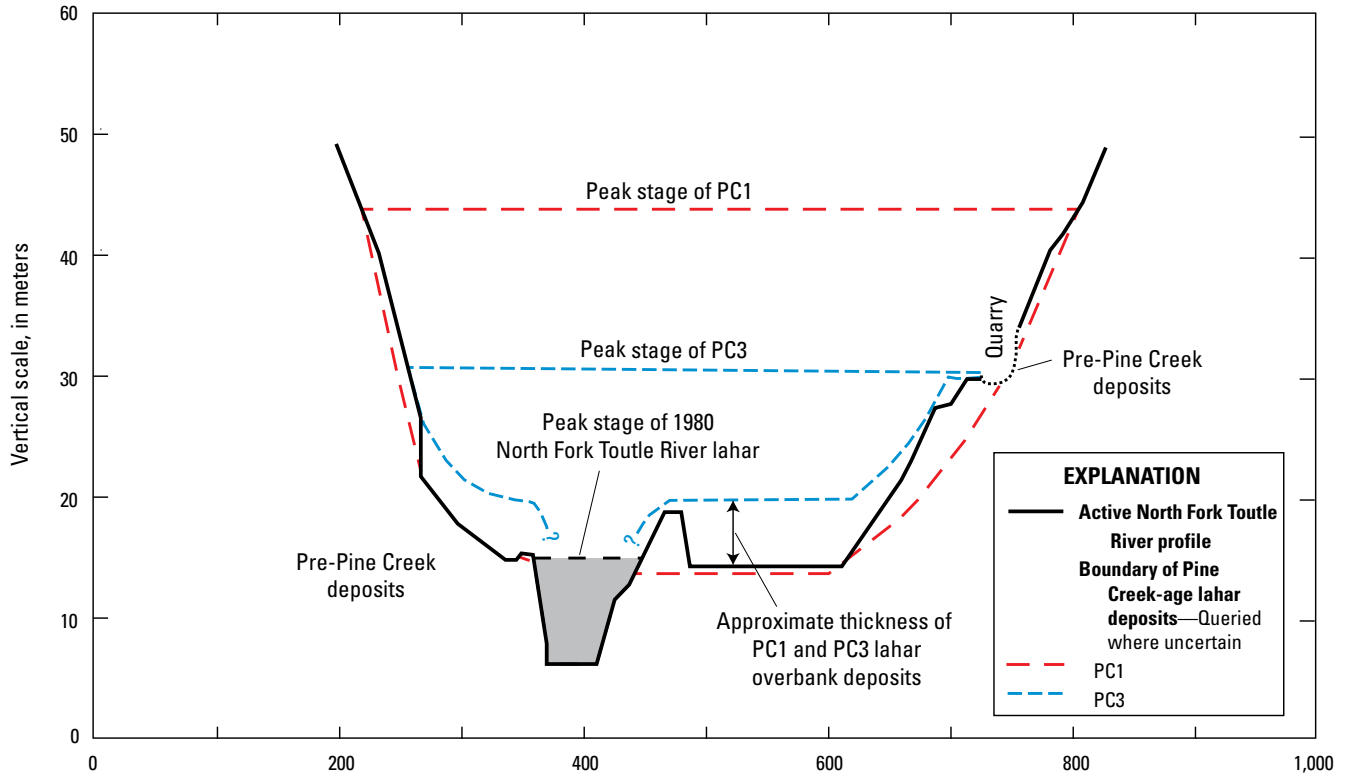


**Figure 21.** Reconstructed lahar-flow cross sections at peak discharge (assuming synchronicity with peak stage) of lahars PC1 and PC3 in the North Fork Toutle River valley at Kid Valley, 10 kilometers northeast of Stop 1. The cross section of the May 18, 1980, lahar is shown for comparison in gray. Modified from Scott (1989).

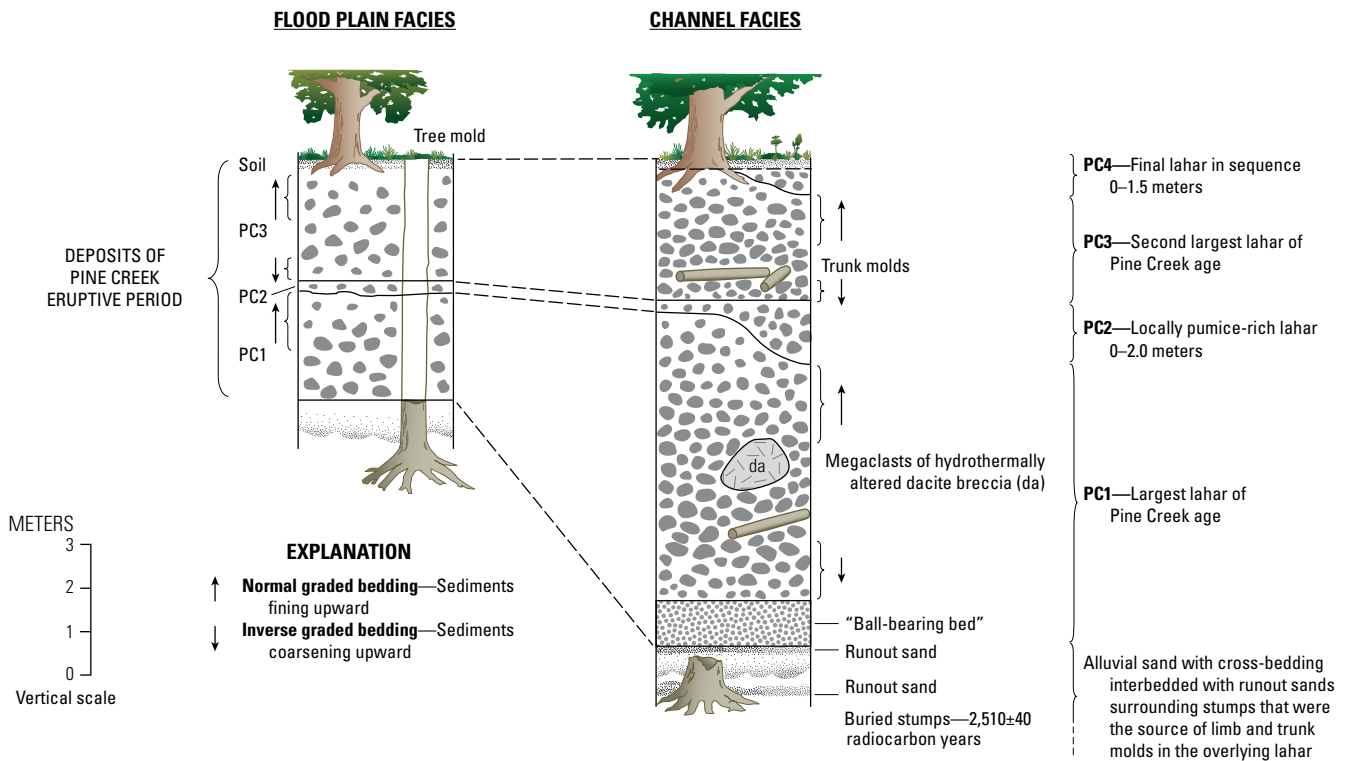


**Figure 22.** Pine Creek eruptive period stratigraphy based on 1980–83 exposures in the North Fork Toutle River valley about 2 kilometers northeast of Stop 1. Both flood plain and channel facies are shown. Note the vertical tree mold (“tree well”) formed in the flood plain facies. Modified from Scott (1988a).

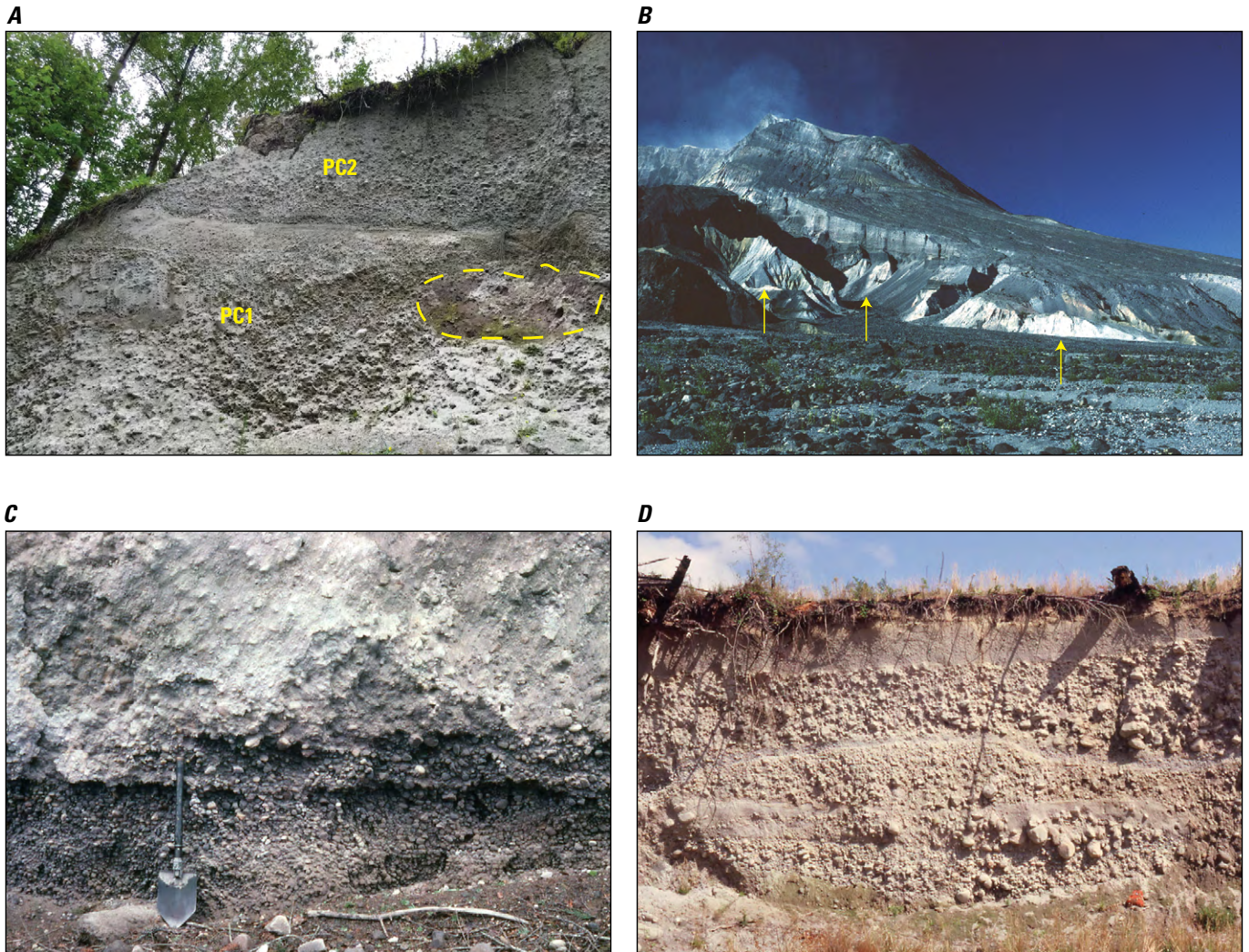


**Figure 23.** Photographs of Pine Creek-age deposits. *A.* Lahar deposits PC1 and PC2 formed by breakouts of the ancestral Spirit Lake at Outlet Creek 2,600 years ago (Stop 1). Clast roundness is notable, indicating origin by entrainment in a water surge. Exposure is on the bank of Outlet Creek, where the lahars dammed and created Silver Lake. Note the 2-meter-wide pink fragile clast of the lake-damming debris-avalanche deposit (outlined) at right in PC1. USGS photograph by K.M. Scott, 2016. *B.* Two Pine Creek-age debris-avalanche deposits (white deposits indicated by arrows) exposed in the incised north flank of Mount St. Helens. The upper deposit probably dammed Spirit Lake and was breached by breakout floods that transformed into the PC1 lahar. USGS photograph by C.J. Harpel, 2003. *C.* Fines-depleted basal section “ball-bearing” bed of the PC1 lahar channel facies deposit on the North Fork Toutle River about 2 kilometers upstream of the South Fork confluence (eroded gravel-rich unit behind shovel; handle is 55 centimeters long). High shear and clast crushing are inferred from the “ball-bearing bed” (Scott, 1988a). USGS photograph by K.M. Scott, 1981. *D.* Lenticular structure in coarse-grained unit at the top of the PC1 lahar deposit protrudes into the PC3 deposit above, which is capped by the finer grained PC4 lahar deposit at the top of the section. Location along North Fork Toutle River near Pullen Creek (PC2 is missing at this locality). Orange backpack for scale. USGS photograph by K.M. Scott, 1981.



**Figure 24.** Photograph of vertical tree mold encased by flood plain facies of PC1 and PC3 lahar deposits (shovel at contact). A horizontal log mold is visible in the upper right. Some trees were encased by deposits of the PC1 and PC3 lahars, indicating that these lahars (plus PC2) occurred in relatively quick succession—before the dead vertical snags of those trees could decay and topple. Tree molds, often filled with loosely compacted material, are easily penetrated by modern tree roots. USGS photograph by K.M. Scott, 1982.

- 11.8 Turn left onto Fiest Road. Harry Gardner Park is to your left.
- 12.1 Stop 2— North and South Fork Toutle River lahar deposits at Harry Gardner Park (lat 46.3247° N, long 122.7076° W)** Turn left into Harry Gardner Park and park your vehicle at the west end of the parking lot. From the parking lot, walk about 450 ft down to the river's edge. Walk downstream along the river, looking for good exposures of 1980 lahar deposits in the cutbank.

The 1980 South Fork Toutle River lahar was triggered by rapid snowmelt at about 8:33 a.m., a minute after the start of the May 18 eruption. This flow began as a PDC, entrained meltwater from scoured snow and transformed to a highly concentrated lahar (debris flow), then became more dilute through incorporation of river water, likely transforming abruptly to hyperconcentrated flow when it joined the North Fork of the river (fig. 25). It traveled 49.8 km to the confluence of the North Fork and South Fork Toutle Rivers in less than 2 hours, arriving at this location at about 10:20 a.m. (Cummans, 1981). Mean peak flow velocity near the source was estimated to be about 28 m/s; in the lower South Fork Toutle River, it was about 7 m/s (Fairchild, 1985). The harrowing account of two people caught and transported downstream by this lahar (and survived) can be found in Waitt (2015, p. 198–201). The larger North Fork Toutle River lahar did not arrive at this site until about 5:50 p.m. (Cummans, 1981).

South Fork Toutle River lahar deposits vary in mean grain size from 0.61 mm in the upstream reach to 0.31 mm in the downstream reach. Sorting varies from 3.3 to 2.8 $\sigma$ . Fines contents range from 11–20 weight percent silt and 2–3 weight percent clay. Nearly continuous exposures of South Fork Toutle River lahar deposits, overlain by North Fork Toutle River lahar deposits, can be seen in high cutbanks north of Harry Gardner Park (fig. 26). The park's namesake, Harry Gardner, constructed Spirit Lake Lodge for Harry Truman, who was a media favorite for his newsworthy refusal to leave his lodge prior to the May 18 eruption (Waitt, 2015). Here, the South Fork Toutle River lahar deposit is as much as 2 m thick and was deposited by a flow in transition between debris flow and hyperconcentrated flow. Note the angularity of coarse clasts in the South Fork Toutle River lahar in contrast with the rounded clasts in the Pine Creek lahar deposits viewed at Stop 1. The recognition in 1980 of hyperconcentrated flow deposits as a downstream “runout facies” of debris-flow lahars was first made in a study of the South Fork Toutle River lahar deposits here by Scott and others (2002).

The larger 1980 North Fork Toutle River lahar (fig. 27) began in the early afternoon of May 18 and lasted 11 hours (Cummans, 1981; Janda and others, 1981; Fairchild, 1985). Flow volume was about 0.14 km<sup>3</sup> downstream of the debris-avalanche deposit and it was nearly that large (0.12 km<sup>3</sup>) when it reached the Toutle and Cowlitz River confluence, approximately 60 km from its source—a liquefaction zone on the avalanche deposit. It had a single broad flow peak that lasted about 2.5 hours (fig. 28); near-source peak discharge was about 7,200 m<sup>3</sup>/s, which slowed to about 6,000 m<sup>3</sup>/s at the mouth of the Toutle River (Fairchild, 1985). The North Fork Toutle River lahar flowed as a fully developed

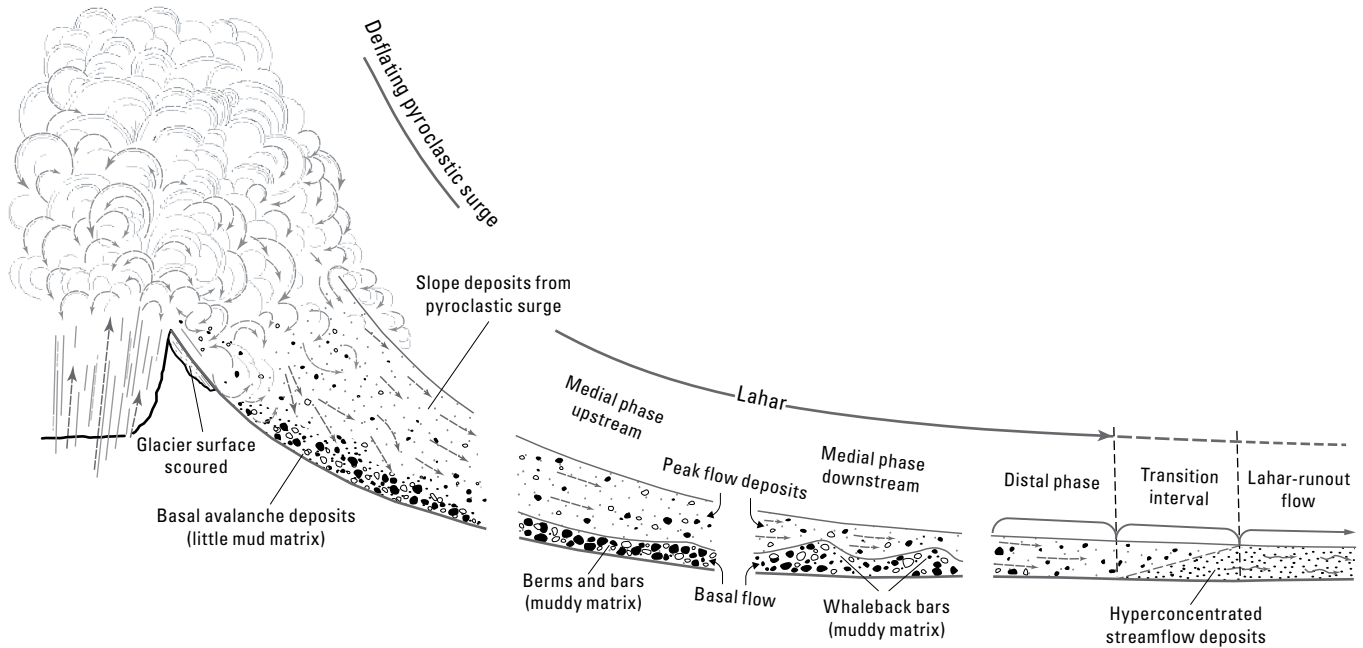


**Figure 25.** Conceptual diagram of origin and transformation of the South Fork Toutle River lahar. The flow likely started as a concentrated pyroclastic density current and transformed first to a debris flow, through entrainment of snow and ice, then gradually to hyperconcentrated flow, through dilution farther downstream (with major dilution at the North Fork Toutle River confluence), and ultimately to a surge of muddy water following wholesale mixing with river water at the confluence with the Cowlitz River (72 kilometers downstream from the volcano’s new crater). Modified from Scott (1988a).

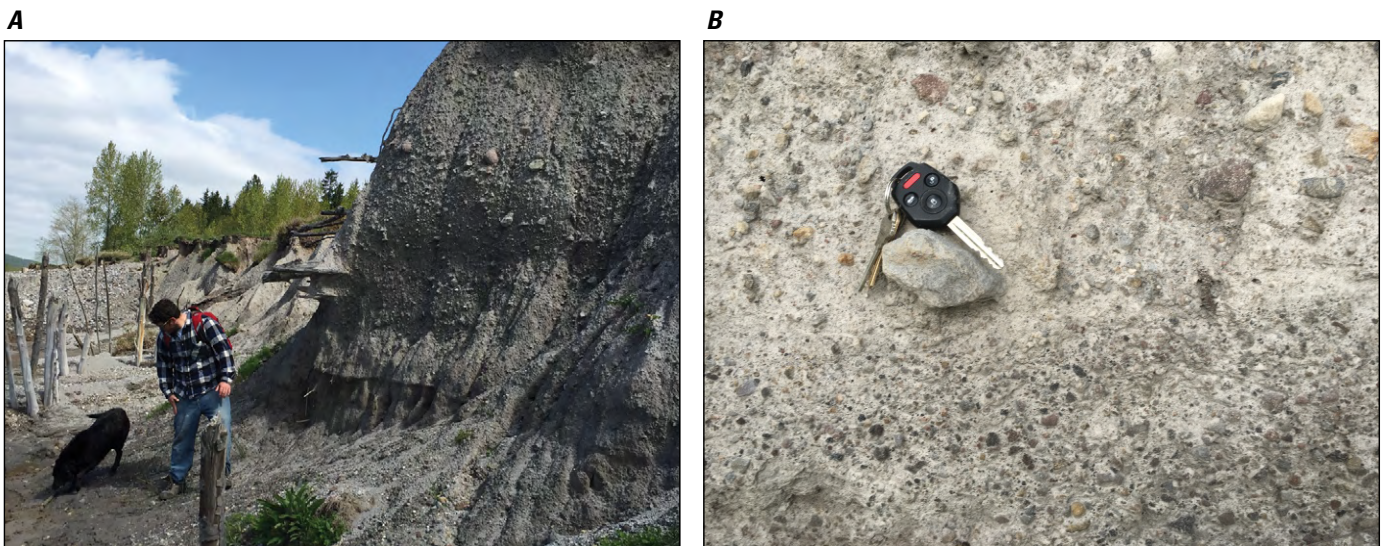


**Figure 26.** Photographs of lahar deposits at Harry Gardner Park (Stop 2). *A.* The North Fork Toutle River lahar deposit (with protruding horizontal logs) overlies the South Fork Toutle River lahar deposit. The North Fork Toutle River lahar flowed some distance up the South Fork Toutle River. The contact is even with the man’s waist, at the center of the photograph. *B.* Closeup photograph of the contact, located just below the keys and coarse clast. Note that the underlying South Fork Toutle River lahar is finer grained and better sorted than the overlying North Fork Toutle River lahar. USGS photographs by K.M. Scott, 2016.

**Figure 27.** Aerial photographic view of the North Fork Toutle River lahar on the afternoon of May 18, 1980. This photograph was taken at the moment the lahar pushed the State Route 504 bridge off its support piers. The location is just downstream of the North and South Fork Toutle River confluence. The bridge deck was never found. Photograph by Roger Werth, The Daily News (Longview, Wash.), copyright 1980.

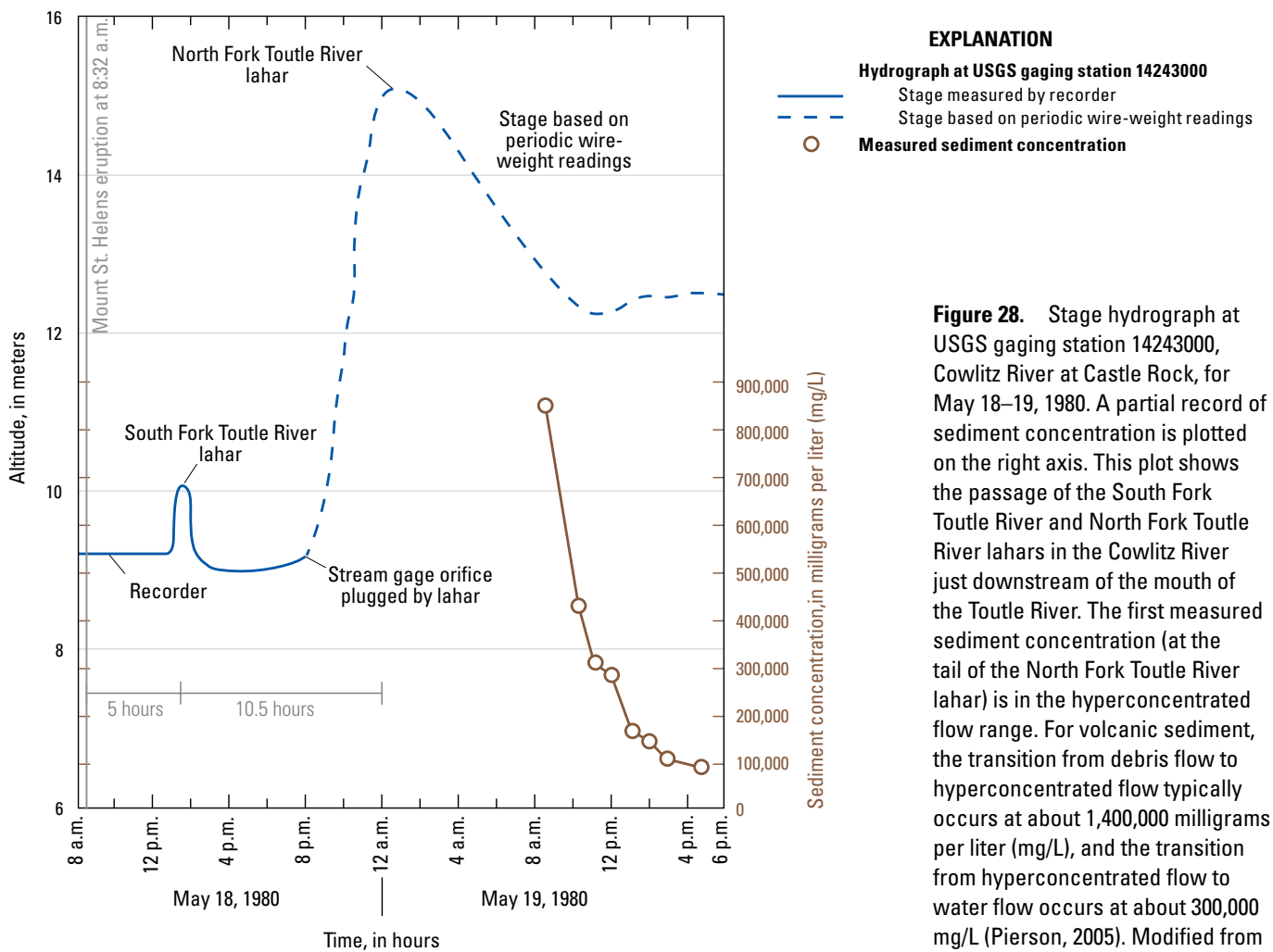


**Figure 28.** Stage hydrograph at USGS gaging station 14243000, Cowlitz River at Castle Rock, for May 18–19, 1980. A partial record of sediment concentration is plotted on the right axis. This plot shows the passage of the South Fork Toutle River and North Fork Toutle River lahars in the Cowlitz River just downstream of the mouth of the Toutle River. The first measured sediment concentration (at the tail of the North Fork Toutle River lahar) is in the hyperconcentrated flow range. For volcanic sediment, the transition from debris flow to hyperconcentrated flow typically occurs at about 1,400,000 milligrams per liter (mg/L), and the transition from hyperconcentrated flow to water flow occurs at about 300,000 mg/L (Pierson, 2005). Modified from Scott (1988a).



debris flow about 90 km to the Columbia River, where it deposited 34–36 million cubic meters of sand and gravel over a reach of more than 10 km and reduced the depth of the Columbia River navigational channel from 12 m to 4 m (Schuster, 1981; Hubbell and others, 1983; Fairchild, 1985). Most of this deposition occurred upstream of the Cowlitz River mouth, where it was carried on an incoming tide. Peak flow velocities varied from 6 to 12 m/s over the total flow distance, although the lahar “flood wave” progressed downstream at only 1.5 to 2.1 m/s (Fairchild, 1985). Typical flow depths ranged from 5 to 8 m, although depths increased to as much as 18 m at channel constrictions (Fairchild, 1985). Back-calculated peak sediment concentration of the lahar was about 65 percent by volume; near the tail of the flow hydrograph, sediment concentration was about 50 percent by volume (Fairchild, 1985) (fig. 28). One sample—collected just upstream of the mouth of the Toutle River at 8:45 p.m. on May 18—had a measured sediment concentration of 67 percent by volume (Scott, 1988a).

Deposits of the North Fork Toutle River lahar have textures indicating that, at its peak, the lahar never transformed from debris flow to hyperconcentrated flow. This probably is owing to the relatively high concentration of fine sediment in the debris mixture—19–28 weight percent silt and clay, of which 3–5 weight percent is clay (Scott, 1988a). Mean grain size of matrix samples decreases slightly from about 0.8 mm to about 0.2 mm (particle size value of 0.2 to 2.0 $\phi$ ), and sorting increases progressively from 4.4 to 2.9 $\sigma$  along the 90-km flow path of the North Fork

Toutle River lahar. Outcrops of this deposit appear as massive, highly consolidated gravelly muddy sand along its full flow path (fig. 29).

- 13.8 Turn right onto S.R. 504.
- 14.3 Coal Bank Bridge. This bridge replaces the original S.R. 504 bridge that was destroyed by the 1980 North Fork Toutle River lahar (fig. 27). At least 35 lahars spanning the Pleistocene and Holocene history of Mount St. Helens have reached the Coal Bank Bridge area, which is about 55 km downstream of Spirit Lake and the volcano. Excellent exposures of lahar deposits upstream of the bridge have in recent years been obscured by vegetation growth and failure of cliff faces.
- 20.5 Kid Valley bridge. This is the only bridge over the North Fork Toutle River that survived the 1980 lahar. After passing through Kid Valley (last service station on S.R. 504) the road begins climbing in elevation. Watch for the sign that advises the sediment retention structure turnoff is approaching.
- 24.3 **Optional Stop B—Sediment Retention Structure (lat 46.3641° N, long 122.5595° W)** Turn right onto Stewart Dam Road and follow until it ends in a parking lot (0.9 mi). A short trail leads to a viewing platform.  
In an effort to keep massive volumes of volcanoclastic sediment from washing into the lower Toutle and Cowlitz Rivers, the U.S. Army Corps of Engineers (USACE) constructed a special type of dam

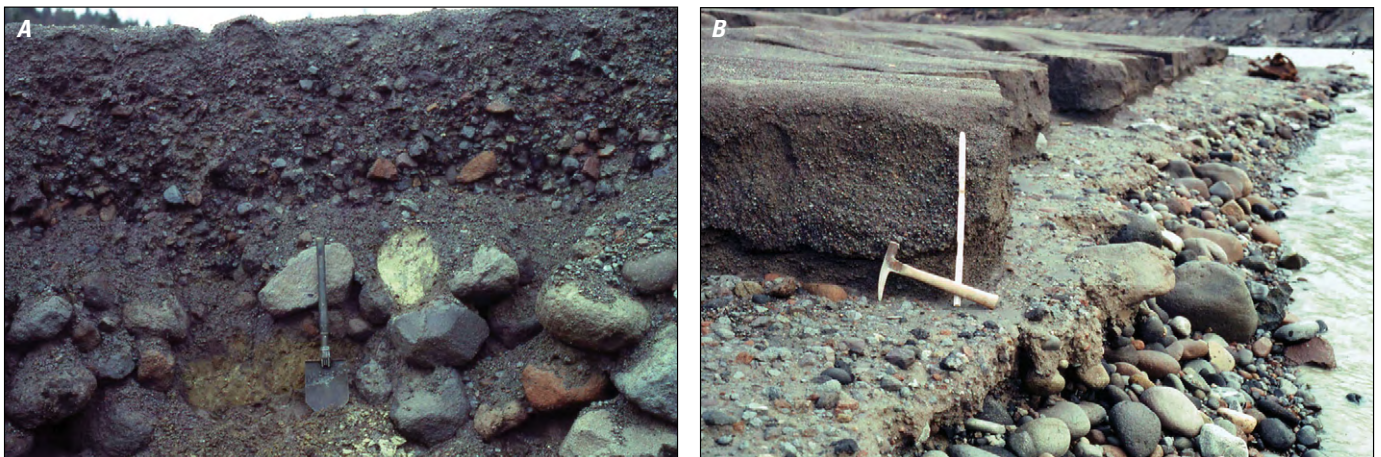


**Figure 29.** Photographs of North Fork Toutle River lahar deposits. *A.* Clast-supported boulder bar in the North Fork Toutle River lahar deposit at the confluence of the two Toutle River forks (near Stop 2). A more fine-grained lahar deposit caps the core of the boulder bar. The high degree of rounding in several boulders attests to the entrainment of stream alluvium in these lahar deposits. Trenching shovel handle is 55 centimeters long. *B.* Fine-grained channel facies of the North Fork Toutle River lahar near Kid Valley. Rounded pre-lahar pebble/cobble alluvium is overlain by a resistant, light-colored “sole layer” at the base of the lahar deposit, with an average thickness of 20 centimeters (layer on which the hammer rests). The dark fine-grained lahar deposit behind the folding ruler (extended 48 centimeters) slopes down from the crest of a whaleback bar, which is partly visible in the upper left corner of the photograph. USGS photographs by K.M. Scott, 1980.

that traps sediment but allows water to pass through to the upper North Fork Toutle River basin (Major and others, 2009). The 550-m-long and 56-m-high, earthen-cored sediment retention structure began trapping sediment in 1987 and construction was completed in 1989 (fig. 30). By 2000 the structure had trapped about 100 metric tons (t) of sediment—about 30 percent of design capacity. However, by then, progressively larger amounts of sediment were passing over the spillway and reducing trap efficiency. In 2013 the spillway was raised 2.1 m in order to improve sediment trapping efficiency. When you are finished, return to S.R. 504, turn right, and continue traveling east.

32.8 Hoffstadt Creek bridge and margin of the devastated zone. One of the highest bridges in Washington State (113 m [370 ft]), the bridge crosses Hoffstadt Creek

near the western limit of the 1980 PDC (lateral blast) deposit, which is 25 km from the volcano. Replanted forests beyond this point obscure evidence of the devastated zone. Also, outside of Mount St. Helens National Volcanic Monument, most tree blowdown was removed by salvage logging in the years following the 1980 eruption.

43.4 **Stop 3—Castle Lake viewpoint (lat 46.2968° N, long 122.2992° W)** Pull into the Castle Lake viewpoint on the right side of the road for a view up-valley towards Mount St. Helens. Castle Lake viewpoint provides an excellent view of the volcano and the 1980 deposits that fill the North Fork Toutle River valley (Major and others, 2009) (fig. 31). Hummocky debris of the 1980 debris avalanche fills much of the valley and blocks local drainages, forming Castle Lake to the south-southeast and Coldwater Lake

**Figure 30.** Photograph of the 575-meter-wide sediment retention structure (SRS) on the North Fork Toutle River. The structure is located 35 kilometers downstream from Mount St. Helens, which is visible in the background, in the North Fork Toutle River basin. The SRS was designed to trap nearly 200 million cubic meters of sediment and nearly reached capacity by 2012, after which the spillway was raised slightly to extend the lifespan of the sediment trap. USGS photograph by A.R. Mosbrucker, 2012.

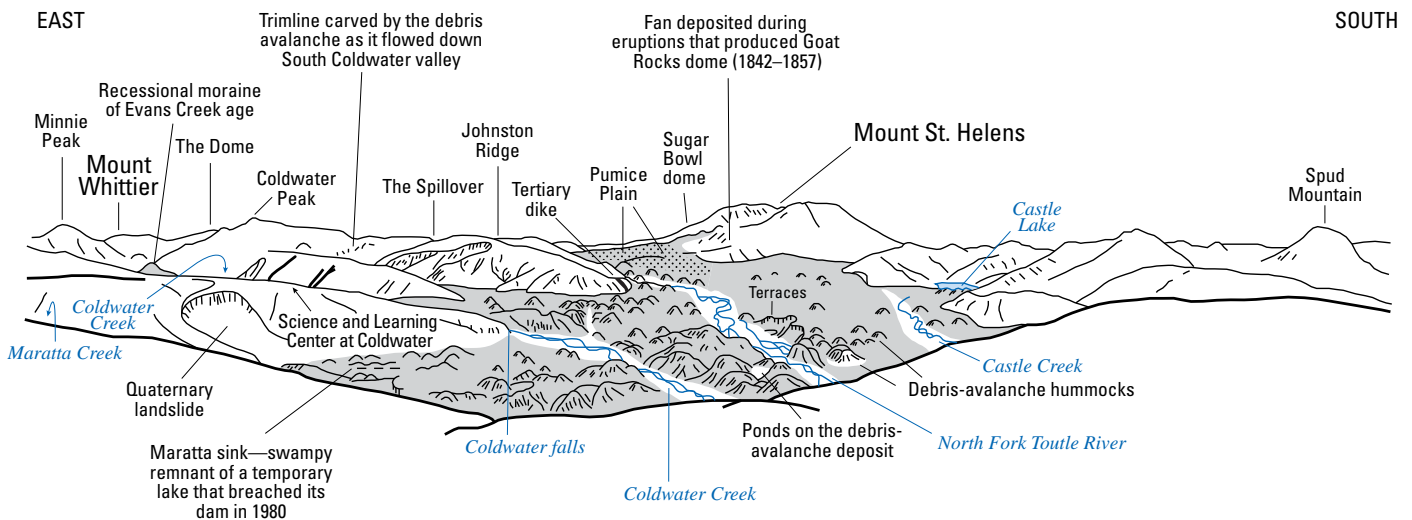


**Figure 31.** Sketch of features visible from Castle Lake viewpoint. Modified from Pringle (2002).

behind the ridge in the east (where the Science and Learning Center at Coldwater is visible). Concern about potential rising waters overtopping and rapidly eroding these unconsolidated barriers and producing catastrophic floods prompted the USACE to create armored spillways for both Castle and Coldwater Lakes.

Johnston Ridge to the southeast divides the North Fork Toutle River from South Coldwater Creek. The 1980 debris avalanche had sufficient momentum to overtop Johnston Ridge at two locations, climbing as much as 380 m above the valley floor and flowing into the valley of South Coldwater Creek before merging with the main body of the avalanche in the North Fork Toutle River valley.

This viewpoint is perhaps one of the best locations to view the spatial distribution of the 1980 debris-avalanche deposits and to understand their kinematics. The first few seconds of the catastrophic edifice collapse were captured in a series of dramatic photographs by Gary Rosenquist and permitted analysis of the movement of discrete slide blocks and onset of the lateral blast (Voight and others, 1981) (fig. 32). The distribution of debris-avalanche deposit components relates directly to the collapse and flow kinematics (fig. 33) (Voight and others, 1981; Glicken, 1996). The initial failure of slide block I involved material from the upper edifice—primarily rocks of Castle Creek and Kalama age (fig. 33). It produced a deposit dominantly of block facies material that forms the hummocky terrain to the south of Coldwater Lake on the west end of Johnston Ridge. Field trip Stop 5 of Day 1 will explore this area in more detail. Downstream of this point, constriction of the valley hindered transport of slide block I. The deposit to the west is formed primarily of slide blocks II and III, which also involved older portions of the edifice (Pine Creek age). Slide block II, seen in photographs to have initiated immediately after slide block I, was disrupted by the initial lateral blast explosions, which provided additional momentum to the avalanche. The area below this viewpoint to the south and west reflects a transition to the more mobile debris from slide blocks II and III. This part of the landscape has a higher proportion of mixed-facies material and a more subdued topography (fig. 34).

From here, continue traveling east. Follow signs to the Johnston Ridge Observatory.

**46.0 Optional Stop C—The Science and Learning Center at Coldwater (lat 46.2976° N, long 122.2669° W)**

At the overpass intersection, follow the signs directing you towards the Science and Learning Center at Coldwater, about 0.3 mi ahead. The Center is only open to the public in winter (November through May)

and on weekends from 10:00 a.m. to 4:00 p.m. It is reserved for special events and educational programs from June through October. Formerly the U.S. Forest Service Coldwater Ridge Visitor Center, the building has been repurposed as the Science and Learning Center at Coldwater. Now operated by the nonprofit Mount St. Helens Institute, the Center provides in-depth and extended education programs to schools and other educational groups visiting the volcano, with programs varying in length from 2 hours to multiple days. The facility offers impressive views of the avalanche-dammed Coldwater Lake, the hummocky debris-avalanche deposit, and Mount St. Helens (fig. 35). From here, you can access a short trail through the blast zone and a trail to Coldwater Lake.

From here, rejoin S.R. 504 and follow the signs towards Johnston Ridge Observatory.

**47.9 Coldwater Lake picnic area and boat launch**

A short spur road to the left leads to a picnic area, boat launch, and restrooms at Coldwater Lake. A short trail with a boardwalk (0.2 mi) traverses around a lakeshore debris-avalanche hummock. Continue driving upvalley; the next stop is shortly after the road turns sharply to the left.

**48.8 Optional Stop D—Logging equipment damaged by 1980 lateral blast (lat 46.2858° N, long 122.2537° W)**

Just after a broad sweeping turn to the left, pull into a small parking lot on the left side of the road. From the parking lot, a hiking trail leads up the ridge. After hiking 1.5 mi and gaining about 1,000 ft in elevation, you will have a view of the heart of the blast zone—the area devastated by the high-velocity, low-concentration PDC—the lateral blast—that initiated the 1980 eruption. At the open viewpoint, you will see scattered logging equipment that was damaged by the 1980 eruption (fig. 36). A bulldozer can be found at about 3,450 feet elevation and other artifacts are nearby—including remnants of commercial logging equipment damaged or destroyed by the eruption. The blast stripped paint off the now-rusted surfaces of machinery facing the volcano. A metal screen on one of the machines trapped wood and rock fragments (as large as 10 centimeters, cm) that were entrained by the hot, turbulent blast cloud (Waite and others, 1989).

When leaving the parking lot, turn left and continue on S.R. 504. The road proceeds along the South Coldwater Creek valley floor, swings sharply to the right (passing over the outlet to the tunnel now draining Spirit Lake), and then climbs the north side of Johnston Ridge. The next stop is at the end of the ridge where the road begins to curve to the ridge's south side.

A

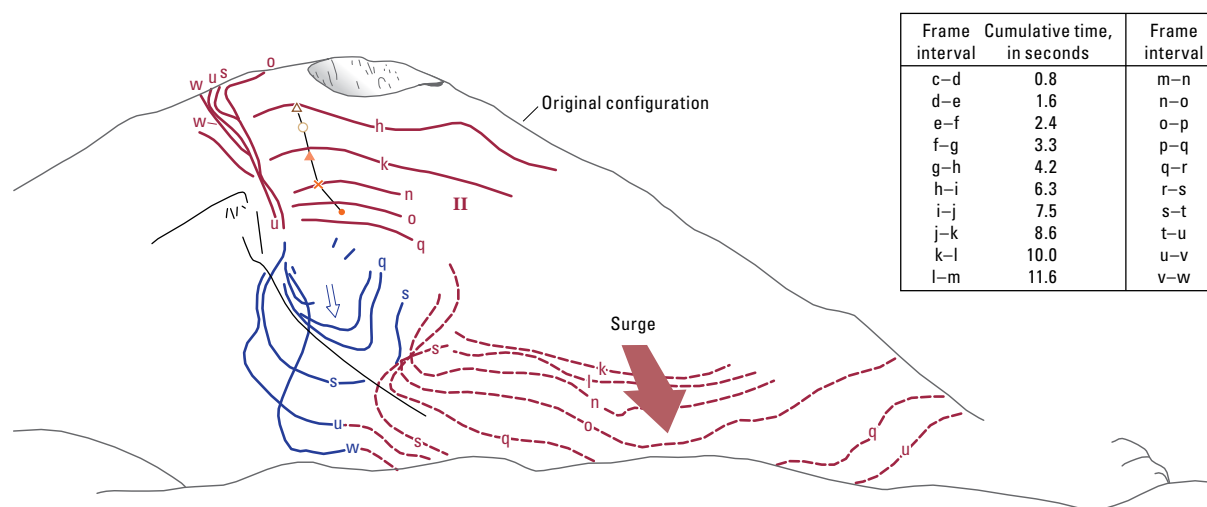
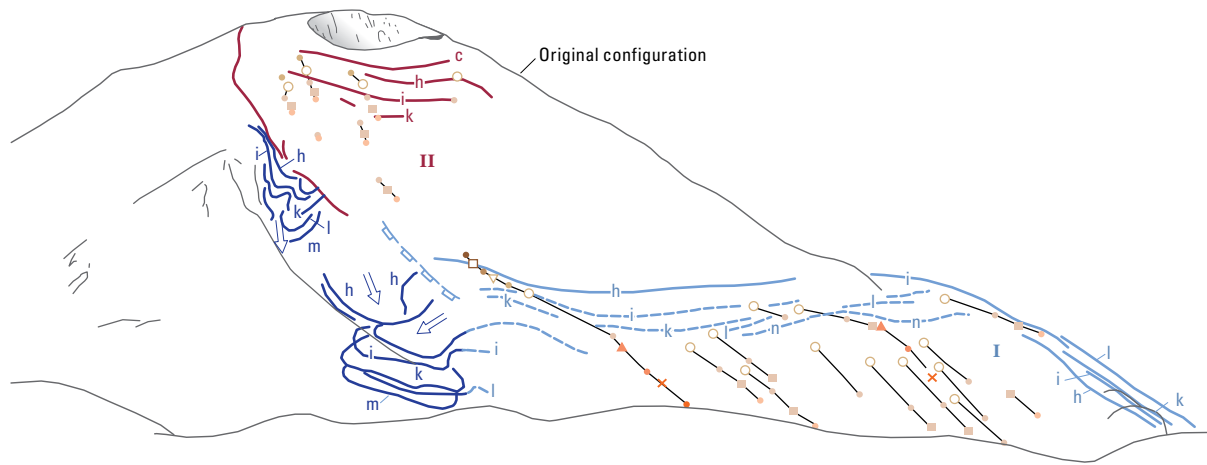
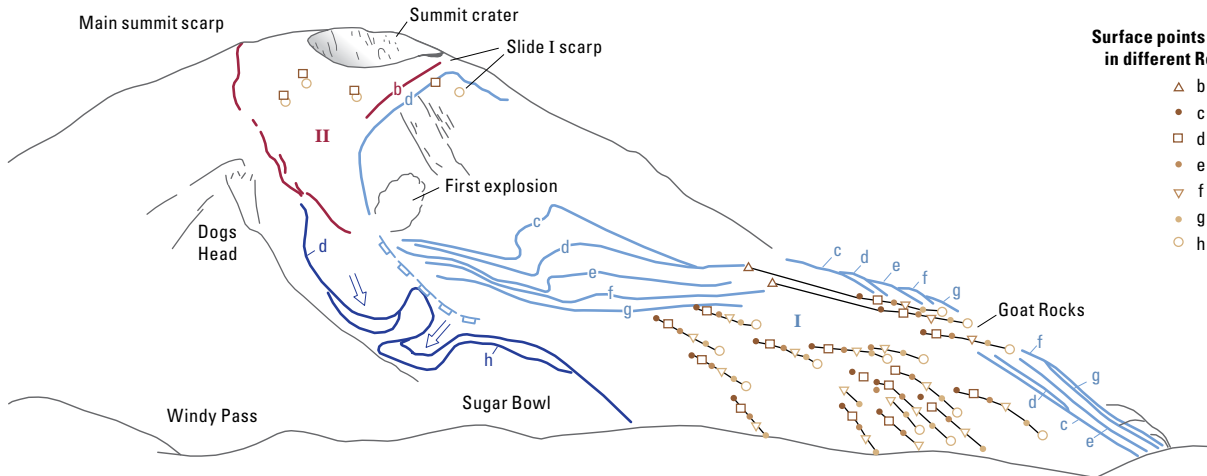
**EXPLANATION**

Line symbols—Drawn from Gary Rosenquist's 1980 photographs; discontinuous where obscured by ash or dust

- Top of slide block I—Solid where certain, dashed where inferred
- Forsyth ice avalanche
- - - Front of Forsyth ice avalanche lobes
- Top of slide block II—Solid where certain, dashed where inferred

Surface points showing positions in different Rosenquist frames

- △ b    ● i
- c    ● j
- d    ● k
- e    ▲ l
- ▽ f    ● m
- g    × n
- h    ● o



Frame interval	Cumulative time, in seconds	Frame interval	Cumulative time, in seconds
c-d	0.8	m-n	13.0
d-e	1.6	n-o	16.7
e-f	2.4	o-p	19.1
f-g	3.3	p-q	21.6
g-h	4.2	q-r	24.1
h-i	6.3	r-s	27.5
i-j	7.5	s-t	28.8
j-k	8.6	t-u	31.8
k-l	10.0	u-v	34.2
l-m	11.6	v-w	36.2



**Figure 32.** Line drawings and photographs depicting 1980 debris-avalanche kinematics. *A.* Line drawings inferred from Gary Rosenquist's time-lapse photographs depicting the onset of edifice collapse by incremental movement (top to bottom) of slide block I (red) and slide block II (blue) material (based on photograph frames b through o) over about 17 seconds. The top two drawings show sequential movement of slide block I and the onset of slide block II movement. By the time of the lower drawing, slide block I had dropped below the level of the foreground ridge, and the arrow labeled "surge" marks the direction of the lateral blast that initiated after passage of slide block I. Figure from Voight and others (1981). *B.* Rosenquist photograph c (8:32:47 a.m. PDT) depicting early collapse configuration. Slide block I, at lower right, was displaced 700 meters with a scarp 600 meters high and slid at a rate of about 50 meters per second. Slide block II, with its headscarp at the summit, was displaced 100 meters. *C.* Rosenquist photograph o (8:33:04 a.m. PDT), taken 16.7 seconds after photograph c, shows the lateral blast penetrating through the moving landslide blocks. Photographs *B* and *C* by Gary Rosenquist, copyright 1980.

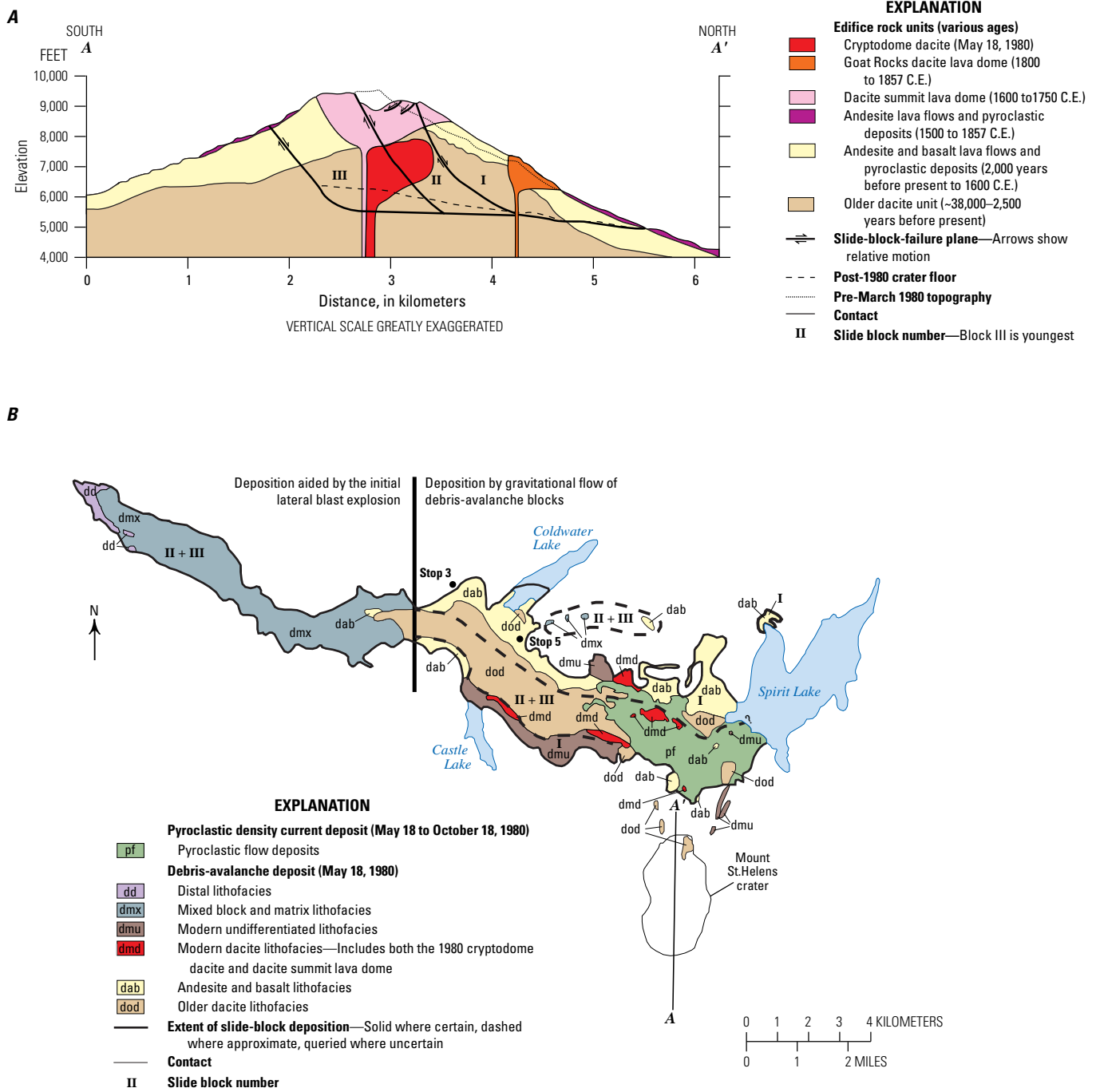


**Figure 33.** Summary of 1980 debris avalanche components before and after edifice collapse. **A.** Generalized north-south cross section of the Mount St. Helens cone showing the inferred May 17, 1980, pre-failure cryptodome topography. The failure planes for slide blocks I, II, and III as well as the post-1980 crater floor are also shown. **B.** Map of the 1980 debris-avalanche deposit showing the distribution of the primary lithofacies. The depositional extent of slide blocks I, II, and III are outlined. Four of the debris-avalanche lithofacies are sourced directly from the pre-1980 volcanic edifice (shown in A). Castle Lake viewpoint (Stop 3) and Hummocks Trail (Stop 5) are labeled on the map. Modified from Glicken (1996).

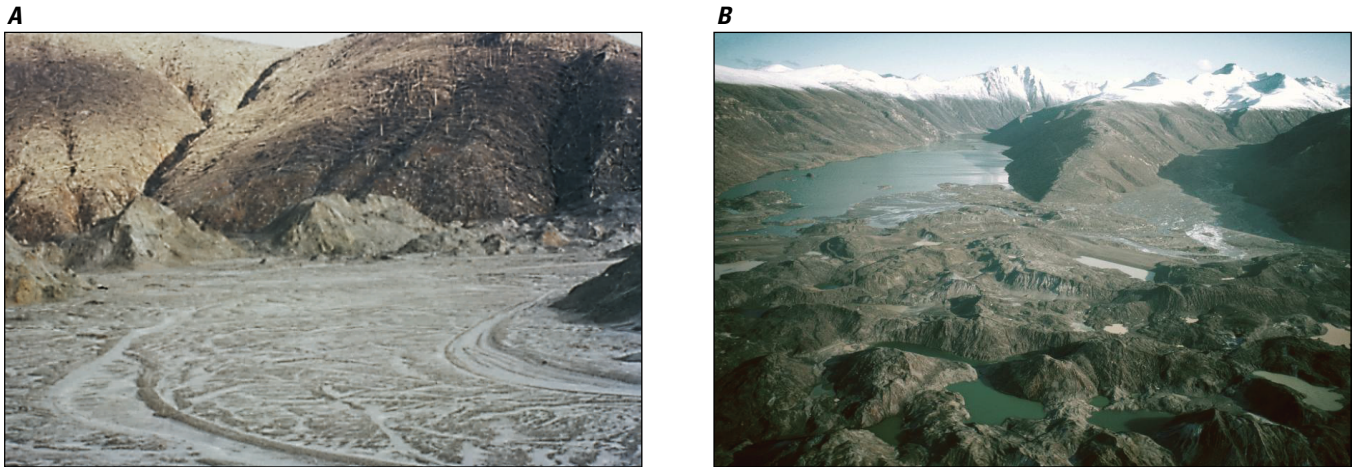


**Figure 34.** Photographs of barren Mount St. Helens 1980 debris-avalanche deposit shortly after emplacement. *A.* View looking north across North Fork Toutle River valley near Elk Rock, about 13 kilometers downstream of the Mount St. Helens crater. Relatively flat, gray terrain in foreground is the mixed block and matrix facies of the debris-avalanche deposit (unit dm<sub>x</sub> in fig. 33*B*). This unit partly liquefied just hours after emplacement and contributed a fine-grained slurry from mud springs of the avalanche deposit in the North Fork Toutle River lahar. Shallow channels, such as seen here, conveyed the lahar slurry downstream. Large hummocks in the middle ground are features of the block facies of the avalanche deposit (not differentiated in fig. 33*B*). Brown valley slopes in background show trees blown down by the lateral blast. The future site of Castle Lake viewpoint (Stop 3) lies above the upper left corner of the image. USGS photograph by K.M. Scott, July 1980. *B.* View north across the hummocky topography of the debris-avalanche deposit block facies (foreground) with numerous pond-filled depressions, composed primarily of andesite and basalt (unit dab in fig. 33*B*). Coldwater Lake (formed by tributary blockage by the avalanche deposit) is visible on the left on the far side of the avalanche deposit. Visible on the right is the flat-floored South Coldwater Creek valley—a valley partly filled by secondary pyroclastic density current deposits (remobilized valley-side lateral-blast deposits) and debris-avalanche material that overrode Johnston Ridge. USGS photograph, 1984.

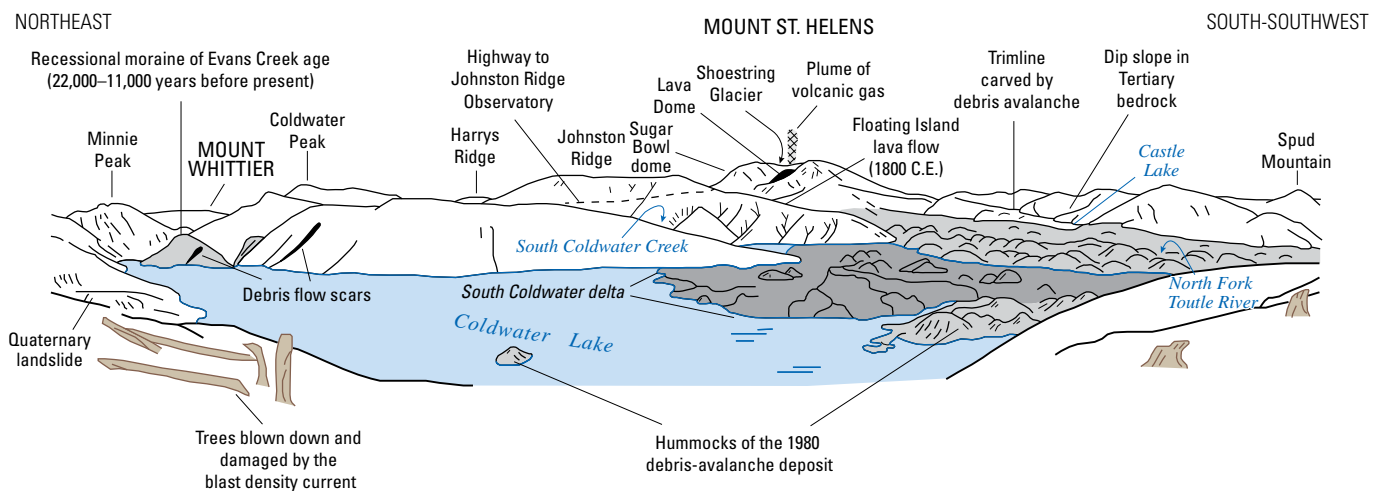


**Figure 35.** Sketch of the view towards Mount St. Helens from the Science and Learning Center at Coldwater, formerly the Coldwater Visitors Center. Modified from Pringle (2002).



**Figure 36.** Photograph of rusted logging equipment damaged and partly buried by the lateral blast, located on Coldwater Ridge. Smithsonian Institution photograph by L. Siebert, 2015.



**Figure 37.** Photograph of logs of trees blown down by 1980 lateral blast, viewed looking southeast from the Boundary Trail west of Loowit viewpoint. Note blowdown orientation is dominantly parallel to the ridge crest, located behind and to the left of this image. Smithsonian Institution photograph by L. Siebert, 2016.

#### 51.9 Spirit Lake tunnel outlet

Just before S.R. 504 makes a nearly 180° turn to the right and crosses over South Coldwater Creek, South Coldwater Creek can be seen emerging from the Spirit Lake tunnel if you park on the shoulder and walk closer to the channel. The tunnel, finished in May 1985, was designed to drain Spirit Lake water into South Coldwater Creek, maintaining the lake level at 1,038 m altitude—and thereby prevent failure of the lake's debris-avalanche natural dam and any potential catastrophic flooding. The 2.6-km-long tunnel, passes 375 m below the crest of Harrys Ridge. Modifications to the tunnel were completed in 2016 after rock deformation threatened blockage in a section of the tunnel.

**54.1 Optional Stop E—Loowit viewpoint (lat 46.2770° N, long 122.2301° W)** Turn right into the Loowit viewpoint for views of Mount St. Helens and the upper North Fork Toutle River valley. This viewpoint, just west of Johnston Ridge Observatory, provides the closest road-side view of tree blowdown from the 1980 eruption on the western approach to the volcano. Tree blowdown—forest tree trunks knocked down, sheared off near the ground surface, and oriented radially away from the volcano—can be seen from an overlook below the parking lot. The Boundary Trail heading west from Loowit viewpoint crosses areas with some radially oriented blowdown and, after traversing the south side of Johnston Ridge for about a half mile, the trail enters a dramatic quarter-mile-

long section through a dense tract of old growth blowdown. Here, ridge-parallel trees mark a change in orientation as the blast cloud deflected around Johnston Ridge (fig. 37). Mount St. Helens National Volcanic Monument regulations require visitors here and on other parts of the Boundary Trail (including those mentioned in this guidebook) to stay on established trails; removal of rock or plant materials is not allowed.

From the parking lot, continue along S.R. 504.

**54.9 Stop 4—Johnston Ridge Observatory (lat 46.2771° N, long 122.2167° W)** S.R. 504 terminates at the parking lot to the Johnston Ridge Observatory. Park and make your way to the visitor center. Here, you can view the Mount St. Helens crater, which is actually an avalanche scar, watch a movie about the 1980 eruption, briefly view exhibits, and hike to the viewpoint on Eruption Trail. Note that you are in the Mount St. Helens National Volcanic Monument, which is a fee site. This is our lunch stop; pick up boxed lunches from the support vehicle.

Johnston Ridge (formerly Coldwater Ridge) was named after USGS volcanologist David Johnston, who lost his life monitoring the volcano when the May 18 lateral blast overran his camp. Johnston Ridge Observatory, built not far from where David Johnson watched the blast cloud that morning, contains a number of well-designed exhibits that explain various aspects of the May 18 eruption. Geological and biological impacts of the eruption to the forested



landscape, the geological context of the May 18 and later eruptions, and USGS volcano monitoring techniques are also treated. A dramatic topographic model with 80,000 multi-colored lights sequentially portrays the emplacement history of the 1980 deposits (fig. 38A), and, combined with repeat showings of a movie about the eruption, provides an excellent overview of the events. A short climb on Eruption Trail leads to a good vantage point for seeing into the 1980 crater, where the composite lava dome (extruded in two eruptive episodes in 1980–86 and 2004–08) and the dome-encircling Crater Glacier can be seen clearly. The debris-avalanche deposit and the thick pumiceous deposits of the Pumice Plain fill the intervening valley below (figs. 38B, C). Farther down the trail, on a loop that returns to the parking lot, is a memorial to victims of the eruption.

Note that Optional Stop F is accessed by foot from Stop 4. Stop 5 is about a 10 minute drive away.

**54.9 Optional Stop F—Boundary Trail to Harrys Ridge (lat 46.2753° N, long 122.2166° W)** The Boundary Trail departs from the east side of the Johnston Ridge Observatory and continues east along the ridge. The trail provides exceptional views of Mount St. Helens and its surroundings. In less than a mile the trail crosses a low point in Johnston Ridge topped by debris-avalanche hummocks. Visitors can walk the trail as far as time permits; even very short walks provide outstanding views away from the crowds at Johnston Ridge Observatory. For those with the better part of a day to spare, the Boundary Trail continues 3.5 mi to Harrys Ridge, which was named after

octogenarian Harry Truman who refused to leave his lodge at Spirit Lake prior to the May 18 eruption. The trail on Harrys Ridge continues right for another 0.6 mi to the crest of the ridge. From here you'll see outstanding views of Spirit Lake—its surface still partly covered by a mat of floating logs from the 1980 tree blowdown—and Mount Adams to the east (fig. 39).

When you are finished, return to your car and begin to backtrack on S.R. 504.

**61.5 Stop 5—Hummocks Trail (lat 46.2869° N, long 122.2717° W)** Watch for the sign marking the Hummocks Trailhead and pull into the parking lot on the left side of the road. Hike on the Hummocks and Boundary Trails to see three types of deposits: (1) the 1980 “lateral blast” deposit; (2) the 1980 debris-avalanche deposit; and (3) post-1980 lahar deposits, as well as the morphologic evolution of the debris-avalanche deposit.

This lengthy stop involves about 3 mi of hiking round trip, mostly on flat terrain (fig. 40). We start on the eastern entrance to the Hummocks Trail and hike 0.7 mi past debris-avalanche hummocks and pond-filled depressions until we reach the junction with the Boundary Trail. On the Hummocks Trail segment we will discuss the surface morphology of this large debris-avalanche deposit and post-avalanche vegetation recovery of the initially barren landscape over the past nearly four decades. Trailside exhibit signs provide visitors with information about the avalanche, biological recovery, and associated research. At the trail junction, we take the Boundary Trail about 0.5 mi eastward and continue nearly to

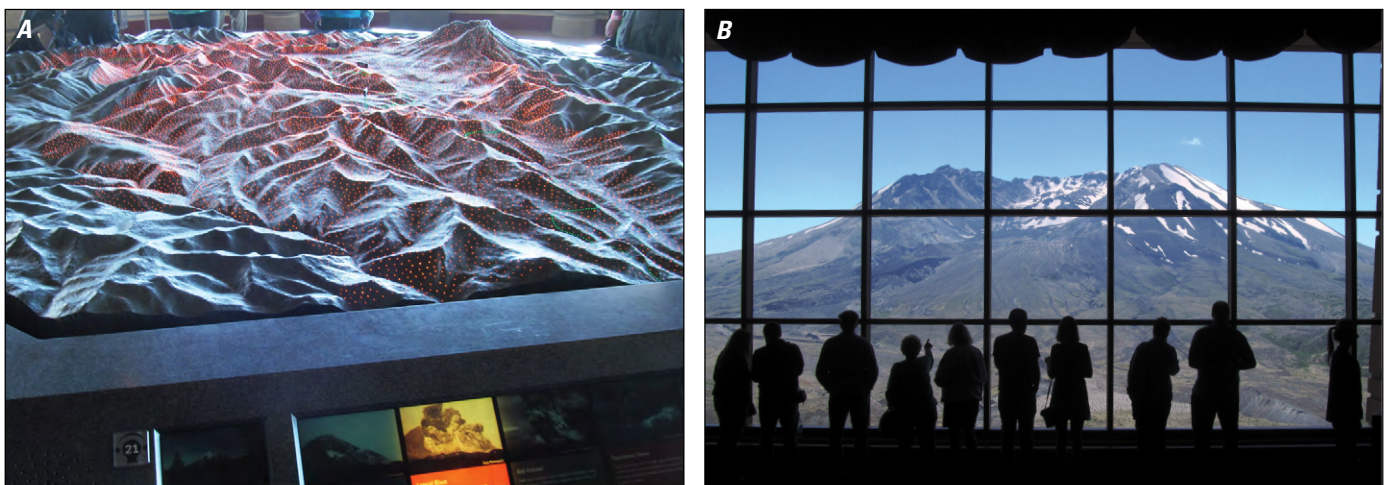


**Figure 38.** Views of the 1980 eruption impacts from Johnston Ridge Observatory (JRO). *A.* Topographic model of the landscape around Mount St. Helens installed at the visitor center, with orange lights showing the extent of the May 18, 1980, lateral blast. Other colored lights sequentially show the extent of the debris avalanche, pumiceous pyroclastic density currents, ashfall, and lahars. *B.* View of Mount St. Helens from the JRO movie theater. Smithsonian Institution photographs *A, B* by L. Siebert, 2016. *C.* Annotated oblique light detection and ranging (lidar) image showing deposits of the 1980 and subsequent eruptions, with JRO in the foreground. Image from Dzurisin and Dreijger (2013).

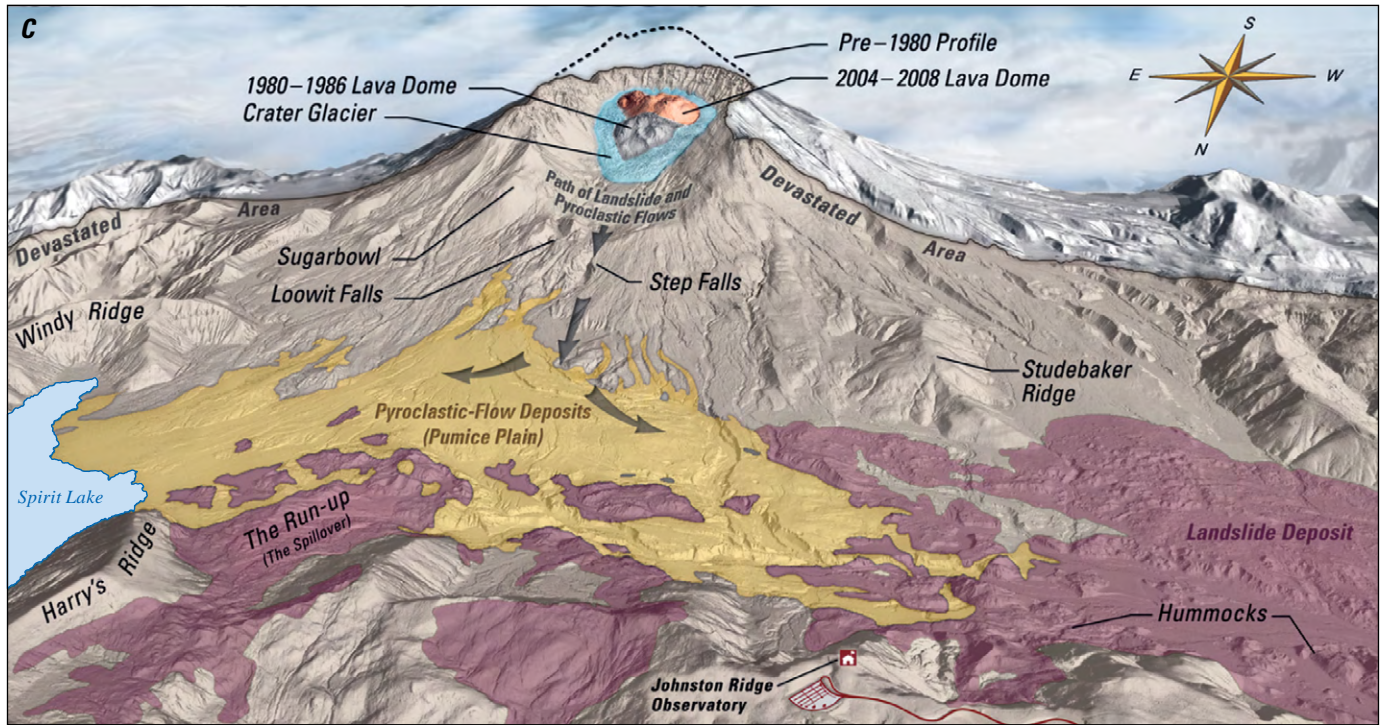
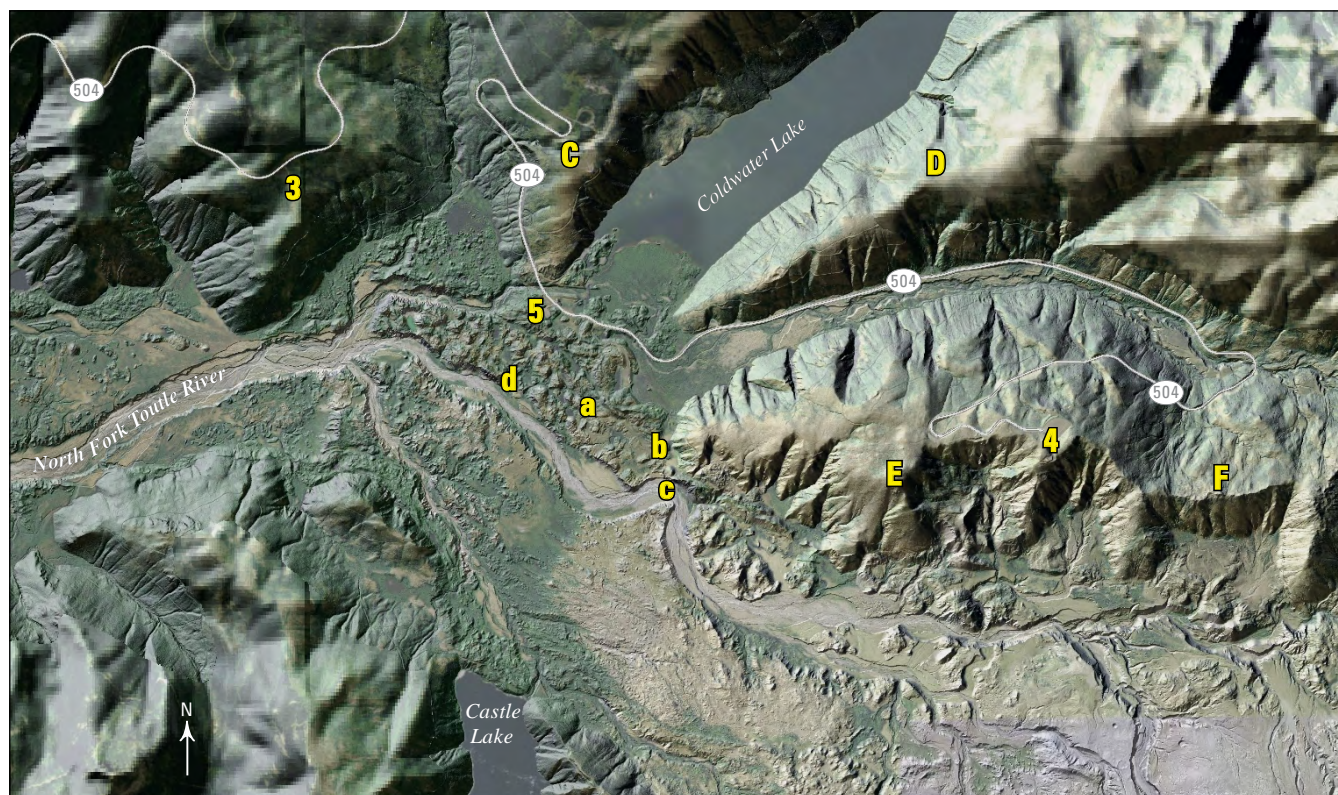


Figure 38.—Continued



**Figure 39.** Photograph of Spirit Lake looking east from Harry's Ridge. The splintered stump of a tree broken off and removed by the lateral blast at Harry's Ridge is visible in the foreground, Spirit Lake to the east with its floating mass of blown down logs (bottom and middle left) in the middle ground, and Mount Adams in the background. The lake surface was raised about 60 meters by deposition of the debris avalanche. Smithsonian Institution photograph by L. Siebert, 1984.



Base from U.S. Geological Survey (USGS) 30-meter Landsat and National Agricultural Imagery Program imagery  
 Shaded relief from USGS 1-meter light detection and ranging (lidar) data  
 Roads from USGS's The National Map

#### EXPLANATION

**5** Field-trip stop—Number is planned stop; letter is optional stop

0 1 2 KILOMETERS  
 0 0.5 1 MILE

**Figure 40.** Map of the Coldwater Lake area. Day 1 planned (numbers) and optional (capital letters) stops and detail of area covered during the hike at Stop 5 (lower case letters) are shown. Stop 5a represents the junction of Hummocks Trail and Boundary Trail; Stop 5b marks the location of tree blowdown and exposure of the lateral blast deposit; Stop 5c indicates where the north bank of the North Fork Toutle River exposes a variety of textures and structures in the debris-avalanche deposit; Stop 5d shows the area along Hummocks Trail where the chaotic topography of the debris-avalanche deposit can be experienced.

the base of Johnston Ridge, where a large protruding Tertiary dike is visible. The hummocky ridge just north of this trail is part of the broad levee that dams Coldwater Lake.

Flat areas between hummocks in this area consist of thin lahar deposits—remnant strands of the liquefied avalanche deposits that coalesced to form the voluminous North Fork Toutle River lahar. Tree blowdown from the lateral blast can be seen on the west end of Johnston Ridge, where deposits of the lateral blast can be found (fig. 41A).

The stratigraphy in this area sheds light on the sequence of events on the morning of May 18. It is known from satellite infrared sensors that the lateral blast reached the Coldwater Lake area about 2.8 minutes after the eruption-triggering earthquake occurred and that the debris avalanche arrived to this point 4–5 minutes afterward (Moore and Rice, 1984). Thus, debris-avalanche deposits should overlie the primary blast deposit. However, some blast deposit in

this area overlies the debris-avalanche deposit. These observations can be explained by the occurrence of more than one blast-generating explosion of hot cryptodome material, separated by a minute or more, as the landslide blocks were sliding downhill and exposing different parts of the cryptodome (Sparks and others, 1986; Criswell, 1987; Hoblitt, 2000).

The North Fork Toutle River has carved some magnificent exposures of the debris-avalanche deposit in this area. South of the Boundary Trail, elk trails provide access to lower terraces along the North Fork Toutle River where deeper parts of the debris-avalanche deposit are exposed, locally capped by debris-flow and fluvial deposits. Higher bluffs expose hummock sections as high as ~50 m, some of which reveal original edifice stratigraphy transported intact (figs. 41B, C, D, E). Large blocks of black and reddish andesitic and basaltic rock layers derive from parts of the edifice formed during the Castle Creek and Kalama eruptive periods (fig. 1). Lighter-colored dacitic blocks

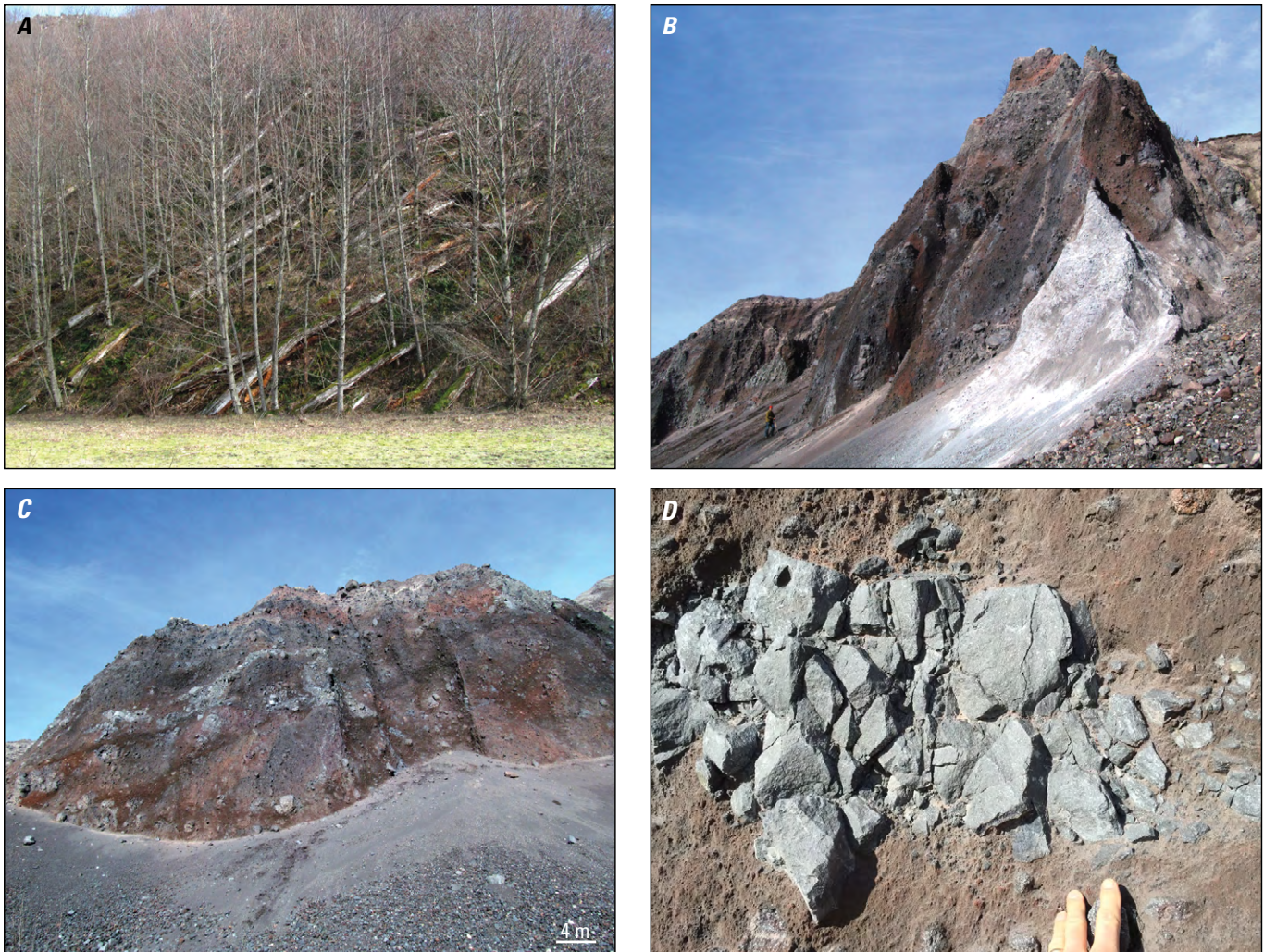
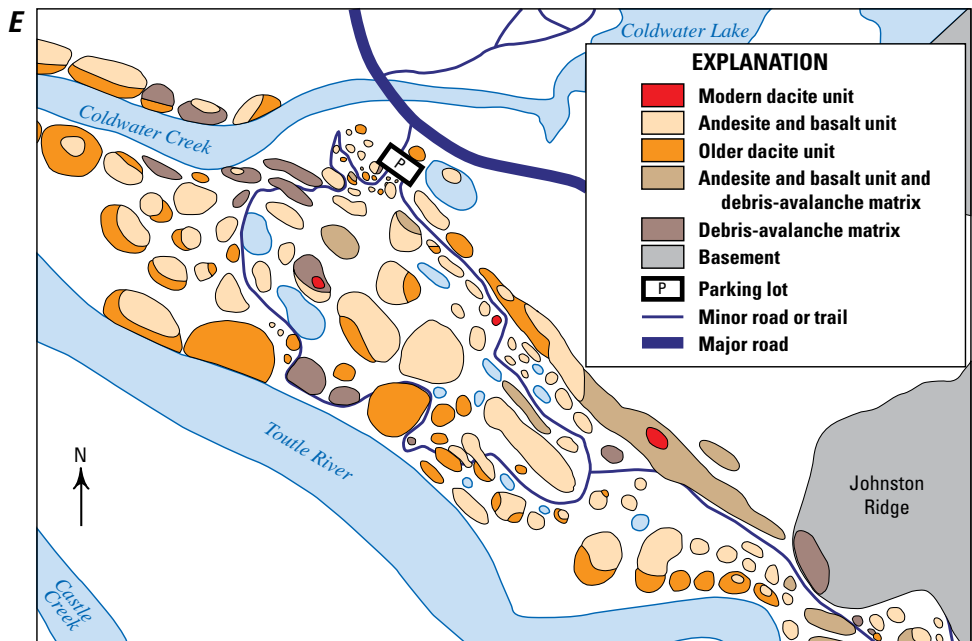


**Figure 41.** Photographs of the 1980 debris-avalanche deposit near Coldwater Lake. *A.* Margin of debris-avalanche deposit where its flat surface is mantled by a thin layer of the North Fork Toutle River lahar deposit (flat green area in foreground). Logs from the 1980 tree blowdown are present on a flank of Johnston Ridge facing away from the volcano—swept by the blast but untouched by the avalanche here. *B.* Debris-avalanche hummock showing tilted and variously oriented basaltic and andesitic Kalama- and Castle Creek-age rocks overlying a sheared fragment of older light-colored dacitic rock of Pine Creek age, consistent with the stratigraphy in the volcano edifice. Note person at lower left for scale. *C.* Debris-avalanche hummock with fractured blocks, color mottling, and shear zones (diagonal dark lineations). *D.* Fractured jigsaw-fit block. *E.* Simplified map of debris-avalanche hummocks near Coldwater Lake, about 10 kilometers downstream of the source crater. Map shows lithologic units from the pre-failure edifice preserved in hummocks. Modified from Takarada (2008). Smithsonian Institution photographs *A, B, C* by L. Siebert; USGS photograph *D* by T.C. Pierson. All photographs from 2016.



derive from the Pine Creek eruptive period. The debris-avalanche deposit at this location was part of slide block I (Glicken, 1996).

The debris-avalanche deposit near Coldwater Lake shows the complex interactions of debris from the different slide blocks that slid sequentially from Mount St. Helens' crater (fig. 33). Debris from slide block I traveled as far as Coldwater Lake at the front of the advancing avalanche. Slide block I material was then shouldered aside and overridden by the more disaggregated and fluidized material from slide blocks II and then III—both of which traveled another 10 km down the valley. Glicken (1996) calls the material of slide block I the block facies, because more than 70 percent of the material is composed of enormous (10–100 m in diameter) avalanche blocks. Glicken (1996) uses mixed block and matrix (or intermediate) facies to describe material containing 10–70 percent avalanche blocks and matrix facies to describe the highly mixed, homogeneous, and distal mixtures of gravel, sand, and fines (less than 10 percent avalanche blocks) (fig. 42). Juvenile clasts of cryptodome dacite in the more disaggregated intermediate and matrix

facies suggest that blast explosions may have added momentum and enhanced the mobility of slide blocks II and III as they slid off the edifice (Glicken, 1996).

Long-term channel cross section surveys document the extent of post-1980 depositional and erosional modification to the North Fork Toutle River drainage at this and other locations (Mosbrucker and others, 2015) (fig. 43). Fluvial incision has widened the river nearly 90 m since initial measurements in 1983 and bank retreat of more than 20 m into the interior of debris-avalanche hummocks has occurred since 2007. The narrow terrace just above river level consists of debris-flow deposits emplaced November 3–8, 2006, by a lahar from Loowit Canyon. The lahar was the result of a prolonged “atmospheric river” rainstorm that dropped 60 cm of rain on Mount St. Helens—including 37 cm on November 7 alone (fig. 44).

Continue backtracking on S.R. 504. We will drive 1.25 hours to Kelso, Wash.

- 106.6 Turn left to merge onto I–5 south toward Portland.
- 116.6 Overnight stay at motel in Kelso, Wash.

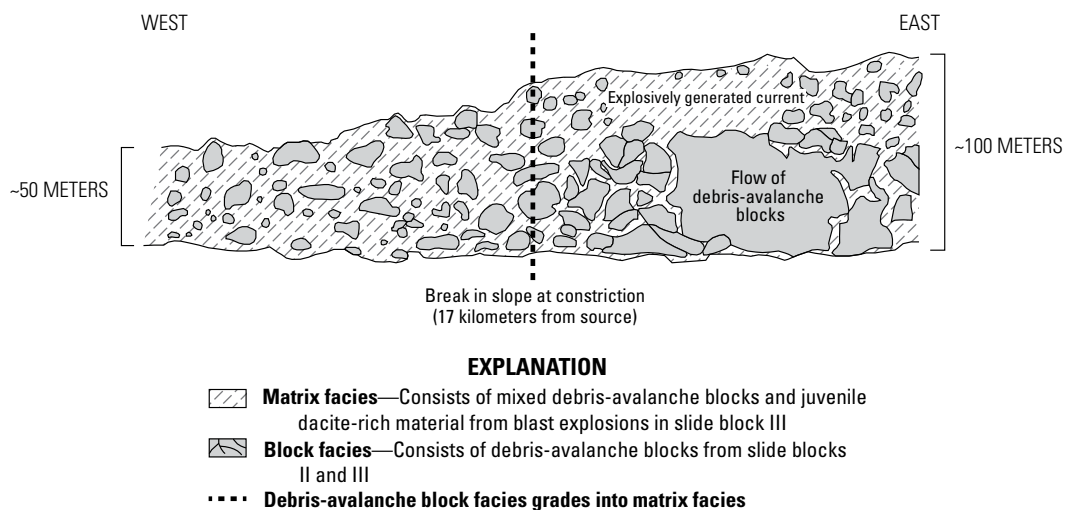


**Figure 42.** Schematic longitudinal cross section through the middle part of the debris-avalanche deposit located within the North Fork Toutle River valley, about 17 kilometers downstream from Mount St. Helens. Cross section shows a proportionately greater amount of matrix facies downstream of the abrupt change in surface slope caused by a constriction in the North Fork Toutle River valley. Sketch modified from Glicken (1996).

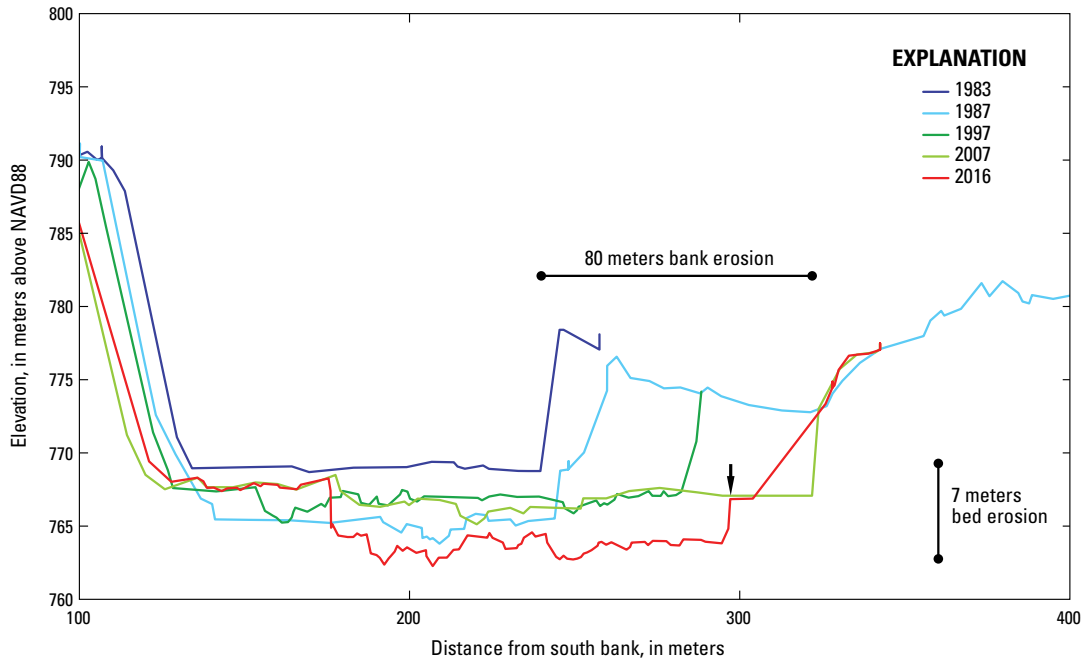


**Figure 43.** Cross-sectional profiles of the North Fork Toutle River at station NF 120, the site of Day 1 Stop 5. Profiles show the evolution of the river from 1983 to 2012, documenting 80 meters of riverbank erosion during this time (Mosbrucker and others, 2015). View is downstream. Arrow shows location of terrace in figure 44. NAVD88, North American Vertical Datum of 1988.

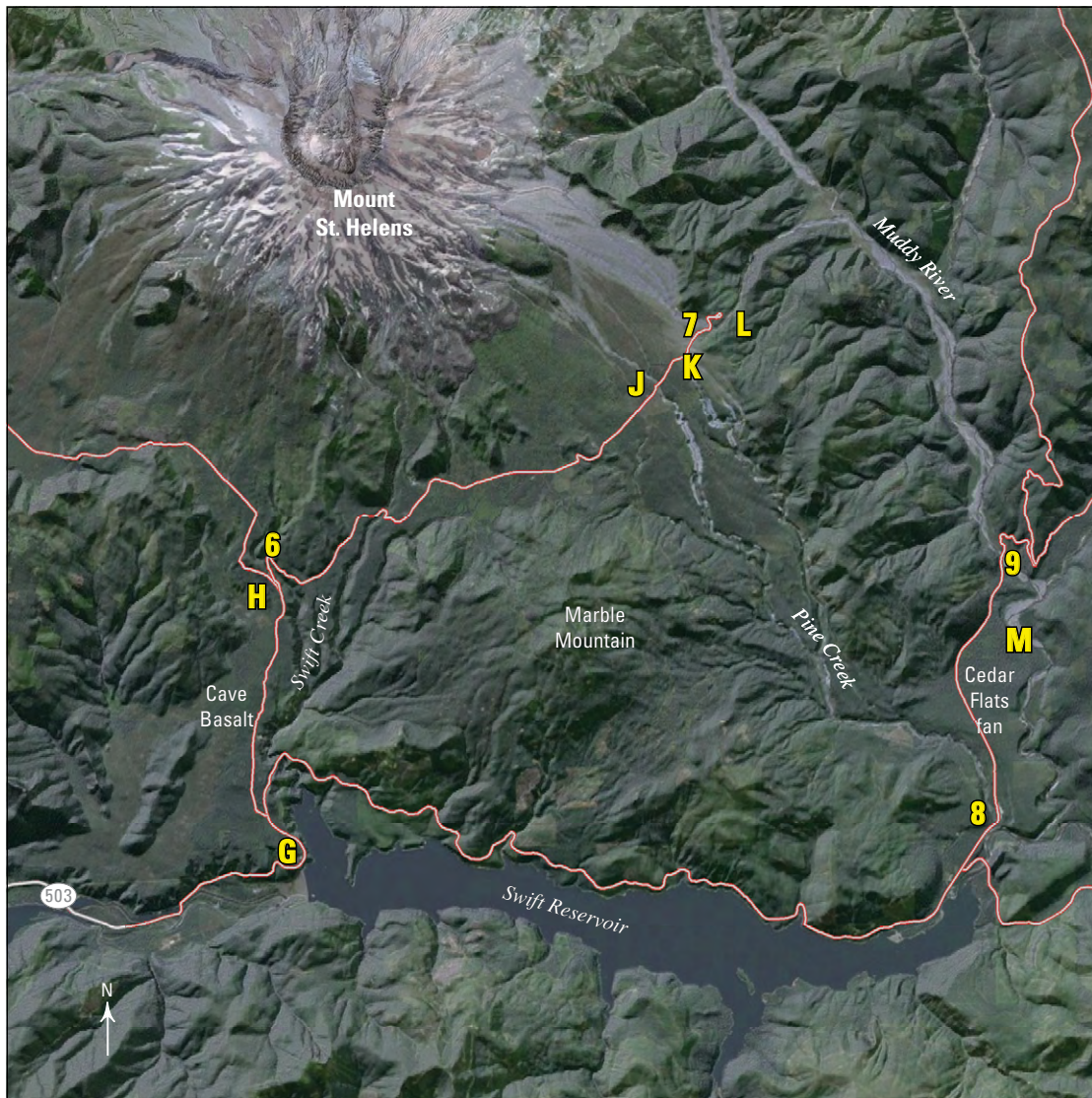


**Figure 44.** Photograph of a low terrace (approximately 3 meters high) in the North Fork Toutle River valley. Section is located on the north side of cross section NF 120 at Stop 5 (marked by arrow in fig. 43). Vertical section includes the multi-hued 1980 debris-avalanche deposit at base; an erosional surface (disconformity); about 2 meters of lahar deposits, emplaced in 2006; and 30–40 centimeters of coarse fluvial gravel on top. Smithsonian Institution photograph by L. Siebert, 2016.

**Day 2: Pyroclastic density current, pyroclastic-fall, lahar, and volcano-fluvial deposits in Lewis River drainage, Mount St. Helens**

Field trip stops for Day 2 are shown in figure 45; note that the sequence of numbered and lettered field trip stops continues from Day 1. Descriptions for each stop are largely extracted from an unpublished field-trip guide written by Michael Clynne and others in 2003 and revised in 2012.

Day 2 begins by driving south on I-5 from Kelso to Woodland. Cumulative mileage for Day 2 begins in Woodland, Washington. Take Exit 21 off I-5. Traveling from the north, the exit ramp becomes Pacific Avenue, which continues for about one mile to a traffic light at S.R. 503 (Lewis River Road); turn left and continue under the freeway. Cumulative mileage starts at the second traffic signal—travelling east on S.R. 503 at the intersection with East CC Street. S.R. 503 parallels the Lewis River. Travel time is about 1.25 hours to the town of Cougar, where Stop 6 is located.



Base from U.S. Geological Survey (USGS) 30-meter Landsat Imagery  
Shaded relief and roads from USGS's The National Map

**EXPLANATION**  
**8** Field-trip stop—Number is planned stop; letter is optional stop

0 2 4 KILOMETERS  
 0 2 MILES

**Figure 45.** Locations of Day 2 planned stops (numbers) and optional stops (letters) on the south and southeast sides of Mount St. Helens. CB: Cave Basalt; CF: Cedar Flats fan; MM: Marble Mountain.

## 50 Geologic Field-Trip Guide of Volcaniclastic Sediments from Snow- and Ice-Capped Volcanoes

0.0 Head east on S.R. 503 at the intersection with East CC Street.

3.5 Missoula Flood terraces and modern flooding  
The catastrophic Missoula Floods emplaced deposits that are preserved as terraces on both sides of the Lewis River for the first 3.5 mi from Woodland (fig. 46). The sediments consist of sand, silt, and gravel deposited by repeated catastrophic breaching of glacial Missoula Lake, which was dammed by an advancing lobe of a continental glacier in western Montana dozens of times between about 20,000 and 15,000 calendar years ago (O'Connor and Benito, 2009). Lower elevation terraces are cut into interstratified Lewis River flood deposits and Holocene lahar and lahar-runout deposits from Mount St. Helens. In 1996, Woodland suffered significant damage from a flood on the Lewis River. Many of the homes you see along the road were inundated with as much as 1.5 m of standing water.

15.0 Tertiary volcanic rocks  
Outcrops on the left side of the road are composed of Tertiary volcanic rocks of the western Cascades. Lake Merwin, on the right side of the road, is one of three major reservoirs maintained for power generation and recreation along the Lewis River.

22.9 Intersection of S.R. 503 with Yale Bridge Road.  
Continue straight through the intersection on S.R. 503.

25.0 Yale Reservoir  
The lake on the right side of the road is Yale Reservoir, the second of three reservoirs on the Lewis River. Note that 4.7 mi before the town of Cougar, S.R. 503 turns south and follows Yale Bridge Road toward Amboy—do not turn here. Continue east on Lewis River Road toward Cougar, Wash.

28.0 Cougar, Washington  
At Cougar, Lewis River Road becomes U.S. Forest Service Road 90 (F.R. 90), and the route continues through the town on this road. Cougar is only 18 km in a straight line from Mount St. Helens, making it the closest community to the volcano. The town is also the last place between here and the volcano to refuel, except for a remote convenience store at Eagle Cliff located at the upstream end of Swift Reservoir. Remnants of Amboy Drift (glacial deposits of ~170–130 ka (Hayden Creek age) are found in roadcuts east of Cougar. Deposits on the south side of Mount St. Helens are dominated by those of the Ape Canyon, Cougar, and Swift Creek eruptive stages (fig. 1).

30.5 Swift Reservoir hydroelectric power canal dam

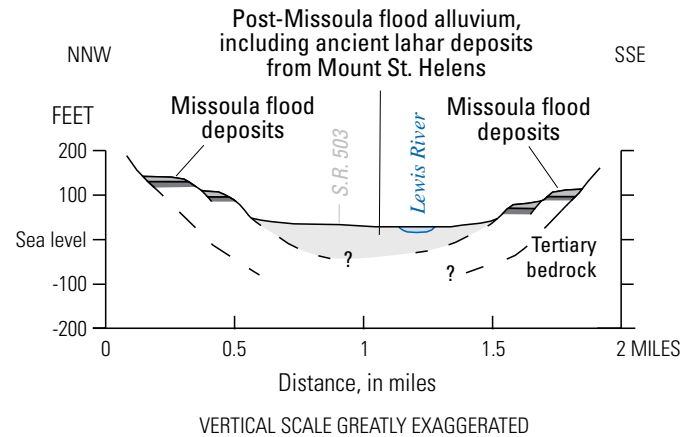


**Figure 46.** Schematic cross section of Lewis River valley, located about 1 mile east of Woodland, Washington. Diagram shows terraces at about 40 meters (140 feet) elevation above sea level, capped by late Pleistocene Missoula Flood deposits (river elevation is about 6 meters [20 feet]). This is the highest level achieved by more than 80 floods that came down the Columbia River and backed up into tributary valleys. Modified from Pringle (2002).

At this point, the road curves to the southeast and you will pass an earthen dam on the left side of the road at the end of a hydroelectric power canal. The canal, operated by PacifiCorp, routes Lewis River water with minimal head loss from Swift Dam to an auxiliary power house located here on the right side of the road. On April 21, 2002, the dam catastrophically failed, destroying parts of the power-generating facility and scouring the canal down to bedrock (Cave Basalt lava flow) (Regan and others, 2008).

Failure of the 25-m-high dam was caused by an unusual piping failure (fig. 47). The 30-ft-thick clay seal on the canal bed was compromised, allowing canal water to enter a lava tube in the basalt beneath the canal. The hydrostatic head created within the lava tube caused a catastrophic blowout at the base of the dam. Leakage began between 3:35 a.m. and 3:50 a.m. and the blowout occurred at 6:55 a.m., creating a 3-m-deep high-velocity torrent aimed directly at the power-generating building.

Just past the building, the road enters a forested flat area that is the surface of the Cave Basalt. Tumuli, push-ups, and pahoehoe surfaces can be seen from the road.

32.2 Bridge over the power canal and Cougar-age debris-avalanche deposits

The route crosses over the power canal 1.5 mi upstream of the downstream end of the canal. From the bridge, the steep slope ahead on the north side of the power canal is composed of Cougar-age debris-avalanche deposits from Mount St. Helens that are mostly obscured by vegetation. The Cave Basalt





**Figure 47.** Failure of the Swift Reservoir power canal dam. *A.* Photograph showing the blowout of the power canal dam and flooding of Forest Road 90 at about 6:55 a.m. on April 21, 2002. PacifiCorp photograph by T. Low, 2002. *B.* Aerial photograph of dam failure and the damage to power-generating facility. Note the sinkhole into the Cave Basalt lava flow at top center of frame. USGS photograph by C.D. Miller, 2002.

flowed through a small notch to the left, near the west end of the power canal, and cascaded downslope into the Lewis River valley to form the surface you just drove over. Just before crossing the bridge, the route passed from Cowlitz County into Skamania County. Continue along F.R. 90 up the hill.

- 34.0 Optional Stop G—Swift Reservoir overlook (lat 46.0663° N, long 122.1998° W)** Pull out at the overlook on the right side of the road, just before the sharp turn to the left. This is a somewhat overgrown viewpoint that offers an upstream view of Swift Reservoir. The overlook lies on a Pleistocene terrace that is a remnant of a Cougar-age debris fan. A vertical exposure of the fan deposits is visible (but extremely difficult to access) downstream on the south Lewis River valley wall, about 70 m lower than the overlook elevation (fig. 8). Terrace stratigraphy (upward from base of section) consists of two Ape Canyon-age lahars, a large Cougar-age debris-avalanche deposit that once blocked the Lewis River valley, a Cougar-age (24.4 ka) two-pumice dacite PDC deposit, and a younger Cougar-age lahar deposit and tephra (Clyne and others, 2005, 2008). The 100-m-thick two-pumice PDC deposit, also visible in a borrow pit across the road to the west, was emplaced as multiple flow units following the debris avalanche after traveling more than 15 km from the volcano. A minimum volume estimate for this PDC is 0.5 km<sup>3</sup>. Lithic blocks of dome rock in the two-pumice PDC deposit suggest that intrusion of magma into a large dome complex (a proto Mount St. Helens—see figure 1B) probably destabilized the edifice and triggered the debris avalanche. It appears to have been the largest

edifice-collapse event in the volcano's history prior to 1980.

From here, continue east and watch for a sign marking the turnoff for F.R. 83 directing you towards Ape Cave, Climbers Bivouac, and Lava Canyon.

- 34.9** Turn left onto F.R. 83. Stay on F.R. 83 until Stop 6.
- 36.6** Turn left onto F.R. 8303 to go to Optional Stops H and I (sign for Ape Cave), otherwise continue straight on F.R. 83.
- 36.8 Optional Stop H—Trail of Two Forests (lat 46.0993° N, long 122.2131° W)** After 0.2 mi on F.R. 8303, pull in to the parking lot on the left side of the road. To get to Optional Stop I, turn left out of the parking lot and continue along F.R. 8303. Otherwise, turn right to return to F.R. 83.
- A short loop trail, the Trail of Two Forests leads to spectacular lava casts (vertical and horizontal) of large trees that formed when the 1.9 ka Cave Basalt lava flowed through the forest. Some of the casts form narrow-diameter tunnel mazes that can be explored by adventurous children and non-claustrophobic adults (bring flashlights).
- 37.5 Optional Stop I—Ape Cave (lat 46.1079° N, long 122.2118° W)** After 0.7 mi on F.R. 8303, pull into the well-marked parking area on the right side of the road. At the end of the parking lot is Ape Cave, a large-diameter and unusually long lava tube that formed in the Cave Basalt lava flow. The lava tube is nearly 4 km long and one of the longest lava tubes in the conterminous United States (Tucker, 2015).

It can be explored individually or with guided walks during summer, but reliable light sources (lanterns or flashlights), sturdy shoes, and warm clothes are needed. The temperature in the cave is about 6 °C (42 °F) year-round with a steady light breeze owing to cold-air drainage.

After finishing with Optional Stops H and I, return to the intersection with F.R. 83. Turn left and continue north along F.R. 83. Note that the mileage from Stops H and I does not contribute to the cumulative mileage.

37.9 Intersection of F.R. 83 with F.R. 8100. Continue straight (north) on F.R. 83.

38.1 **Stop 6—Swift Creek PDC deposits (lat 46.1198° N, long 122.2061° W)** Watch for a large roadcut on the left side of the road. There is a place to park on the right side of the road just as you arrive at the outcrop.

PDC deposits of the younger part of the Swift Creek volcanic assemblage (fig. 48) (Hyde, 1975) are exposed in a road cut along the west side of the West Fork Swift Creek valley on F.R.83 (fig. 45). The outcrop consists of three PDC deposits erupted during the Swift Creek eruptive stage (fig. 1) overlying a “flowage deposit”, which in turn rests directly on till emplaced during the Last Glacial Maximum. Clasts in

the lowest PDC deposit consist of 73 percent pumice and 27 percent nonvesicular andesite and dacite, but only 23 percent of the fragments in the overlying middle PDC deposit are pumice. Tephra set S separates these two deposits from an upper PDC deposit in which pumice is absent. This third PDC deposit is only about 1 m thick and contains angular, radially jointed rock fragments with diameters of 10–20 cm.

When finished with this outcrop, continue in the same direction along F.R. 83. Drive 20 minutes to Stop 7.

38.4 Swift Creek lava flow

Just after a sharp curve to the right, F.R. 83 begins to contour around the edge of the largest lava flow in the history of Mount St. Helens. You will begin to see outcrops of this lava on the left side of the road. The 200-m-thick Cougar-age (20–18 ka) andesite flow originated from a vent that was then at or near the summit at 1,830 m elevation, and traveled about 6 km to the south (Clynne and others, 2008). The flow is overlain by PDC deposits of the same age. Climbers Bivouac—the access point for the Monitor Ridge climbing route to the summit—lies atop the flow. Summit climbs during the summer months are by permit only; daily allotments of 100 permits often sell out well in advance.

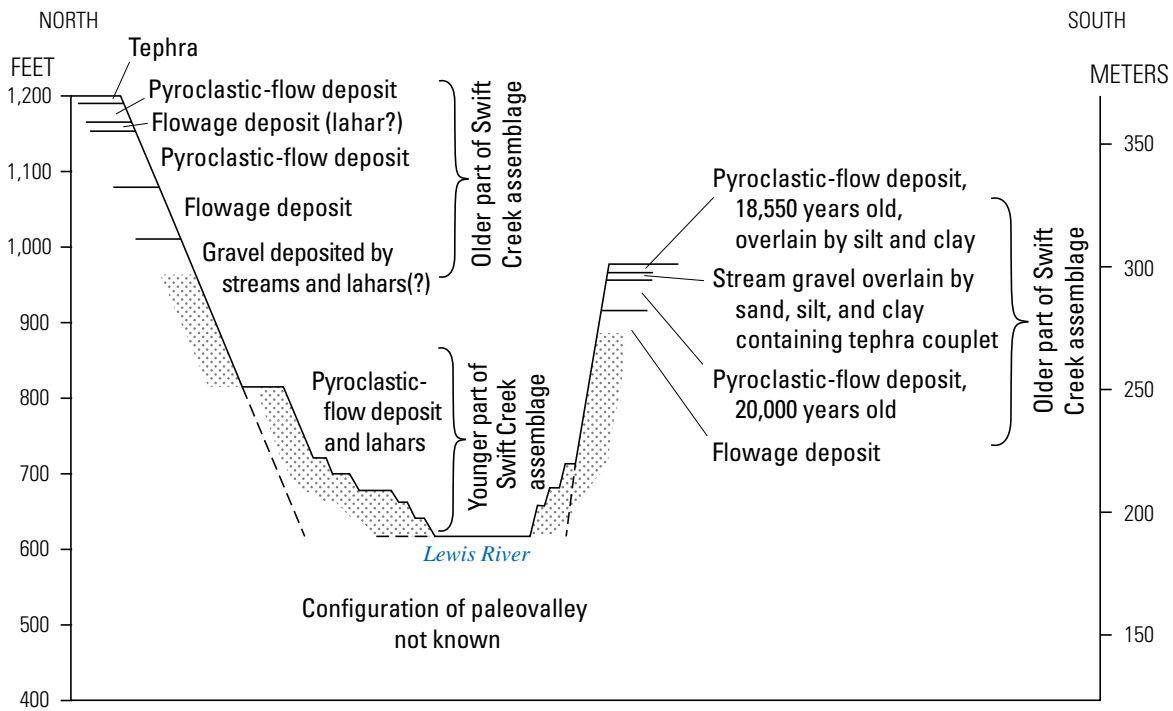
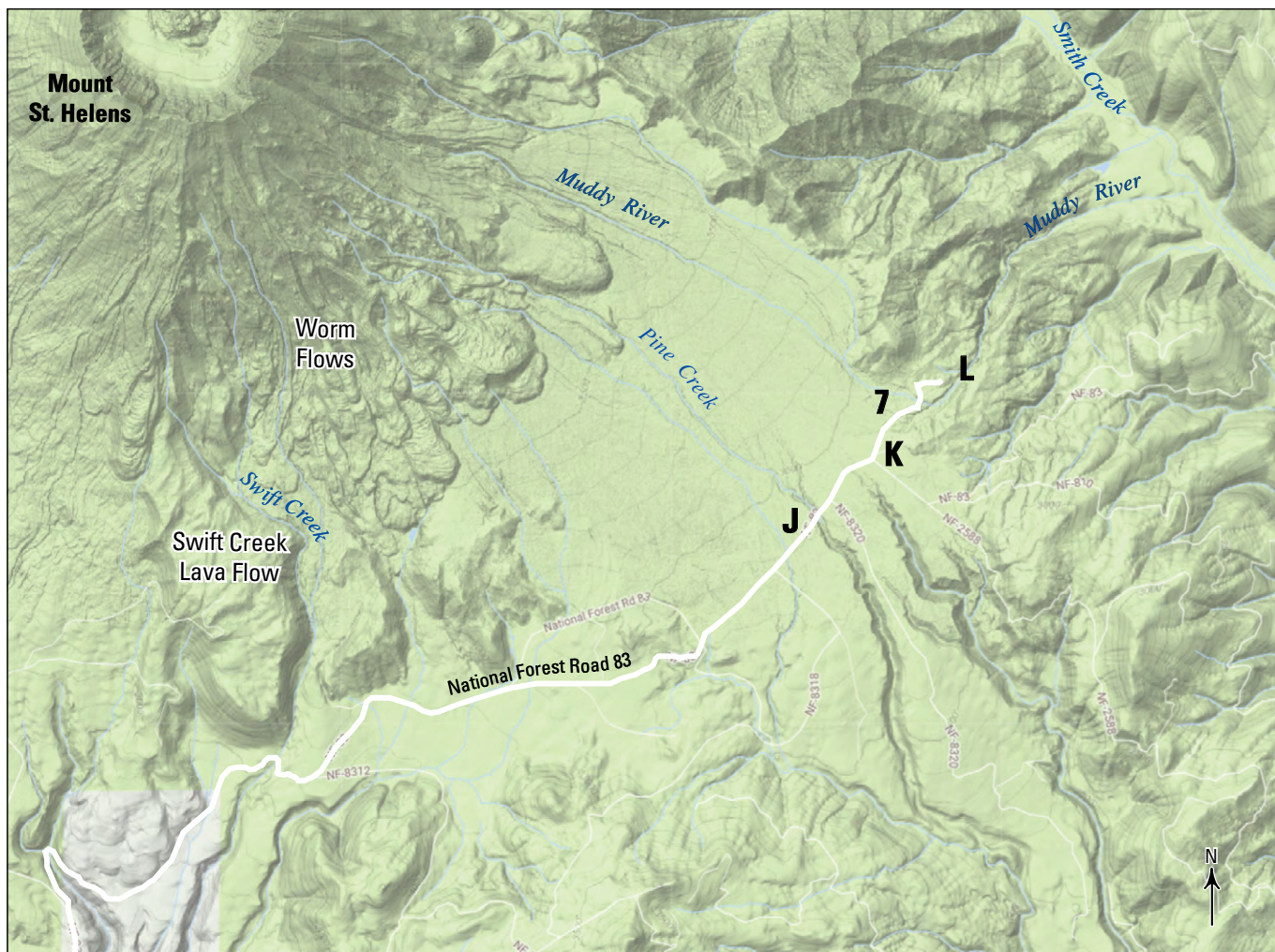


**Figure 48.** Cross-sectional view of deposits of the Swift Creek eruptive stage exposed in the Lewis River valley near the mouth of Swift Creek. The younger part of the Swift Creek assemblage is exposed at Stop 6. Stippled pattern marks areas of limited exposure. Modified from Hyde (1975).

- 40.4 **Swift Creek**  
The roadcut on the east side of Swift Creek exposes an early Kalama-age lahar deposit underlain by Pine Creek-age dacitic lithic PDC deposits. Over the next few miles, the road crosses forested areas underlain by Pine Creek lithic PDC deposits, early Kalama-age lahar and PDC deposits, and an older Castle Creek-age lahar.
- 41.8 **June Lake trailhead**  
The Worm Flows lava complex is visible to the north from this point (fig. 49). This sinuous complex of fresh andesitic lava flows, with prominent flow levees, was emplaced in the early- to mid-1500s during the Kalama eruptive period. We will see better views of these flows at the Lahar Viewpoint (Optional Stop K) and Stratigraphy Viewpoint (Stop 7).

- 43.5 **Tertiary bedrock knoll and tephra-fall deposits**  
F.R. 83 passes through a small knoll of Tertiary volcanic rocks that is almost completely buried by Mount St. Helens deposits. The entire set of Spirit Lake stage tephra-fall deposits is present on the Tertiary bedrock, including 1980, X, W, B, P, and Y tephra sets. The next bridge that you reach is the location of Optional Stop J.
- 44.8 **Optional Stop J—West Pine Creek bridge (lat 46.1535° N, long 122.1048° W)** Pull off the road in a safe location. Lithic PDC deposits of Pine Creek age are exposed in the channel banks. This channel conveyed part of the Pine Creek lahar on May 18, 1980, which eroded the channel and destroyed the pre-eruption bridge at this location. From here, continue in the same direction on F.R. 83.



Base from Google Maps, 2017

**EXPLANATION**  
**7** Field-trip stop—Number is planned stop; letter is optional stop

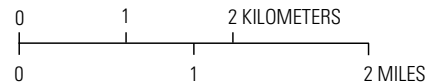


**Figure 49.** Topographic map of the southeast quadrant of Mount St. Helens showing Day 2 stops. This map shows the Pine Creek-Muddy River debris fan at center and surrounding terrain, with planned field-trip stops (numbers) and optional stops (letters) labeled.

## 45.3 Pine Creek-Muddy River fan

The road passes onto the Pine Creek-Muddy River debris fan—a broad surface underlain by a very thick (approximately 200–400 m) sequence of lahar and PDC deposits that has nearly filled the paleovalley of upper Pine Creek (Crandell and Mullineaux, 1973). The deposits were emplaced mainly during the Pine Creek and Kalama eruptive periods. Much of the fan surface was swept clear of vegetation by a large lahar in 1980 (Pierson, 1985).

45.6 **Optional Stop K—Lahar Viewpoint (lat 46.1593° N, long 122.0956° W)** Pull into the Lahar Viewpoint parking lot on the right side of the road.

Streams on the Pine Creek-Muddy River debris fan now form a mainly parallel drainage pattern. Pine Creek stays within the Pine Creek valley, but Muddy River, having captured some of the Pine Creek drainage, now spills through a low divide at the head of Lava Canyon on the ridge between the Pine Creek and Muddy River valleys and descends the flank of the ridge that once separated the two fluvial systems (fig. 49).

The 1980 Pine Creek-Muddy River lahar was triggered during the first minutes of the May 18 eruption

by the action of a lithic PDC scouring, entraining, and melting snow and ice from the outer flanks of Mount St. Helens (Brugman and Meier, 1981; Pierson, 1985; Waitt, 1989) (fig. 50). The complex lahar path is shown in figure 51. An average of 6 m of snow and ice (as much as 10 m locally) were eroded from the volcano's southeast flank. The initiating PDC, generated by “boiling over” of hot fragmental material during the first minutes of the eruption, was partly funneled through Shoestring Notch, a low point on the crater rim, accelerated down the outer flank of the volcano as fast as 50 m/s (Moore and Rice, 1984), and transformed to a high-concentration, high-velocity (40 m/s) lahar by the time it reached the upper Pine Creek-Muddy River fan. Pumiceous PDCs formed by column collapse during the afternoon that day also swept through this area and triggered a lahar composed almost purely of pumice in Muddy River (Pierson, 1985).

Lahar Viewpoint is located where the 1-km-wide lahar split into two flows—one continuing down Pine Creek, and the other descending Lava Canyon to the Muddy River, where it joined a lahar from Smith Creek traveling down that channel (Pierson, 1985). At Lahar Viewpoint, the lahar was only a few meters deep but moving at about 20 m/s. The Pine Creek lahar reached

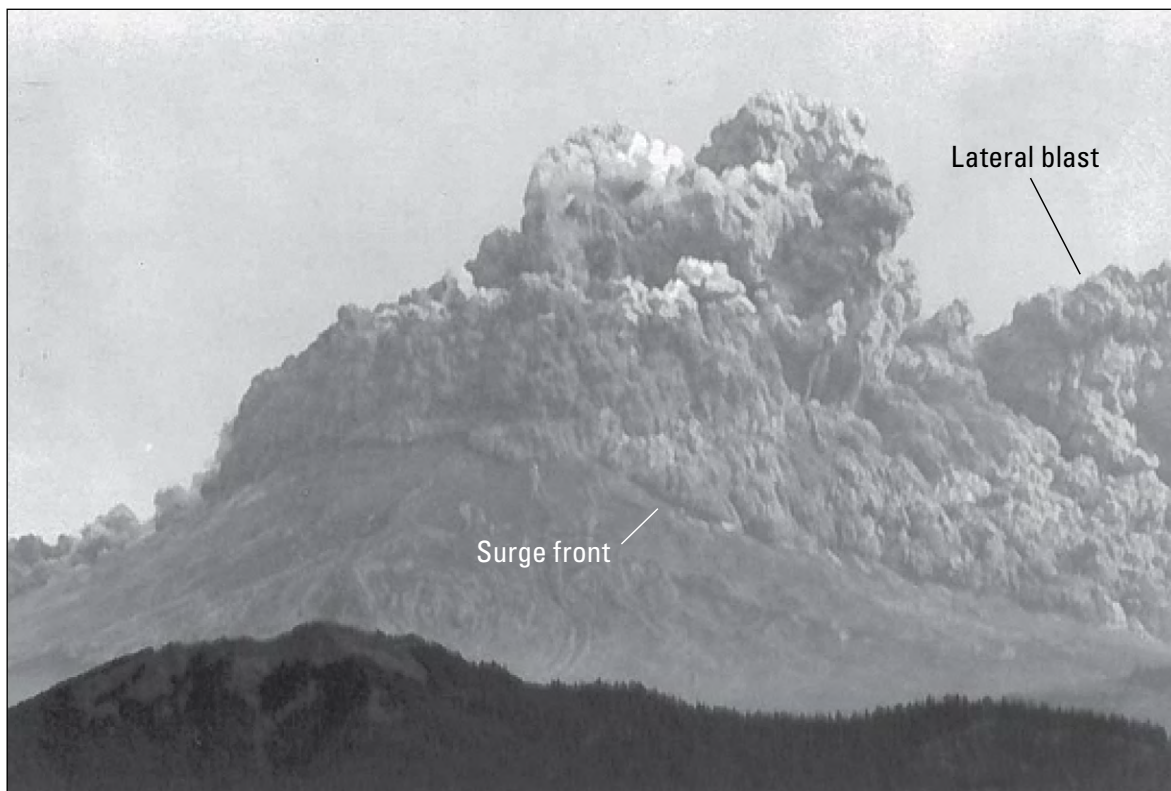


**Figure 50.** Photographic view of the south flank of Mount St. Helens between 8:33 and 8:34 a.m. on May 18, 1980 (eruption began at 08:32 a.m.). As the lateral blast moved northward (away from camera), lithic pyroclastic density currents “boiled over” onto the west, south, and east flanks. The front of a major pyroclastic density current (labeled surge front) moved down the southeast flank at 50 meters per second. Photograph by K. Seibert, 1980.

Swift Reservoir 23 km downstream from the crater only about 20 minutes after the beginning of the eruption; the Muddy River lahar arrived shortly thereafter. The combined lahars deposited 14 million cubic meters of muddy debris in a delta at the head of Swift Reservoir (Pierson, 1985).

Most trees encountered by the high-velocity lahar were sheared off a few inches above ground level, and a levee of tangled tree trunks can still be seen along the western flow margin just upstream of F.R. 83. Post-1980 tree growth here has reduced visibility of the lahar deposits, which are now better exposed near Stop 7 (Stratigraphy Viewpoint).

From here, turn right out of the parking lot and continue east on F.R. 83 to Stop 7.

**46.0 Stop 7—Stratigraphy Viewpoint (lat 46.1633° N, long 122.0922° W)** Pull into the pullout along the left side of the road just before crossing the bridge over the Muddy River (a small stream here).

Much of the eruptive history of Mount St. Helens is recorded by bedded pyroclastic-fall deposits (Mullineaux, 1986, 1996). At this stop, a short walk across the Muddy River channel leads to streambank outcrops that reveal an impressive stratigraphic section of tephra and interbedded lahar deposits of the Spirit Lake eruptive stage (3.9 ka to present) and older deposits of Mount St. Helens (fig. 52). This outcrop exposure is occasionally modified by slumping and

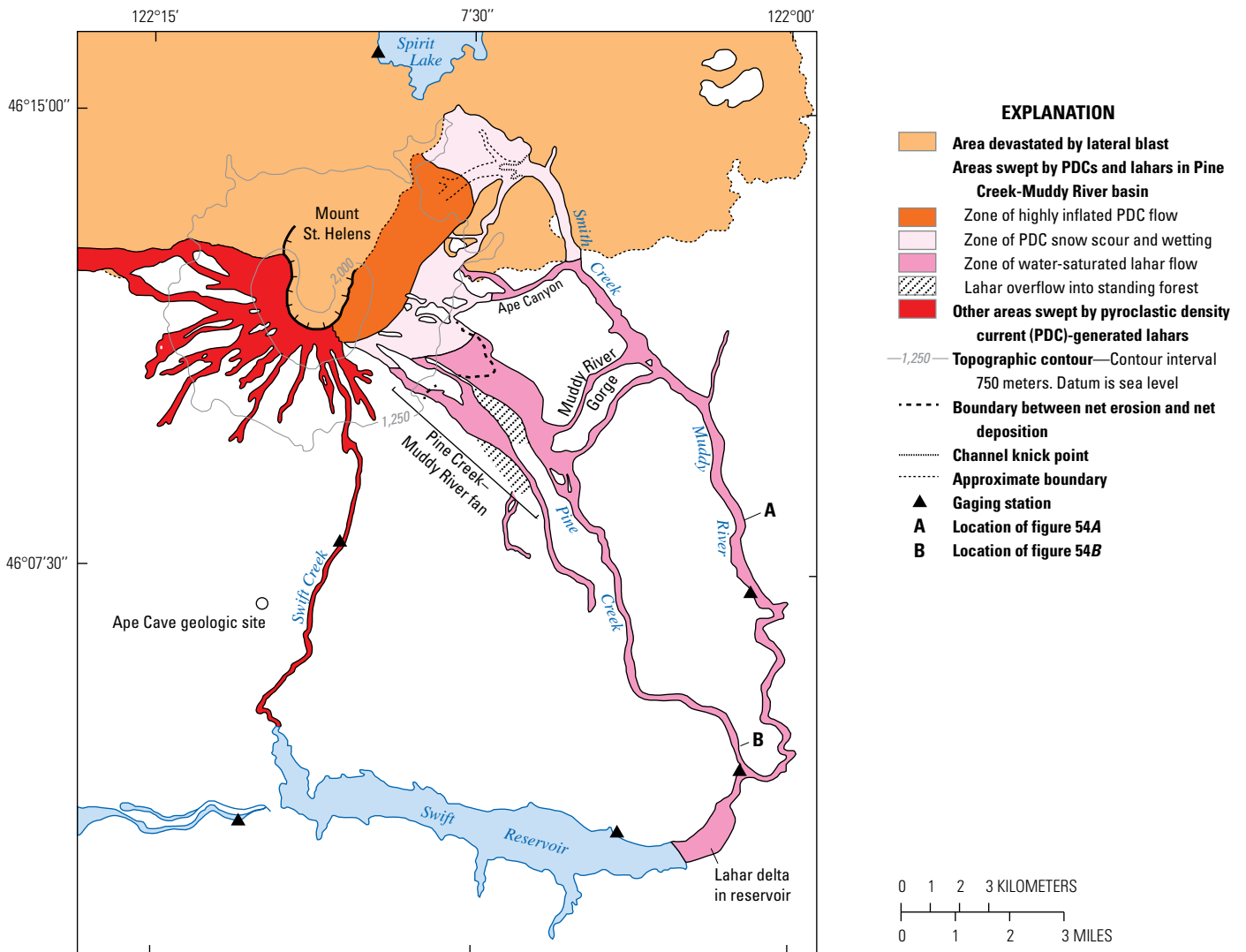


**Figure 51.** Map of volcanic slopes and river channels on west, south, and east flanks of Mount St. Helens that were impacted by May 18, 1980, lahars (see recent aerial view in fig. 45). Topographic contours (gray) in meters above sea level. Modified from Pierson (1985). See figure 54 for descriptions of A and B.



**Figure 52.** Pyroclastic-fall, pyroclastic density current, and lahar deposits at Stratigraphy Viewpoint along the Pine Creek-Muddy River debris fan margin (Stop 7). *A.* Photograph of the Pine Creek-Muddy River debris fan and Stratigraphy Viewpoint (light-colored bluff) along its margin. Shoestring Notch in Mount St. Helens' crater rim can be seen in the background. Smithsonian Institution photograph by L. Siebert, 2016. *B.* Photograph of the stratigraphic section at bluff outcrop (stream cutbank) showing major tephra sets labeled by letters; intervening units are lahar and pyroclastic density current deposits (see fig. 1 for approximate ages). Note long-handled shovel for scale. USGS photograph by R. Waitt, 1981. *C.* Map of the tephra fall distribution from three major Holocene explosive eruptions at Mount St. Helens. Modified from Clynne and others (2005). *D.* Photograph of the stratigraphic section in *A*, as seen today. Scale bar marked in red and white intervals of 10 centimeters. Smithsonian Institution photograph by L. Siebert, 2016.



May 18, 1980, lahar

Tephra set W

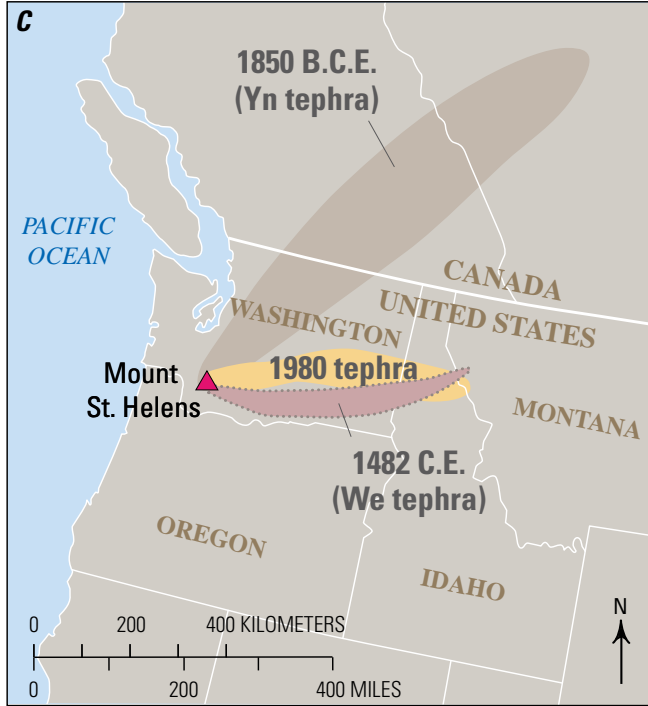
Tephra set B

Tephra set P

Tephra set Y

Tephra set J

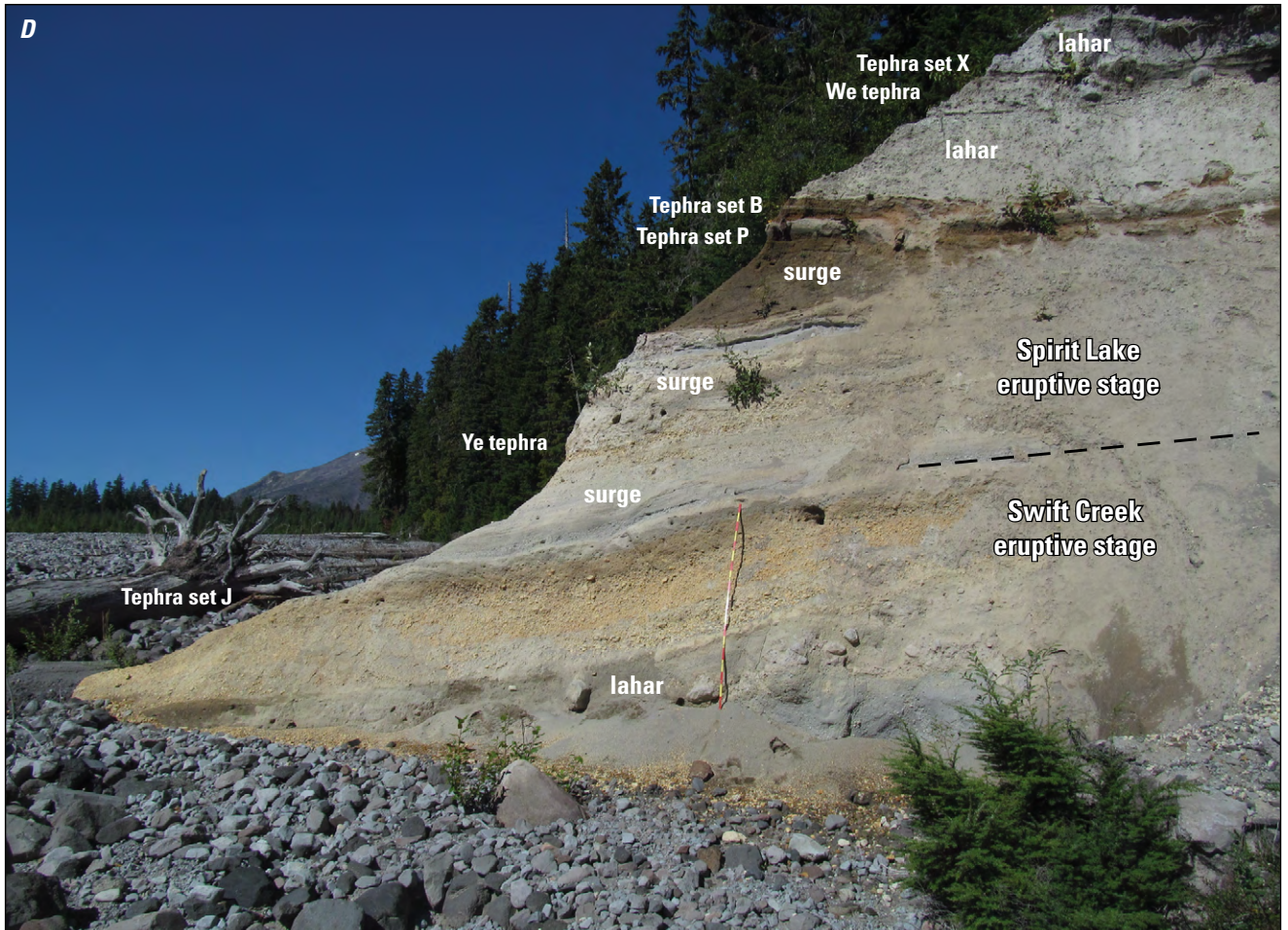
Lahar



erosion and the stratigraphic section varies along the cutbank.

The exposed sequence includes the thick pumice tephra set S (about 16 ka) at the base, the highly oxidized set J (about 13 ka) of the Swift Creek stage (fig. 53), and tephra layers Ye (3.3 ka) and We (1482 C.E.) of the Spirit Lake stage. The section also contains several intercalated lahar and PDC deposits and is capped by tephra set X (about 1500 C.E.) and the 1980 lahar deposit (fig. 53). Sets We and X are precisely dated by anomalously narrow growth rings on adversely affected trees (Yamaguchi, 1983). Tephra set J may now be the lowest pyroclastic-fall unit exposed; most of the basal tephra set S has been buried by the aggrading stream channel. A more detailed section of tephra set S, which comprises at least three major pumiceous air-fall tephra layers, can be seen at nearby exposures to the northeast.

If you wish to go to Optional Stop L, continue on from the pullout for Stop 7 and continue on F.R. 83 for another 0.5 mi to the end of the road. If you are not going to Optional Stop L, turn right out of the parking lot and backtrack on F.R. 83. Drive 45 minutes to Stop 8.



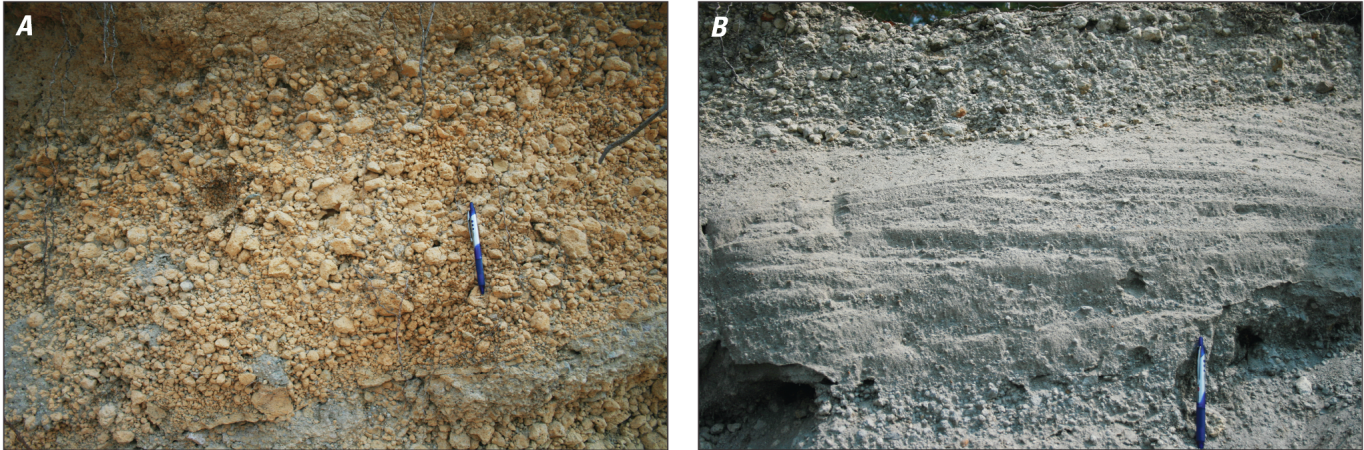


**Figure 53.** Close-up photographs of two volcaniclastic units at Stratigraphy Viewpoint (Stop 7). *A*, Coarse air-fall pumice unit of tephra set J (upper part). *B*, Low-concentration pyroclastic surge deposit (Smith Creek eruptive period) sandwiched between two air-fall pumice units. Deposit displays the low-angle crossbedding characteristic of many surge deposits. USGS photographs by T. Pierson, 2017.

**46.5 Optional Stop L—Lava Canyon Trail (lat 46.1658° N, long 122.0882° W)** The Lava Canyon trailhead is at the end of F.R. 83. The Lava Canyon trail traverses deceptively hazardous terrain. Make sure everyone in your party stays on the trail. The fast-moving water can sweep a person over the waterfalls if he or she slips in.

The trail descends into Lava Canyon, an incision cut by the Muddy River into an andesitic lava flow that flowed down the canyon 1,900 years ago. In places the canyon cuts into weaker Tertiary rocks lying beneath the lava flow. Several waterfalls drop over cliffs in the Kalama-age lava flow, which is about 16 m thick here. It displays two common features of columnar jointing: an upper 8-m-thick set of small, irregular, ill-formed columns (“entablature”), and a lower set of well-formed columns (“colonnade”) of equal thickness. A 0.4-mi wheelchair-accessible section of the trail leads to views of Lava Canyon at the uppermost waterfall. Here, a large boulder from the 1980 lahar is perched on top of the scoured lava flow surface. An extended 0.6-mi loop that crosses the Muddy River on a swinging suspension bridge provides good views of the young lava flow overlying oxidized lower Oligocene rocks. The trim line cut by part of the 1980 Pine Creek-Muddy River lahar can be seen in the prominent change in canyon-side vegetation from post-lahar alder trees to old-growth trees above.

When you are finished, turn around and backtrack on F.R. 83, passing Stops 7 and 6, until you reach the intersection with F.R. 90.

56.9 Turn left onto F.R. 90 towards Windy Ridge.

60.7 The third of the large reservoirs on the Lewis River, Swift Reservoir, is on the right. The road parallels the

reservoir until you are nearly to Stop 8, about 10 mi ahead.

68.7 U.S. Forest Service Pine Creek Information Center is on the left side of the road. The information center is usually open in summer during normal business hours. The next stop is about 500 ft ahead.

68.8 Intersection with F.R. 25

Continue straight on F.R. 25 to follow the field-trip route. If you need gas or diesel, turn right on F.R. 90 and drive 0.7 mi to a convenience store with fuel pumps on the left. If you are continuing northward to Windy Ridge Viewpoint or Randle, Wash., this station provides the last fuel available before Randle.

**69.5 Stop 8—Pine Creek Boulder and inactive quarry (lat 46.0725° N, long 122.0182° W)** Pull into the parking area located on the right side of the road. Stop 8 (fig. 45) consists of two adjacent localities highlighting volcaniclastic sediment that has been transported down Pine Creek, (1) a massive boulder transported by the 1980 Pine Creek lahar (fig. 54A), located approximately at location C in figure 52; and (2) a small inactive quarry showing a sequence of Pine Creek-age flow units (fig. 54B). After parking, walk behind the boulder and carefully make your way down the informal trail leading to a beach along the Lewis River. The informal trail is steep, descending about 20 m in 60 m. Please proceed carefully. We will eat lunch here, on the Lewis River beach, while viewing pre-1980 lahar deposits in riverside bluffs.

At this location, the Pine Creek lahar had a peak flow velocity of about 12 m/s, a peak flow depth of about 6 m, and a peak flow width of about 100 m; its



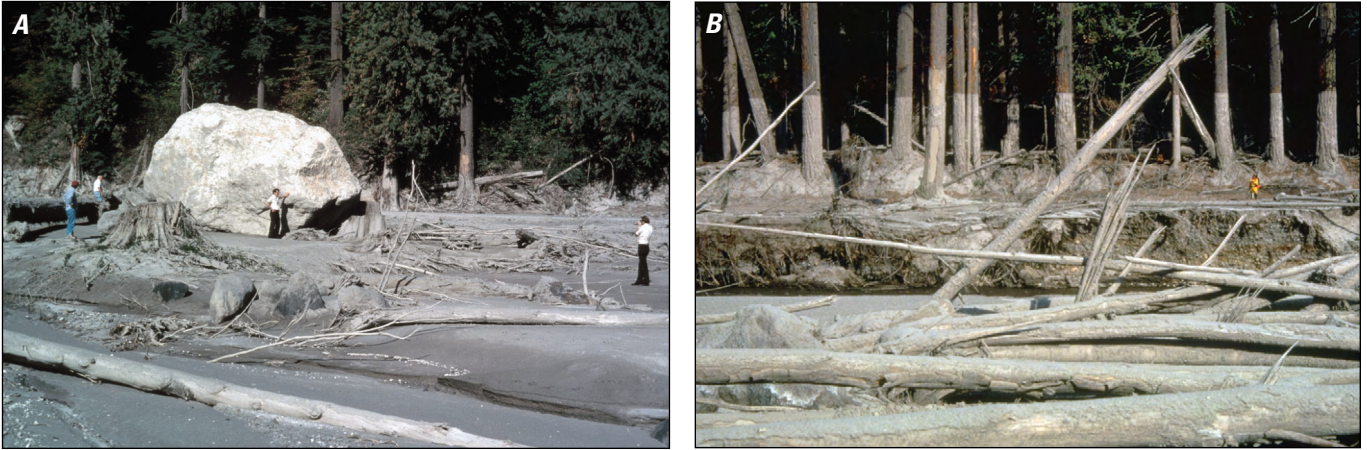


**Figure 54.** Signs of passage left by 1980 lahars other than major deposits. *A.* Photograph of a boulder weighing 37 short tons that was transported to this location by the Pine Creek lahar. Note mud marks on background trees indicating that the boulder was never more than half submerged by the lahar that emplaced it. USGS photograph, September 1980. *B.* Photograph of mud coatings on trees that mark the peak inundation depth of the 1980 Muddy River lahar. Note how much less material was emplaced by the lahar in comparison to this maximum depth. Person in yellow for scale. USGS photograph by L. Topinka, October 1980. These photograph locations can be viewed in figure 51 of this report.

peak discharge was about  $7,300 \text{ m}^3/\text{s}$  (Pierson, 1985). Such lahars can transport massive clasts (fig. 54A). The 37-ton (short ton) Pine Creek Boulder (approximate dimensions  $8 \times 5 \times 5 \text{ m}$ ) was deposited on the road 10 m above the creek bed by the 1980 Pine Creek lahar, making use of bed aggradation during lahar passage to reach that height. It was later moved off the road to its present location. The largest known boulder transported by 1980 lahars ( $10.4 \times 6.0 \times 4.6 \text{ m}$ ) was found resting on a terrace of 1980 lahar deposits along the Muddy River near location A in figure 51. It must have rolled there as bedload, because the lahar depth at that location is only 4 m—too shallow to have transported such a large clast as suspended load (Pierson, 1985). Older deposits of Pine Creek age are seen in the cutbank along the Lewis River below Pine Creek Boulder, where we plan to have lunch. As you walk to and from the outcrops along the Lewis River you pass through a young forest that has grown on the surface of the 1980 lahar deposits. In contrast, the large tree stumps here are rooted into the underlying Kalama-age deposits that formed the pre-1980 surface. Note that where lahar deposits are thin, trees growing on underlying surfaces can survive inundation and abrasion injury (fig. 54B). They also record the impact date by producing tree rings for a decade or two that are much thinner than average.

From the Pine Creek Boulder parking area, continue about 100 m on F.R. 25 across the bridge over Pine Creek. Just after the bridge, a small dirt road enters a quarry on the right side of the road (lat  $46.0743^\circ \text{ N}$ , long  $122.0164^\circ \text{ W}$ ). Note this is a privately owned quarry and we recommend that you get permission from the landowners (Three Rivers Recreational Area, LLC) prior to entering. The quarry

provides excellent exposures of Pine Creek-age lahars emplaced within a paleochannel that cuts into older Swift Creek-age deposits (fig. 55). These lahars overlie a PDC deposit of Pine Creek age that is exposed in the bank of the Lewis River.

From the quarry, continue in the direction you were traveling on F.R. 25 for about 10 minutes. Watch for the next bridge, located just before the parking place for the next site.



**Figure 55.** Cross-sectional photograph of Pine Creek-age lahar deposits and volcano-fluvial layers in quarry at Stop 8. The view is nearly parallel to flow direction (from left to right), with a coarse gravel bar at center right. Smithsonian Institution photograph by L. Siebert, 2016.

**73.0 Optional Stop M—Cedar Flats Natural Area (lat 46.1117° N, long 122.0186° W)** Driving back toward Cougar, watch on the left side of the road for an unsigned pullout next to a split-rail log fence that marks a trailhead. Pull off the road and park at the fence. This is the start of a 1 mi loop trail through a spectacular remnant of lowland Pacific Northwest old-growth forest. Rare examples of fully mature Douglas fir (*Pseudotsuga menziesii*), western hemlock (*Tsuga heterophylla*), and western redcedar (*Thuja plicata*) are present. Cedar Flats Natural Area, on which the forest grows, occupies a large debris fan at the mouth of Pine Creek. The debris fan is underlain by a Cougar-age debris-avalanche deposit, which likely transformed to a lahar by the time it was deposited here (fig. 56). Its exposure at Cedar Flats suggests that the debris avalanche diverted around the Marble Mountain massif and traveled down both the Swift Creek and Pine Creek valleys.

The debris-avalanche deposit at Cedar Flats is overlain by Swift Creek-age lahars and lithic PDC deposits and Kalama-age deposits from hyperconcentrated flows and muddy streamflows (M. Clynne, oral commun., 2016). The Swift Creek deposits are mostly oligomictic and dominated by porphyritic hornblende-hypersthene dacite blocks, which were derived from lava domes. Clasts of the Kalama-age deposits are mostly weakly vesiculated bread-crust andesite with rare blocks of highly vesiculated andesite as much as several meters in diameter. As many as five beds of the Kalama-age deposits are visible here and are related to eruption of the middle Kalama PDCs, which are identical in lithology and composition to the Worm Flows lava complex. About half way through the loop, the trail passes along a steep embankment that overlooks the Muddy River. The Cougar-stage debris-avalanche and younger deposits crop out along this embankment, but off-trail access is steep and difficult.

**73.4 Stop 9—1980 Muddy River lahar deposits (lat 46.1223° N, long 122.0145° W)** Cross the Muddy River bridge and park on the right side of the road or in the parking area on the left a short distance away. You are on the northeast bank of the Muddy River. As you look downstream from the bridge, the cutbank on the northeast side of the river is composed of 1980, Kalama-age, and older (unknown age) lahar deposits. From the road, walk down the embankment on the downstream side of the bridge and proceed along the river. Note that the vertical cutbank can be unstable, owing to undercutting by the river. However, the continuous erosion also exposes excellent outcrops along the cutbank in the few hundred meters downstream from the bridge. Please locate an outcrop that can be safely accessed to view the stratigraphic sequence.



**Figure 56.** Photograph of a Cougar-age debris-avalanche deposit at Cedar Flats, which had already transformed to a lahar by the time it reached this location. This exposure shows an extremely compact and poorly sorted deposit in a cutbank of the Muddy River. Scraped outcrop surface shows abundant vesicles and small polymictic angular to subrounded clasts with characteristic mottled pastel-colored texture of hydrothermally altered material. Head of military trenching tool for scale; looser material above is colluvium. Smithsonian Institution photograph by L. Siebert, 2016.

As was noted at Stop 8, young trees are growing on the surface of the 1980 lahar deposits, and mixed among them are stumps of trees that were growing on the underlying Kalama-age deposit and killed by lahar inundation in 1980.

Two lahars flowed down Muddy River on May 18, 1980 (fig. 57): (1) a large lahar in the morning that was composed dominantly of lithic clasts and (2) a much smaller lahar in the afternoon composed entirely of rounded pumice clasts (Pierson, 1985). Deposits of both can be seen along the northeast bank about 100 m downstream of the Muddy River bridge (fig. 58A), although the upper unit is only locally preserved. Evolution of the morning lahar is described in detail at Optional Stop K. In this area, the morning lahar was at least 4.2 m deep and capable of inflicting severe damage to trees growing on low river terraces (fig. 58B). The afternoon lahar derived water from rapid snowmelt generated by pumiceous PDCs descending Mount St. Helens' southeast flank during the main Plinian phase of the eruption (Pierson, 1985).

In its lower reach, the Muddy River channel has a flatter gradient than the lower Pine Creek channel. The morning lahar was probably partly hydraulically dammed by a sharp bend in the river just downstream of Stop 9. In fact, the back-calculated flow velocity here was less than 4 m/s—one of the slowest velocities measured (Pierson, 1985). The Muddy River lahar

entered the Lewis River with a peak flow rate of about 5,000 m<sup>3</sup>/s and reached the head of Swift Reservoir about 34 minutes behind the 1980 Pine Creek lahar.

Particle-size distributions for the Pine Creek and Muddy River lahars are broadly similar and typical of granular debris-flow lahars (fig. 58C). Slurry matrix samples of both of these east flank deposits are coarser than those of the North and South Fork Toutle River deposits. Deposits are, in places, as thick as 2.5 m, but, in general, they are less than 0.5 m and thin relative to the depth of the flows that deposited them. Thin coatings of muddy sand adhered to steep channel banks and tree trunks, providing estimates of flow depth (fig. 58B).

This is the field trip's last site at Mount St. Helens. After finishing at this stop, backtrack on F.R. 25 to the junction with F.R. 90. From here there are two possible routes (detailed below) to the starting point for Day 3 in Hood River, Oregon. Both routes have optional stops, but alternative route 1 is about

75 mi shorter than route 2. Alternative route 1 follows narrow and winding paved rural roads without services to the town of Carson, Wash., crosses the Columbia River at the Bridge of the Gods, and proceeds to Hood River on I-84. This route passes through the Indian Heaven volcanic field (Scott and others, 1995), a field with numerous small Quaternary monogenetic volcanoes between Mount St. Helens and Mount Adams. However, the volcanic field is heavily forested and no notable geologic features are visible along this route. Alternative route 2 returns to I-5 at Woodland, connects with I-205 just north of Vancouver, and joins I-84 in northeast Portland before continuing east to Hood River.

## Day 2: Alternative Route 1

- 73.4 Backtrack toward Cougar on F.R. 25.
- 77.9 Turn left onto F.R. 90 at the intersection with F.R. 25.
- 78.3 Eagle Cliff bridge  
You are now crossing the Eagle Cliff bridge, which replaces a bridge destroyed by lahars during the May 18, 1980, eruption. You will soon pass the Eagle Cliff store and campground, which typically has gas available during the summer months. If your car is running low on gas, this will be your last chance to refuel for the next 35 miles. Continue on F.R. 90 and watch for an intersecting paved road on the right.
- 82.1 Turn right onto Curly Creek Road. When the road begins to climb a low hill with a series of curves, watch for your next turn.
- 84.9 Optional Stop N1—McClellan overlook (lat 46.0403° N, long 122.9194° W)** Turn right into the parking lot for McClellan overlook, which provides an excellent view of the south side of Mount St. Helens. When finished, turn right out of the parking lot and continue in the direction you were traveling along Curly Creek Road.
- 87.1 Curly Creek Road ends in a T-intersection with Meadow Creek Road; turn right. Meadow Creek Road eventually turns into Wind River Road, also known as F.R. 30.

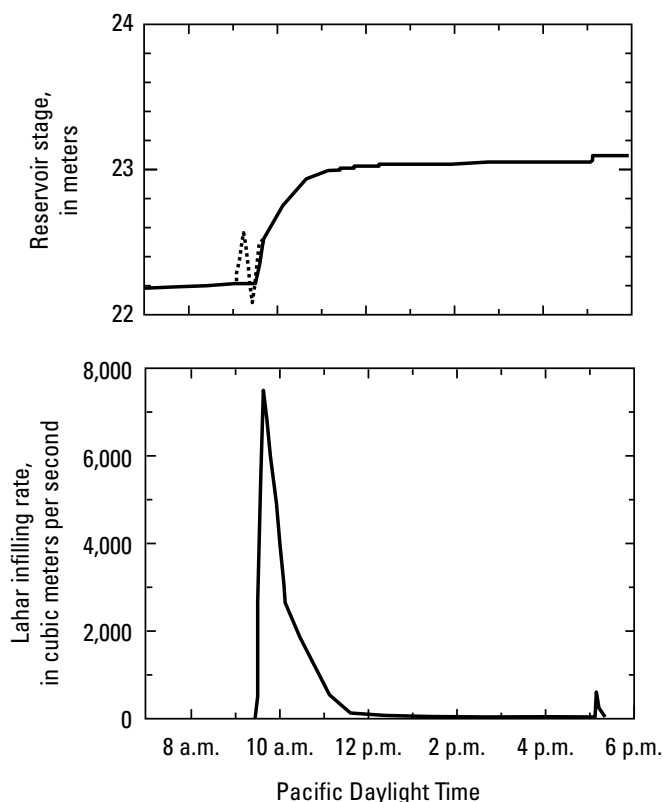


**Figure 57.** Lake-level record for Swift Reservoir on May 18, 1980, and reconstructed hydrographs for the Pine Creek and Muddy River lahars as they entered Swift Reservoir. The Pine Creek lahar arrived about 34 minutes before the Muddy River lahar and 30 minutes after being triggered on the flank of the volcano. The total sediment volume deposited underwater was 13,431,000 cubic meters (m<sup>3</sup>). A second, smaller Muddy River lahar, composed of pumice fragments, arrived in the late afternoon with a volume of about 520,000 m<sup>3</sup>. Modified from Pierson (1985).

- 111.0 Wind River bridge  
The relatively flat valley that you have been traveling along is underlain by a late Pleistocene mafic lava flow from the Trout Creek Hill volcanic vent. Erosion by the river has exposed the lava flow in a deep canyon below the bridge. Continue along Wind River Road, also commonly referred to as the Wind River highway.

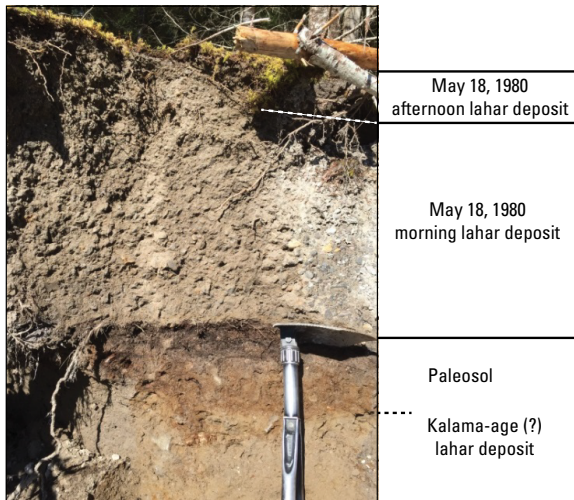
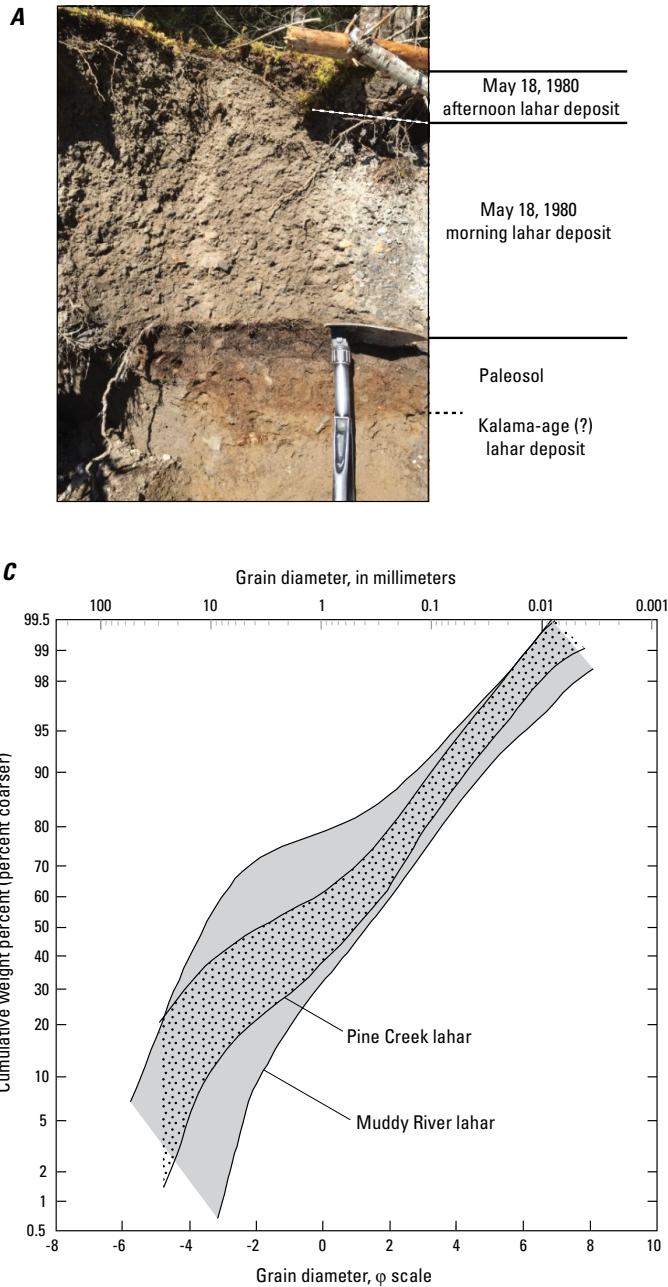


**Figure 58.** Evidence of lahars in the lower Muddy River. **A.** Photograph of the sequence of lahar deposits at Stop 9. Bottom unit was emplaced by a probable Kalama-age lahar. A moderately mature paleosol (with A and B<sub>ox</sub> horizons) is developed on the top of this unit (the pre-1980 forest floor). Shovel blade (20 centimeters long) at top of paleosol. Overlying that is the May 18 morning lahar deposit, containing mostly pebble-size lithic clasts. At the top of the section is the discontinuous deposit emplaced by the May 18 afternoon pumice lahar. USGS photograph by T.C. Pierson, 2016. **B.** Photograph of a tree near the lahar flow margin abraded by the May 18 Muddy River morning lahar. Note the removal of tree bark and the thin coating of mud on the tree trunk as well as the burial of the trunk base in the lahar deposit (thickness here unknown). USGS photograph by G. Beach, 1981. **C.** Plot of grain-size distribution of Pine Creek and morning Muddy River lahar deposits. Phi ( $\phi$ ) scale represents grain diameter as the negative logarithm (base 2) of grain diameter in millimeters (at top). Modified from Pierson (1985).

- 112.0 You are now entering the community of Carson, Wash. Continue through Carson on Wind River Road.
- 114.5 Turn right onto S.R. 14. You are now in the Columbia Gorge.
- 117.3 Pass through the town of Stevenson, Wash.
- 118.1 Rock Cove  
As you leave Stevenson, the road is on a causeway that divides Rock Cove on the right from the mainstream of the Columbia River on the left. The islands in Rock

Cove are hummocks in the Red Bluff landslide, derived from Greenleaf Peak, 3.7 mi (6 km) away on the ridge to your right. Continue traveling along S.R. 14.

- 120.5 Bridge of the Gods  
Turn left onto the narrow, two-lane Bridge of the Gods, and cross the Columbia River. The bridge toll is currently \$2.00 for cars. You are now entering Oregon. At the end of the bridge, follow the road as it loops around. Turn right at the bottom of the ramp onto Wa Na Pa Street (Cascade Locks Highway). Proceed east through the town of Cascade Locks.

Cascade Locks takes its name from an early navigational lock, finished in 1896, that was constructed to help river boats pass the notorious Cascade Rapids (from which the Cascade Range gets its name). This became a moot issue after 1937, when the rapids (and the lock) were drowned by the backwater pool from Bonneville Dam (elevation around 21 m above sea level, a.s.l.). If you are going to Optional Stop P, proceed 0.5 mi from the end of the bridge ramp, and turn left on SW Portage Road into Marine Park. If continuing directly to Hood River, drive 1.0 mi farther and merge onto I–84. At this point, alternative routes 1 and 2 follow the same path to Hood River, Oreg. Skip ahead to Optional Stop P (at mile marker 176.0 on alternative route 2) to continue with the road log from this point.

## Day 2: Alternative Route 2

- 73.4 Begin the return to Woodland, Wash. by heading south on F.R. 90 from the F.R. 25 and F.R. 90 junction.
- 96.2 Pass through the town of Cougar, Wash. Continue on Lewis River Road.
- 101.5 Continue straight on S.R. 503.
- 124.6 Woodland, Wash. Turn left onto I–5 southbound towards Portland, Oreg.
- 137.6 Merge onto I–205 southbound towards Salem, Oreg.
- 148.1 Glenn L. Jackson Memorial Bridge  
The Glenn L. Jackson Memorial Bridge on I–205 over the Columbia River has support piers on Government Island, a large mid-channel bar composed in part of volcanoclastic sediment from Mount Hood. In clear weather you can see a spectacular view of Mount Hood from the bridge.  
The Columbia River forms the border between Washington and Oregon. The low hills on the Oregon side of the river are volcanoes of the Pliocene–Pleistocene Boring Volcanic Field (fig. 59). The volcanic field is named for the town of Boring, Oregon (not for being uninteresting). Boring Volcanic Field vents extend from the Portland area eastward, nearly parallel to the Columbia Gorge. Other vents probably related to the Boring Volcanic Field and of similar age extend eastward nearly to the Hood River. More than 80 vents, located on both sides of the Columbia River, were active from about 3.3 Ma to 57 ka.
- 141.4 Take Exit 22 for I–84 eastbound towards The Dalles.  
The junction of I–205 and I–84 crosses channels scoured by the Missoula floods that diverged around

Rocky Butte, the intrusive core of a 285±16 ka basaltic andesite volcano of the Boring Volcanic Field just west of this junction.

- 150.3 Bridge over the Sandy River  
On the last day of the field trip (Day 4 Stop 9), we will visit Timberline-age lahar deposits from Mount Hood on the Sandy River delta, visible here on the north side of the I–84 bridge.
- 164.0 Optional Stop O2—Multnomah Falls (lat 45.5788° N, long 122.1185° W)** To visit the falls, take Exit 31 (left exit) to Multnomah Falls parking. Hide or take valuables and lock your car; this is a high-theft area. Walk along the pathway, crossing through a pedestrian underpass, to Multnomah Falls Lodge (restaurant and concessions); continue past these to the waterfall. This 620-ft (189 m) two-tiered waterfall is the highest of many along “Waterfall Alley” in the western part of the Columbia Gorge and the most visited natural recreation site in the Pacific Northwest. Multnomah Creek plunges off vertical cliffs composed of Miocene-age Columbia River Basalt lava flows. A short trail leads to the iconic Benson footbridge between the upper and lower falls, and a longer trail leads to an overlook above the upper falls. To the west, the loop trail to Wahkeena Falls leads to additional waterfalls. Multnomah Falls Lodge is on the National Register of Historical Places; a gift shop and restrooms are available on the ground level.  
From the parking lot, merge back onto I–84 eastbound. Note, for those with more time, Multnomah Falls is also accessible by a scenic loop road between Exit 22 (Corbett) and Exit 35 (Ainsworth State Park). This is one of several remnants of the Historic Columbia River Highway—the first road across the Cascades—which celebrated its centennial in 2016. The narrow highway also passes by Vista House at Crown Point, with spectacular views of the Columbia Gorge and several other major waterfalls.
- 166.0 Dodson debris fan  
You are passing the westernmost of several boulder-rich debris-flow deposits near Dodson, Oreg., that were emplaced during an extreme rainstorm in early February 1996. The deposits are on the south side of the road, but are heavily vegetated. As a result of the debris flow, I–84 was closed for five days and Union Pacific railroad tracks were severely damaged. The debris flow also inundated a house, whose residents escaped only moments before the flow arrived.
- 169.6 Beacon Rock  
The monolith visible on the Washington side of the Columbia River is Beacon Rock, a volcanic plug composed of basaltic andesite that stands 848 ft (258 m)

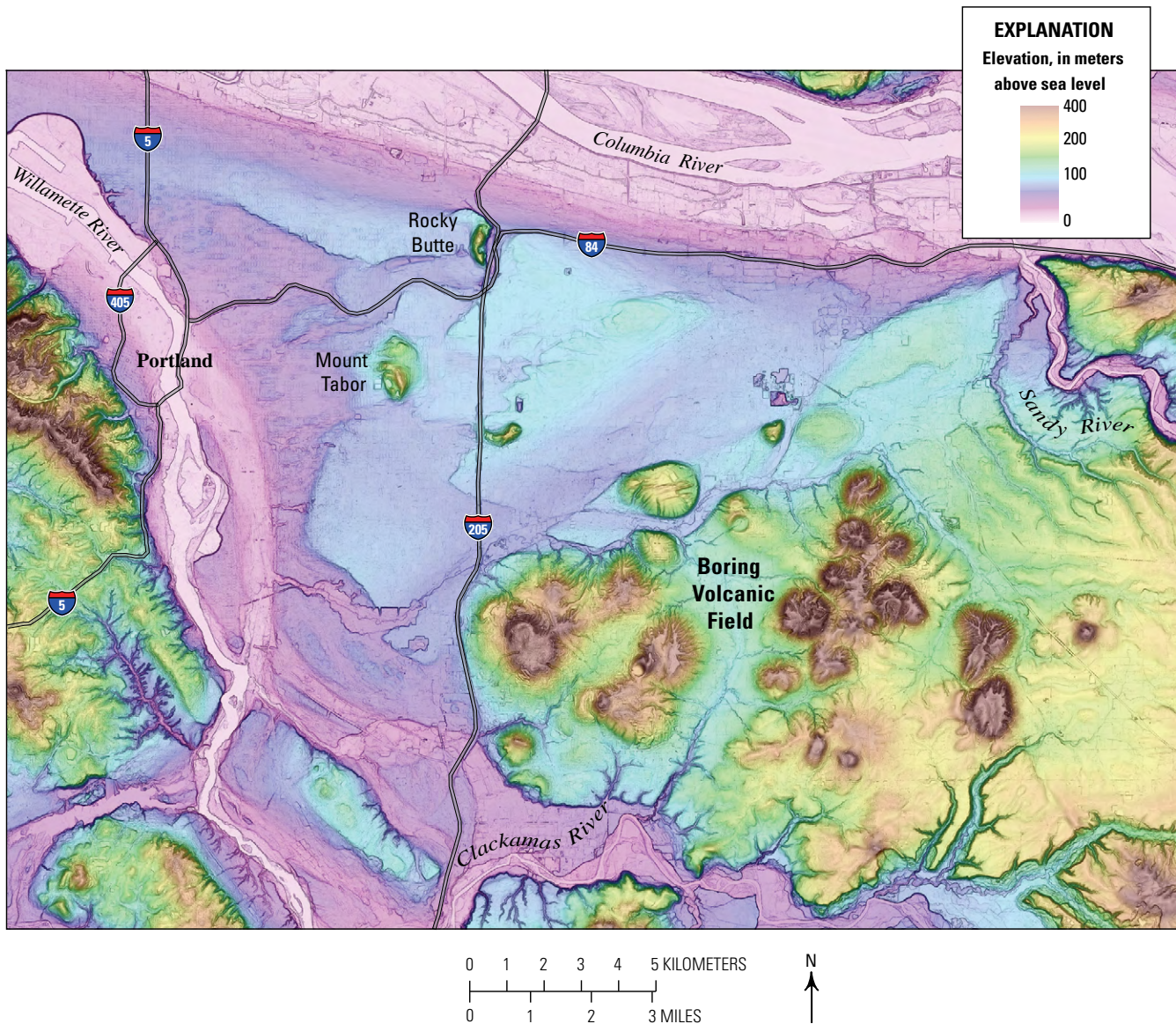


**Figure 59.** Colored digital elevation model of the Portland area. The upper limit of Missoula flooding here was approximately 125 meters above sea level, corresponding to the transition between blue and green. Higher elevation areas of roughly circular shape in darker brown are volcanoes of the Boring Volcanic Field, including Rocky Butte and Mount Tabor. Modified from O'Connor and Burns (2009).

tall. Emplaced 57 ka, it is the youngest dated vent of the Boring Volcanic Field. The plug is the congealed magma in the conduit of a cinder cone, which was exposed when the Missoula floods stripped away the volcaniclastic ejecta that formed the surrounding cone.

### 173.3 Bonneville Dam

Bonneville Dam is a large hydroelectric dam that was the first one built on the Columbia River, completed in 1937 to bring ample electric power to the Pacific Northwest. Part of Bonneville Dam is built on a massive landslide deposit emplaced by the ~600-year-old Bonneville landslide. A navigational lock at Bonneville Dam was completed in 1938—the highest

single-lift lock in the world at that time. A second powerhouse was added to the dam, finished in 1981. A larger lock was constructed and opened to ship and barge traffic in 1993. Bonneville Dam produces more than 1,000 megawatts of electric power today.

Just after the exit for Bonneville Dam and east of the Eagle Creek fish hatchery, roadcuts on the south side of the freeway expose lower Miocene Eagle Creek Formation lahar deposits, which underlie the Columbia River Basalt Group.

### 176.1

Alternate routes 1 and 2 merge together here at the town of Cascade Locks. Cascade Locks takes its name from an early navigational lock, finished in

1896, that was constructed to help river boats pass the notorious Cascade Rapids (from which the Cascade Range gets its name). This became a moot issue after 1937, when the rapids (and the lock) were drowned by the backwater pool from Bonneville Dam (pool elevation around 21 m a.s.l.).

**176.1 Optional Stop P—Bonneville landslide**

(lat 45.6710° N, long 121.8926° W) Take Exit 44 off I-84 to Cascade Locks. The exit ramp turns into Wa Na Pa Street. Follow Wa Na Pa Street east into the town and drive 0.5 mi. Turn left on SW Portage Road into Marine Park, passing through the railroad underpass and staying left. Park by the old lock, then walk across the lock on the pedestrian bridge and continue north to the river's edge for a view of the Bonneville landslide.

Weak, tilted layers of volcanoclastic sediments are responsible for a large number of landslides on the Washington side of the Columbia Gorge (Palmer, 1977; O'Connor and Burns, 2009; Pierson and others, 2016). The town of Cascade Locks provides several viewpoints of what remains of the natural Bridge of the Gods—a “bridge” across the Columbia River recorded in the legends of local native people. This “bridge” has been inferred to be the natural dam that held back the Columbia River for months to possibly years, forming when the Bonneville landslide broke loose from the northern side of the Columbia Gorge in the early 15th century and slid completely across the river to the southern shore (fig. 60A). Stumps of trees killed by submersion in the landslide-dammed lake were preserved until they were resubmerged in the backwater pool behind Bonneville Dam (fig. 60B). The

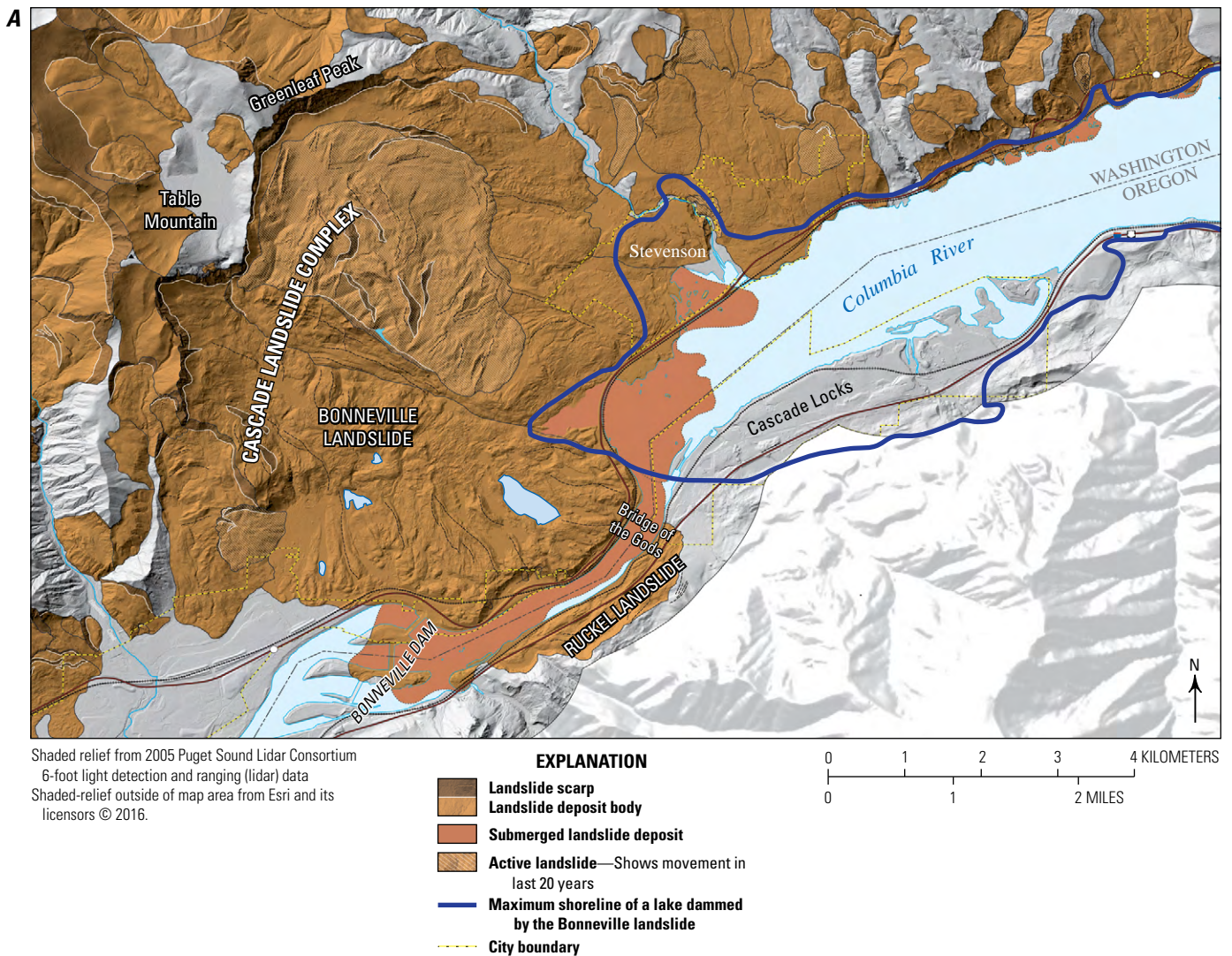


**Figure 60.** Large landslides in Columbia Gorge. *A.* Map of the Bonneville and surrounding landslides on the Washington side of the western Columbia Gorge. The blue line shows the approximate location of the maximum shoreline of a lake dammed by the Bonneville landslide (O'Connor and Burns, 2009). Modified from Pierson and others (2016). *B.* Photograph of remnants of the submerged forest of the Columbia Gorge drowned by the temporary lake formed behind the Bonneville landslide in the early 15th century. Archival photograph 3931 by D.B. Lawrence, Oregon Historical Society, 1933.

Figure 60.—Continued



lake-forming blockage was partly breached sometime after the landslide occurred, allowing formation of a new river channel about 1 km south of the former channel. This new channel was quite narrow (140 m) and steep (dropping 12 m over 3.2 km), and it was filled with large landslide blocks. A formidable set of rapids—first described by Lewis and Clark as the Cascade Rapids—prompted construction of a canal and locks that were completed in 1896. Operation of the canal and locks, and bypassing of the Cascade Rapids, permitted steamboat navigation up the Columbia River and, thus, large-scale commerce between the west and east sides of the Cascade Range. Marine Park in Cascade Locks provides a clear view of the eroded toe of the landslide blockage, but the rapids here are now submerged beneath the backwater pool of Bonneville Dam (fig. 61).

Bonneville landslide is one of several large landslides making up the Cascade landslide complex, several of which can be seen from Marine Park in Cascade Locks (fig. 61) (Pierson and others, 2016). Both the Bonneville and Red Bluffs landslide, each about a cubic kilometer in volume, traveled between 5 and 6 km from their 400- to 500-m-high headscarps to their toes. Both are less than 600 years old (Pierson and others, 2016). A reactivated, 8 km<sup>2</sup> portion of the Red Bluffs landslide, the Crescent Lake landslide (fig. 60A), currently creeps during the wet winter months at an average rate of about 15–20 centimeters per year.

Breaching of the lake dammed by the Bonneville landslide occurred in stages (O'Connor, 2004; O'Connor and Burns, 2009). Prominent deltaic surfaces at both 75–80 and 40 m a.s.l. indicate that the lake

surface was at or near maximum capacity for some time, followed by a prolonged interim stable lower lake level. Additional incision into the blockage lowered the lake to its pre-1937 historical elevation of 13 m a.s.l. At least one episode of lowering the lake level was cataclysmic, leaving behind boulder-rich flood bars and bedded sands just downstream of the landslide blockage. Distinctive beds of relatively coarse sediment in floodplain and estuary deposits farther downstream suggest a large dam-breach flood occurred. These beds underlie 1479–1482 C.E. tephra from Mount St. Helens (O'Connor and others, 1996; Atwater, 1994). This suggests that a large flood affected the lower Columbia River within a few decades of landslide emplacement. The most plausible scenario to create the downstream flood features is partial breaching of the stable 75–80 m a.s.l. lake level and release of water downstream, lowering lake level to 40 m a.s.l. decades after emplacement of the landslide deposit. The timing and nature of further incision to attain historical lake levels is uncertain but may have occurred just before Lewis and Clark's visit (1805–06), based on the degree of preservation of drowned forest trees that were exposed to air after the lake level dropped to 13 m a.s.l.

Once finished with this stop, turn left on Wa Na Pa Street. Merge onto I–84 eastbound ahead.

#### 186.9 Wind Mountain

Across the Columbia River to the north, Wind Mountain is a ~6 Ma quartz diorite intrusion (Korosec, 1987). Another of the great Columbia Gorge landslides, the Collins Point landslide was active a few decades ago





**Figure 61.** Photograph of headscarps of the Bonneville landslide (left) and Red Bluffs landslide (right) in the background, with the truncated toe of the Bonneville landslide deposit in the left foreground (covered in vegetation). The water surface here is directly above the submerged Cascade Rapids. The mountain peak on the left is Table Mountain; on the right is Greenleaf Peak. The view is from the Oregon shore at Cascade Locks, looking north. Smithsonian Institution photograph by L. Siebert, 2014.

and is sourced from the north. It wraps around both sides of Wind Mountain and its eastern arm protrudes about 0.25 mi out into the Columbia River channel.

#### 187.7 Shellrock Mountain

To the south, you are passing Shellrock Mountain, which has been dated to  $5.7 \pm 0.6$  Ma and is the southern continuation of the quartz diorite intrusion at Wind Mountain (Korosec, 1987).

199.0 Take Exit 63 off I-84. Turn left at the end of the ramp. Once across the freeway overpass, take the next available right turn, onto Riverside Drive. Turn right onto Nichols Parkway. Proceed a few hundred feet to Hampton Inn and Suites hotel, our stop for the night.

### Day 3: Hyaloclastites, glacial tills, and other diamicts in the Hood River and Sandy River basins, Mount Hood

Numbered and lettered stops restart at 1 and A, respectively, for field trip Days 3 and 4 here at Mount Hood. Day 3 includes visits to exposures of various volcanoclastic sediments on three sides of Mount Hood (fig. 62). The route starts south of Hood River, Oreg., on the north side of the volcano, traverses the east flank on Oregon Route 35 (O.R. 35), and then turns west on U.S. Highway 26 (U.S. 26) across the volcano's south flank.

0.0 Cumulative mileage for Day 3 begins at the Hampton Inn and Suites hotel in Hood River. We begin by backtracking a short distance on I-84. From the hotel,

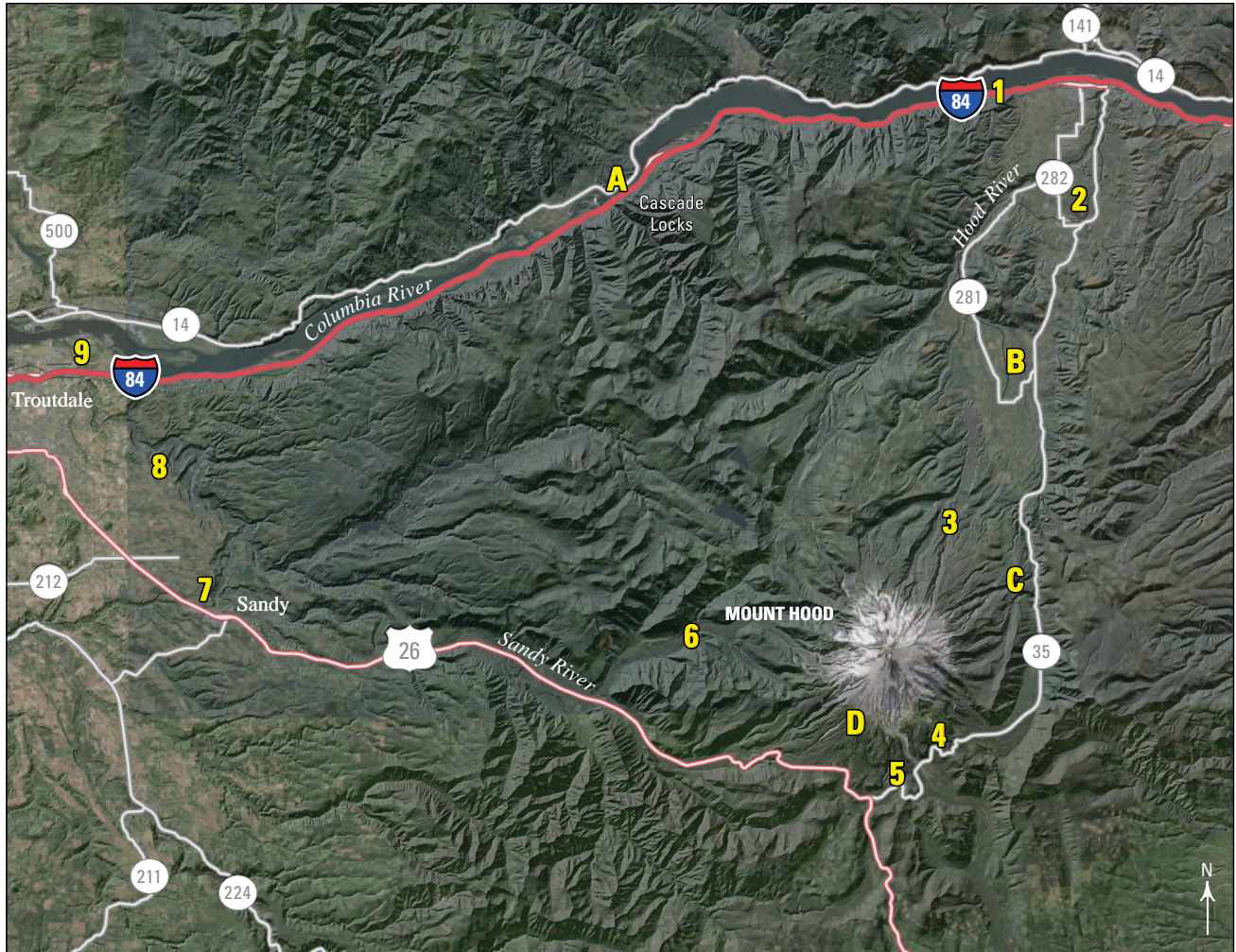
turn left onto Nichols Parkway, left onto Riverside Drive, left onto North 2nd Street, and then merge onto I-84 westbound. Drive 3.4 mi west to a high roadcut of orange-yellow deposits on the right with a wide pullout area.

**3.4 Stop 1—Hyaloclastite deposits along I-84 (lat 45.7072° N, long 121.5791° W)** Park along the shoulder of the road just past the intersection with Morton Road.

The hyaloclastites at this stop formed when basaltic lava flows rapidly quenched and shattered as they flowed into the cold water of the Columbia River. These roadcuts expose pillow lavas and orange-colored palagonitized hyaloclastite debris—including glassy, chemically altered, coarse sand and fine gravel (fig. 63). These units are part of a pillow lava-palagonite sequence that outcrops westward along the base of Pliocene lava flows in the Columbia Gorge. The pillows commonly are aligned and the clastic beds dip steeply owing to emplacement as submerged delta-front foreset beds. A K-Ar age of  $3.53 \pm 0.08$  Ma was obtained from the base of this sequence at Perham Creek, about 5.5 km southwest of this site (Conrey and others, 1996). The lava source is uncertain.

Once finished at the outcrop, merge back onto I-84 westbound. Stay in the right lane because you will be using the next exit to make a U-turn. The drive to Stop 2 takes about 10 minutes.

3.9 Take the next right exit, marked as a service road, to make a U-turn onto I-84 eastbound. Follow the service



Base from U.S. Geological Survey (USGS) 30-meter Landsat imagery  
Shaded relief and roads from USGS's The National Map

**EXPLANATION**  
**5** Field-trip stop—Number is planned stop; letter is optional stop

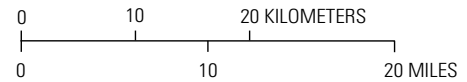


**Figure 62.** Locations of planned stops (numbers) and optional stops (letters) for field trip Days 3 and 4 at Mount Hood.

road to the left as it passes under I-84 and curves back the right. At the intersection with Mitchell Point Drive, turn right and merge onto I-84 eastbound.

7.8 **Mount Adams view**  
 Mount Adams is briefly visible across the Columbia River to the north-northeast up the White Salmon River valley. Hood River lies about halfway between Mount Hood and Mount Adams, and volcanic mass flows from both volcanoes have reached as far as the Columbia River (Vallance, 1999).

8.7 Back in the town of Hood River, take Exit 64 with signs for O.R. 35, leading to White Salmon and

Government Camp. Turn right at the end of the ramp and follow O.R. 35 southward towards Mount Hood and Government Camp. At highway mile marker 100, you are nearing Stop 2.

11.4 **Stop 2—Mount Hood flank-collapse lahar deposit (lat 45.6804° N, long 121.5085° W)** Just after mile marker 100, watch for a railroad bridge over the road. Pull off into a parking area located on the right side of the road just after passing under the railroad bridge. From the parking area, walk down to the railroad tracks and continue to the south along the tracks for about 200 m to lat 45.6785° N, long 121.5097° W. The outcrop is located in the railroad cut on the east

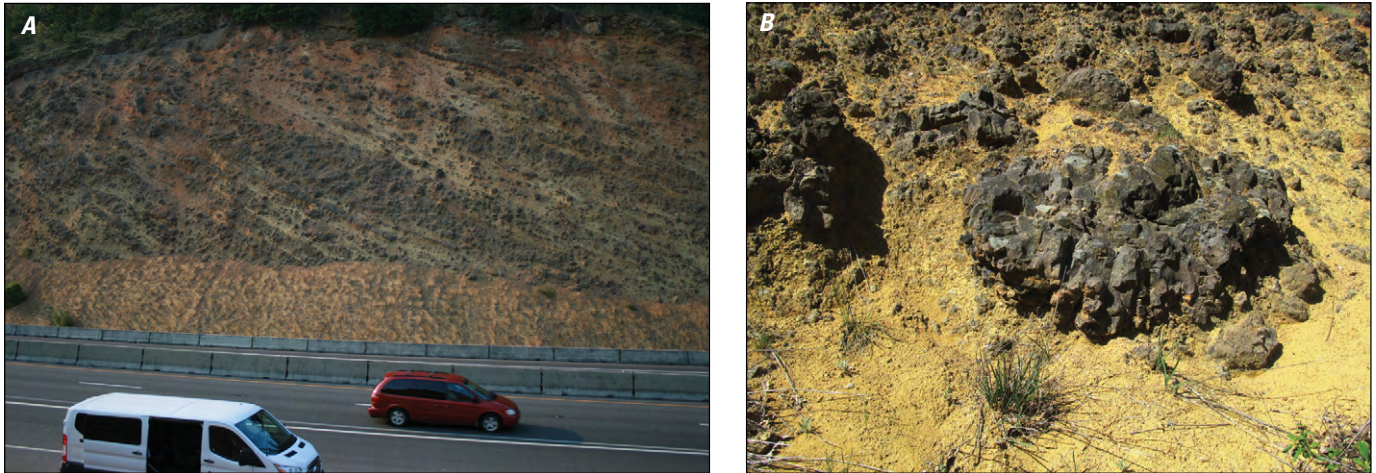


**Figure 63.** Deposits of a late Pliocene basaltic hyaloclastite delta, located along Interstate 84, just west of Hood River, Oregon (field trip Day 3 Stop 1). The deposits formed when basaltic lava flows entered standing water. *A.* Photograph of delta-front foreset beds dipping to the right (west). Highway barriers are about one meter tall. View is to the south, taken from the north side of Interstate 84. USGS photograph by T. Pierson, 2017. *B.* Photograph of a fractured pillow lava, about 1 meter wide, surrounded by a palagonitized matrix. Smithsonian Institution photograph by L. Siebert, 2016.

side of the tracks. Be extremely careful because this is an active rail line with trains passing several times a day, albeit slowly.

The Hood River lahar originated from edifice collapse on the north flank of Mount Hood and transformed from a debris avalanche to a large debris-flow lahar that flowed down the Hood River valley, crossed the Columbia River valley (filling it ~100 m deep), and then flowed at least 4 km up the White Salmon River valley on the Washington shore—a total distance of about 50 km (Vallance, 1999). The lahar deposit has been estimated to be ~100,000 years old (Scott and Gardner, 2017), but it could be younger. It contains wood too old for radiocarbon dating (implying the lahar must be older than 38,000 years) and the probable failure scar on the north flank of Mount Hood has filled in with lavas as old as 50 ka, providing an older minimum age (W.E. Scott, 2016, oral commun.). Additionally, the deposit contains an andesite clast that has a K-Ar age of  $61 \pm 21$  ka, suggesting the lahar must be younger than ~80 ka to have entrained this clast (Scott and others, 2003). An arcuate scarp at Cooper Spur on the northeast flank of Mount Hood may represent the east edge of the in-filled edifice-collapse scarp. At least two other large clay-rich lahar deposits are found in the Hood River valley, suggesting a history of edifice instability at Mount Hood. One of these lies between an andesite lava flow dated at  $475 \pm 14$  ka and the 424-ka basaltic andesite of Cloud Cap; the other remains undated.

At this outcrop along the railroad tracks, 38 km downstream of the volcano, the top of the deposit is

about 60 m above the valley floor and is locally as thick as 40 m, although at this location it is about 20 m thick (fig. 64A). The massive, matrix-supported diamict is extremely well indurated. The matrix is a highly cohesive, yellowish- to brownish-gray muddy sand that contains 7–9 percent clay, including expandable smectite-vermiculite, and, locally, kaolinite (Vallance, 1999; Cook, 2002). The unit overlies local alluvium from the Hood River that contains clasts that were not sourced from Mount Hood. It is, in turn, overlain by poorly exposed sandy deposits emplaced by the Missoula floods—catastrophic late Pleistocene glacial outburst floods that swept down the Columbia Gorge dozens of times (O'Connor and Benito, 2009; O'Connor and Burns, 2009).

After finishing at the outcrop, turn right out of the parking area and continue driving south on O.R. 35. The route takes you over Middle Mountain, a bedrock knob in the middle of the Hood River valley. Watch for signs marking U.S. 281 to Parkdale and Cooper Spur. The drive to Stop 3 takes about 30 minutes.

### 21.3 Optional Stop A—View of Mount Hood

(lat  $45.5539^\circ$  N, long  $121.5682^\circ$  W) After going over Middle Mountain, Mount Hood comes into full view. Pull onto the shoulder of the road to take photographs of the volcano from one of its best vantage points. In contrast to the smooth, broad fans of volcanoclastic sediments of latest Pleistocene and Holocene age that form much of the south flank of Mount Hood (fig. 9), the north flank is steep and rugged, formed more by mass wasting and lava flows than by accumulation of

volcaniclastic sediment. Because the summit vent at Crater Rock is located south of the summit ridge, the north volcano flank and Hood River valley have not received primary eruptive products (except minor tephra) since late Pleistocene time.

Continue south on O.R. 35. The Hood River valley is one of the major pear-, cherry-, and apple-producing regions in Oregon. Mount Hood is an essential ingredient in this agricultural enterprise beyond merely providing

great logos for fruit crates and a dramatic backdrop for the “Fruit Loop” scenic drive of the Hood River valley, which for several weeks in April is awash in blossoms. The soils in the upper valley, the Parkdale Series and its relatives, form chiefly in thick ash-cloud deposits of Polallie age (Harris, 1973). The fertile soils are typically well draining but have good moisture-holding capacity and allow deep rooting. Of equal importance, the perennial snow and ice on Mount Hood provide an



**Figure 64.** Photographs of edifice-collapse deposits from the Hood River lahar at Mount Hood. *A.* Deposit in lower Hood River valley at Day 3 Stop 2, about 38 kilometers from the volcano. The deposit contains large angular clasts, supported by a muddy sand matrix. A fragile clast about 3 meters long and composed of unconsolidated gray diamict is visible at the lower right. Smithsonian Institution photograph by L. Siebert, 2014. *B.* Massive, clay-rich lahar deposit in the town of Hood River, approximately 42 kilometers downstream of Mount Hood. Large andesite clasts were cut (rather than plucked) by an excavator at this building site, revealing the degree of induration of the matrix material. The notebook at center right is 20 centimeters tall. USGS photograph by T.C. Pierson, 2003. *C.* Hood River lahar deposit along the White Salmon River at Underwood, Washington. The lahar traveled north from Mount Hood, up the Hood River valley, and across the Columbia River to the White Salmon River valley, 46 kilometers from source. The deposit here is about 12 meters thick and 100 meters above the current river level. Note that the size of the largest clasts (small boulder) has not diminished with distance—a characteristic of clay-rich debris-flow lahars. USGS photograph by W. Scott.

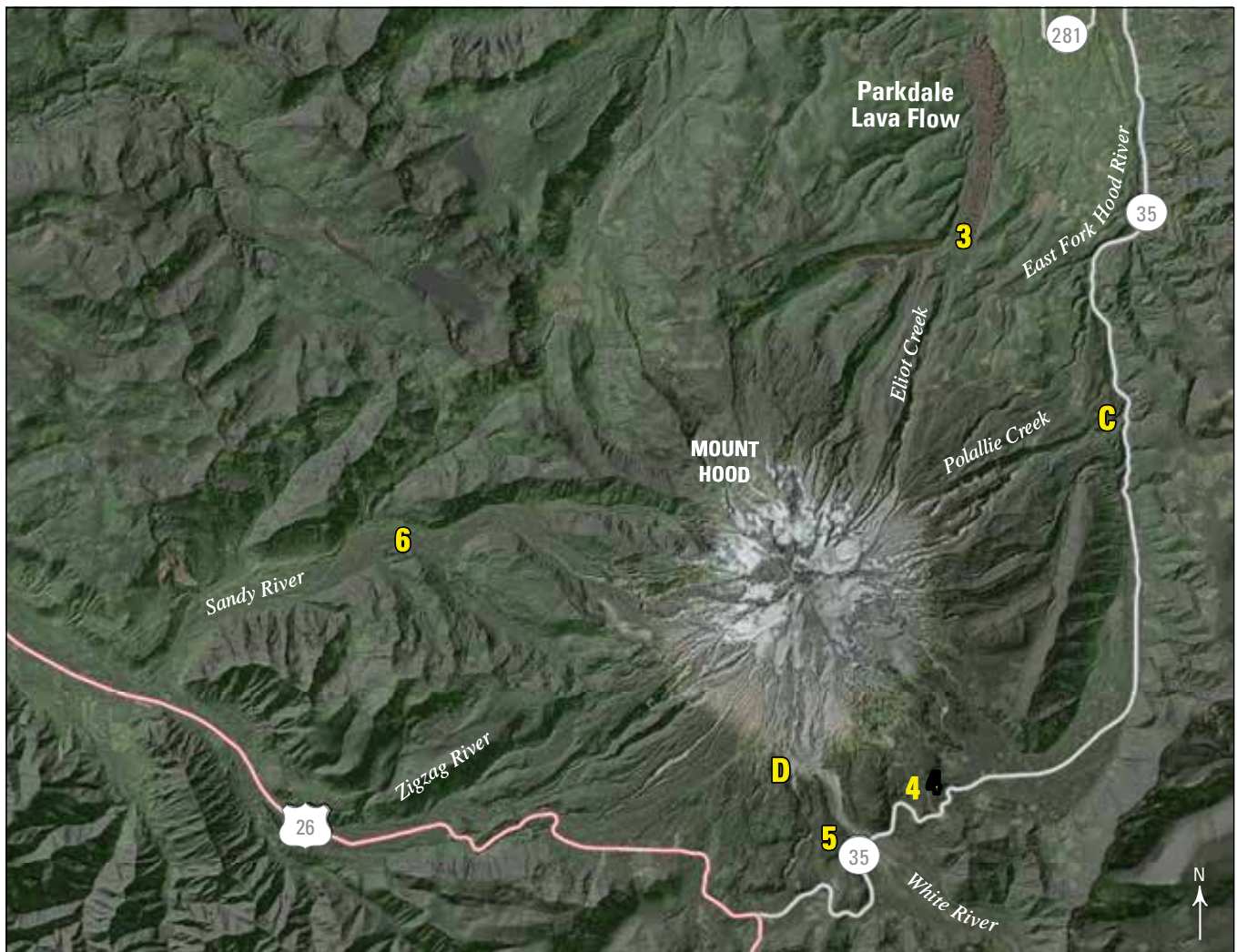
ample and relatively low-cost supply of irrigation water during the summer.

Proximal stops at Mount Hood begin with a look at recent debris-flow deposits at Eliot Branch on the north flank, west of O.R. 35 (fig. 65).

- 22.4 Turn right onto U.S. 281 (Cooper Spur Road) toward Parkdale.
- 24.2 After a short distance, you will come to the intersection with Baseline Drive (Parkdale is to the right). Continue straight on Cooper Spur Road.
- 27.0 Turn right onto Evans Creek Drive and follow it as it curves to the right.

- 27.5 Just after the curve on Evans Creek Drive, make a hard-left turn onto Laurance Lake Drive. Drive 2.5 mi (past a large pond on the left) until a bouldery debris field is reached.

**30.0 Stop 3—Eliot Branch debris-flow deposit (lat 45.4604° N, long 121.6329° W)** The Eliot Branch lahar was triggered in the early morning of November 7, 2006, by intense and prolonged rainfall from an “atmospheric river” rainstorm. Approximately 30 cm (12 inches) of rain fell at the 4,000-ft elevation level on the mountain over 5 days. The lahar was triggered by coalescing of a series of relatively small moraine-debris landslides on buried stagnant ice below the toe of the Eliot Glacier (fig. 66A). This granular lahar and



Base from U.S. Geological Survey (USGS) 30-meter Landsat imagery  
Shaded relief and roads from USGS's The National Map

**EXPLANATION**  
**6** Field-trip stop—Number is planned stop; letter is optional stop

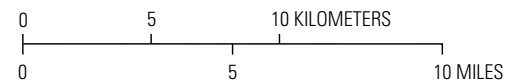


**Figure 65.** Location of planned stops (numbers) and optional stops (letters) on Days 3 and 4 that are proximal to Mount Hood.

its derivative phases flowed a total of 47 km down the Middle Fork Hood River, then down the main stem of the Hood River, and all the way to the Columbia River. The flow path included 28 km as a debris flow, which was in the process of transforming to hyperconcentrated flow, and 19 km as a muddy water flood following wholesale dilution by a major tributary. Our stop is on the debris field that was the primary depositional area for the debris-flow phase of the flow (fig. 66*B–D*). The debris flow transported clasts as large as about 5 m in diameter (fig. 66*B*) and spread debris as much as several meters thick across an area almost 2 km long and about 500 m wide (figs. 66*C, D*). Deposition of the debris flow was promoted by both a decrease in channel slope and an abrupt narrowing of the channel,

caused by the presence of the 7.7 ka basaltic andesite Parkdale lava flow (fig. 67).

Once finished with this stop, return toward O.R. 35 on Laurance Lake Drive. You will not follow the same route to the highway; instead travel south on Cooper Spur Road.

- 32.4 At the intersection, turn right onto Evans Creek Road.
- 32.9 Turn right onto Cooper Spur Road and continue following this road until it ends at a T-intersection with O.R. 35 at Polallie Creek.
- 40.5 Turn right at the O.R. 35 intersection. Just after the intersection, the road crosses a bridge over Polallie



**Figure 66.** Photographs of the Eliot Branch lahar source and deposit. *A.* Bank failure of debris from Eliot Glacier moraine—one of many streambank failures contributing debris to the Eliot Branch lahar. USGS photograph by J. Griswold, 2007. *B.* A large boulder, approximately 5 meters in diameter, that was transported by the debris-flow phase of the Eliot Branch lahar. *C.* View of the debris-flow depositional area, looking upstream (to the south). Damage to trees that are still standing indicates the flow depth at this point. Person to the right of the boulder for scale. *D.* Log jam at the downstream end of the debris field; view is looking downstream (northeast). The vertical tree fragment in the center foreground is approximately 2 meters tall. USGS photographs *B, C, D* by T.C. Pierson, 2006.



**Figure 67.** Eliot Branch channel before and after deposition of the Eliot Branch debris flow, with the Parkdale lava flow largely blocking the channel. *A.* Composite oblique aerial view of the 7,700-year-old Parkdale lava flow with vent and Eliot Branch at lower left. View is to the north-northeast, looking downstream. The town of Parkdale, Oregon, is to the upper right. Darker portion of the image on the left is compiled from photographs taken on June 28, 2005, and the lighter portion at right from photographs taken on June 16, 2006—both prior to the November 7, 2006, Eliot Branch debris flow. Image data from Google Earth, U.S. Department of Agriculture Farm Service Agency, and the State of Oregon, 2006. *B.* Oblique aerial view of the 2006 Eliot Branch debris-flow deposits at lower left. The debris flow primarily deflected around the Parkdale vent, forming the light-colored area along the West Fork Hood River on the west side of the Parkdale lava flow, with very little material deflecting down the east side of the lava flow. Image from Google Earth, 2010.



Creek. Turn left into the parking area for a restroom stop.

**40.6 Optional Stop B—Polallie Creek debris fan (lat 45.4177° N, long 121.5702° W)** On Christmas night in 1980, an intense winter storm triggered a ~5,000 m<sup>3</sup> landslide of water-saturated volcaniclastic debris. The landslide quickly liquefied and flowed down Polallie Creek on the east flank of Mount Hood at velocities as much as 15 m/s (Gallino and Pierson, 1985). The debris flow—15 m deep and moving at least 12 m/s—buried a Forest Service campground on a debris fan at the mouth of the creek with about 100,000 m<sup>3</sup> of debris (fig. 68A). One person staying at the campground in a pickup truck camper was killed. This deposit, as much as 10 m thick, dammed the East Fork Hood River for 10–20 minutes with a debris blockage more than 200 m long. The blockage was subsequently breached by rising water impounded upstream, releasing a dam-break flood that destroyed about 8 km of O.R. 35 (fig. 68B). Similar events have swept down most of the valleys draining Mount Hood during the past century, but flows on White River, Newton Creek, Eliot Branch, and Ladd Creek have done the most damage to roads and bridges.

From here, continue south on O.R. 35 and watch for signs to Mount Hood Meadows Ski Resort.

**52.1** Take the exit for Mount Hood Meadows Ski Resort and Bennett Pass Sno-Park. At the end of the offramp, turn left on Bennett Pass Road and cross the bridge over O.R. 35. Pull into the parking lot for the Bennett Pass Sno-Park on the left side of the road after crossing the bridge.

**52.5 Stop 4—Glacial till at Bennett Pass (lat 45.3102° N, long 121.6421° W)** Walk back over the bridge and at the far end climb down to the outcrop on the left side (lat 45.3106° N, long 121.6443° W). There is a wide margin along the road in front of the outcrop. However, vehicles travel at high speed along O.R. 35 and this is on the inside of a blind curve. Be extremely cautious about vehicle traffic at this site.

Mount Hood was extensively glaciated during the Last Glacial Maximum (known locally as the Evans Creek glaciation, table 3) and previous Pleistocene glaciations, and glacial deposits composed of volcaniclastic rock fragments are widespread on the volcano's flanks. However, glaciers on the volcano today are small in comparison to what they once were (fig. 69). The roadcut on O.R. 35 at Bennett Pass here on the south flank of Mount Hood originally exposed three diamicts, interpreted by Crandell (1980) as glacial tills separated by buried soils (fig. 70) (Scott, Gardner, and others, 1997; Scott and Gardner, 2017). Today, the lowest unit is obscured by talus eroded from the outcrop face.

The tills mantle the crest of a ridge of Miocene volcanic rock, which is buried farther upslope by Mount Hood lavas. The tills display several characteristics that can be used to distinguish them from similar-looking volcaniclastic deposits: emplacement on a ridge instead of a valley floor, striated and faceted clasts, unusually high silt content in the matrix compared to lahar and PDC deposits in the area, and a high degree of compaction locally.

In general, these glacial units are unstratified, but the middle unit locally displays crude bedding, suggesting a flow-till origin (Scott, Gardner, and

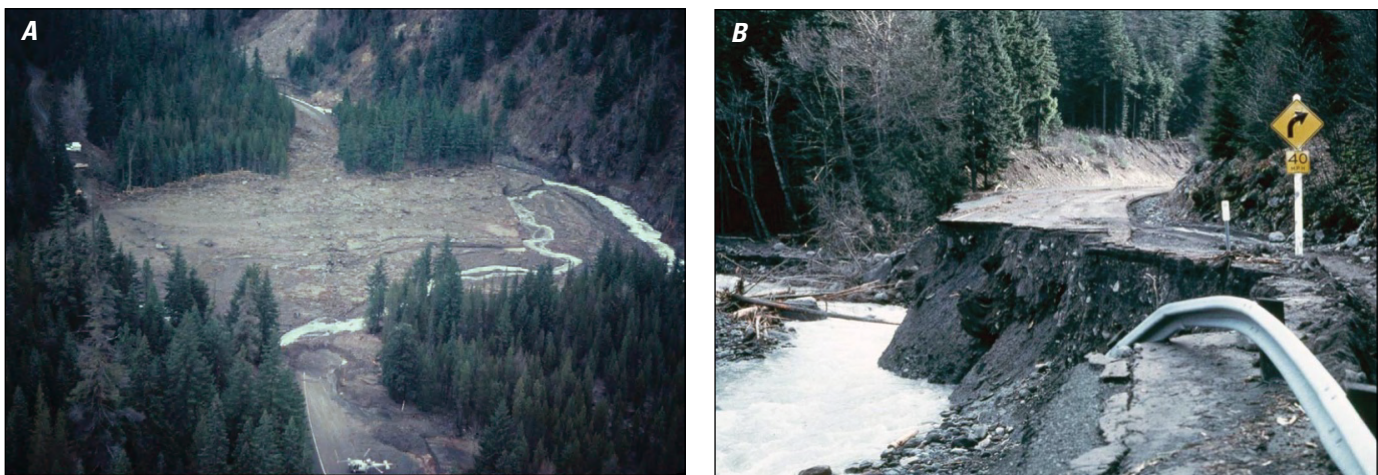


**Figure 68.** Impacts of Polallie Creek debris flow on December 25, 1980, on the east side of Mount Hood. *A.* Aerial photograph of the debris fan crossing Oregon Route 35 (O.R. 35), taken two days after the event. The view is to the north. Helicopter at lower center for scale. *B.* Photograph of damage to a section of O.R. 35 along the East Fork Hood River. The dam-break flood released from blockage of the river caused extensive erosion along the riverbank, undercutting the highway here. U.S. Forest Service photographs, 1980.



**Figure 69.** Photograph of small glaciers remaining on Mount Hood. The glacier at the head of this valley (the Sandy River) is the Sandy Glacier on the west flank of Mount Hood. View is to the east. This glacier, as part of a Pleistocene summit ice cap, once extended as far as 27 kilometers down the Sandy River. Reid Glacier is to the right. USGS photograph by T.C. Pierson, 2005.



**Figure 70.** Photographs of glacial till deposits at Bennett Pass. *A.* Outcrop of till units exposed at Bennett Pass, 11 kilometers southeast of Mount Hood summit. View is to the northwest, with Mount Hood in the background. Most of the roadcut exposure consists of the middle of three till units (compact pebbly diamicts). The lowermost till is covered by talus. Smithsonian Institution photograph by L. Siebert, 2016. *B.* Closeup view of the middle till unit texture—an extremely poorly sorted pebbly diamict. Shovel blade is about 20 centimeters long. USGS photograph by T.C. Pierson, 2016.

others, 1997). The upper two units appear to date from the Last Glacial Maximum (Evans Creek glaciation) and the lowest till likely dates from either 150 ka or 75 ka, estimated by the degree of soil development on its top and the probable timing of pre-Evans Creek glaciations in this area (Scott, Gardner, and others, 1997; Scott and Gardner, 2017).

Clasts in the upper till correlate this unit to the Polallie eruptive period. About half of the clasts are highly porphyritic and vesicular, similar to clasts derived from collapse of Polallie-age lava domes on Mount Hood. A terminal moraine of Evans Creek age east of this location contains a high proportion of similar clasts, many of them showing weak prismatic jointing. This suggests dome growth and collapse were occurring during this glacial advance and shedding debris onto glacial ice. The glacier then transported the material to moraines as supraglacial drift (Scott and Gardner, 2017).

From the Bennett Pass Sno-Park turn right onto Bennett Pass Road to cross back over the bridge. Turn left just past the bridge and merge back onto O.R. 35 westbound. Continue about 5 minutes to Stop 5.

**54.8 Stop 5—White River PDC and debris-flow deposits (long 45.3032° N, long 121.6740° W)** Just after crossing the White River, pull into the large parking lot for the White River West Sno-Park on the right side of the road. Park at the far end of the lot. We will eat lunch at this stop.

Lithic PDC and lahar deposits from the latest eruption of Mount Hood funneled down White River canyon. The PDCs originated as collapses of a lava dome growing at the Crater Rock vent between 1781 and 1793 C.E. (Old Maid eruptive period) (Crandell, 1980; Cameron and Pringle, 1987; Scott, Gardner, and others, 1997). Crater Rock is visible from this vantage point as well as the ski lifts of the Timberline Lodge and Ski Area along the axis of the debris fan below the lava dome.

Leave your car and walk upstream for about 0.6 mi. A bluff on the southwest bank of the river provides good exposure of one Old Maid-age PDC deposit, located at 45.3087° N, 121.6804° W. The PDC deposit varies in thickness from 5 to 20 m (Scott and Gardner, 2017) (fig. 71). Farther upstream, several overlying lahar deposits can be found. This PDC deposit contains several identifying features that are useful in distinguishing PDC units from other volcaniclastics: (1) an abundance of slightly to moderately vesicular clasts, many displaying prismatic jointing; a friable sandy matrix; entrained charcoal fragments; pinkish coloration near the top of the deposit; and gas-escape pipes. In addition, uniform thermoremanent

magnetization was determined from numerous clasts; it matches that of other PDC deposits of Old Maid age and at least part of the Crater Rock lava dome (Scott and Gardner, 2017).

Lahar and PDC deposits on the northeast riverbank opposite the White River West Sno-Park were emplaced during the Polallie eruptive period. Modern deposits mantling the wide valley floor are from repeated floods and debris flows that continue to be triggered by rainstorms in the steep upper canyon. The previous O.R. 35 bridge at this location was closed 20 times since 1907 owing to washouts, including five closures since 1998 and most recently in 2006 (fig. 72) (Anderson and others, 2006). That bridge was replaced in 2012 with a new bridge that is 4 m higher and considerably longer, providing a larger cross-sectional area for material to pass under.

Once finished with this outcrop, return to the cars. Turn right onto O.R. 35 heading west. Stop 6 is about 45 minutes away.

58.6 Turn onto U.S. 26 west toward Portland.

58.7 “The Barlow Road”

U.S. 26 roughly follows the historic Barlow Road—part of the Oregon Trail. We will follow this route for the rest of today and part of tomorrow. Early settlers traveling the Barlow Road passed through the area about 50 years after Mount Hood’s last eruption.

61.1 Turn right onto Timberline Highway (sign for Timberline Lodge).

**66.2 Stop 6—Timberline Lodge (lat 45.3303° N, long 121.7078° W)** Timberline Lodge is both the last stop for the day as well as the overnight accommodation. The historic Timberline Lodge (fig. 73) is situated on the southwest flank of Mount Hood on the volcaniclastic debris fan downslope of Crater Rock (fig. 12). The lodge, one of the iconic mountain lodges of the western United States, was constructed from 1936 to 1938 by the depression-era Works Progress Administration and lavishly furnished by local artisans. This National Historical Landmark is one of Oregon’s most visited sites and provides year-round skiing and snowboarding on the Palmer snowfield, as well as expansive views of the Mount Hood summit to the north and Mount Jefferson and other central Oregon volcanoes to the south. The Pacific Crest National Scenic Trail, extending from Mexico to Canada, passes by 0.2 mi uphill of the lodge and provides good views of volcaniclastic deposits in the upper Zigzag River (3 mi west of the lodge) and White River valleys (0.7 mi east of the lodge) (fig. 17).

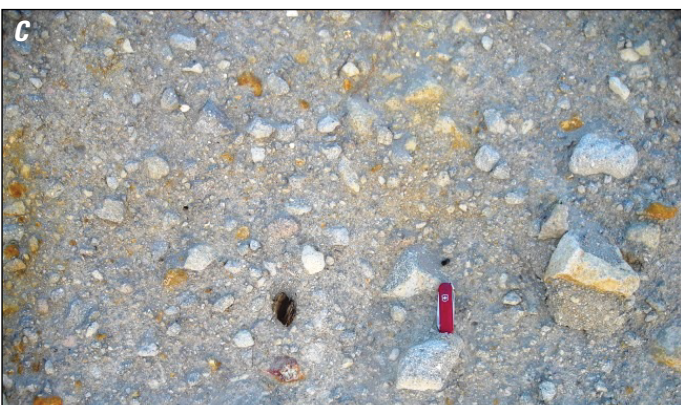
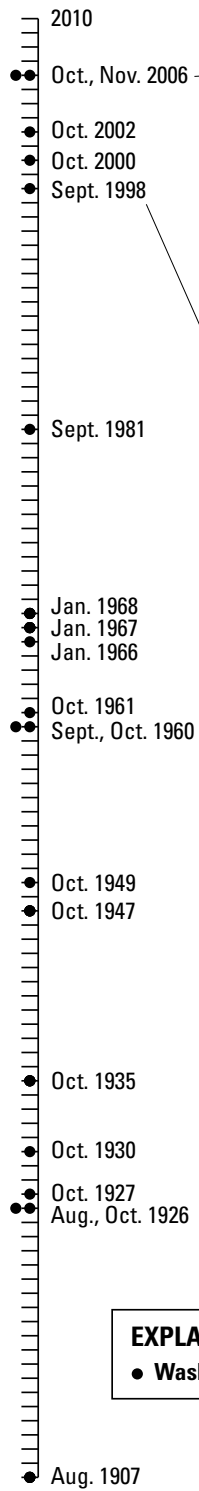


**Figure 71.** Photographs of lithic pyroclastic density current (PDC) and secondary lahar deposits in the upper White River valley. *A.* Old Maid-age PDC (block-and-ash flow) deposit exposed in vertical face of a low terrace on left side of photograph. View is upstream to the north, toward Mount Hood summit. Old Maid deposits are inset within the canyon that has been cut into light-colored and thicker Polallie-age deposits at far right. Smithsonian Institution photograph by L. Siebert, 2013. *B.* Closeup view of PDC deposit in *A*, showing the massive structure, uniform lithology of clasts, and poorly sorted nature of these deposits. Note that the larger clasts are angular to subangular (the largest here is about 0.5 meters in diameter). Lahar deposits typically show crude rounding of coarse clasts. This deposit lacks a well-developed pinkish oxidized zone at the top of the deposit, possibly due to a relative cool emplacement temperature. *C.* Closeup view of a finer grained part of the PDC deposit in *A* and *B*, with small pieces of black charred wood at top center and left. Red pocketknife is approximately 6 centimeters long. Orange color of some clasts is probably due to degassing alteration products along cracks in the dome prior to collapse. *D.* Modern debris-flow and hyperconcentrated-flow deposits in low terrace within the active White River channel near the Oregon Route 35 bridge. These deposits are composed of eroded and reworked material from the PDC deposits upstream. Black pencil for scale is 15 centimeters long. Note that coarse clasts are more rounded than in the PDC deposit upstream. USGS photographs *B*, *C*, *D* by T.C. Pierson, 2009.

TIMELINE, IN YEARS



**EXPLANATION**  
 ● Washout event



**Figure 72.** History of debris-flow damage to the Oregon Route 35 bridge crossing the White River. Washouts have caused the bridge to close 20 times since 1907. Modified from Anderson and others (2006). Mount Hood National Forest photographs by D. Jones (top) and T. DeRoo (bottom).



**Figure 73.** Photograph of the Timberline Lodge on the southwest flank of Mount Hood in winter. Arcuate scarp of edifice collapse during the Timberline eruptive period can be seen behind the lodge. The post-collapse Crater Rock lava dome casts a shadow on the left side of the scarp. Timberline Lodge and Ski Area photograph.

#### Day 4: Distal lahar and volcano-fluvial deposits downstream of Mount Hood

Stops on Day 4 examine deposits along the Sandy River, including lahar and fluvial aggradational valley-fill deposits of the Timberline and Old Maid eruptive periods. Stop numbers and letters continue from Day 3.

- |      |   |      |   |
|------|---|------|---|
| 0.0  | Timberline Lodge. Return to U.S. 26 by way of Timberline Highway.   | 17.0 | When entering the small community of Zigzag, watch for the Mount Hood National Forest Zigzag Ranger Station on the left side of the road. Just after passing the ranger station, turn right onto the East Lolo Pass Road. Continue on the East Lolo Pass Road, which parallels the Sandy River.   |
| 5.3  | Turn right onto U.S. 26 and continue west past the small community of Government Camp, which originally provided housing for workers building Timberline Lodge. It is about a 50-minute drive to Stop 7.  | 18.4 | The Sandy River comes very close to the right side of the East Lolo Pass Road here. Look for signs of significant bank erosion and damage to some of the houses and buildings along the river, which were caused by a flood with a high sediment load in January 2011.  |
| 6.7  | Tom Dick and Harry Mountain cirques<br>If a good view of glacial cirques is desired, turn left into the parking lot for Mount Hood Ski Bowl. Look south to see Pleistocene-age glacial cirques on Tom Dick and Harry Mountain (1,544 m a.s.l.). The mountain is composed of Pliocene-Pleistocene andesite and basaltic-andesite lava flows emplaced on top of the Miocene-age Laurel Hill pluton and Rhododendron Formation volcanoclastic rocks (Sherrod and Scott, 1995). The upper portion of the ski area is located within a glacial cirque carved into the mountain. When you are finished, turn left out of the parking lot to rejoin U.S. 26 and continue westward. | 21.2 | After passing the sign indicating entrance into Mount Hood National Forest, take a slight right at the fork in road onto Muddy Fork Road. This turn is not marked well, but is located at the point where East Lolo Pass Road begins to climb uphill out of the valley. Muddy Fork Road follows the valley floor and parallels the Sandy River. |
| 14.9 | Town of Rhododendron built on lahar deposits<br>U.S. 26 soon begins a long curving downgrade. Recent widening of the highway has produced fresh   | 21.9 | At the next intersection, turn right to continue on Muddy Fork Road. In a short distance, the road crosses a bridge over the Sandy River.   |

exposures of the Laurel Hill pluton in this location. At the bottom of the grade, the highway flattens out onto a forested low-gradient surface in the valley floor. This is a broad lahar deposit consisting mostly of Timberline-age lahar units and locally includes Old Maid-age deposits. The large boulders scattered among the trees were emplaced as part of these lahars.

- 22.1 Stop 7—Old Maid Flat (lat 45.3837° N, long 121.8681° W)** At the entrance to McNeil Recreation Site (the next left turn), park on the shoulder of the road and walk into the campground. There are only a few places to park in the campground that are not fee-site campsites. Walk to campsite 16 (lat 45.3868° N, long 121.8676° W), and from here proceed about 400 ft northwest between campsites into the forest to the edge of the cutbank overlooking the Sandy River. Find a place to safely descend to the river where you can view the cutbank.
- Old Maid Flat was a primary depositional site for lahar and volcano-fluvial sediments during the Timberline and Old Maid eruptive periods. It also was, and continues to be, a major sediment source, supplying coarse volcaniclastic sediment to channel reaches farther downstream the Sandy River during major rainstorms. This stop, about 15 km downstream of the Crater Rock vent, provides the opportunity to examine a variety of syneruptive and posteruptive depositional units, including debris-flow, hyperconcentrated-flow, and volcano-fluvial deposits related to Old Maid volcanic activity. Timberline-age deposits are buried at this location, but exposed farther upstream. The Old Maid units show a variety of sedimentary textures and features (fig. 74). The Sandy River channel in this steep reach is very active during winter high flows, transporting large volumes of coarse volcanic sediment. Modern sedimentary features and structures can also be seen here. Tree wells on the surface of Old Maid Flat and tree snags exposed in the channel bed indicate that old-growth forest trees were rapidly buried in growth position by these sediment-rich flows. Note that these banks are unstable. Please be careful.
- Dendrochronologic evidence indicates that the first major lahar during the Old Maid eruptive period occurred in late summer or early autumn of 1781—the year the dome-building eruption started. Other significant flows include an outbreak flood from the formerly dammed Muddy Fork tributary in 1787, a lahar in 1791, and another lahar in 1800 (Pringle and others, 2002, 2010). The 1781 lahar was the largest generated during the Old Maid eruptive period (Pierson and others, 2011). An unknown number of smaller lahars that did not injure trees along the valley sides also contributed sediment between 1781 and 1805, when sedimentary infill of Old Maid Flat was complete and forest vegetation became established over much of that surface (Cameron and Pringle, 1986; Pierson and others, 2011). Following infill, parts of the original depositional surface at Old Maid Flat were carved 2–15 m deep and as much as ~50 m wide by erosional channels. Based on the maturity of trees growing within these channels today, much of the erosion on the surface of Old Maid Flat appears to have occurred shortly after lahar deposition and before widespread establishment of forest vegetation. Stops 8 and 9 explore downstream deposits in the depositional reach at Oxbow Regional Park and at the Sandy River delta.
- When you are finished at this stop, backtrack the way you came to U.S. 26 westbound.
- 22.3 Turn left onto Muddy Fork Road.
- 23.0 Turn left onto East Lolo Pass Road.
- 27.2 Turn right onto U.S. 26 westbound.
- 43.9 Sandy, Oregon. Note that the speed limit is strictly enforced in town. The city of Sandy was founded as a trading post for pioneers traveling on the Barlow Road segment of the Oregon Trail (now U.S. 26 here). Established in 1845, the Barlow Road connected The Dalles, Oreg., at the eastern end of the Columbia Gorge, to the Willamette River near Oregon City. This overland route was an alternative to the faster, but more dangerous, river route that rafted wagons through the treacherous Cascade Rapids on the Columbia River.
- 44.7 At far end of town, turn right onto Bluff Road. The next optional stop is just ahead.
- 45.6 Optional Stop C—Jonsrud viewpoint (lat 45.4099° N, long 122.2736° W)** Pull into the parking lot of the Jonsrud viewpoint on the right side of the road. The view here looks up the Sandy River valley, incised about 150 m deep at this location, with Mount Hood in the distance, about 45 km away (fig. 75). From here, turn right out of the parking lot onto Bluff Road. Continue traveling on this road as it curves to the left.
- 49.8 Turn right onto 347th Avenue, which becomes SE Cottrell Road.
- 51.1 Turn left onto SE Lusted Road.
- 51.3 Turn right onto SE Hosner Road. Continue on SE Hosner Road, continuing straight through next 4-way intersection. Road begins steep descent into Sandy River canyon and becomes SE Oxbow Parkway.
- 52.8 Where the road makes a sharp turn to the right along the steep curving descent, you will pass a small wedge of Missoula flood deposits, largely overgrown with vegetation, on the inside of the curve.
- 53.3 At the bottom of the steep grade, continue straight to enter Oxbow Regional Park, which is a fee site. Enter the park and follow SE Oxbow Parkway through the park.



**Figure 74.** Photographs of volcaniclastic deposits of mainly Old Maid age exposed at Old Maid Flat, about 15 kilometers downstream of Mount Hood. *A.* Poorly sorted bouldery debris-flow deposit. Wooden shovel handle is 3.5 centimeters (cm) in diameter. *B.* Sequence of crudely stratified hyperconcentrated-flow deposits. Trenching shovel at lower right for scale, handle 55 cm long. *C.* Vertical and lateral transitions from gravelly to sandy facies in hyperconcentrated-flow deposits. *D.* Modern volcano-fluvial deposit emplaced by a major flood in November 2006, composed of moderately sorted medium- to fine-grained sand. *E.* Granular (noncohesive) debris-flow deposit overlain by a hyperconcentrated-flow deposit. Trenching shovel at lower center for scale. *F.* Outsized clast of nonvesiculated dacite in a hyperconcentrated-flow deposit. Pencil for scale. USGS photographs by T.C. Pierson, 2009.

**Figure 75.** Photographic view of Sandy River from Jonsrud viewpoint outside of Sandy, Oregon. The grassy terrace in the center of the photograph is underlain by Polallie-age lahar and lahar-runout deposits. Mount Hood is in the background. Smithsonian Institution photograph by L. Siebert, 2016.



**53.7 Stop 8—Oxbow Regional Park (lat 45.4972° N, long 122.2908° W)** Drive most of the length of the park and turn into the parking area for the boat ramp on the left side of the road. If you enter the one-way campground loop, you have gone too far. From the boat ramp, find the trailhead on the east right (upstream) side of the parking lot and walk the trail along the river, heading upstream.

Oxbow Regional Park lies along the low-gradient lower reach of the Sandy River, about 70 km downstream of Mount Hood and about 15 km upstream of the river mouth (fig. 76). It showcases past rapid syneruptive channel aggradation in a river system with high rates of sediment transport (Pierson and others, 2009, 2011). An episode of profound channel aggradation occurred in this lower reach around 1.5 ka during the Timberline eruptive period, when excessive sedimentation rates caused the channel bed to be raised ~30 m. After the sediment supply waned, the channel re-incised to near its original level. Again, between 1781 and 1793 during the Old Maid eruptive period, the channel bed rose ~23 m due to high rates of eruption-related sedimentation and thereafter re-incised to its present level. Both aggradation episodes engulfed standing old-growth forests in sediment. Those trees are now gradually being re-exposed by bank erosion, revealing “ghost forests” (figs. 15, 16).

Posteruptive channel incision occurred following periods of aggradation associated with past eruptions. Incision occurred in a stepwise fashion, leaving flights of fill terraces along the riverbanks (figs. 15, 16, 77, 78). Primarily only terraces of Old Maid age remain

visible today; older flights are mostly buried. Exposed terraces are commonly capped by fine-grained fluvial sand emplaced by major floods. A radiocarbon date from one sand unit suggests it is a backwater deposit from the outbreak flood that was caused by initial breaching of the Bonneville landslide dam in the 15th century. This flood surge would have had to back-flood about 15 km up the Sandy River from the Columbia River to reach this location. Dendrochronologic evidence permits reconstruction of the timing of the Old Maid aggradation-degradation cycle, and suggests the aggradation phase lasted about a decade and the degradation phase 50–100 years (Pierson and others, 2011).

Sedimentary textures and lithofacies of the aggradational valley-fill deposits demonstrate that most of the rapid deposition was accomplished by normal fluvial processes. Though lahars did occur and emplace deposits near the base of both the Timberline and Old Maid sedimentary sequences, they were not the dominant contributors of sediment, as is common in other more proximal volcanic settings (for example, Smith, 1987a,b, 1991; Pierson and others, 1996). Lithofacies and historical records also indicate that the Sandy River channel was braided during most of the two aggradation-degradation cycles (Smith, 1987a,b; 1991; Moulton and Dunlay, 1990; Miall, 1996; Manville and others, 2005). Width of the active braidplain (250–600 m) was constrained by the walls of the incised valley and may partly explain the unusually thick sedimentary fill accumulations in this river reach.



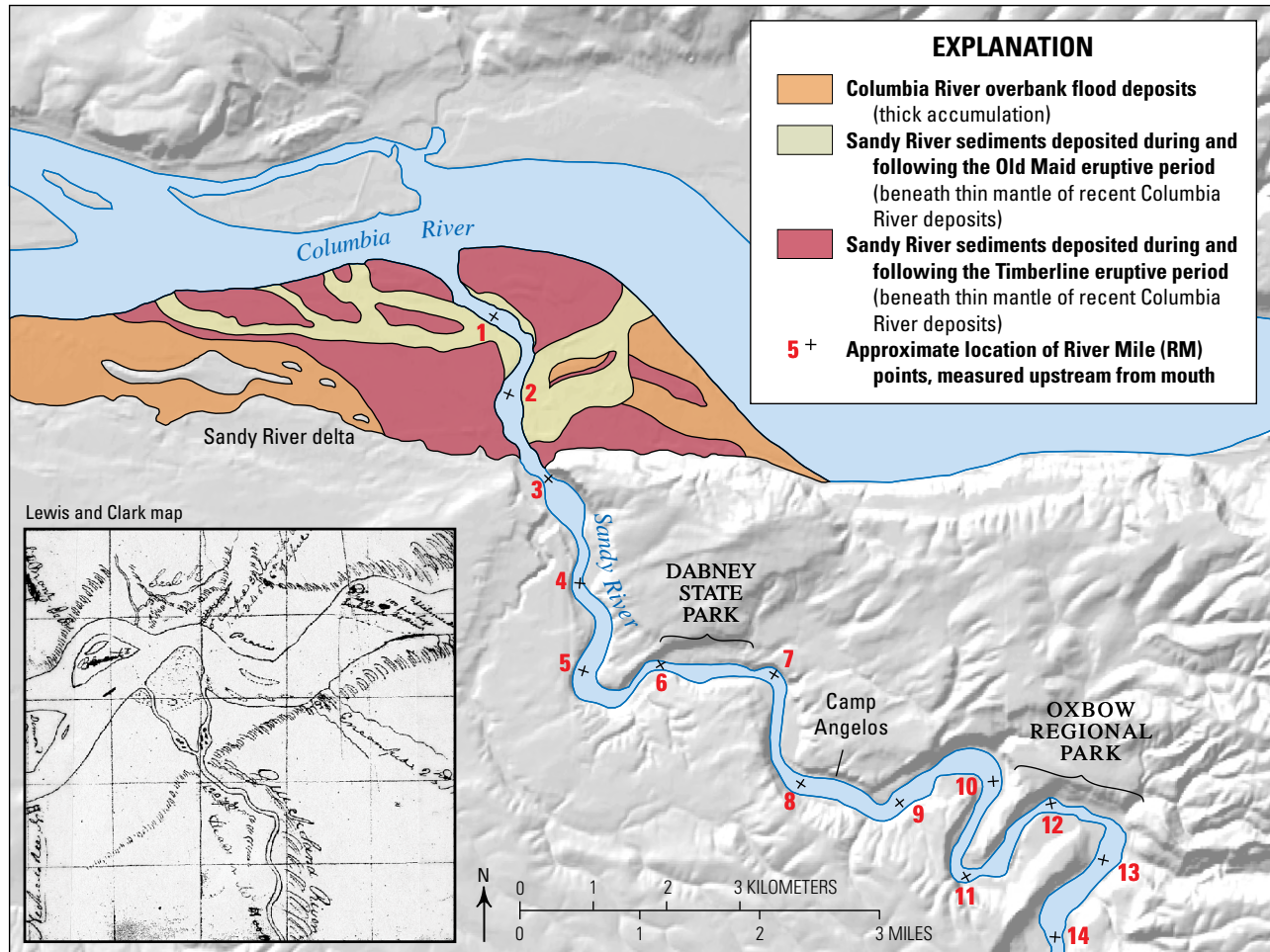


**Figure 76.** Shaded-relief map of the lower Sandy River with geology of the Sandy River delta shown. Stop 8 examines exposures between river miles 11 and 12 at Oxbow Regional Park and Stop 9 is located at river mile 2.2, west bank, at the apex of the Sandy River delta. Inset map at lower left is a sketched map drawn by Lewis and Clark in 1805–1806, showing the same area with the Sandy River labeled “Quick Sand River” (O’Connor, 2004). The eastern delta distributary channel shown on Lewis and Clark’s map, active into the 20th century, was closed off by an engineering diversion in the 1930s, but was restored in 2013. Figure from Pierson and others (2011).

Sediments composing the valley-fill aggradational deposits in this Sandy River reach are dark gray immature volcanic sands and gravels (Pierson and others, 2011). Most of the rock fragments within the deposits appear fresh and have similar compositions to those that were erupted during the Timberline and Old Maid eruptive periods. Small amounts of epiclastic particles are also found. Sediments deposited during aggradation are dominantly crossbedded medium to coarse fluvial sands with minor gravel lenses. Sediments in the top few meters of the lower degradation terraces, that is, sediments deposited during the degradation phase of the cycle, are more gravel rich and crudely bedded.

Four lithofacies associations (FAs) comprise the Timberline and Old Maid aggradation-degradation

sequences (fig. 79), originally defined and categorized by Smith (1987a), and described below.

**FA-1—Fluvial channel deposits.** Poorly to moderately sorted medium to coarse sand, locally including fine gravel lenses and beds. Sand beds display mainly trough crossbedding and planar crossbedding, with local ripple cross-laminations.

FA-1 reflects dune and ripple migration and braid bar formation at conditions of dominantly subcritical flow in shallow sand-dominated channels at moderate to high rates of sediment transport (Miall, 1996). It is common in aggradational braided river systems (Manville and others, 2005) and was directly observed by the Lewis and Clark Expeditions in 1805 and 1806 at the mouth of the Sandy River (Moulton and Dunlay, 1990).

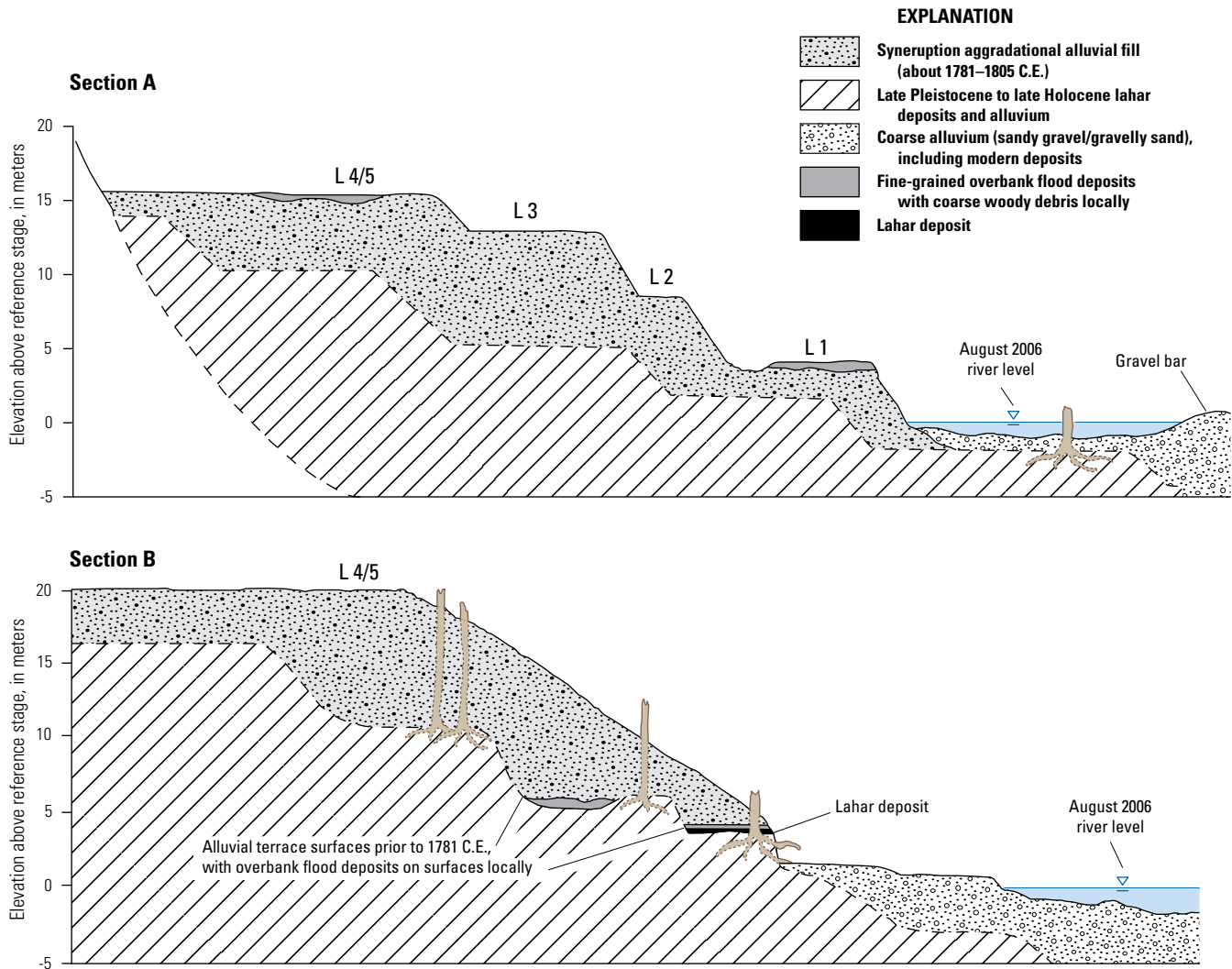


**Figure 77.** Simplified cross sections along the low-gradient depositional reach of the Sandy River in Oxbow Regional Park. Section A is located at river mile 12.8; section B is located at river mile 11.6 (see fig. 76). Terrace levels L1 through L4/5 (a level encompassing two closely spaced surfaces) were cut during the decades following the end of the Old Maid eruption. Two generations of paleoterrace surfaces and forests (undifferentiated in figure) were buried by subsequent channel-fill deposits during the Timberline and Old Maid eruptive periods. Modified from Pierson and others (2011).

**FA-2—Overbank floodplain deposits.** Moderately to well-sorted medium to very fine sand and silt. Bedding mainly consists of ripple-drift cross-laminations or bed-parallel laminations. Sand beds commonly capped by a layer of silt less than 1 cm thick.

FA-2 is observed at the base of the Old Maid stratigraphic section wherever it rests on a pre-Old Maid paleoterrace surface as well as on some degradation terrace surfaces. It is interpreted as the result of one or more episodes of overbank flooding that occurred as the aggrading channel bed brought paleoterrace surfaces within the vertical range of peak flood flows. On degradation terraces these sands represent floodplains

that were soon abandoned above the range of floods as the channel incised. FA-2 deposits beneath the basal lahar deposit could have been formed by a sediment-charged wave of river water pushed ahead of the 1781 lahar (see Cronin and others, 1999). These overbank sediments were laid down by shallow low-velocity overbank flows, which also stranded woody debris on paleoterrace surfaces and gently buried layers of undisturbed forest duff.

**FA-3—High-energy braided-channel deposits.** Poorly sorted coarse to very coarse sand, gravelly sand, and sandy gravel. Strata are horizontally bedded, low-angle crossbedded, or massive (with coarse gravel

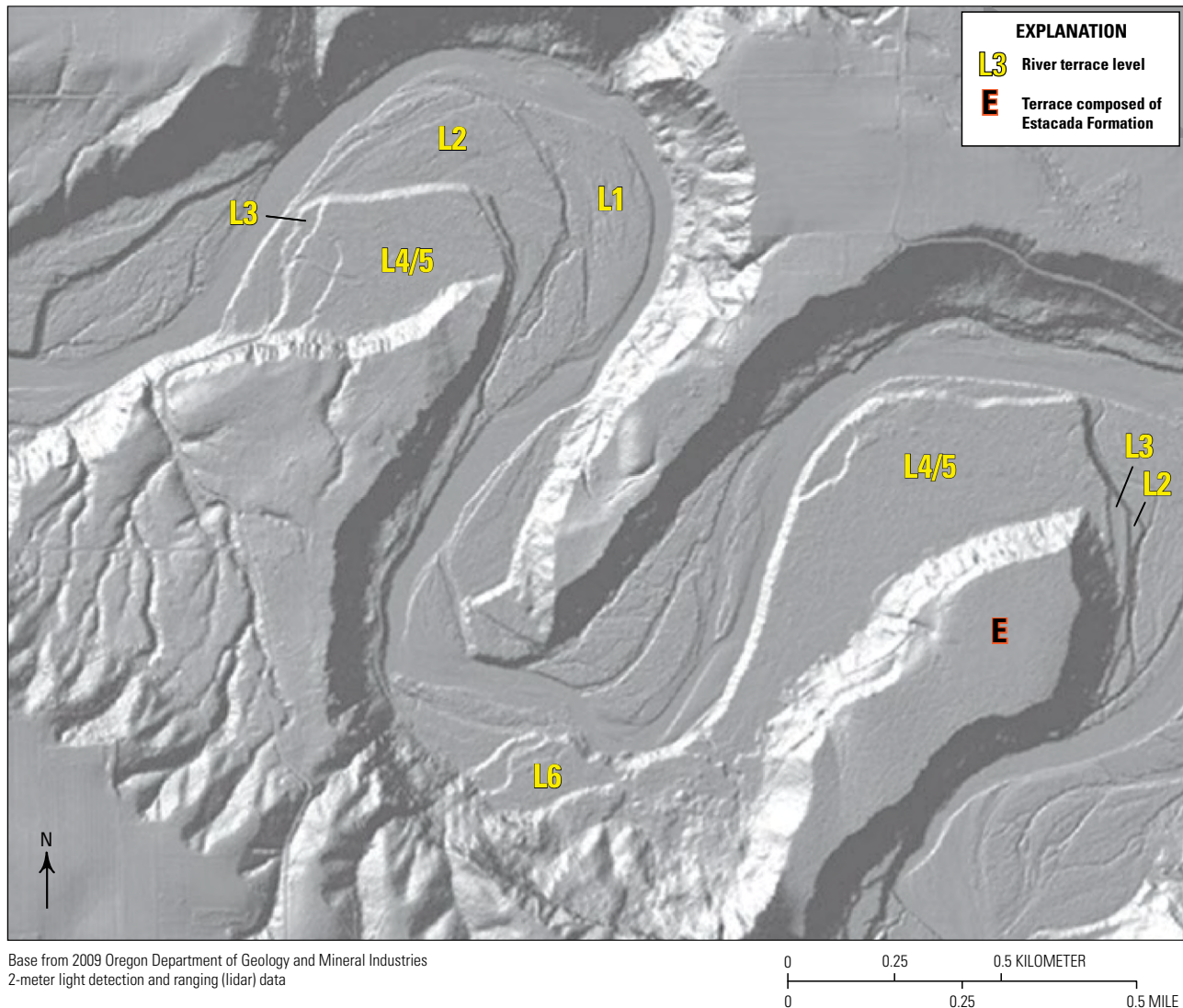


**Figure 78.** Digital elevation model with 2-meter resolution of the Sandy River at Oxbow Regional Park, approximately between river miles 8.8 and 13.8 (see fig. 76). Image derived from 2009 Oregon Department of Geology and Mineral Industries bare-earth light detection and ranging (lidar) data. This river reach is about 66–75 kilometers downstream of Mount Hood, with the river flowing from right to left. The broad, flat terraces in the river valley were cut by incision of aggradational fill deposits following various eruptive periods. The L4/5 and lower terraces were formed following the Old Maid eruptive period and the L6 terrace was formed at the end of the Timberline eruptive period. The high terrace at the center of the right oxbow (labeled “E”) is a late Pleistocene surface composed of the Estacada Formation—an older volcaniclastic unit from Mount Hood (Trimble, 1963).

lenses). Also labeled sheetflood deposits in Smith (1987a).

FA-3 is typical of high sediment transport rates and high bed shear stress at the transition between subcritical and supercritical flow (Miall, 1996). It probably reflects narrowing and deepening of active channels as degradation begins, but while sediment transport rates are still high. These are conditions common in the deeper parts of braided rivers (Smith, 1987a; Miall, 1996).

**FA-4—Debris-flow and hyperconcentrated-flow lahar deposits.** Massive, extremely poorly sorted, indurated beds of muddy sandy gravel or

muddy gravelly sand, having both matrix-supported and clast-supported textures.

FA-4 represents lahar deposition on paleoterrace surfaces. Both the Timberline and Old Maid aggradational sequences begin with lahars—two closely spaced in time at the beginning of Timberline deposition and one at the beginning of Old Maid deposition. All of these early lahars were in excess of 3 m flow depth, inferred from the presence of flood-intolerant conifers growing on the inundated paleoterrace surfaces (Pierson and others, 2011).

Once finished at this stop, we will eat lunch in the picnic area prior to departure. The drive to the

next stop takes about 30 minutes. From the boat ramp, backtrack to exit the park.

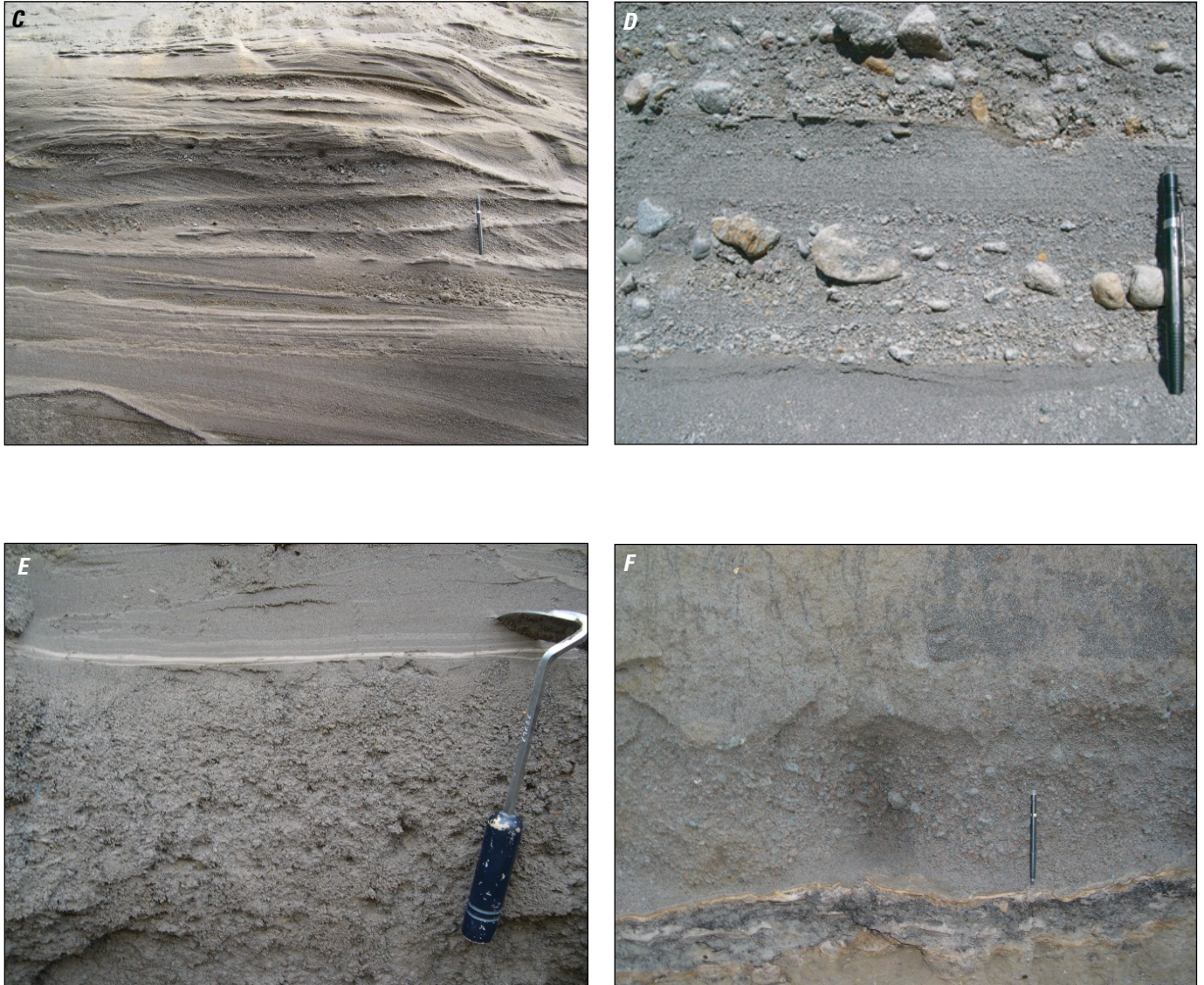
- 54.1 At the park exit, continue straight uphill on SE Oxbow Parkway (becoming SE Hosner Road).
- 55.5 Turn right at the stop sign onto SE Oxbow Drive.
- 57.7 The road intersects and continues as SE Division Drive.
- 59.2 The road forks as it approaches a blinking-light, four-way stop. Take the fork to the right onto SE Troutdale Road.
- 61.9 At the traffic light intersection with SW Cherry Park Road and Buxton Road, veer right through the intersection onto Buxton Road.
- 62.4 At the T-intersection with Historic Columbia River Highway, turn left and stay in the right lane.
- 62.5 Take the first right at the traffic light onto Graham Road. Follow Graham Road as it passes over the railroad tracks and under I-84, staying in the right lane. After passing under I-84 you will see the Troutdale Airport ahead; two lanes of traffic curve to the left parallel to the freeway, but keep straight instead.
- 63.1 Turn right onto NE Harlow Road.

**63.4 Stop 9— Timberline lahar deposits at the Sandy River delta (lat 45.5457° N, long 122.3863° W)**  
 Once you pass the storage facility on the right, you will notice several pullouts along the left side of the road. Pull into one of these and park. Short steep trails descend to outcrop exposures; vegetation may need to be cleared.

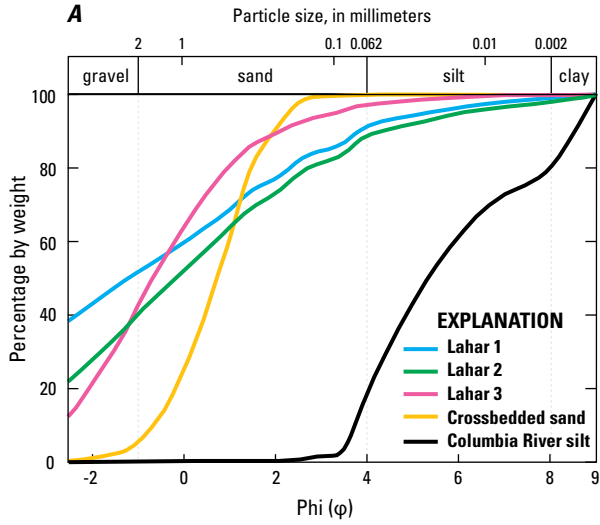
The Sandy River delta is a depositional structure as much as ~90 m thick that is predominantly built of Mount Hood volcaniclastic sediment (fig. 76) (Rapp, 2005). Drill cores reveal that delta deposits rest on the Troutdale Formation (indurated Columbia River sediment of Pliocene age) and largely predate the Timberline eruptive period (fig. 80). Interbedded Columbia River overbank flood deposits appear in the uppermost 15 m of the section but are apparently absent below that, although well-logging methods may not detect thin layers at depth. The full age range of the delta is not known, but organic material from 12–14 m depth (5 m below the base of the Timberline deposits) in a drill core from the delta center dates to about 5 ka (Rapp, 2005).

The 8.5-m section along the bluff on the west side of the Sandy River here consists of lahar and volcano-fluvial deposits of Timberline age that overlie pre-Timberline Columbia River flood deposits. Old

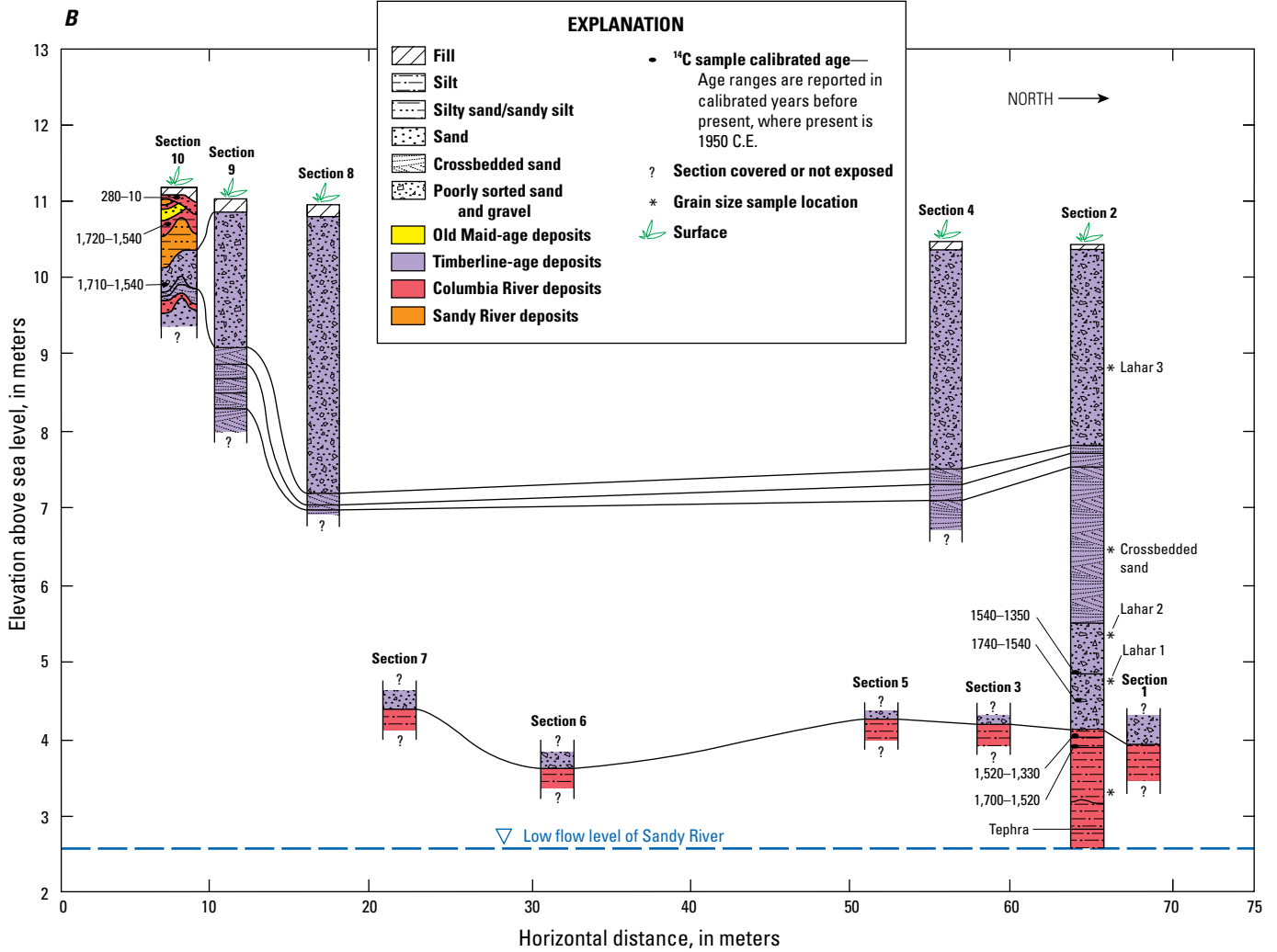




**Figure 79.** Photographs of sediments emplaced during the Old Maid eruptive period at Oxbow Regional Park. Photographs *A*, *B*, *C*, *E*, and *F* were taken at outcrops located between river miles 11 and 12 (fig. 76). *A*. A recently exposed face of the highest Old Maid-age alluvial terrace (L4/5) at Oxbow Regional Park. View looks downstream, showing trees that were rapidly buried in growth position. The surface of the Timberline-age paleoterrace on which the trees were growing is at the contact just below the man's waist. USGS photograph by T.C. Pierson, 2009. *B*. Closeup cross-sectional view of a Timberline-age paleoterrace surface soil overlain by fine to very fine overbank flood sands of lithofacies association 2 (FA-2). Paleoflow direction was approximately left to right. Note the infilled macropores in the soil and the thin, light-colored silt partings in the overbank flood sands (probably separating individual flood events). Scraper shaft is 0.7 millimeters wide. USGS photograph by T.C. Pierson, 2005. *C*. Crossbedded medium to coarse sand (FA-1) in lower third of the 20-meter-high L4/5 terrace. Paleoflow was from left to right. Pencil at center right for scale. USGS photograph by T.C. Pierson, 2006. *D*. Horizontal plane-bed stratification with localized low-angle crossbedding in alternating coarse sand and fine gravel layers (FA-3). Paleoflow was approximately from right to left. Pencil at right for scale. *E*. Normally graded top of a lahar deposit (FA-4) at the base of the Old Maid section beneath terrace L4/5. Paleoflow was approximately from left to right. Note the thin, white silty layer at the top of lahar unit, which probably formed during dewatering of the deposit. FA-2 deposits cap the lahar unit. Scraper at right for scale. *F*. Inversely graded base of the same lahar deposit in *E*. The lahar unit rests on a thin silty layer with groundwater iron staining, which, in turn, overlies a thin overbank flood deposit resting on a Timberline-age paleoterrace surface. Pencil at bottom right for scale. USGS photographs *D*, *E*, *F* by T.C. Pierson, 2009.



**Figure 80.** Holocene stratigraphy and chronology at Stop 9, as exposed in a riverbank outcrop along the west bank of the Sandy River delta at river mile 2.5. *A*, Plot of grain size distribution in select sediment samples from section 2. *B*, Correlated stratigraphy in sections 1–10 of the Sandy River delta. Age ranges are reported in calibrated years before present (cal. yr B.P.), where present is 1950 C.E. Present-day downstream is to the right. Modified from Rapp (2005), in which the stratigraphy is described in more detail.



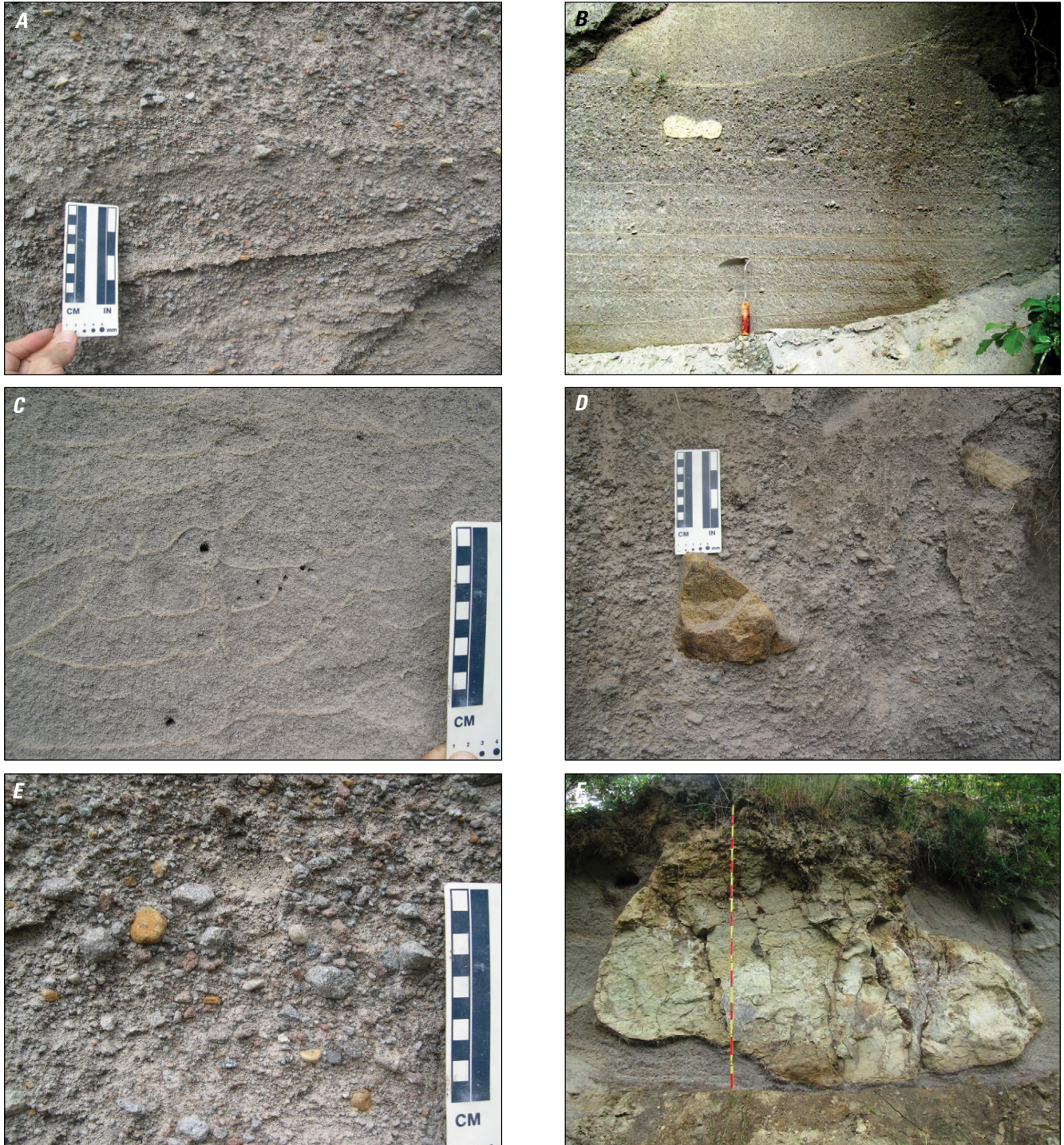


**Figure 81.** Photographs of lithofacies within the uppermost Timberline-age lahar deposit exposed at the mouth of the Sandy River at the delta apex at Stop 9. *A.* Sandy gravel unit within the youngest Timberline-age lahar deposit showing poorly developed stratification. *B.* Faint horizontally bedded coarse sand with fine sandy silt partings between sand beds. The thin silty “cap layers” form quickly between surges as depositional units consolidate and the expelled pore water transports fines to the surface. These repeating units typically are deposited by individual surges within a lahar; bedded units underlie a more massive layer. Shovel for scale. *C.* Dish structures and soft-sediment deformation within the same unit as in *B* caused by localized upward expulsion of pore water during consolidation, which disrupts silty partings between depositional units. *D.* Outsized clasts in a coarser lahar lithofacies. *E.* Coarsest lithofacies within the uppermost lahar deposit of the Timberline section here, with texture probably reflecting the relatively high concentration of the flow at the time of deposition. Faint layering at bottom of photograph suggests increasing concentration, from hyperconcentrated flow to debris flow, during progressive deposition. *F.* Large fragile clast of the semi-consolidated Pliocene Sandy River Mudstone, probably entrained by bank collapse from farther upstream and carried by the uppermost lahar. The material below the clast is talus. Vertical scale is 2 meters. USGS photographs *A* and *C–E* by T.C. Pierson, 2005; Smithsonian Institution photograph *B* and *F* by L. Siebert, 2016.

Maid-age deposits are present nearby but inset within the Timberline-age deposits at a slightly lower elevation. They can be seen from this location across the channel on the east side of the delta.

## Stratigraphy of Timberline-age Section

This bluff exposes a compressed version of the Timberline aggradation sequence (fig. 81) seen at Stop 8 farther upstream—6 m thick here but about 30 m thick at Oxbow Regional Park, located 16 km upriver (fig. 79). The two lahar units at the base of the section (together about 1.3 m thick) were emplaced as debris flows and are massive, very compact, extremely poorly sorted pebbly diamicts. Above them are about 2 meters of crossbedded fluvial sand, which grades upward to a third lahar deposit at the top of the section that is nearly 3 m thick. This top lahar unit shows evidence of emplacement by a flow at the concentration boundary between debris flow and hyperconcentrated flow. It has faint horizontal bedding, isolated outsized clasts, and thin silty partings that locally break up into dish structures caused by rapid vertical dewatering—all characteristics of hyperconcentrated-flow deposits. The Timberline volcaniclastic units overlie a micaceous clayey silt deposit at least 2.5 m thick. Abundant mica implies a Columbia River provenance (little mica found in the Sandy River basin), and the texture suggests deposition by overbank flooding. Radiocarbon dates for this section (fig. 80) confirm that the volcaniclastic units in this outcrop are from the Timberline eruptive period.

## Historical accounts of the Sandy River delta during and following the Old Maid eruptive period

Historical evidence suggests that high rates of sediment transport, perhaps accompanied by channel aggradation, were occurring in the Sandy River delta in 1792 (Cameron and Pringle, 1987). Direct observations were made at the river mouth by Lt. William Broughton of the Vancouver expedition. Broughton was the first European to cross the notorious Columbia River bar, enter the estuary, and verify that the mighty Columbia River—long hypothesized by cartographers and explorers—actually existed. He left his ship anchored in the estuary and continued up the Columbia River in a small boat, reaching as far as Point Vancouver, just upriver from the Sandy River mouth, and claimed the river's drainage basin for Great Britain. Broughton noted a

shallow sand bar actively forming at the river's mouth—a location where the Columbia River's current is particularly swift and where a sand bar could not persist without a large and continuous sediment supply (Cameron and Pringle, 1987).

Members of the Lewis and Clark expedition described and mapped the mouth and lower ~5 km of the Sandy River on November 3, 1805, and explored it further on their return on April 1, 1806 (fig. 76, inset) (Cameron and Pringle, 1986, 1987; Moulton and Dunlay, 1990; O'Connor, 2004). Based on these descriptions, the Sandy River was a wide braided channel, transporting predominantly sand-size sediment at a high rate on an unstable and unarmored sandy bed, where flow depth was nowhere more than about 10 cm. The expedition members named it the Quick Sand River, because they could not wade across it owing to the quick condition of the sandy bed. In their notes, they compared this channel to the shallow sediment-choked Platte River they had visited in Nebraska at the beginning of the expedition.

On the return trip in spring of 1806, an exploring party noted the river had low banks easily overtopped by high water—a location where today there is a terrace surface 18 m above the channel. The expedition must have observed the lower Sandy River near maximum aggradation. Based on other evidence, maximum aggradation level was reached at Oxbow Regional Park by 1793, more than a decade earlier (Pierson and others, 2011). In 1805, the Sandy River channel was noted to be about 110–275 m wide with numerous mid-channel sand islands and very turbid flow. Today, the main active channel across most of the delta is 80–140 m wide and several meters deep, with only a few large mid-channel islands. The channel widens to 250 m at the river mouth.

## Acknowledgments

This guidebook draws on earlier field-trip guides to Mount St. Helens (Waitt and others, 1989; Doukas, 1990; Waitt and Pierson, 1994; Pringle, 2002; Major and others, 2009) and Mount Hood (Scott, Gardner, and others, 1997; Pierson and others, 2009; Scott and Gardner, 2017), as well as unpublished field-trip guides by Michael Clynne, John Pallister, William E. Scott, and colleagues. The material presented is a distillation of myriad contributions illuminating the history of these two volcanoes from many more researchers than can be referenced here. Dave Ramsey facilitated preparation of location map graphics.



## References Cited

- Anderson, D.A., DeRoo, T.G., and Hedeon, C.D., 2006, Response to 1998 debris flow in the upper White River valley, Oregon: *Oregon Geology*, vol. 67, p. 7–10.
- Atwater, B.F. (compiler), 1994, *Geology of Holocene liquefaction features along the lower Columbia River at Marsh, Brush, Price, Hunting, and Wallace Islands, Oregon and Washington*: U.S. Geological Survey Open-File Report 94–209, 64 p.
- Banks, N.G., and Hoblitt, R.P., 1981, Summary of temperature studies of 1980 deposits, *in* Lipman, P.W., and Mullineaux, D.R., eds., *The 1980 eruptions of Mount St. Helens*, Washington: U.S. Geological Survey Professional Paper 1250, p. 295–313.
- Branney, M.J., and Kokelaar, P., 2002, *Pyroclastic density currents and the sedimentation of ignimbrites*: Geological Society Memoir No. 27, The Geological Society, London, 143 p.
- Brantley, S.R., and Waitt, R.B., 1988, Interrelations among pyroclastic surge, pyroclastic flow, and lahars in Smith Creek valley during first minutes of 18 May 1980 eruption of Mount St. Helens, USA: *Bulletin of Volcanology*, v. 50, p. 304–326.
- Brown, R.J., and Andrews, G.D.M., 2015, Deposits of pyroclastic density currents, *in* Sigurdsson, H., Houghton, B.F., McNutt, S.R., Rymer, H., and Stix, J., eds., *Encyclopedia of Volcanoes* (2d ed.): Elsevier, Amsterdam, p. 631–648.
- Brugman, M.M., and Meier, M. F., 1981, Response of glaciers to the eruptions of Mount St. Helens, *in* Lipman, P.W., and Mullineaux, D.R., eds., *The 1980 eruptions of Mount St. Helens*, Washington: U.S. Geological Survey Prof. Paper 1250, p. 743–756.
- Bryan, S.E., Peate, I.U., Peate, D.W., Self, S., Jerram, D.A., Mawby, M.R., Marsh, J.S., and Miller, J.A., 2010, The largest volcanic eruptions on Earth: *Earth-Science Reviews*, v. 102, p. 207–229.
- Cameron, K.A., and Pringle, P.T., 1986, Post-glacial lahars of the Sandy River basin, Mount Hood, Oregon: *Northwest Science*, v. 60, p. 225–237.
- Cameron, K.A., and Pringle, P.T., 1987, A detailed chronology of the most recent major eruptive period at Mount Hood, Oregon: *Geological Society of America Bulletin*, v. 99, p. 845–851.
- Carey, S.N., 1991, Transport and deposition of tephra by pyroclastic flows and surges, *in* Fisher, R.V., and Smith, G.A., eds., *Sedimentation in volcanic settings*: Society for Sedimentary Geology Special Publication 45, p. 39–57.
- Carey, S.N., Gardner, J., and Sigurdsson, H., 1995, The intensity and magnitude of Holocene plinian eruptions from Mount St. Helens volcano: *Journal of Volcanology and Geothermal Research*, v. 66, p. 185–202.
- Cas, R.A.F., and Wright, J.V., 1987, *Volcanic successions modern and ancient*: Allen and Unwin, London, 528 p.
- Charbonnier, S.J., and Gertisser, R., 2008, Field observations and surface characteristics of pristine block-and-ash flow deposits from the 2006 eruption of Merapi Volcano, Java, Indonesia: *Journal of Volcanology and Geothermal Research*, v. 177, p. 971–982.
- Christiansen, R.L., and Peterson, D.W., 1981, Chronology of mudflows in the South Fork and North Fork Toutle River following the May 18 eruption, *in* Lipman, P.W., and Mullineaux, D.R., eds., *The 1980 eruptions of Mount St. Helens*, Washington: U.S. Geological Survey Prof. Paper 1250, p. 17–30.
- Clynne, M.A., Calvert, A.T., Wolfe, E.W., Everts, R.C., Fleck, R.J., and Lanphere, M.A., 2008, The Pleistocene eruptive history of Mount St. Helens, Washington, from 300,000 to 12,800 years before present, *in* Sherrod, D.R., Scott, W.E., and Stauffer, P.H., eds., *A Volcano Rekindled—The Renewed Eruption of Mount St. Helens, 2004–2006*: U.S. Geological Survey Professional Paper 1750, p. 593–627.
- Clynne, M.A., Ramsey, D.W., and Wolfe, E.W., 2005, Pre-1980 eruptive history of Mount St. Helens, Washington: U.S. Geological Survey Fact Sheet 2005–3045, 4 p.
- Collins, B.D., and Dunne, T., 1986, Erosion of tephra from the 1980 eruption of Mount St. Helens: *Geological Society of America Bulletin*, v. 97, p. 896–905.
- Conrey, R.M., Sherrod, D.R., Uto, K., and Uchiumi, S., 1996, Potassium–argon ages from Mount Hood area of Cascade Range, northern Oregon: *Isochron/West*, no. 63, p. 10–20.
- Cook, R.C., 2002, Differentiation of three Quaternary Mt. Hood lahars by particle size, clay mineralogical, bulk mineralogical, and geochemical analyses: Middlebury College, BA senior thesis, 104 p.
- Crandell, D.R., 1971, *Postglacial lahars from Mount Rainier volcano*, Washington: U.S. Geological Survey Professional Paper 677, 73 p.
- Crandell, D.R., 1980, Recent eruptive history of Mount Hood, Oregon, and potential hazards from future eruptions: U.S. Geological Survey Bulletin 1492, 81 p.
- Crandell, D.R., 1987, Deposits of pre-1980 pyroclastic flows and lahars from Mount St. Helens volcano, Washington: U.S. Geological Survey Professional Paper 1444, 91 p.
- Crandell, D.R., and Mullineaux, D.R., 1973, Pine Creek volcanic assemblage at Mount St. Helens, Washington: U.S. Geological Survey Bulletin 1383–A, 23 p.
- Criswell, C.W., 1987, Chronology and pyroclastic stratigraphy of the May 18, 1980, eruption of Mount St. Helens, Washington: *Journal of Geophysical Research*, v. 92, p. 10237–10266.

- Cronin, S.J., LeCointre, J.A., Palmer, A.S., and Neall, V.E., 2000, Transformation, internal stratification, and depositional processes within a channelized, multi-peaked lahar flow: *New Zealand Journal of Geology and Geophysics*, v. 43, p. 117–128.
- Cronin, S.J., Neall, V.E., Lecointre, J.A., and Palmer, A.S., 1999, Dynamic interactions between lahars and stream flow: A case study from Ruapehu volcano, New Zealand: *Geological Society of America Bulletin*, v. 111, p. 28–38.
- Cummins, J., 1981, Chronology of mudflows in the South Fork and North Fork Toutle River following the May 18 eruption, *in* Lipman, P.W., and Mullineaux, D.R., eds., *The 1980 eruptions of Mount St. Helens*, Washington: U.S. Geological Survey Professional Paper 1250, p. 479–486.
- Dinehart, R.L., 1999, Sediment transport in the hyperconcentrated phase of the March 19, 1982 lahar, *in* Pierson, T.C., ed., *Hydrologic consequences of hot-rock/snowpack interactions at Mount St. Helens volcano, Washington 1982–84*: U.S. Geological Survey Professional Paper 1586, p. 37–52.
- Doukas, M.P., 1990, Road guide to volcanic deposits of Mount St. Helens and vicinity, Washington: U.S. Geological Survey Bulletin 1859, 53 p.
- Druitt, T.H., 1992, Emplacement of the 18 May 1980 lateral blast deposit ENE of Mount St. Helens, Washington: *Bulletin of Volcanology*, v. 54, p. 554–572.
- Dufek, J., Ongaro, T.E., and Roche, O., 2015, Pyroclastic density currents—Processes and models, *in* Sigurdsson, H., Houghton, B.F., McNutt, S.R., Rymer, H., and Stix, J., eds., *Encyclopedia of Volcanoes* (2d ed.): Elsevier, Amsterdam, p. 617–629.
- Dzurisin, D., and Driedger, C.L., 2013, Mount St. Helens, 1980 to now—What’s going on?: U.S. Geological Survey Fact Sheet 2013–3014, 6 p.
- Evarts, R.C., O’Connor, J.E., and Tolan, T.L., 2013, Geologic map of the Washougal quadrangle, Clark County, Washington, and Multnomah County, Oregon: U.S. Geological Survey Scientific Investigations Map 3257, pamphlet 46 p., scale 1:24,000, <http://pubs.usgs.gov/sim/3257/>.
- Fairchild, L.H., 1985, Lahars at Mount St. Helens, Washington: Seattle, University of Washington, Ph.D. dissertation, 374 p.
- Fisher, R.V., 1961, A proposed classification of volcaniclastic sediments and rocks: *Geological Society of America Bulletin*, v. 72, p. 1409–1414.
- Fisher, R.V., 1966, Rocks composed of volcanic fragments and their classification: *Earth-Science Reviews*, v. 1, p. 287–298.
- Fisher, R.V., 1983, Flow transformations in sediment gravity flows: *Geology*, v. 11, p. 273–274.
- Fisher, R.V., 1990, Transport and deposition of a pyroclastic surge across an area of high relief—the 18 May 1980 eruption of Mount St. Helens, Washington: *Geological Society of America Bulletin*, v. 102, p. 1038–1054.
- Fisher, R.V., Glicken, H.X., and Hoblitt, R.P., 1987, May 18, 1980, Mount St. Helens deposits in South Coldwater Creek, Washington: *Journal of Geophysical Research*, v. 92, p. 10,267–10,283.
- Fisher, R.V., and Schmincke, H-U., 1984, *Pyroclastic rocks*: Springer-Verlag, Berlin, 472 p.
- Fisher, R.V., and Waters, A.C., 1970, Base surge bed forms in maar volcanoes: *American Journal of Science*, v. 268, p. 157–180.
- Folk, R.L., 1974, *Petrology of Sedimentary Rocks*: Hemphill, Austin, 184 p.
- Freundt, A., Wilson, C.J.N., and Carey, S.N., 2000, Ignimbrites and block-and-ash deposits, *in* Sigurdsson, H., Houghton, B.F., McNutt, S.R., Rymer, H., and Stix, J., eds., *Encyclopedia of Volcanoes*: Academic Press, San Diego, p. 581–599.
- Gallino, G.L., and Pierson, T.C., 1985, Polallie Creek debris flow and subsequent dam-break flood of 1980, East Fork Hood River Basin, Oregon: U.S. Geological Survey Water-Supply Paper 2273, 22 p.
- Gardner, C.A., Scott, W.E., Major, J.J., and Pierson, T.C., 2000, Mount Hood—History and hazards of Oregon’s most recently active volcano: U.S. Geological Survey Fact Sheet 060-00, 4 p.
- Glicken, H., 1996, Rockslidedebris avalanche of May 18, 1980, Mount St. Helens Volcano, Washington: U.S. Geological Survey Open-File Report 96–677, 90 p.
- Harris, B.L., 1973, Genesis, mineralogy, and properties of Parkdale soils, Oregon: Corvallis, Oregon State University, Ph.D. dissertation, 174 p.
- Hausback, B.P., 2000, Geologic map of the Sasquatch Steps area, north flank of Mount St. Helens, Washington: U.S. Geological Survey Map I-2463, scale 1:4,000.
- Hausback, B.P., and Swanson, D.A., 1990, Record of pre-historic debris avalanches on the north flank of Mount St. Helens volcano, Washington: *Geoscience Canada*, v. 17, p. 142–145.
- Hoblitt, R.P., 2000, Was the 18 May 1980 lateral blast at Mt. St. Helens the product of two explosions?: *Philosophical Transactions of the Royal Society A*, v. 358, no. 1770, p. 1639–1661.
- Hoblitt, R.P., and Kellogg, K.S., 1979, Emplacement temperatures of unsorted and unstratified deposits of volcanic rock debris as determined by paleomagnetic techniques: *Geological Society of America Bulletin*, Part I, v. 90, p. 633–642.

- Hoblitt, R.P., Miller, C.D., and Vallance, J.W., 1981, Origin and stratigraphy of the deposit produced by the May 18 directed blast, *in* Lipman, P.W., and Mullineaux, D.R., eds., *The 1980 eruptions of Mount St. Helens*, Washington: U.S. Geological Survey Professional Paper 1250, p. 401–420.
- Houghton, B.F., and Carey, R.J., 2015, Pyroclastic fall deposits, *in* Sigurdsson, H., Houghton, B.F., McNutt, S.R., Rymer, H., and Stix, J., eds., *Encyclopedia of Volcanoes* (2d ed.): Elsevier, Amsterdam, p. 599–616.
- Houghton, B.F., Wilson, C.J.N., Smith, R.T., and Gilbert, J.S., 2000, Phreatoplinian eruptions, *in* Sigurdsson, H., Houghton, B.F., McNutt, S.R., Rymer, H., and Stix, J., eds., *Encyclopedia of Volcanoes*: Academic Press, San Diego, p. 513–525.
- Hubbell, D.W., Laenen, J.M., and McKenzie, S.W., 1983, Characteristics of Columbia River sediment following the eruption of Mount St. Helens on May 18, 1980: U.S. Geological Survey Circular 850–J, 21 p.
- Hyde, J.H., 1975, Upper Pleistocene pyroclastic-flow deposits and lahars south of Mount St. Helens volcano, Washington: U.S. Geological Survey Bulletin 1383–B, 20 p.
- Iverson, R.M., 2005, Debris-flow mechanics, *in* Jakob, M., and Hungr, O., eds., *Debris-flow Hazards and Related Phenomena: Praxis*—Springer, Berlin, p. 103–134.
- Iverson, R.M., and Vallance, J.W., 2001, New views of granular mass flows: *Geology*, v. 29, p. 115–118.
- Janda, R.J., Scott, K.M., Nolan, K.M., and Martinson, H.A., 1981, Lahar movement, effects, and deposits, *in* Lipman, P.W., and Mullineaux, D.R., eds., *The 1980 eruptions of Mount St. Helens*, Washington: U.S. Geological Survey Professional Paper 1250, p. 461–478.
- Korošec, M.A., 1987, Geologic map of the Hood River quadrangle, Washington and Oregon: Washington Division of Geology and Earth Resources Open-File Report 87-6, 41 p., 1 map sheet, scale 1:100,000.
- Lawrence, D.B., 1948, Mt. Hood's latest eruption and glacier advances: *Mazama*, v. 30, no. 13, p. 22–29.
- Letsinger, S., 1994, Late-stage syneruption sedimentation in the South Fork Toutle River, Toutle, Washington: Moscow, University of Idaho, M.S. thesis, 38 p.
- Lipman, P.W. and Mullineaux, D.R. eds., 1981, *The 1980 eruptions of Mount St. Helens*, Washington: U.S. Geological Survey Professional Paper 1250, 844 p.
- Lombard, R.E., Miles, M.B., Nelson, L.M., Kresh, D.L., and Carpenter, P.J., 1981, The impact of mudflows of May 18 on the lower Toutle and Cowlitz Rivers, *in* Lipman, P.W. and Mullineaux, D.R., eds., *The 1980 eruptions of Mount St. Helens*, Washington: U.S. Geological Survey Professional Paper 1250, p. 693–699.
- Lorenz, V., 1974, Vesiculated tuffs and associated features: *Sedimentology*, v. 21, p. 273–291.
- Major, J.J., 1997, Depositional processes in large-scale debris-flow experiments: *Journal of Geology*, v. 105, p. 345–366.
- Major, J.J., Crisafulli, C.M., Frenzen, P., and Bishop, J., 2009, After the disaster—The hydrogeomorphic, ecological, and biological responses to the 1980 eruption of Mount St. Helens, Washington, *in* O'Connor, J.E., Dorsey, R.J., and Madin, I.P., eds., *Volcanoes to Vineyards—Geologic Field Trips through the Dynamic Landscape of the Pacific Northwest*: Geological Society of America Field Guide 15, p. 111–134, doi: 10.1130/2009.fld015(06).
- Major, J.J., Pierson, T.C., Dinehart, R.L., and Costa, J.E., 2000, Sediment yield following severe volcanic disturbance—a two-decade perspective from Mount St. Helens: *Geology*, v. 28, p. 819–822.
- Major, J.J., and Scott, K.M., 1988, Volcaniclastic sedimentation in the Lewis River valley, Mount St. Helens, Washington—Processes, extent, and hazards: U.S., Geological Survey Bulletin 1383–D, 38 p.
- Majors, H.M., 1980, Three newly discovered accounts of activity on Mount St. Helens: *Northwest Discovery*, v.1, p. 36–41.
- Manville, V., Nemeth, K., and Kano, K., 2009, Source to sink—A review of three decades of progress in the understanding of volcaniclastic processes, deposits, and hazards: *Sedimentary Geology*, v. 220, p. 136–161.
- Manville, V., Newton, E.H., and White, J.D.L., 2005, Fluvial responses to volcanism—Resedimentation of the 1800a Taupo ignimbrite in the Rangitaiki River catchment, North Island, New Zealand: *Geomorphology*, v. 65, p. 49–70.
- McPhie, J., Doyle, M., and Allen, R., 1993, *Volcanic textures—A guide to the interpretation of textures in volcanic rocks*: Hobart, University of Tasmania, Centre for Ore Deposit and Exploration Studies, 196 p.
- Miall, A.D., 1996, *The Geology of Fluvial Deposits*: Springer, Berlin, 582 p.
- Moore, J.G., 1967, Base surge in recent volcanic eruptions: *Bulletin Volcanologique*, v. 30, p. 1–27.
- Moore, J.G., and Rice, C.J., 1984, Chronology and character of the May 18, 1980, explosive eruptions of Mount St. Helens, *in* *Explosive Volcanism—Inception, Evolution, and Hazards*: Washington, D.C., National Academy Press, p. 133–142.
- Moore, J.G., and Sisson, T.W., 1981, Deposits and effects of the May 18 pyroclastic surge, *in* Lipman, P.W., and Mullineaux, D.R., eds., *The 1980 eruptions of Mount St. Helens*, Washington: U.S. Geological Survey Professional Paper 1250, p. 421–438.

- Mosbrucker, A.R., 2014, High-resolution digital elevation model of Mount St. Helens crater and upper North Fork Toutle River basin, Washington, based on an airborne lidar survey of September 2009: U.S. Geological Survey Data Series 904, <https://doi.org/10.3133/ds904>.
- Mosbrucker, A.R., Spicer, K.R., Major, J.J., Saunders, D.R., Christianson, T.S., and Kingsbury, C.G., 2015, Digital database of channel cross-section surveys, Mount St. Helens, Washington: U.S. Geological Survey Data Series 951, 9 p. and supplemental data, <http://dx.doi.org/10.3133/ds951>.
- Moulton, G.E., and Dunlay, T.W., eds., 1990, *The Journals of the Lewis and Clark Expedition*, v. 6—November 2, 1805–March 22, 1806: Lincoln, University of Nebraska Press, 548 p.
- Mullineaux, D.R., 1986, Summary of pre-1980 tephra-fall deposits erupted from Mount St. Helens, Washington State, USA: *Bulletin of Volcanology*, v.48, p. 17–26.
- Mullineaux, D.R., 1996, Pre-1980 tephra-fall deposits erupted from Mount St. Helens, Washington: U.S. Geological Survey Professional Paper 1563, 99 p.
- Mullineaux, D.R., and Crandell, D.R., 1981, The eruptive history of Mount St. Helens, *in* Lipman, P.W., and Mullineaux, D.R., eds., *The 1980 eruptions of Mount St. Helens*, Washington: U.S. Geological Survey Professional Paper 1250, p. 3–15.
- Neuendorf, K.K.E., Mehl, J.P., and Jackson, J.A., 2005, *Glossary of Geology*, 5th Edition: American Geological Institute, Alexandria, VA, 779 p.
- O'Connor, J.E., 2004, The evolving landscape of the Columbia River Gorge—Lewis and Clark and cataclysms on the Columbia: *Oregon Historical Quarterly*, v. 105, no. 3, p. 390–437.
- O'Connor, J.E., and Benito, G., 2009, Late Pleistocene Missoula Floods—15,000–20,000 calendar years before present from radiocarbon dating: *Geological Society of America Abstracts with Programs*, v. 41, no. 7, p. 169.
- O'Connor, J.E., and Burns, S.F., 2009, Cataclysms and controversy—Aspects of the geomorphology of the Columbia River Gorge, *in* O'Connor, J.E., Dorsey, R.J., and Madin, I.P., eds., *Volcanoes to Vineyards—Geologic Field Trips through the Dynamic Landscape of the Pacific Northwest*: Geological Society of America Field Guide 15, p. 237–251.
- O'Connor, J.E., and Costa, J.E., 2005, The world's largest floods, past and present—Their causes and magnitudes: U.S. Geological Survey Circular 1254, 13 p.
- O'Connor, J.E., Pierson, T.C., Turner, D., Atwater, B.F., and Pringle, P.T., 1996, An exceptionally large Columbia River flood between 500 and 600 years ago—breaching of the Bridge-of-the-Gods landslide?: *Geological Society of America Abstracts with Programs*, v. 28, no. 5, p. 97.
- Orton, G.J., 1996, Volcanic environments, *in* Reading, H.G., ed., *Sedimentary Environments—Processes, Facies and Stratigraphy*: London, Blackwell Science, p. 485–567.
- Palmer, L., 1977, Large landslides of the Columbia River Gorge, Oregon and Washington: *Geological Society of America, Reviews in Engineering Geology*, v. 3, p. 69–83, doi: 10.1130/REG3-p69.
- Pierson, T.C., 1985, Initiation and flow behavior of the 1980 Pine Creek and Muddy River lahars, Mount St. Helens, Washington: *Geological Society of America Bulletin*, v. 96, p. 1056–1069.
- Pierson, T.C., 1999, Transformation of water flood to debris flow following the eruption-triggered transient-lake breakout from the crater on March 19, 1982, *in* Pierson, T.C., ed., *Hydrologic consequences of hot-rock/snowpack interactions at Mount St. Helens volcano, Washington 1982–84*: U.S. Geological Survey Professional Paper 1586, p. 19–36.
- Pierson, T.C., 2005, Hyperconcentrated flows—Transitional process between water flow and debris flow, chap. 8 of Jakob, M., and Hungr, O. eds., *Debris-flow hazards and related phenomena*: Praxis–Springer, Berlin, p. 159–202.
- Pierson, T.C., Daag, A.S., Delos Reyes, P.J., Regalado, M.T.M., Solidum, R., and Tubianosa, B.S., 1996, Flow and deposition of posteruption hot lahars on the east side of Mount Pinatubo, July–October 1991, *in* Newhall, C.G., and Punungbayan, R.S., eds., *Fire and Mud—Eruptions and Lahars of Mount Pinatubo, Philippines*: Philippine Institute of Volcanology and Seismology, Quezon City, and University of Washington Press, Seattle, p. 921–950.
- Pierson, T.C., Evarts, R.C., and Bard, J.A., 2016, Landslides in the Western Columbia Gorge, Skamania County, Washington: U.S. Geological Survey Scientific Investigations Map 3358, scale 1:12,000, pamphlet 22 p., <http://dx.doi.org/10.3133/sim3358>.
- Pierson, T.C., Pringle, P.T., and Cameron, K.C., 2011, Magnitude and timing of downstream channel aggradation in response to a dome-building eruption at Mount Hood, Oregon: *Geological Society of America Bulletin*, v. 123, p. 3–20.
- Pierson, T.C., and Scott, K.M., 1985, Downstream dilution of a lahar—Transition from debris flow to hyperconcentrated streamflow: *Water Resource Research*, v. 21, p. 1511–1524.
- Pierson, T.C., Scott, W.E., Vallance, J.W., and Pringle, P.T., 2009, Eruption-related lahars and sedimentation response downstream of Mount Hood—Field guide to volcaniclastic deposits along the Sandy River, Oregon, *in* O'Connor, J.E., Dorsey, R.J., and Madin, I.P., eds., *Volcanoes to Vineyards—Geologic Field Trips through the Dynamic Landscape of the Pacific Northwest*: Geological Society of America Field Guide 15, p. 229–244.

- Pringle, P.T., 2002, Roadside geology of Mount St. Helens National Volcanic Monument and vicinity (rev. ed.): Washington Department of Natural Resources Division of Geology and Earth Resources Information Circular 88, 122 p.
- Pringle, P.T., Pierson, T.C., and Cameron, K.A., 2002, A circa A.D. 1781 eruption and lahar at Mount Hood, Oregon—Evidence from tree-ring dating and from observations of Lewis and Clark in 1805–6 [abs]: *Geological Society of America Abstracts with Programs*, v. 34, no. 6, p. 511.
- Pringle, P.T., Pierson, T.C., Cameron, K.A., and Sheppard, P.R., 2010, Late eighteenth century Old Maid eruption and lahars at Mount Hood, Oregon (USA) dated with tree rings and historical observations, *in* Stoffel, M., Bollschweiler, M., Butler, D.R., and Luckman, B.H., eds., *Tree Rings and Natural Hazards, A State-of-Art—Advances in Global Change Research 41*: Springer Science + Business Media B.V., p. 487–491, [https://doi.org/10.1007/978-90-481-8736-2\\_46](https://doi.org/10.1007/978-90-481-8736-2_46).
- Rapp, B.K., 2005, The Holocene stratigraphy of the Sandy River delta, Oregon: Portland State University, M.S. thesis, 93 p.
- Regan, P.J., Huhta, G., and Lagnion, W.N., 2008, Failure of Swift No. 2 Forebay Dam, *in* Annual Conference, 28th, Portland, Oreg., 2008, Proceedings: Denver, Colo., United States Society on Dams, p. 85.
- Reid, M.E., Keith, T.E.C., Kayen, R.E., Iverson, N.R., Iverson, R.M., and Brien, D.L., 2010, Volcano collapse promoted by progressive strength reduction—New data from Mount St. Helens: *Bulletin of Volcanology*, v. 72, p. 761–766.
- Rowley, P.D., Kuntz, M.A., and Macleod, N.S., 1981, Pyroclastic-flow deposits, *in* Lipman, P.W., and Mullineaux, D.R., eds., *The 1980 eruptions of Mount St. Helens*, Washington: U.S. Geological Survey Professional Paper 1250, p. 489–512.
- Sarna-Wojcicki, A.M., Shipley, S., Waitt, R.B., Dzurisin, D., and Wood, S.H., 1981, Areal distribution, thickness, mass, volume, and grain size of air-fall ash from the six major eruptions of 1980, *in* Lipman, P.W., and Mullineaux, D.R., eds., *The 1980 eruptions of Mount St. Helens*, Washington: U.S. Geological Survey Professional Paper 1250, p. 577–60.
- Sarocchi, D., Sulpizio, R., Macias, J.L., and Saucedo, R., 2011, The 17 July 1999 block-and-ash flow (BAF) at Colima Volcano: New insights on volcanic granular flows from textural analysis: *Journal of Volcanology and Geothermal Research*, v. 204, p. 40–56.
- Savage, S.B., 1984, The mechanics of rapid granular flows: *Advances in Applied Mechanics*, v. 24, p. 289–376.
- Schuster, R.L., 1981, Effects of the eruptions on civil works and operations in the Pacific Northwest, *in* Lipman, P.W., and Mullineaux, D.R., eds., *The 1980 eruptions of Mount St. Helens*, Washington: U.S. Geological Survey Professional Paper 1250, p. 701–718.
- Schuster, R.L., and Crandell, D.R., 1984, Catastrophic debris avalanches from volcanoes, *in* Proceedings of the 4th International Conference on Landslides, Toronto: v. 1, p. 567–572.
- Scott, K.M., 1988a, Origins, behavior, and sedimentology of lahars and lahar-runout flows in the Toutle-Cowlitz River system, Mount St. Helens, Washington: U.S. Geological Survey Professional Paper 1447–A, 74 p.
- Scott, K.M., 1988b, Origin, behavior, and sedimentology of prehistoric catastrophic lahars at Mount St. Helens, Washington: Geological Society of America Special Paper 229, p. 23–36.
- Scott, K.M., 1989, Magnitude and frequency of lahars and lahar-runout flows in the Toutle–Cowlitz River system: U.S. Geological Survey Professional Paper 1447–B, 33 p.
- Scott, W.E., and Gardner, C.A., 2017, Field-trip guide to Mount Hood, Oregon, highlighting eruptive history and hazards: U.S. Geological Survey Scientific Investigations Report 2017–5022–G, 115 p., <https://doi.org/10.3133/sir20175022g>.
- Scott, W.E., Gardner, C.A., Sherrod, D.R., Tilling, R.I., Lanphere, M.A., and Conrey, R.M., 1997, Geologic history of Mount Hood volcano, Oregon—A field-trip guidebook: U.S. Geological Survey Open-File Report 97–263, 38 p.
- Scott, W.E., Gardner, C.A., Tilling, R.I., and Lanphere, M.A., 2003, Geologic History of Mount Hood Volcano, Oregon—A Field-Trip Guidebook: State of the Arc Conference Proceedings, Timberline Lodge, Oreg., 39 p.
- Scott, W.E., Iverson, R.M., Vallance, J.W., and Hildreth, W., 1995, Volcano hazards in the Mount Adams region, Washington: U.S. Geological Survey Open-File Report 95–492, 11 p., 2 sheets.
- Scott, K.M., Macias, J.L., Naranjo, J.A., Rodriguez, S., and McGeehin, J.P., 2002, Catastrophic debris flows transformed from landslides in volcanic terrains—Mobility, hazard assessment, and mitigation strategies: U.S. Geological Survey Professional Paper 1630, 59 p.
- Scott, W.E., Pierson, T.C., Schilling, S.P., Costa, J.E., Gardner, C.A., Vallance, J.W., and Major, J.J., 1997, Volcano hazards in the Mount Hood region, Oregon: U.S. Geological Survey Open-File Report 97–89, 14 p., 1 sheet.
- Sheppard, P.R., Weaver, R., Pringle, P.T., and Kent, A.J.R., 2010, Dendrochronological evidence of the 1781 eruption of Mount Hood, Oregon, *in* Stoffel, M., Bollschweiler, M., Butler, D.R., and Luckman, B.H., eds., *Tree Rings and Natural Hazards, A State-of-Art—Advances in Global Change Research 41*: Springer Science + Business Media B.V., p. 465–467, [https://doi.org/10.1007/978-90-481-8736-2\\_43](https://doi.org/10.1007/978-90-481-8736-2_43).

- Sherrod, D.R., and Scott, W.E., 1995, Preliminary geologic map of the Mount Hood 30- by 60-minute Quadrangle, northern Cascade Range, Oregon: U.S. Geological Survey Open-File Report 95-219, 35 p.
- Sherrod, D.R., Scott, W.E., and Stauffer, P. H., 2008, A volcano rekindled—The renewed eruption of Mount St. Helens, 2004–2006: U.S. Geological Survey Professional Paper 1750, 856 p.
- Siebert, L., 1984, Large volcanic debris avalanches—Characteristics of source areas, deposits, and associated eruptions: *Journal of Volcanology and Geothermal Research*, v. 22, p. 163–197.
- Siebert, L., 1996, Hazards of large volcanic debris avalanches and associated eruptive phenomena, *in* Scarpa, R. and Tilling, R.I., eds., *Monitoring and mitigation of volcano hazards*: Springer-Verlag, Berlin, p. 541–572.
- Smith, G.A., 1986, Coarse-grained nonmarine volcaniclastic sediment—Terminology and depositional process: *Geological Society of America Bulletin*, v. 97, p. 1–10.
- Smith, G.A., 1987a, The influence of explosive volcanism on fluvial sedimentation—The Deschutes Formation (Neogene) in central Oregon: *Journal of Sedimentary Petrology*, v. 57, p. 613–629.
- Smith, G.A., 1987b, Sedimentology of volcanism-induced aggradation in fluvial basins—Examples from the Pacific Northwest, U.S.A., *in* Ethridge, F.G., Flores, R.M., and Harvey, M.D., eds., *Recent Developments in Fluvial Sedimentology*: Society of Economic Paleontologists and Mineralogists Special Publication No. 39, p. 217–228.
- Smith, G.A., 1991, Facies sequences and geometries in continental volcaniclastic sediments, *in* Fisher, R.V., and Smith, G.A., eds., *Sedimentation in volcanic settings*: Society for Sedimentary Geology Special Publication 45, p. 109–121.
- Smith, G.A., and Fritz, W.J., 1989, Volcanic influences on terrestrial sedimentation: *Geology*, v. 17, p. 375–376.
- Smith, G.A., and Lowe, D.R., 1991, Lahars—Volcano-hydrologic events and deposition in the debris flow-hyperconcentrated flow continuum, *in* Fisher, R.V., and Smith, G.A., eds., *Sedimentation in Volcanic Settings*: Society for Sedimentary Geology Special Publication 45, p. 59–70.
- Sparks, R.S.J., Moore, J.G., and Rice, C.J., 1986, The initial giant umbrella cloud of the May 18th, 1980, explosive eruption of Mount St. Helens: *Journal of Volcanology and Geothermal Research*, v. 28, p. 257–274.
- Sparks, R.S.J., Self, S., and Walker, G.P.L., 1973, Products of ignimbrite eruptions: *Geology*, v. 1, p. 115–118.
- Sulpizio, R., Dellino, P., Doronzo, D.M., and Sarocchi, D., 2014, Pyroclastic density currents—State of the art and perspectives: *Journal of Volcanology and Geothermal Research*, v. 283, p. 36–65.
- Takarada, S., 2008, Recent Developments in Explosive Volcanism—Debris Avalanches: Report of the Commission on Explosive Volcanism Short Course, International Association of Volcanology and Chemistry of the Earth's Interior (IAVCEI), available at [http://iavceicev.clas.asu.edu/reports/2008\\_sc/cev\\_sc\\_takarada.pdf](http://iavceicev.clas.asu.edu/reports/2008_sc/cev_sc_takarada.pdf).
- Trimble, D.E., 1963, Geology of Portland, Oregon, and adjacent areas: U.S. Geological Survey Bulletin 1119, 119 p.
- Tucker, D.S., 2015, *Geology underfoot in Western Washington*: Mountain Press Publishing Company, 352 p.
- Ui, T., 1983, Volcanic dry avalanche deposits—Identification and comparison with nonvolcanic debris stream deposits: *Journal of Volcanology and Geothermal Research*, v. 18, p. 135–150.
- Ui, T., 1989, Discrimination between debris avalanche and other volcaniclastic deposits, *in* Latter, J.H., ed., *Volcanic Hazards, IAVCEI Proceedings in Volcanology*: Springer-Verlag, Heidelberg, v. 1, p. 201–209.
- Ui, T., Takarada, S., and Yoshimoto, M., 2000, Debris avalanches, *in* Sigurdsson, H., Houghton, B.F., McNutt, S.R., Rymer, H., and Stix, J., eds., *Encyclopedia of Volcanoes*: Academic Press, San Diego, p. 617–626.
- Valentine, G.A., and Fisher, R.V., 2000, Pyroclastic surges and blasts, *in* Sigurdsson, H., Houghton, B.F., McNutt, S.R., Rymer, H., and Stix, J., eds., *Encyclopedia of Volcanoes*: Academic Press, San Diego, p. 571–580.
- Vallance, J.W., 1999, Postglacial lahars and potential hazards in the White Salmon River system on the southwest flank of Mount Adams, Washington: U.S. Geological Survey Bulletin 2161, 49 p.
- Vallance, J.W., 2000, Lahars, *in* Sigurdsson, H., Houghton, B.F., McNutt, S.R., Rymer, H., and Stix, J., eds., *Encyclopedia of Volcanoes*: Academic Press, San Diego, p. 601–616.
- Vallance, J.W., and Iverson, R.M., 2015, Lahars and their deposits, *in* Sigurdsson, H., Houghton, B.F., McNutt, S.R., Rymer, H., and Stix, J., eds., *Encyclopedia of Volcanoes* (2d ed.): Elsevier, Amsterdam, p. 649–664.
- Vallance, J.W., and Scott, K.M., 1997, The Osceola Mudflow from Mount Rainier—Sedimentology and hazard implications of a huge clay-rich debris flow: *Geological Society of America Bulletin*, v. 109, p. 143–163.

- van Wyk de Vries, B., and Davies, T., 2015, Landslides, debris avalanches, and volcanic gravitational deformation, *in* Sigurdsson, H., Houghton, B.F., McNutt, S.R., Rymer, H., and Stix, J., eds., *Encyclopedia of Volcanoes* (2d ed.): Elsevier, Amsterdam, p. 665–685.
- Voight, B., and Davis, M.J., 2000, Emplacement temperatures of the November 22, 1994 nuée ardente deposits, Merapi Volcano, Java: *Journal of Volcanology and Geothermal Research*, v. 100, p. 371–377.
- Voight, B., Glicken, H., Janda, R.J., and Douglass, P.M., 1981, Catastrophic rockslide avalanche of May 18, *in* Lipman, P.W., and Mullineaux, D.R., eds., *The 1980 eruptions of Mount St. Helens*, Washington: U.S. Geological Survey Professional Paper 1250, p. 347–377.
- Voight, B., Janda, R.J., Glicken, H., and Douglass, P.M., 1983, Nature and mechanics of the Mount St. Helens rockslide-avalanche of 18 May 1980: *Geotechnique*, v. 33, p. 243–273.
- Waite, R.B., 1981, Devastating pyroclastic density flow and attendant air fall of May 18—Stratigraphy and sedimentology of deposits, *in* Lipman, P.W., and Mullineaux, D.R., eds., *The 1980 eruptions of Mount St. Helens*, Washington: U.S. Geological Survey Professional Paper 1250, p. 439–458.
- Waite, R.B., 1989, Swift snowmelt and floods (lahars) caused by great pyroclastic surge at Mount St. Helens volcano, Washington, 18 May 1980: *Bulletin of Volcanology*, v. 52, p. 138–157.
- Waite, R.B., 2015, *In the Path of Destruction—Eyewitness Chronicles of Mount St. Helens*: Pullman, Washington State University Press, 413 p.
- Waite, R.B., Hoblitt, R.P., Criswell, C.W., Scott, K.M., Glicken, H., and Brantley, S.R., 1989, Recent volcanoclastic deposits and processes at Mount St. Helens volcano, Washington—Excursion 2A, *in* Chapin, C.E., and Zidek, J., eds., *Field excursions to volcanic terranes in the western United States, Volume 2—Cascades and Intermontane West*: New Mexico Bureau of Mines and Mineral Resources Memoir 47, p. 51–64.
- Waite, R.B., and Pierson, T.C., 1994, The 1980 (mostly) and earlier explosive eruptions of Mount St. Helens volcano, *in* Swanson, D.A., and Haugerud, R.A., *Geologic field trips in the Pacific Northwest*, vol. 2: Dept. of Geological Sciences, University of Washington (1994 GSA Guidebook), p. 2I-1–37.
- Waite, R.B., Pierson, T.C., MacLeod, N.S., Janda, R.J., Voight, B., and Holcomb, R.T., 1983, Eruption-triggered avalanche, flood and lahar at Mount St. Helens—Effects of winter snowpack: *Science*, v. 221, p. 1394–1397.
- Walker, G.P.L., 1971, Grain-size characteristics of pyroclastic deposits: *Journal of Geology*, v. 79, p. 696–714.
- Walker, G.P.L., 1981, Generation and dispersal of fine ash and dust by volcanic eruptions: *Journal of Volcanology and Geothermal Research*, v. 11, p. 81–92.
- White, J.D.L., and Houghton, B.F., 2006, Primary volcanoclastic rocks: *Geology*, v. 34, p. 677–680.
- Willingham, W.F., 2005, The Army Corps of Engineers’ short-term response to the eruption of Mount St. Helens: *Oregon Historical Quarterly*, v. 106, no. 2, p. 174–203.
- Wilson, C.J.N., and Houghton, B.F., 2000, Pyroclast transport and deposition, *in* Sigurdsson, H., Houghton, B.F., McNutt, S.R., Rymer, H., and Stix, J., eds., *Encyclopedia of Volcanoes*: Academic Press, San Diego, p. 545–554.
- Wilson, C.J.N., and Walker, G.P.L., 1982, Ignimbrite depositional facies—The anatomy of a pyroclastic flow: *Journal of the Geological Society (London)*, v. 139, p. 581–592.
- Wise, W.S., 1969, Geology and petrology of the Mt. Hood area—A study of High Cascade volcanism: *Geological Society of America Bulletin*, v. 80, p. 969–1006.
- Wright, J.V., Self, S., and Fisher, R.V., 1981, Towards a facies model for ignimbrite-forming eruptions, *in* Self, S., and Sparks, R.S.J., eds., *Tephra Studies*: D. Reidel Publishing Co., Dordrecht, p. 433–439.
- Wright, J.V., Smith, A.L., and Self, S., 1980, A working terminology of pyroclastic deposits: *Journal of Volcanology and Geothermal Research*, v. 8, p. 315–336.
- Yamaguchi, D.K., 1983, New tree-ring dates for recent eruption of Mount St. Helens: *Quaternary Research*, v. 20, p. 246–250.
- Yamaguchi, D.K., and Hoblitt, R.P., 1995, Tree-ring dating of pre-1980 volcanic flowage deposits at Mount St. Helens, Washington: *Geological Society of America Bulletin*, v. 107, p. 1077–1093.

